The Dissertation Committee for Michael Douglas Brown certifies that this is the approved version of the following dissertation:

Design for Shear in Reinforced Concrete Using

Strut-and-Tie and Sectional Models

Committee:

_____

Oguzhan Bayrak, Supervisor

_____

Eric B. Becker

_____

John E. Breen

_____

James O. Jirsa

_____

Sharon L. Wood

Design for Shear in Reinforced Concrete Using

Strut-and-Tie and Sectional Models

by

Michael Douglas Brown, B.S.C.E., M.S.E.

Dissertation

Presented to the Faculty of the Graduate School of

The University of Texas at Austin

in Partial Fulfillment

of the Requirements

for the Degree of

Doctor of Philosophy

The University of Texas at Austin

August 2005

Acknowledgements

This dissertation was made possible only with help from many individuals. The help that was provided by the staff at the Ferguson Structural Engineering Laboratory over the years had been greatly appreciated. The practical knowledge I gained from the technical staff is invaluable, as was the assistance of the administrative staff.

I would also like to thank the students who worked on the project with me. The work of both Ivan Ornelas and Cameron Sankovich helped to make this dissertation possible along with the help of Kyle Stueck, Annika Trevino, and Mike Ziemenski. They all put many hours into the research project assisting in fabricating the test specimens as well as interpreting the data. I would also like to thank Hyo-Jeong Shin for her help with the last series of beam tests. Thanks are also due for the rest of the students who worked in the lab with me. Hopefully they all learned as much from me, as I have learned from them. I wish them all the best of luck with their future plans.

A great many thanks are in order for my advisor, Oguzhan Bayrak. Thank you for teaching me to ask questions regardless of where the answer may lead. I am also in debt to all of my committee (Eric Becker, John Breen, Jim Jirsa, and Sharon Wood) for their help with my dissertation. They each viewed the work with a unique perspective, and made the final product that much better.

Finally my deepest thanks are reserved for my parents. Isaac Newton once said, "If I have seen further, it is by standing on the shoulders of giants." He used to phrase to pay homage to the thinkers that came before him. I would like to use the phrase to honor my parents who made all of my education possible. If I have been able to succeed, it is only through their hard work.

July 15, 2005

Design for Shear in Reinforced Concrete Using

Strut-and-Tie and Sectional Models

Publication No. _____

Michael Douglas Brown, Ph.D.

The University of Texas at Austin, 2005

Supervisor: Oguzhan Bayrak

The design of reinforced concrete members for shear was studied. Both strut-and-tie models (STM) and sectional methods were examined. Initially, the response of isolated struts was observed. Various layout of reinforcement were used within the isolated struts. Three series of deep beam tests were also conducted. The first series was used to examine the effects of load distribution (uniform or concentrated) and distribution of shear reinforcement (horizontal and vertical) on shear strength of deep beams. The effects of beam width and shear span-to-depth ratio on shear strength were studied using the second series of beam tests. In the final series, the effects of load distribution on specimens without shear reinforcement were observed. A database of approximately 1,200 experimental results was compiled. The database, along with the experimental program, was used to evaluate the levels of conservatism of North American STM

code provisions as well as sectional design provisions. A new design procedure was developed to improve the safety of STM design procedures. Along with the new procedures, an expression was created to determine the necessary amount of reinforcement within a bottle-shaped strut. Finally, recommendations to improve the conservatism of sectional design provisions were developed.

Table of Contents

List of Tables

List of Figures

Notation

a = shear span

a/d = shear span-to-depth ratio

$A_{bearing}$ = bearing area of the reaction or applied load

A_c = minimum cross-sectional area of the strut

A_{core} = the area of concrete confined by spirals or ties

A_H = area of horizontal shear reinforcement

A_{ps} = area of prestressing steel

A_s = area of tensile reinforcement

A_{si} = area of surface reinforcement in the ith layer crossing a strut

A_{sk} = area of skin reinforcement

A_v = area of shear reinforcement

A_{vh} = the area of shear reinforcement parallel to the span

A_1 = area of strut at node faces

A_2 = area of strut at point of maximum spreading

b = the width of the strut perpendicular to the plane of the reinforcing bars

b_{ef} = the maximum strut width

b_{min} = the minimum strut width

b_v = beam width

b_w = width of web

c = neutral axis depth at ultimate moment capacity

c_a = approximate neutral axis depth

C_P = Coefficient for insufficiently reinforced struts

C_R = Coefficient for sufficiently reinforced struts

d = effective depth of section

d_e = effective beam depth

D = the diameter of spiral confinement

f_b = allowable bearing stress

$f_{bearing}$ = bearing stress of supported by the anchorage device

f_c' = the concrete compressive strength

f_{ck} = concrete cylinder strength

f_{ce} = effective compressive strength

f_{lat} = the lateral confining stress provided by spirals or ties:

$$\frac{2A_s f_y}{Ds} \quad \text{for spirals}$$

$$\frac{A_s f_y}{Ss} \quad \text{for ties}$$

f_y = yield strength of the reinforcement

F = nominal capacity of a bottle-shaped strut

F_t = the force in the tie

$F_\perp$ = force due to the reinforcement crossing the splitting crack

h = overall section depth

H = length of the strut from face of the node to face of the node

k_b = conversion factor for the efficiency of the face of a node in bearing

k_s = conversion factor for the efficiency of the face of a node abutting a strut

k_t = conversion factor for the efficiency of the face of a node anchoring a tie

K_c = coefficient reflecting influence of transverse tensile straining

K_f = coefficient reflecting influence of nominal strength of concrete

l = the length of the strut

m = slope of the dispersion of compression

M = factored moment at a section

M_n = nominal flexural strength at a section

M_u = factored moment at section

n = ratio of modulus of elasticity of steel to modulus of elasticity of concrete

r = longitudinal reinforcement ratio (%)

s = stirrup spacing

s = the pitch of spiral steel or the spacing of tie steel

s_i = spacing of reinforcing bars in the ith layer adjacent to the surface of the member

s_H = spacing of horizontal shear reinforcement

s_V = spacing of vertical shear reinforcement

s_2 = spacing of horizontal shear reinforcement in a direction perpendicular to the longitudinal reinforcement.

S = the width tie reinforcement

T = total transverse tension force

V_c = nominal shear strength provided by concrete

V_s = nominal shear strength provided by shear reinforcement

V_u = factored shear force at section

$V_{Ultimate}$ = maximum shear (including self-weight)

α = factor for confinement of surrounding concrete

α = reduction factor considering f_{lcd} versus strength of cylindrical test

α_s = the smallest angle between the compressive strut the adjoining tie

β = factor for aspect ratio of strut

β_s = the strut efficiency factor

β_1 = parameter used to define the compressive stress block

γ_c = partial safety factor

γ_i = the angle between the axis of the strut and the bars in the ith layer of reinforcement crossing that strut

ε_s = the tensile strain in the concrete in the direction of the tension tie

ε_1 = average principle tensile strain

ε_2 = average principle compressive strain

θ = the smallest angle between the compressive strut the adjoining tie

v = efficiency factor

v_{exp} = experimentally determined efficiency factor

v_P = efficiency factor for insufficiency reinforced struts

v_R = efficiency factor for sufficiency reinforced struts

v_1 = efficiency factor

v_2 = efficiency factor

       $v_2 = 0.80$ for struts with cracks parallel to the strut with bonded reinforcement; the reduction is due to the transverse tension and to the disturbances by the reinforcement and the irregular crack surfaces.

       $v_2 = 0.60$ for struts transferring compression across cracks with normal crack widths, e.g. in webs of beams.

       $v_2 = 0.45$ for struts transferring compression over large cracks e.g. in members with axial tension.

$$\rho_w = A_s \Big/ b_w d$$

$\rho_\perp$ = reinforcement ratio perpendicular to the splitting crack

$$\omega = \frac{A_s f_y}{b_w d f'_c}$$

CHAPTER 1

Introduction

1.1 OVERVIEW

In concrete structures, design engineers often encounter portions of structures that are subjected to significant shear stresses. Traditional design assumptions, specifically those regarding plane sections remaining plane after deformation, do not apply to such locations. These locations these have traditionally been designed using empirical formulations or past experience. A strut-and-tie model or strut-and-tie modeling (STM) offers an alternative to such methods.

Strut-and-tie modeling provides design engineers with a more flexible and intuitive option for designing structures, or portions thereof, that are heavily influenced by shear. The method allows for the stress flows within a structure to be approximated with simple truss-elements that can be designed using basic structural mechanics.

Strut-and-tie modeling was first introduced into American code provisions in the AASHTO Guide Specifications for Design and Construction of Segmental Concrete Bridges in 1989. In the segmental guide specification STM can be used to design for shear and torsion as well as the forces induced by the anchorage of post-tensioned prestressing forces. In recent years STM has become an increasingly popular method for design and detailing of structural concrete members subjected to large shear stresses. Code provisions for STM have been adopted for design by both ACI 318 (2002) and the AASHTO LRFD Bridge Design Specifications (1998).

1.2 PROJECT DIRECTION AND SCOPE

Project 4371 was sponsored by the Texas Department of Transportation (TxDOT) to study the AASHTO LRFD Bridge Design Specification provisions for STM. To examine those provisions an extensive literature review was conducted. The experimental results presented within the literature were then compiled into a large database. Based on the analysis of the data obtained from the literature, an experimental program was developed to fill gaps in technical literature. In the experimental program, a series of small-scale isolated strut tests was used to examine the effects of reinforcement on the strength of a strut. Additionally, three series of beam tests were conducted on shear-critical reinforced concrete members to examine the effects of shear reinforcement, shear span-to-depth ratio, and load distribution on shear strength.

Using the data compiled into the aforementioned database, current code provisions within ACI 318 and AASHTO LRFD were examined. The results indicate that the application of both codes produces relatively large numbers of unconservative estimates of strength. Due to the apparent unconservative nature of the current code provisions, a new design procedure was developed to increase levels of safety as well as to simplify the design processes required for implementation of STM. As part of that new procedure, a new method for determining the minimum reinforcement required within a strut was developed.

Finally, the database was used to examine current ACI 318 code provisions regarding shear in reinforced concrete beams. The current version of AASHTO LRFD allows the calculation of shear strength in reinforced concrete members using the same method and equations of ACI 318. However, the requirements for minimum shear reinforcement within AASHTO LRFD are different than those in ACI 318-05. The focus of the discussion regarding sectional design methods for shear is the ACI 318-05 provisions, but much of the

discussion is also relevant to the provisions of the AASHTO LRFD Bridge Design Specifications as well. The results indicate that the current code provisions for the concrete contribution to shear strength may be unconservative for concentrated loads, but conservative for distributed loads. A simple change to current code provisions is proposed to address this deficiency.

Strut-and-tie modeling is a wide-ranging method for designing reinforced and prestressed concrete structures. This dissertation limits the discussion of STM to conventionally reinforced, deep beams. Furthermore, the discussion of STM is limited to prismatic beams without openings or other changes in cross section. The use of STM has been shown to provide safe estimations of nominal capacity in past studies (Cook and Mitchell 1988 and Breen et al. 1994).

1.3 DISSERTATION ORGANIZATION

This dissertation comprises seven chapters. Together, these chapters provide a review of STM based on the available technical literature and on an experimental investigation. Chapter 2 contains the background and literature review regarding STM as well as discussions of various codes that have implemented provisions for STM. The first series of tests consisted of 26 small-scale test specimens that were used to investigate the behavior of isolated struts. The results of the isolated strut tests are presented in Chapter 3. Following the isolated strut tests, three series of beam tests were undertaken. The first and second series of beam tests each contained ten specimens and the third series contained 4 specimens. The beam tests were used to examine struts in a more realistic environment than had been done in the isolated strut tests. All three series of beam tests are presented in Chapter 4. The data discussed in Chapter 5 was used to evaluate the STM provisions of ACI 318-05 and AASHTO LRFD Bridge Design Specification. Ultimately the database was used to develop and evaluate a

new STM design procedure. Chapter 5 contains all of the information about the test results in the database as well as the new design procedure. Chapter 6 focuses on more traditional sectional design methods as opposed to STM. The database described in Chapter 5 was also used to evaluate sectional design methods and develop recommendations to improve the conservatism of those methods. Finally, conclusions developed throughout the research program are presented in Chapter 7.

CHAPTER 2

Background on Strut-and-Tie Modeling

2.1 INTRODUCTION

Strut-and-Tie Modeling (STM) is a method of design for reinforced and prestressed concrete that reduces complex states of stress within a structure to a collection of simple stress paths. The stress paths result in truss members loaded with uniaxial stress that is parallel to the axis of the stress path. Truss members that are in compression are called struts, while the force paths that are in tension are named ties. The intersections of struts and/or ties form the nodes. The collection of struts, ties and nodes is called a truss mechanism or model. The forces within a strut-and-tie model can be calculated using static equilibrium if the truss is statically determinate.

Such a reduction in complexity allows for simple design of structural concrete. With the forces in each strut and tie having been determined from basic statics and any necessary compatibility conditions, only the stresses within these elements (struts, ties, and nodes) need be compared with permissible stresses. To determine the allowable stress for a strut or node, empirical observations of their behavior must be made. The empirical observations of the strength of isolated members can be combined with truss mechanisms to develop an accurate model for prediction of the strength of the concrete member. A strut-and-tie model consists of elements in pure tension or compression. Appropriate reinforcement must be provided in the portions of the structure where tension is indicated by the strut-and-tie model or where additional strength, confinement, or both are required by the struts. By using a simple truss model, an estimation of strength of a structural element can be made and the element can be appropriately detailed.

Strut-and-tie modeling is most useful as a design tool when applied to structures, or portions of structures, in which plane sections do not remain planar after the application of load. The behavior of such elements (corbels, deep beams, dapped-end beams, or post-tension anchorage zones) is not dominated by flexural deformations. The difficulty in analyzing these types of elements often arises due to the inability to apply kinematic compatibility. STM disregards kinematic constraints. Overall equilibrium and equilibrium of the nodes are considered during the analysis stage. The constitutive relationships are determined by empirical observation of struts, ties and nodes to establish the yield conditions for those elements. STM, therefore, conforms to the lower bound theory of plasticity, which requires that only equilibrium and yield conditions be satisfied. The lower bound theory of plasticity states that if the load has such a magnitude that it is possible to find a stress distribution corresponding to stresses within the yield surface and to maintain internal and external equilibrium, then this load will not cause collapse of the body (Nielson 1998). In other words, the capacity of a structure as estimated by a lower bound method will be less than or at most equal to the actual collapse load of the structure in question. The most appealing quality of a lower bound theory is its inherent conservatism.

2.1.1 Elements of a Strut-and-Tie Model

Each of the types of elements in a strut-and-tie model serves a unique purpose, but must act in concert to describe accurately the behavior of a structure. Before discussing STM as a whole, each of its components must be examined.

2.1.1.1 Struts

Struts are the elements within strut-and-tie models that carry compressive stresses. The geometry of a strut varies widely and depends upon the force path from which each individual strut arises. The most basic type of strut is prismatic.

Prismatic struts have a uniform cross section over their length (Figure 2-1). Such a strut can occur in beam bending where the compressive stresses are confined by the neutral axis. The compressive stress block of a beam in a section of constant moment is an example of a prismatic strut.

The second major type of strut is a compression fan. A compression fan is characterized by stresses that focus onto a very small area. The stresses flow radially from a large area to a much smaller one. A compression fan can develop when large distributed loads flow into a support (Figure 2-1). There are no tensile stresses developed within a compression fan because the forces are collinear without any tension components perpendicular to the radii of the fan.

When the flow of compressive stresses is not confined to a portion of a structural element, a bottle-shaped strut can form (Figure 2-1). In this case, the force is applied to a small zone and the stresses disperse as they flow through the member. As the compression disperses, it changes direction forming an angle to the axis of the strut. To maintain equilibrium a tensile force is developed to counteract the lateral component of the angled compression forces. A bottle-shaped strut can be modeled by a collection of struts and ties to adequately account for the tensile force.

(a) Prism

(b) Bottle

(c) Fan
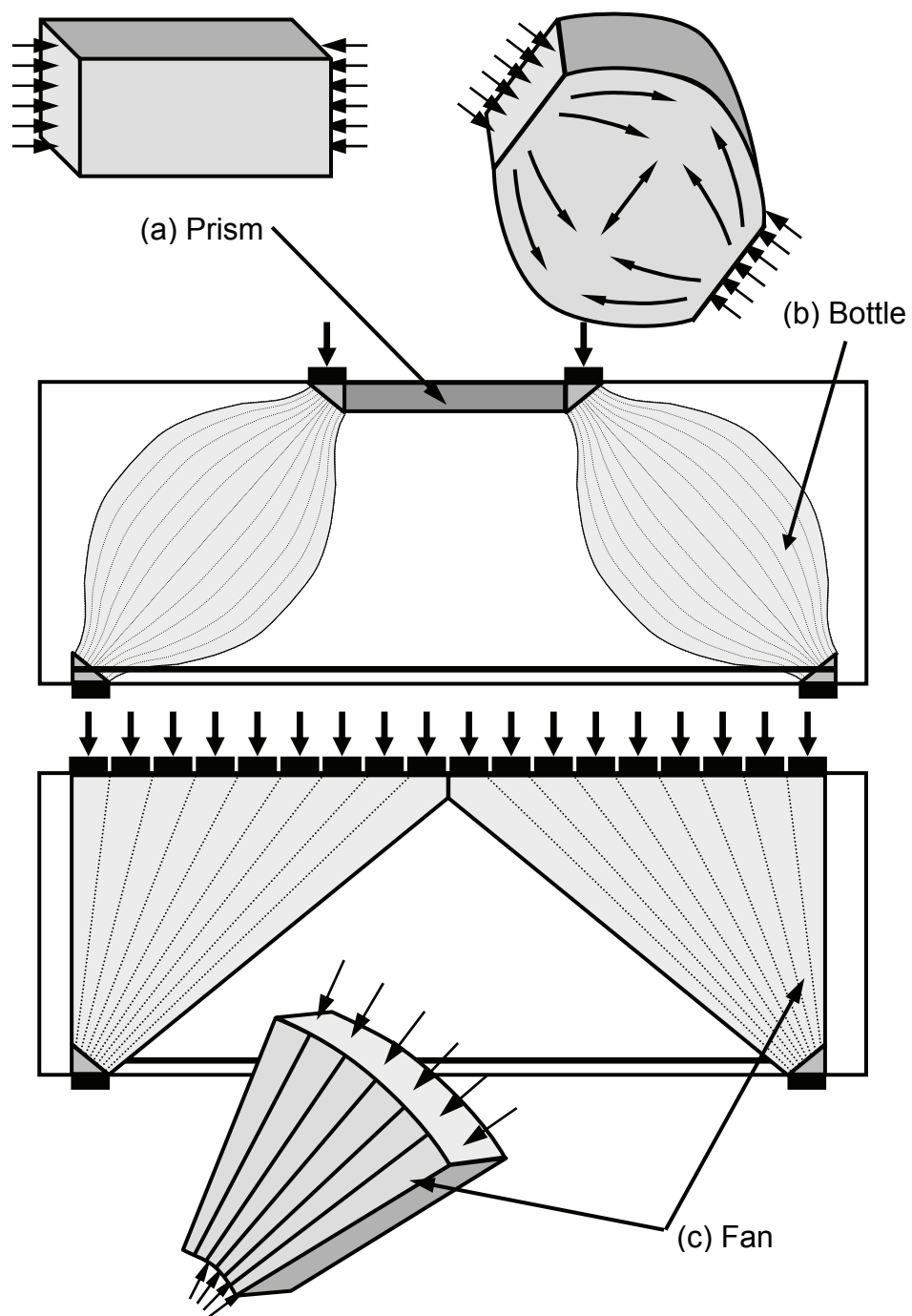
Figure 2-1: Common types of struts

8

The dispersion of compression was described in great detail by Guyon (1953). Guyon used isostatic lines to determine the dispersion of tensile and compressive stresses in a post-tension anchorage zone (Figure 2-2). Guyon reasoned that isostatic lines of compression (1 thought 6 in Figure 2-2) must be parallel to the applied force at the point where the force was applied and at some distance away from the point of application. St. Venant's principle suggests that at a distance equal to the member depth, the stress distribution is nearly uniform. The isostatic lines are therefore distributed uniformly across the section as on line CD in Figure 2-2. As the isostatic lines of compression curve, tension is produced normal to those lines along the lines E and E'. Although this derivation was based on anchorage zones, it can be used to describe the dispersion of compression for externally applied loads as well.
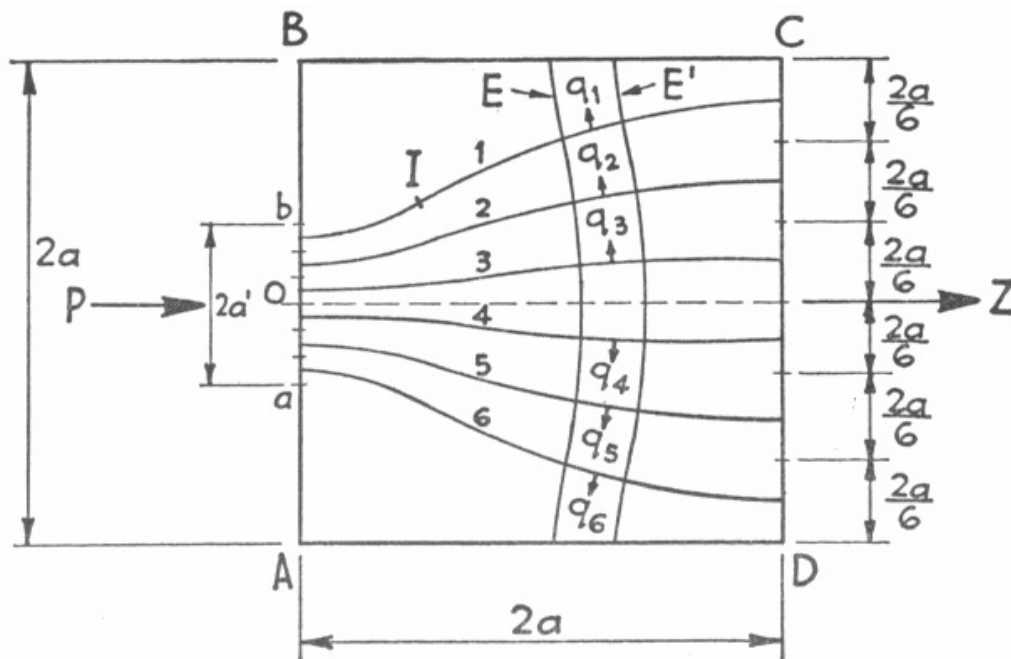
Figure 2-2: Dispersion of compression (Guyon 1953)

2.1.1.2   Ties

Ties are the elements within a strut-and-tie model that carry tension, and are generally confined to reinforcing or prestressing steel. The geometry of a tie is therefore much simpler. The tie is geometrically confined to elements that can carry high tensile forces, and the allowable force is generally given as a fraction of the yield force.

Appropriate attention must be given to the anchorage of ties. If the yield force of a tie is expected at any point in the strut-and-tie model, the proper anchorage must be provided beyond that point. The necessary anchorage requirement for ties (Thompson 2002) has been studied recently.

2.1.1.3   Nodes

Nodes form where struts and ties intersect (Figure 2-3). Nodes are described by the types of element that intersect at the node. For example, a CCT node is one which is bounded by two struts (C) and one tie (T). Using this nomenclature nodes are classified as CCC, CCT, CTT, or TTT. A CCC node is expected to have a higher strength than any of the other types due to the effect of confinement. Each of the other node types has some tensile stresses acting upon it due to the presence of the tie(s). Tensile stresses can cause cracking within the nodal zone, and reduce the strength.

The geometry of a node may be defined by the details of the structure. Wherever concentrated loads are applied to the structure, there will be some finite bearing area. The dimensions of that bearing area will define the geometry of the adjacent node. Nodes that do not occur on the boundary or are not influenced by a bearing area of a structural member are much harder to define geometrically.

Nodes may be assumed to be hydrostatic. Hydrostatic nodes are loaded with a stress that is applied perpendicular to each face of the node and that stress

is equal in magnitude on all faces of the node. Since the stresses are normal to the surfaces of the node, there are no shear stresses at the boundaries of the node or within the body of the node. Non-hydrostatic nodes are also possible and permissible due to the inherent shear strength of concrete. If such nodes are used, the ratio of the maximum stress on a node to the minimum stress on that same node should not exceed a value of two (Schlaich, Schäfer, and Jennewein 1987). The states of stress in both hydrostatic and non-hydrostatic nodes are shown in Figure 2-4.

CCC Node

CTT Node

CCT Node
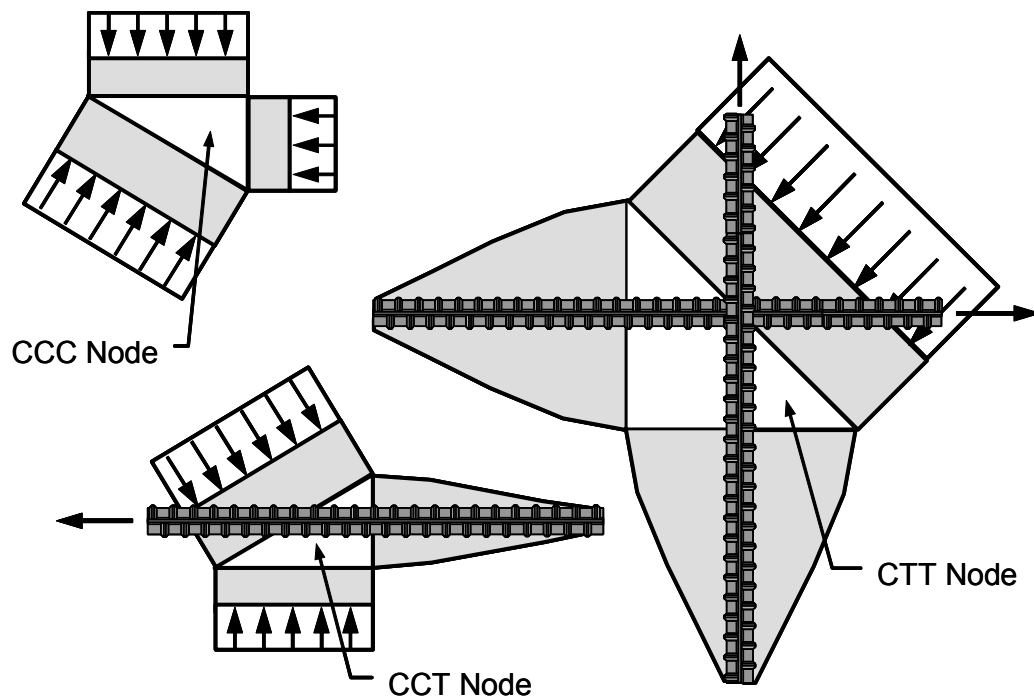
Figure 2-3: Schematic depictions of nodes (after Thompson et al. 2003)

i. Hydrostatic Node

ii. Non-Hydrostatic Node

Axis 1

F_2

w_2

σ_2

Axis 2

F_1

σ_1

w_1

θ

σ_s

w_s

F_s

$\sigma_1 = \sigma_2 = \sigma_s$

F_2

w_2

σ_2

F_1

σ_1

w_1

θ

σ_s

w_s

F_s

$\sigma_1 > \sigma_s > \sigma_2$

Mohr's Circle

$+\tau$

$\sigma_1 = \sigma_2 \rightarrow$ no shear

$-\sigma$
(tension)

$+\sigma$
(compression)

$-\tau$

$+\tau$

$\sigma_1 > \sigma_2 \rightarrow$ shear

τ_{node}

σ_2

σ_1

$-\sigma$
(tension)

$+\sigma$
(compression)

$-\tau$
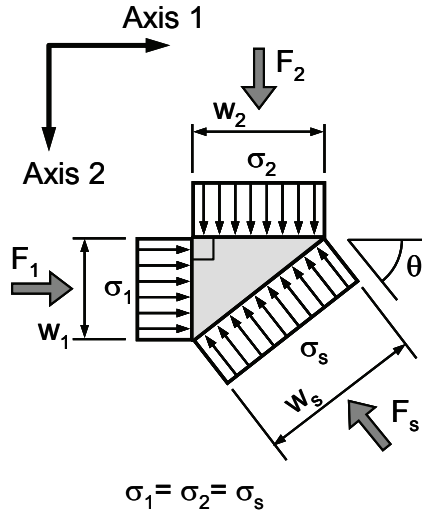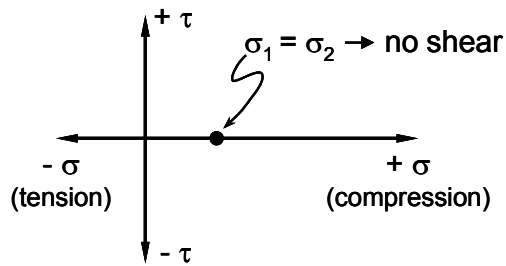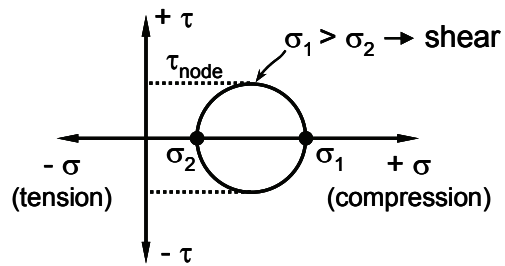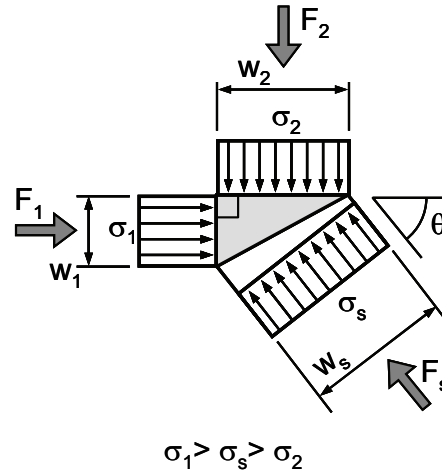
Figure 2-4: Mechanics of hydrostatic and non-hydrostatic nodes (Thompson 2002)

2.2 HISTORICAL DEVELOPMENT OF STRUT-AND-TIE MODELING

The beginnings of STM date back to the infancy of reinforced concrete design. In 1899, Wilhelm Ritter developed a truss mechanism to explain the role of transverse reinforcement in the shear strength of a beam. Previously it was believed that transverse steel bars provided dowel action that resisted horizontal shear deformations. Based on Ritter's truss model (Figure 2-5), it is clear that the stirrups are in tension, and dowel action is not the primary shear resistance

mechanism. Ritter's model was later refined by Mörsch in 1902. Mörsch believed that the discrete diagonal forces that Ritter had used in his truss would be better represented by a continuous field of diagonal compression (Figure 2-6).
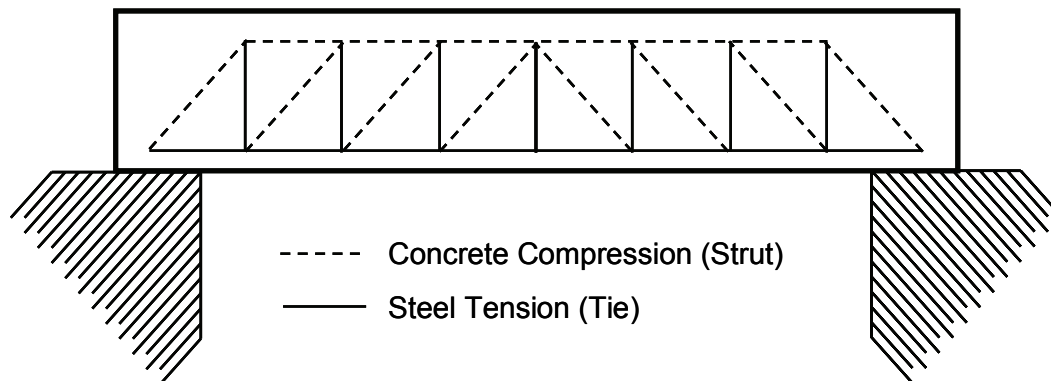
Figure 2-5: Ritter's original truss model (1899)
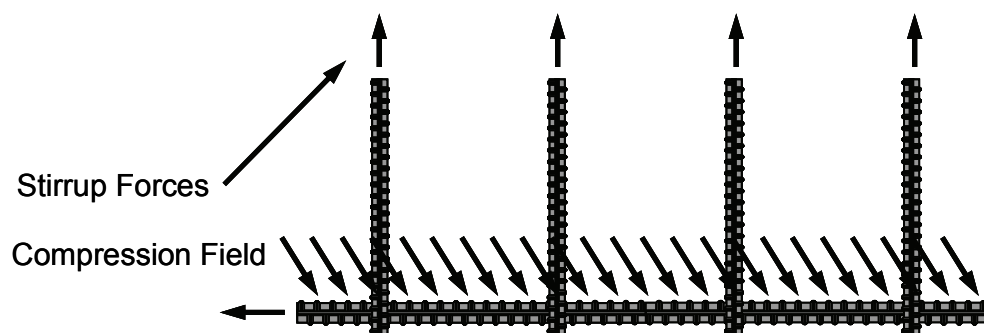
Figure 2-6: Mörsch's adaptation of Ritter's model (1902)

Experimental testing in the United States showed that the truss models produced overly conservative estimates of strength (Talbot 1909). The truss models neglected the tensile strength of the concrete which can play an important part in resistance to shear. In 1927, Richart proposed a method of shear design in which the concrete and steel contributions to shear strength were calculated independently then summed to determine the overall shear strength. In this method the concrete contribution to shear strength (V_c) was based on empirical observations of beams failing in shear and the steel contribution (V_s) was based

13

on a truss model whose concrete compression field was at an angle of 45 degrees from the longitudinal reinforcement. With a simple and safe sectional model available, truss modeling soon fell out of favor in North America.

Revival in the use of STM began in the United States in the early 1970s. At that time STM was first applied to concrete members subjected to a combination of shear and torsion. For this case a tubular truss which formed a hollow box near the outside face of the members was used (Figure 2-7) (Lampert and Thürlimann 1971). The tubular truss model was later refined to a space truss model (Lüchinger (1977), Ramirez and Breen (1983), Mitchell and Collins (1986)). The space truss could adequately account for all the actions of bending, shear, torsion and axial load.
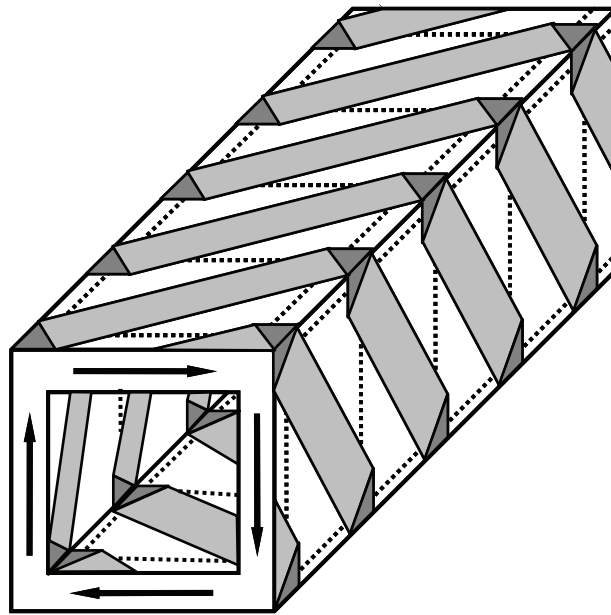
Figure 2-7: Idealized truss model for torsion of a square section (After Thompson et al. 2003)

Following the increased interest in STM regarding complex load states, general methods for the application of STM began to appear. Both Marti (1985a,

1985b) and Schlaich, Schäfer, and Jennewein (1987) presented modeling approaches for use in discontinuity regions (Figure 2-8). These approaches provided basic tools that could be applied to complex structures for safe designs based on behavioral models. Following this work, STM began appearing in North American codes for general design use. The Canadian CSA Standard was the first to adopt STM in 1984. Soon afterwards it was adopted by AASHTO for the segmental guide specification in 1989 and by the Bridge Design Specifications in 1994. Most recently ACI has included STM provisions in the 2002 edition of the Building Code Requirements for Structural Concrete (ACI 318-02).
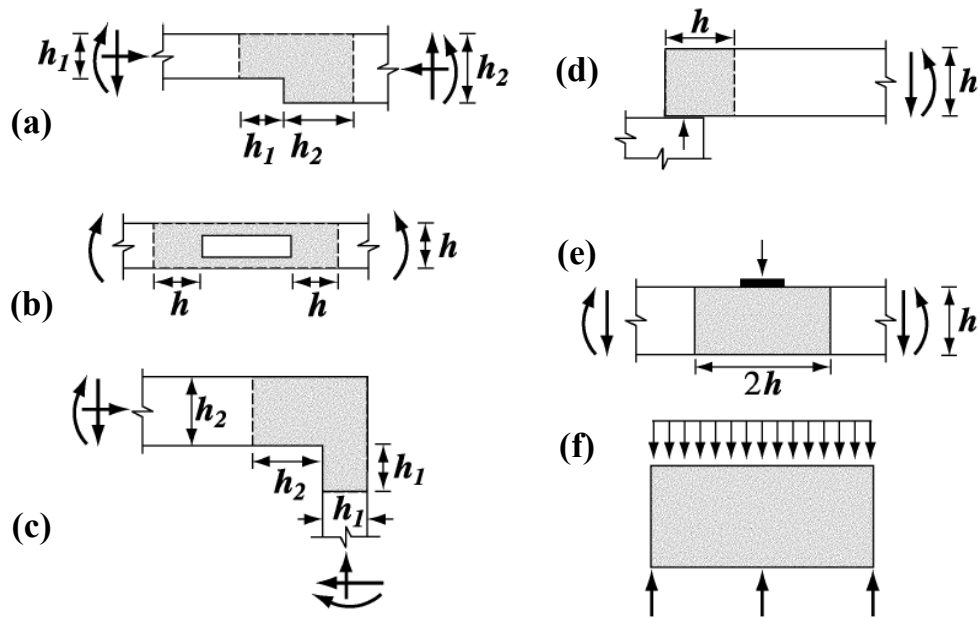
Figure 2-8: Typical D-regions (geometric discontinuities a-c and statical discontinuities d-f) (From Appendix A of ACI 318-05)

2.3 CURRENT CODE PROVISIONS FOR STRUT-AND-TIE MODELING

Many code authorities world-wide have added STM specifications to their traditional design specifications. Each of the codes (ACI 318-05, AASHTO

15

LRFD Bridger Design Specifications, CSA A23.3-94, NZS 3101:1995, and fib recommendations 1999) handles the elements of a strut-and-tie model differently. The major codes are discussed individually below.

2.3.1 ACI 318-05

Provisions for the use for STM were added as an appendix to the main body of the ACI building code in 2002. The ACI 318-05 Appendix A provisions provide estimations of the strength of the struts of a strut-and-tie model as a fraction of the specified compressive strength of the concrete:

$$f_{ce} = 0.85 \beta_s f_c' \tag{2-1}$$

Where: β_s = the strut efficiency factor (Table 2-1)

                f_c' = the concrete compressive strength

                f_{ce} = effective compressive strength

The efficiency factor, β_s, is based on the type of strut. There are five classes of struts listed in Table 2-1. The first category is a strut with uniform cross section over its length as would occur normally in the compression zone of a beam (Figure 2-1). Bottle-shaped struts are the most prevalent and general of the classes. A bottle-shaped strut is one with a varying cross-sectional area. Typically, if a force is applied to a small region of a concrete element, the stresses will disperse in the lateral direction as they flow through that element. Figure 2-9 shows the elastic stress distribution of a bottle-shaped strut as well as a possible strut-and-tie model.

Table 2-1: Node and strut efficiency factors

	Strut and Node Efficiencies[†]	ACI 318-05[‡]		AASHTO LRFD[*]		NZS 3101:1995	
		β_s	ϕ	ν	ϕ	ν	ϕ
Struts	Strut with uniform cross-section over its length	1.00	0.75	Eqn. 2-3	0.70		
	Bottle-shaped struts with reinforcement satisfying A.3.3	0.75	0.75	Eqn. 2-3	0.70	NZS 3101:1995 specifies only nodal efficiency factors.	
	Bottle-shaped struts without reinforcement satisfying A.3.3	0.60	0.75	Eqn. 2-3	0.70		
	Struts in tension members	0.40	0.75	Eqn. 2-3	0.70		
	All other cases	0.60	0.75	Eqn. 2-3	0.70		
Nodes	Nodes bounded by compression or bearing CCC Node	1.00	0.75	0.85	0.70	0.65	0.80
	Nodes anchoring one tie CCT Node	0.80	0.75	0.75	0.70	0.55	0.80
	Nodes anchoring more than one tie CTT and TTT Nodes	0.60	0.75	0.65	0.70	0.45	0.80

[†]fib factors are not listed in this table as they do not conform to the same classification system.
[‡]Efficiency factors for ACI are applied to $0.85 f_c'$ while for the other code documents the efficiency multiplies f_c' directly
[*]The provisions are CSA A23.3-94 differ from AASHTO LRFD due only to the use of partial safety factors.
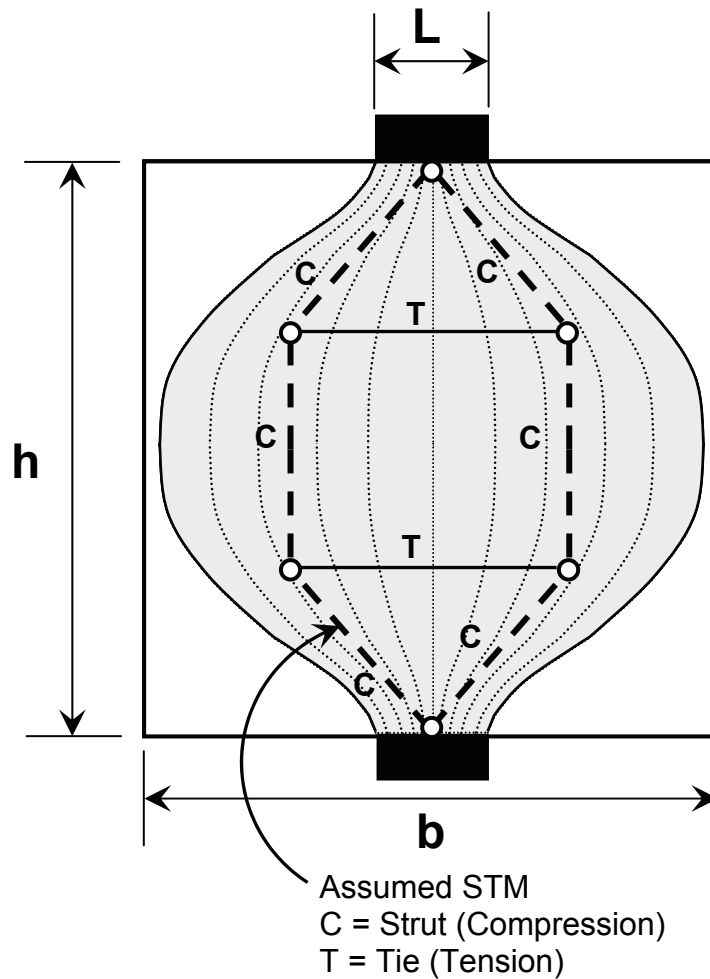
Figure 2-9: Elastic stress distribution for bottle-shaped strut and strut-and-tie model

Note that there are two efficiency factors associated with bottle-shaped struts. These two factors are based on the reinforcement within the strut. As the compression spreads out from the support, tension is developed. In Figure 2-9, the compression is applied vertically, and the induced tension is horizontal. When the induced tensile stress exceeds the tensile strength of the concrete, a vertical crack will form. Without any horizontal reinforcement, the strut could split causing a brittle failure. This phenomenon is the basis of the split cylinder test (ASTM C

18

496) used to determine the tensile strength of concrete. Nevertheless, if sufficient transverse reinforcement exists, brittle failure can be avoided, and the strut can continue to carry load beyond the cracking load. If a particular strut satisfies Equation A-4 in Section A.3.3.1 of ACI 318-05 or the more general provisions of A.3.3, the larger β_s factor of 0.75 may be used. The more general provisions of Section A.3.3 of ACI 318-05 allow the designer to determine the necessary transverse reinforcement for a bottle-shaped strut based on a 2:1 spread of compression.

For equation A-4 of ACI 318-05 (Eqn. 2-2), reinforcement that crosses the anticipated crack is included as can be seen in Figure 2-10. Struts that do or do not meet the minimum reinforcement criterion (Eqn. 2-2) make up the second and third classes of struts. The provisions of Appendix A of ACI 318-05 allow the use of bottle-shaped struts without transverse reinforcement. Without transverse reinforcement, a bottle-shaped strut can not maintain equilibrium after the splitting crack has formed. Currently in ACI 318-05 there are minimum reinforcement requirements for deep beams if Appendix A is used. The required reinforcement presented in Chapter 11 of ACI 318-05 restrains the growth of diagonal tension cracks. The use of bottle-shaped struts without transverse reinforcement allows diagonal tension cracks to grow without restraint. The use of bottle-shaped strut without transverse reinforcement is questionable.

$$\sum \frac{A_{si}}{bs_i} \sin\alpha_i \geq 0.003 \qquad (2\text{-}2)$$

Where: A_{si} = area of surface reinforcement in the ith layer crossing

a strut

s_i = spacing of reinforcing bars in the ith layer adjacent to

the surface of the member

b = the width of the strut perpendicular to the plane of the
reinforcing bars

α_i = the angle between the axis of the strut and the bars in
the ith layer of reinforcement crossing that strut
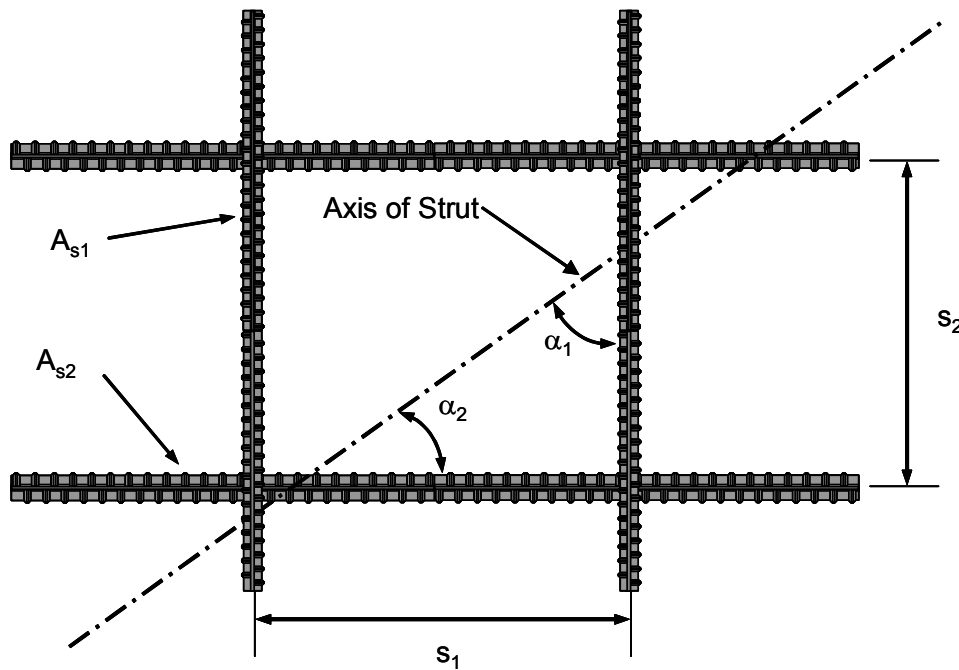
Figure 2-10: Nomenclature for Equation 2-2

The fourth class of strut is one that occurs in a tension member. A strut such as this can occur in the tension flange of a prestressed T-beam. As the prestress diffuses from the web to the extreme edges of the flange, struts are produced in the plane of the flange. If a T-beam happens to be in negative curvature (tension in the flange), the struts representing the dispersion of the prestress force will be in a zone of tension. The final class of struts is for all struts that do not meet the requirements for the previous classes of struts.

Additionally, ACI 318 places limits on the allowable stresses at the faces of the nodes (Table 2-1). The nodal efficiency factors are based on the elements that intersect to form the node and are listed in Table 2-1.

The strength of a strut must be checked at its minimum cross-sectional area. For a strut, especially a bottle-shaped strut, the minimum area will occur at the ends of the strut where it intersects a node. Using the efficiency factors presented in Appendix A (ACI 318-05), the strength of the strut will control the strength of that interface except in the case of a CTT node. It is only in a CTT node that the nodal efficiency could be less than the efficiency of struts framing into that node.

ACI 318-05 Appendix A also provides one more restriction on the modeling process. The angle between the axes of any strut and any tie entering a common node may not be less than 25 degrees. This provisions stems from the idea that struts will lose capacity as they approach the direction of a tie. Clearly a strut that is coincident with a tie will have no compressive capacity. The angle of 25 degrees was chosen to eliminate potential problems with struts that form a slight angle with a tie. Figure 2-11 shows the relationship between strut efficiency and the angle between the strut and tie based on the ACI 318-05 guidelines.

21
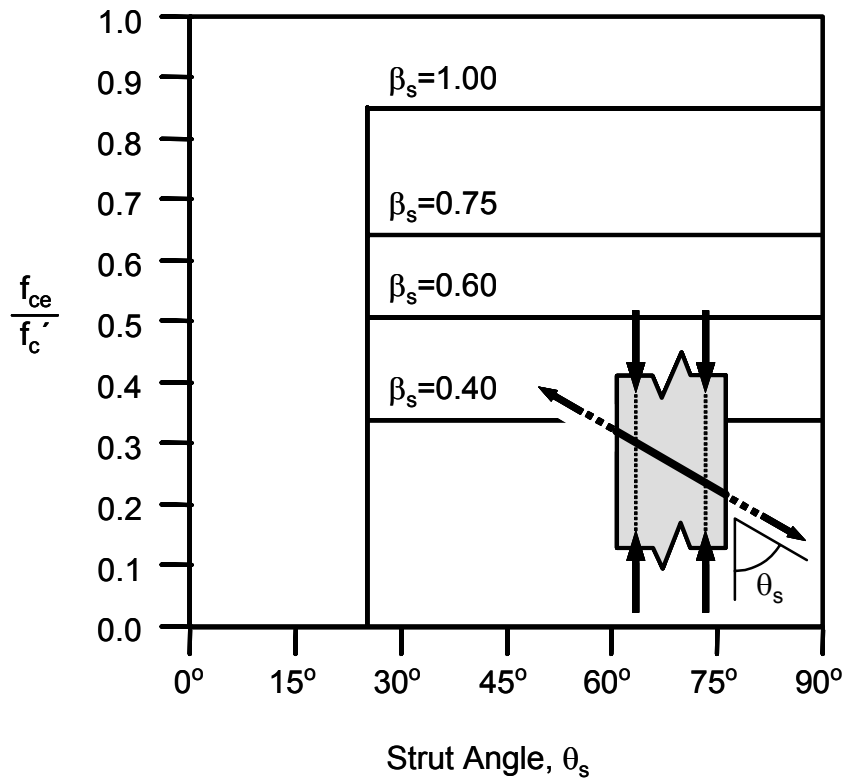
Figure 2-11: Relationship between strut efficiency on the angle between the strut and tie used in ACI 318-05

2.3.2 AASHTO LRFD Bridge Design Specifications

The AASHTO LRFD Bridge Design Specifications, like ACI 318-05, place limits on the allowable stress at the faces of the nodes and struts. However, the AASHTO approach for the allowable stress in a strut is based on Modified Compression Field Theory (MCFT) (Collins and Mitchell 1991) rather than the reinforcement ratios used by ACI. The MCFT based equations are presented below:

22

$$f_{cu} = \frac{f'_c}{0.8 + 170\varepsilon_1} \leq 0.85 f'_c \qquad (2\text{-}3)$$

$$\varepsilon_1 = \varepsilon_s + (\varepsilon_s + 0.002) \cot^2 \alpha_s \qquad (2\text{-}4)$$

Where: α_s = the smallest angle between the compressive strut and the adjoining tie

ε_s = the tensile strain in the concrete in the direction of the tension tie

f'_c = specified concrete strength

f_{cu} = usable compressive strength

Rather than using the amount of reinforcement that crosses the anticipated crack as in ACI, AASHTO bases the efficiency on an average strain in the concrete at the location of a tie. The strut strengths as presented in AASHTO were developed based on tests of reinforced concrete panels. Panels were subjected to a planar loading scheme, in which stress was applied to the four edges of the panels. That stress consisted of both a normal and shearing components. This experimental program (Vecchio and Collins 1982) allowed the researchers to examine concrete under complex stress states and develop mechanics-based models based on that data. The model, MCFT, was then converted into a design tool. In order to apply the design form of MCFT, one must choose an appropriate tensile concrete strain (ε_s).

In the experiments performed by Vecchio and Collins (1982) the average tensile concrete strain was measured using a displacement transducer that was placed on the specimen. That displacement transducer measured the relative motion of the ends of the instrument, and that displacement was then divided by the original gage length. Therefore the strain was averaged over cracks in the concrete.

Such a measurement of strain is simple to determine in a laboratory environment. However, many practicing engineers and TxDOT designers have had difficulty in choosing an appropriate average tensile concrete strain to use in design and have expressed reservations about using these provisions. If the process could be simplified and the strain term eliminated, it would likely help design engineers.

The angle between the strut and any adjoining tie is explicitly considered in the AASHTO LRFD STM provisions. Therefore, no limit is placed on that angle as in ACI. As the angle between the strut and the tie approaches zero, the strength of the strut also approaches zero (Figure 2-12). While very small angles are allowed by AASHTO, they become impractical due to the diminished efficiency factor. The diminished efficiency factors and the associated reductions in the allowable strength of struts encourage the design engineer to seek a more refined truss mechanism.
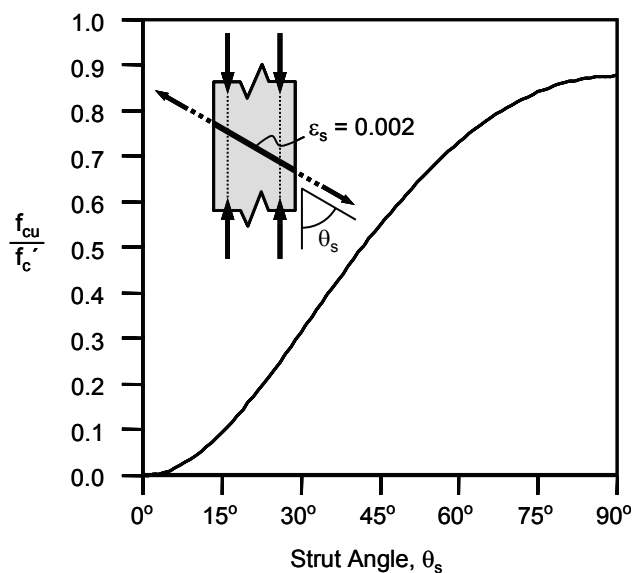
Figure 2-12: Relationship between strut efficiency on the angle between the strut and tie used in AASHTO LRFD

24

For the nodal stress limits, AASHTO, like ACI, simply specifies factors based on the type of node (Table 2-1). It should be noted that the AASHTO nodal efficiency factors are multiplied f_c' directly rather than $0.85f_c'$ as specified in ACI 318 Appendix A.

The AASHTO LRFD STM specifications require that the truss model must be very near the plane that is defined by the legs of the transverse reinforcement (Figure 2-13a) for struts anchored by reinforcement (CTT Nodes). For example, in the case of a very wide beam the CTT nodes, and the struts that abut them, must lie in a plane that contains the ties. The entire width of the structural member may not be used for the truss unless additional transverse reinforcement (i.e. intermediate stirrup legs) is provided. The provisions regarding the width of a strut are base on earlier research regarding torsion of concrete members (Mitchell and Collins 1986). Its applicability to CTT nodes requires further systematic research.

2.3.2.1 *Minimum Shear Reinforcement Requirements*

The AASHTO LRFD Bridge Design Specifications have four distinct provisions for minimum shear reinforcement. Each of them is presented individually. The first requirement (Section 5.8.2.5) requires that:

$$A_v \geq 0.0316\sqrt{f_c'}\,\frac{b_v s}{f_y} \qquad (2\text{-}5)$$

Where: A_v = area of shear reinforcement [in.^{2}]

f_c' = specified concrete strength [ksi]

b_v = beam width [in.]

s = stirrup spacing [in.]

f_y = yield strength of the reinforcement [ksi]

This requirement is equivalent to providing enough shear reinforcement to resist a stress equal to half of the concrete contribution to shear strength when using sectional analysis. This provision is based on strength requirements. The other three detailing requirements are based on serviceability.

The second of the four shear reinforcement requirements is presented in Section 5.7.3.4. and is intended for use in members that exceed 36 in. in depth. The reinforcement requirement is:

$$A_{sk} \geq 0.012(d_e - 30) \leq \frac{A_s + A_{ps}}{4} \qquad (2\text{-}6)$$

Where: A_{sk} = area of skin reinforcement [in.^{2}/ft]

d_e = effective beam depth [in.]

A_s = area of tensile reinforcement [in.^{2}]

A_{ps} = area of prestressing steel [in.^{2}]

The required skin reinforcement must be distributed along the vertical faces of the component for a distance equal to $d_e/2$ from the tension face of the component. The spacing of the bars which comprise the skin reinforcement must be less than $d/6$ and 12 in.

In Section 5.13.2.3 of AASHTO LRFD, detailing requirements for deep beams is:

$$\phi f_y A_s \geq 0.12 b_v s \qquad (2\text{-}7)$$

Where: f_y = yield strength of the reinforcement [ksi]

A_s = area of shear reinforcement [in.^{2}]

b_v = beam width [in.]

s = stirrup spacing [in.]

As per the provisions of AASHTO LRFD both horizontal and vertical reinforcement must be provided along the vertical faces of the element. The amount of both vertical and horizontal reinforcement must satisfy Eq. 2-7. Additionally, the spacing must not exceed $d/3$ or 12 in.

The final detailing provisions in AASHTO LRFD pertain to reinforcement to control cracks in D-regions (Section 5.6.3.6). This requirement must be satisfied if STM is used to design the element. The area of this reinforcement must be at least 0.003 times the gross concrete area in each direction. Therefore, an orthogonal grid of reinforcement must be provided. For thick members, such as bent caps, the crack control reinforcement must be distributed across the cross section with internal stirrup legs.
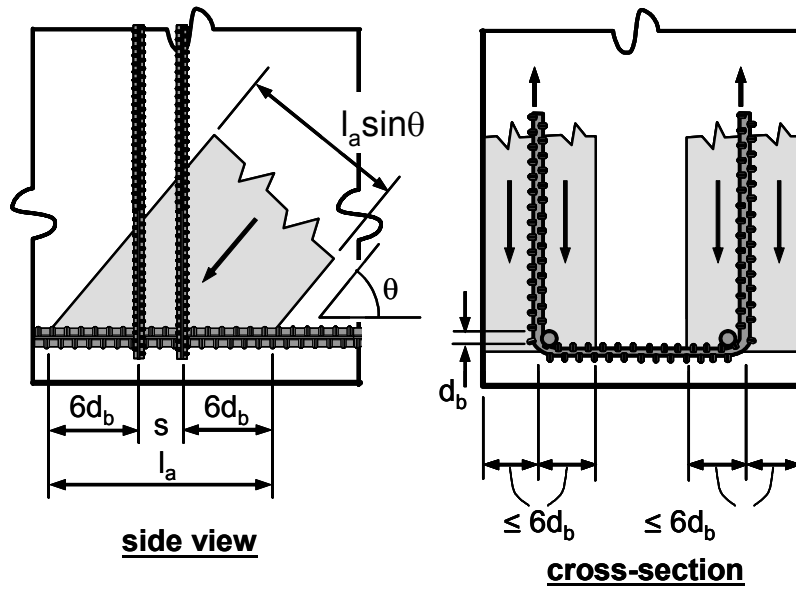
(a) Strut anchored by reinforcement (CTT node)
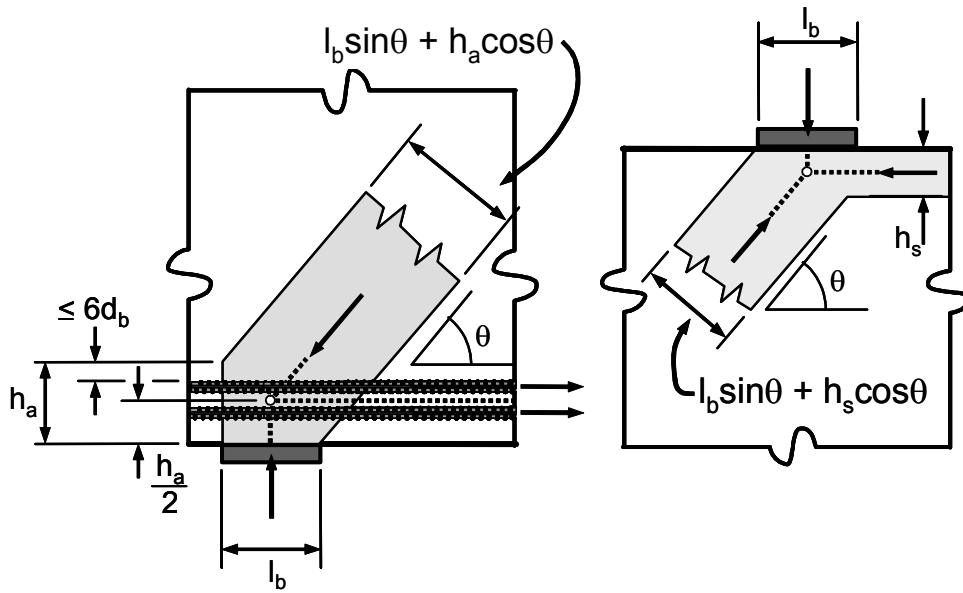
(b) Strut anchored by bearing and reinforcement (CCT node)

(c) Strut anchored by bearing and strut (CCC node)

Figure 2-13: AASHTO Recommendations for dimensioning nodes

2.3.3 CSA A23.3-94

The STM procedures in the Canadian Building Code, CSA A23.3, are the same as those presented in AASHTO LRFD Bridge Design Specifications. All nodal stress limits as well as the MCFT based equation for the strength of a strut are identical. However, CSA A23.3-94 requires slightly less crack control reinforcement than the AASHTO LRFD STM provisions. CSA A23.3 requires a reinforcement ratio of at least 0.002 in each direction.

2.3.4 NZS 3101:1995

The New Zealand Standard for concrete structures contains provisions for STM in its Appendix. These provisions are the most general of the code provisions presented. The NZS 3101 does not present any limits on the geometry of the truss regarding the angle between the strut and tie or regarding the width of the strut. Only the strength of nodes and ties are specified. The forces within the ties are limited to the amount of force that can be developed within the steel. If less than the full development length is provided, then less than the full yield strength of the tie can be carried. The NZS 3101:1995 efficiencies are listed in Table 2-1.

2.3.5 fib Recommendations 1999

The fib model code takes a different approach to the specification of STM than the ACI 318-05 or AASHTO LRFD Bridge Design Specification. The first major difference is the use of partial safety factors; the second is the classification of a strut by the amount and direction of anticipated cracking rather than the strut geometry. The strength of a strut is given by the following equations. Note that SLS and ULS stand for service and ultimate limit states, respectively.

$$f_{1cd} = \alpha \frac{f_{ck}}{\lambda_c} \qquad (2\text{-}8)$$

$$f_{cd,eff} = v_1 f_{lcd} \text{ or } f_{cd,eff} = v_2 f_{lcd} \qquad (2\text{-}9)$$

Where: α = reduction factor considering f_{lcd} versus strength of cylindrical test specimen and duration of loading:

    α = 1.00 for SLS

    α = 0.85 for ULS

  γ_c = partial safety factor

    γ_c = 1.00 for SLS

    γ_c = 1.50 for ULS

  f_{ck} = specified concrete cylinder strength (MPa)

  v_1 = efficiency factor

    $v_1 = (1 - f_{ck}/250)$

  v_2 = efficiency factor

    $v_2 = 0.80$ for struts with cracks parallel to the strut with bonded reinforcement; the reduction is due to the transverse tension and to the disturbances by the reinforcement and the irregular crack surfaces.

    $v_2 = 0.60$ for struts transferring compression across cracks with normal crack widths, e.g. in webs of beams.

    $v_2 = 0.45$ for struts transferring compression over large cracks e.g. in members with axial tension.

FIB also provides recommendations for the strength of confined struts. The increase in strength is indexed to a volumetric reinforcement ratio that is common in many confinement models.

Confinement is also accounted for in the efficiency of nodes. There are three classes of nodes within the fib recommendations: nodes anchoring ties (both CCT and CTT), nodes in biaxial compression (CCC), and nodes in triaxial compression. The efficiency factors for those nodes are 0.85, 1.20, and 3.88 respectively.

FIB provides very thorough specifications about detailing. Recommendations regarding appropriate bend diameters for the bars are presented as well as the nodal geometry produced by such bends.

2.4 STRUT-AND-TIE MODELING PROCEDURE FOR DESIGN AND DETAILING

The first step of the STM process is to determine the location of the disturbed regions. Disturbed regions occur wherever there is a local disruption of the stress flows within a member. Such disturbances can be classified into two groups: static and geometric. Static disturbances are due to the presence of concentrated loads. The loads can be the result of concentrated loads applied to a structure or to reactions. Geometrical disturbances arise from local changes in a structure's geometry such as a dapped end or a beam, joint, or opening. Examples of both types of discontinuity are depicted in Figure 2-8 with geometric discontinuities on the left (a-c) and static discontinuities on the right (d-f). The complete STM process is shown in Figure 2-14.

```
┌─────────────────────────┐
│   Delineate D-Regions    │
│     and B-Regions        │
└─────────────────────────┘
            │
            ▼
┌─────────────────────────┐
│ Determine Resultant Forces at │
│     D-Region Boundaries   │
└─────────────────────────┘
            │
            ▼
┌─────────────────────────┐
│   Sketch the Flow of Forces   │
│ and Develop a Basic Truss Model │
└─────────────────────────┘
            │
            ▼
┌─────────────────────────┐
│ Develop a Truss Model that Mimics the │
│   Flow of Forces and Ensure that   │
│     Each Node is in Equilibrium     │
└─────────────────────────┘
            │
            ▼
┌─────────────────────────┐        ┌─────────────────────────┐
│   Calculate Forces in the   │◄──────│   Refine Geometry of    │
│     Struts and Ties       │        │   Truss Model based     │
└─────────────────────────┘        │     on Tie Locations      │
            │                        └─────────────────────────┘
            ▼                                    ▲
      ◇ Size the Steel for ◇──────────────────────┘
      ◇     the Ties      ◇
            │
            ▼
   ◇ Check Allowable ◇        ┌─────────────────────────┐
   ◇ Stress Levels in Nodes ◇──►│   Resize Nodes/Struts as   │
   ◇    and Struts     ◇        │   Necessary to Satisfy     │
            │                    │       Stress Limits        │
            ▼                    └─────────────────────────┘
┌─────────────────────────┐
│   Detail Any Necessary    │
│ Confining Steel or Anchorages │
│   for Tie Reinforcement   │
└─────────────────────────┘
```

Figure 2-14: Flowchart for STM process

32

The size of a D-region is determined using Saint-Venant's Principle which states that the stress distribution due to an applied disturbance approaches a uniform stress distribution as the distance between the applied disturbance and the cross-section in question increases (Figure 2-15). Using this idea, the length of a D-region is assumed to be approximately the same size as the depth of the member.
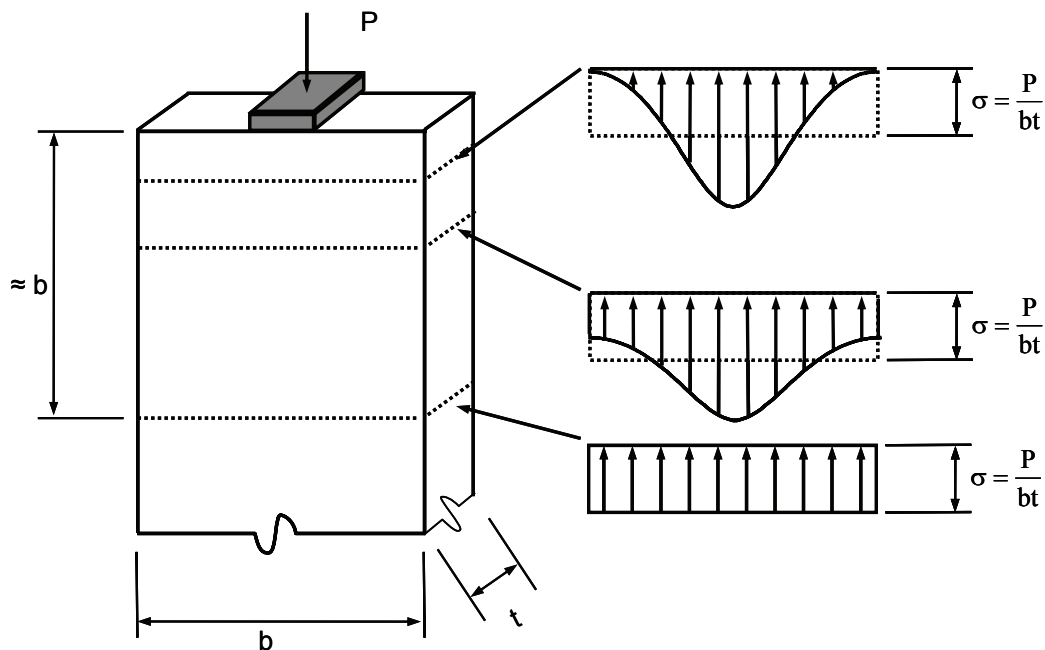
Figure 2-15: St. Venant's principle

After the D-regions have been identified, the resultant forces acting on the boundary of the D-region must be determined. The forces on the D-region shown in Figure 2-8(d) could be calculated based on the compressive stress block and the force in the longitudinal reinforcement of the B-region. Similarly, all forces on the boundary of D-regions must be calculated based on compatibility with the adjoining B-regions as well as any forces applied directly to the D-region. Not only must the magnitudes of the forces be determined appropriately, the locations

of the forces are also critical. Equilibrium must be maintained on the boundary between B- and D-regions.

Once the forces acting on the boundary of the D-regions have been determined, the flow of forces within the D-region can be sketched. Finite element analysis (FEA) may be conducted to determine the stress paths within an uncracked D-region, and a strut-and-tie model can be established on such stress paths. To minimize cracking under service and ultimate loads the axes of the struts and ties should match the directions of principle stresses as closely as possible (Schlaich, Schäfer, and Jennewein 1987). However, for many D-regions FEA is unnecessary as the stress paths can be estimated with relative ease.

After the stress paths have been determined, they can be used to establish a working truss model. The working truss model must meet equilibrium at all nodes. The truss model should not contain members that intersect at small angles. Struts that intersect ties at shallow angles typically suffer from a drastic reduction in strength; this phenomenon is addressed in both ACI and AASHTO codes. If the truss model contains such undesirable elements, refinement of the truss itself may be necessary.

For any given D-region there are many truss models that will satisfy equilibrium. Based on the lower bound theorem, any model that satisfies equilibrium and constitutive relationships will safely approximate the strength of the structure. When evaluating various truss models, a model with fewer ties is preferable. The optimal truss model will be that which contains the minimum strain energy at ultimate load. Schlaich, Schäfer, and Jennewein (1987) proposed that strain energy would be concentrated in the ties and minimizing the number and length of ties would also minimize the strain energy of the truss, which would produce an optimal or near-optimal truss model.

34

Additionally, it is preferable to have a truss model that is statically determinate. A determinate truss will require only equilibrium to determine the forces in each member. An indeterminate model will require some estimate of the member stiffnesses. It is difficult to estimate accurately the stiffness of the elements within a strut-and-tie model due to the complex geometry. Struts are in general not prismatic, and could display non-linear material behavior. The exact cross-sectional area of a strut is accurately known only at the location where the strut is influenced by an external bearing area. At other locations the geometry is not clearly defined. Consequently the stiffness will be difficult to assess.

Once a truss model has been defined, the forces in all members can be calculated. With the forces in each of the truss members known, the appropriate amount of reinforcing steel can be determined very simply by dividing the force in the tie by the yield stress of the steel and the appropriate strength reduction factor. Once the necessary amount of reinforcement has been determined, the truss geometry may need to be refined. For example, if more reinforcing steel is needed than the initially expected amount, the location of the tie could be changed in order to accommodate the increased amount of steel. The centroid of the reinforcement that will act as the tie should coincide with the location of the tie in the strut-and-tie model.

Once the ties have been designed and the truss model refined to include the final tie positions, the struts and nodes can be checked for necessary strength. The stress levels in the struts and nodes must be kept below allowable stresses. The allowable stress is determined differently by different codes.

The most critical elements in the strut-and-tie model will be those that are in contact with the external boundary of the member. Boundary elements will be influenced by bearing areas and support reactions. Bearing areas and reactions

will limit the size of the adjacent nodes, and therefore limit the allowable force in those elements.

Internal strut-and-tie model elements have more potential for plastic redistribution of stresses. The geometry of internal struts and nodes is not confined to a bearing area and can increase in size to develop all available strength. In most cases, variable geometry of internal elements may make it difficult to calculate stresses accurately, but the same variable geometry allows redistribution that makes accurate calculations unnecessary. Nevertheless, the stresses in the internal elements must be compared with permissible stresses. Using the appropriate code recommendations, the minimum required area of the internal elements (based on permissible stresses computed using efficiency factors) should be calculated, and provided within the member.

If the stresses in the nodes and struts are higher than the permissible stresses, an increase in the available area over which the nodes or struts act may be necessary. To increase the area, the bearing areas can be made bigger, or the overall geometry of the structural member can be increased. If neither of those options is practicable, the concrete strength can be increased or confinement can be added to the critical areas of the member. Proper confinement can locally augment the strength of the elements where necessary.

The final step in STM is to detail all the reinforcement within the member. Detailing involves ensuring that all ties are adequately anchored to develop the necessary strength at the critical locations, and ensuring adequate steel to confine the concrete anywhere confinement is necessary.

2.5   INVESTIGATIONS OF STRUT-AND-TIE MODELING

Many researchers have conducted experimental investigations to examine the application of STM. The individual elements of STM (nodes and struts) as

well as the overall system performance of members have been studied. First the research regarding struts will be discussed. That will be followed by the research on nodes and finally research on the application of STM structural systems and components will be presented.

2.5.1 Research Programs Focused on the Behavior of Struts

Many different approaches to determining the behavior of struts have been presented in the technical literature. Some researchers have relied entirely on FEA while others have conducted experimental investigations. The majority of the research presented in this section focused on bottle-shaped struts and the longitudinal crack associated with those struts.

2.5.1.1 *Thürlimann (1976)*

In 1976, Thürlimann presented the following equation for maximum compressive stress in a strut:

$$v = 0.35 + \frac{696}{f_c'} \text{ with } vf_c' \leq 2,400\,psi \qquad (2\text{-}10)$$

Where: v = efficiency factor

f_c' = specified concrete strength (psi)

Equation 2-10 was based on test evidence and practical experience with applying STM to design calculations. The limit of 2,400 psi corresponds approximately to a compressive strength of 4,800 psi. This limit was imposed because the maximum compressive strength in the test series was 4,800 psi.

Thürlimann's equation for strut efficiency was presented in a lecture at the University of Texas at Austin, and appears to be unpublished at least in regards to English language sources. The equation is briefly described in Ramirez and Breen (1983) and Bergmeister et al.(1993).

2.5.1.2 Ramirez and Breen (1983)

Ramirez and Breen examined published test data and conducted an experimental program to evaluate shear and torsion in reinforced and prestressed concrete beams. They used a variable angle truss model to determine the behavior of beams subject to combinations of shear, flexure, and torsion.

In their recommendations, limits were placed on the angle, α, between the diagonal struts and the longitudinal reinforcement. The limits (26 degrees $< \alpha <$ 63 degrees) were chosen such that neither the longitudinal nor transverse reinforcement yielded prematurely. By balancing the stresses in the longitudinal and transverse reinforcement, crack widths were kept to a relative minimum since the cracks could be restrained by reinforcement in both directions.

To determine allowable efficiency factors, Ramirez and Breen examined the specimens that failed due to web-crushing rather than any yielding the reinforcement. For such specimens, Ramirez and Breen determined the allowable diagonal stress to be:

$$f_{ce} = 30\sqrt{f_c'} \hspace{3cm} \text{(2-11)}$$

Where: f_{ce} = effective stress in diagonal truss members

f_c' = specified concrete strength (psi)

2.5.1.3 Marti (1985)

Based on comparisons with experimental research, Marti suggested using 60% of the compressive strength of the concrete as a first approximation to the strength of a strut. That value could then be altered based on the specific characteristics of the strut. For example, the efficiency of the strut could be increased if well distributed reinforcement or confinement were provided. Marti also suggested that for members with large reinforcement ratios, the concrete

efficiency be reduced. If the reinforcement ratio is large, the strength of the member will likely be controlled by the concrete strength and additional conservatism may be necessary.

2.5.1.4 Batchelor, George, and Campbell (1986)

Batchelor, George, and Campbell (1986) assembled a database of 48 beam tests to examine the efficiency of a concrete strut. Their database included only specimens that were explicitly described as "web-crushing" failures by the originating papers; however, the database included both conventionally reinforced beams as well as prestressed beams. No attempt was made to distinguish between the shear behavior of conventionally reinforced and prestressed beams.

Based on the database, the following equation was proposed:

$$ln\left(v\frac{d}{b_w}\right) = 3.342 - 0.199\left(\frac{a}{d}\right) - 7.471\left(\frac{d}{b_w}\right) \quad (2\text{-}12)$$

Where: v = efficiency factor

d = effective depth of section

a = shear span

b_w = width of web

The above equation was developed as a best-fit regression to the data, and was intended only for beams with shear span-to-depth (a/d) ratios less than 2.5. For larger a/d ratios, Batchelor, George, and Campbell indicated that a flexural failure rather than a shear failure will control the strength of a beam making efficiency factors unnecessary. For the purposes of design, they suggested that a constant value of $v = 0.60$ be used for the practical ranges of b_w/d between 0.1 and 0.2. Additionally, they recommend that systematic research be performed for the same range of b_w/d. The final recommendation of their paper was that additional

research needs to be performed to determine appropriate values of the efficiency factor for beams supporting distributed loads.

2.5.1.5   Collins and Mitchell (1986)

In this paper, was written to present the background research relevant to the 1984 Canadian code provisions was presented. No new experimental or analytical research was reported. Detailed design examples using the Canadian specifications were carried out. The relevant equations (Equations 2-13 and 2-14) for determining the efficiency of a strut were:

$$v = \frac{1}{0.8 + 170\varepsilon_1} \tag{2-13}$$

$$\varepsilon_1 = \varepsilon_s + \frac{(\varepsilon_s + 0.002)}{\tan^2 \theta} \tag{2-14}$$

Where: θ = the smallest angle between the compressive strut the adjoining tie

   ε_s = the tensile strain in the concrete in the direction of the tension tie

These two equations were later adopted by AASHTO in a slightly different form and an alternate nomenclature (Eqn. 2-3 and 2-4).

2.5.1.6   Chen (1988) and Nielsen (1998)

Chen conducted a statistical analysis of a database containing the results of "almost 700 tests including ordinary beams, deep beams, and corbels" (Nielsen 1998). The empirical efficiency factor that he derived is given in Equation 2-15.

$$v = \frac{0.6\left(2 - 0.4\dfrac{a}{h}\right)(r + 2)(1 - 0.25h)}{\sqrt{f_c'}} \tag{2-15}$$

For: $\dfrac{a}{h} \leq 2.5$; $\quad r \leq 2\%$; $\quad h \leq 1\,m$

Where: a = shear span (m)

h = overall section depth (m)

r = longitudinal reinforcement ratio (%)

f_c' = specified concrete strength (MPa)

Based on Chen's database the mean value of the ratio of experimental efficiency factors to predicted efficiency factors is 1.0, and the coefficient of variation is 16%. It was recommended that if any of the input values of Equation 2-12 exceed the limits placed up on them that the upper limit be used. The database upon which the equation is based contained specimens with $f_c' < 100MPa$ (14.5 ksi), $a/h < 10$, and $h < 1.20m$ (47 in.), and the statistical regression was intended to be used for the full range.

2.5.1.7 *Adebar and Zhou (1993)*

Adebar and Zhou conducted experiments to determine the ability of plain concrete to confine a strut and therefore increase its capacity. These tests were part of a larger study of STM for a deep pile cap. In a pile cap it can be uneconomical to provide large amounts of confining reinforcement. The tests consisted of plain concrete cylinders that were loaded in the axial direction to mimic an unreinforced strut within the pile cap.

The test setup is called a double punch test (Chen 1970; Marti 1989). The specimen is loaded by a circular bearing plate that is smaller than the cross-section of the specimen itself (Figure 2-16). Adebar and Zhou conducted 60 such tests. Based on those tests the following design recommendation was presented:

41

$$f_b \leq 0.6 f_c' \left(1 + 2\alpha\beta\right) \tag{2-16}$$

$$\alpha = 0.33 \left(\sqrt{\frac{A_2}{A_1}} - 1 \right) \leq 1.0 \tag{2-17}$$

$$\beta = 0.33 \left(\frac{H}{d} - 1 \right) \leq 1.0 \tag{2-18}$$

Where f_b = allowable bearing stress

α = factor for confinement of surrounding concrete

β = factor for aspect ratio of strut

H = length of the strut from face of the node to face of the node (in.)

d = width of strut, measured at the node faces (in.)

A_1 = area of strut at node faces (in.^{2})

A_2 = area of strut at point of maximum spreading (in.^{2})
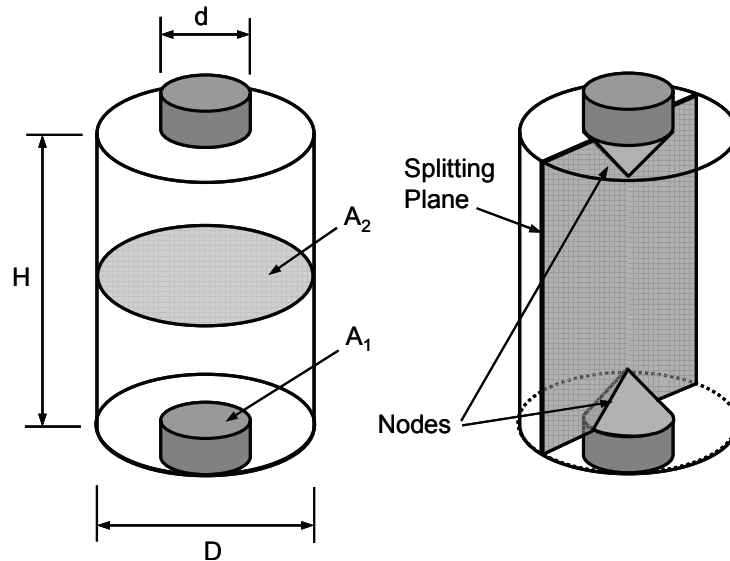
Figure 2-16: Schematic representation of the double punch test

The lower limit on bearing stress of $0.6 f_c'$ was found to be acceptable in cases where no confinement was present. The upper limit of $1.8 f_c'$ was chosen to correspond with bearing strength given in the ACI 318-89. ACI 318-89 was the governing code document at the time the research was conducted. Under the current ACI design specifications (ACI 318-05) the upper limit on bearing strength is $2.0 f_c'$.

2.5.1.8 *Vecchio and Collins (1993)*

In an attempt to refine the equations developed for the Modified Compression Field Theory (MCFT), Vecchio and Collins examined new panel test data. The original panel tests used to develop MCFT, were all performed at the University of Toronto whereas the new data were obtained from tests conducted at other institutions (Kollegger and Mehlhorn (1990); Belarbi and Hsu (1991)). Based on the evaluation of the new and old data, a new model for concrete softening was presented.

$$v = \frac{1}{1.0 + K_c K_f} \qquad (2\text{-}19)$$

$$K_c = 0.35 \left(\frac{-\varepsilon_1}{\varepsilon_2} - 0.28 \right)^{0.80} \geq 1.0 \qquad (2\text{-}20)$$

$$K_f = 0.1825 \sqrt{f_c'} \geq 1.0 \qquad (2\text{-}21)$$

Where: K_c = coefficient reflecting influence of transverse tensile straining

K_f = coefficient reflecting influence of nominal strength of concrete

ε_1 = average principle tensile strain

43

ε_2 = average principle compressive strain

f_c' = specified concrete compressive strength (MPa)

For all the tests upon which the above model is based, a uniform stress was applied to the edges of the panels rather than a force. Therefore, the principle strains could be readily determined from the experimental data. This model may be difficult to implement as a design tool because such quantities will be unknown to a designer.

Vecchio and Collins concluded that the new model was not very different from the original MCFT model (Vecchio and Collins 1986). Additionally, they concluded that when the new compression softening models were applied within a nonliner FEA, analytical and experimental results were in good agreement.

2.5.1.9 *Foster and Gilbert (1996)*

Using a database of the results of approximately 40 deep beam and corbel tests, Foster and Gilbert examined various models for the efficiency factor for concrete in compression. Two new models for determining the efficiency factor were presented, and evaluated using the database. The first model was an adaptation of Collins and Mitchell's MCFT expression (Equations 2-3 and 2-4). Equation 2-4 requires that a tensile concrete strain be input into the model. Warwick and Foster 1993 developed a relation between the concrete tensile strain and the compressive strength (Eqn 2-22). Combining Equations 2-4 and 2-22 a new relation was produced. Note that the angle, α_s, was replaced by a shear span-to-depth ratio, a/d. Foster and Gilbert called this equation "the modified Collins and Mitchell relationship."

$$\varepsilon_s = -0.002 - 0.001\left(\frac{f_c' - 20}{80}\right) \qquad (2\text{-}22)$$

$$v = \frac{1}{1.14 + (0.64 + f_c'/470)(a/d)^2} \qquad (2\text{-}23)$$

Where: $\quad \alpha_s$ = the smallest angle between the compressive strut the adjoining tie

ε_s = the tensile strain in the concrete in the direction of the tension tie

f_c' = specified concrete strength (20 MPa < f_c' <100 MPa)

Another model that was developed using FEA of the deep beam and corbel test database was also presented. Foster and Gilbert (1996) conducted a parametric study to examine the effects of shear span-to-depth ratio, concrete strength, and the amount of horizontal and vertical web reinforcement. Based on the parametric study the following model was developed:

$$v = 1.25 - \frac{f_c'}{500} - 0.72\left(\frac{a}{d}\right) + 0.18\left(\frac{a}{d}\right)^2 \leq 0.85 \text{ for a/d} < 2 \qquad (2\text{-}24)$$

$$v = 0.53 - \frac{f_c'}{500} \text{ for a/d} \geq 2 \qquad (2\text{-}25)$$

Where: $\quad f_c'$ = specified concrete strength (20 MPa < f_c' <100 MPa)

a = shear span

d = effective depth of the cross-section

When compared with the small database of experimental results used by Foster and Gilbert, both of the new models appear to be an upper bound on the data, and yielded unconservative results for a majority of tests.

2.5.1.10 Yun and Ramirez (1996)

Yun and Ramirez conducted detailed non-linear finite element analysis (FEA) to determine the behavior of a reinforced concrete beam. The beam was tested in a previous research study regarding the detailing of reinforcement

(Anderson and Ramirez 1987). In the paper by Anderson and Ramirez twelve beams tests were conducted. Yun and Ramirez undertook a FEA of one of those twelve beams. After the nonlinear FEA was conducted, the principle stresses within each nodal zone were tabulated. Based on the ratio of the principle stresses an allowable concrete stress in each nodal zone was determined (Figure 2-17).
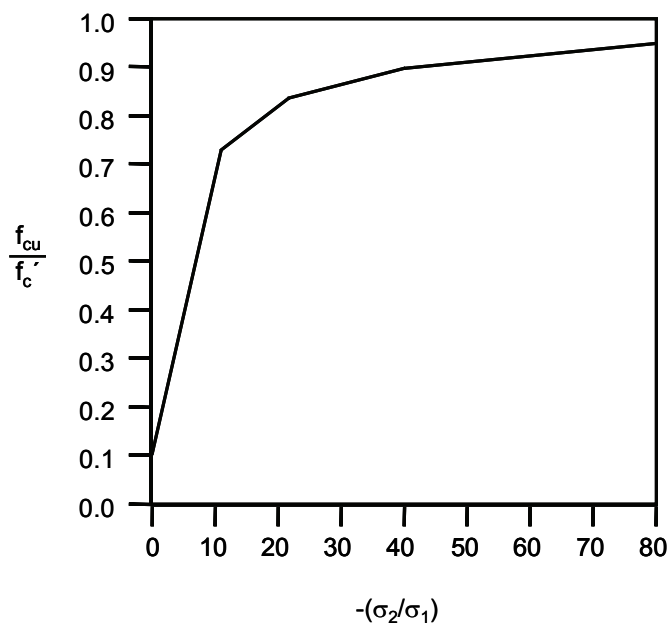
Figure 2-17: Concrete efficiency factor as used by Yun and Ramirez (1996)

After a FEA was performed for the entire beam, more detailed analyses were conducted on the nodal zones only. Nonlinear material properties were used for the FEA of the nodal zone. By applying the failure criterion Yun and Ramirez developed (Figure 2-17) the actual failure mechanisms of the beam could be determined based on the FEA of the nodal zones which indicated local zones of crushing. If a FEA of the nodal zone indicated the presence a failure mechanism, it was assumed that the actual beam failed in a similar mechanism at the same node. The observed failure of beam was indeed the same as that produced in the FEA of the nodal zone. Yun and Ramirez' (1996) approach produced good

estimations of the capacity of the beam; however, those estimations required very detailed and complex FEA.

2.5.1.11 Foster and Gilbert (1998)

Sixteen conventionally reinforced concrete deep beams were tested to failure in order to evaluate the ACI sectional shear design model as presented in ACI 318-89 and a plastic truss model. The plastic truss model was based on previous work by Warwick and Foster (1993). In the Warwick and Foster study an efficiency factor was developed through FEA (Equations 2-22 and 2-23).

The deep beams consisted of a single span with concrete strength ranging from 7,250 psi to 17,400 psi, and the shear span-to-depth ratio varied from 0.5 to 1.32. The results of the tests indicated that the FEA based model yielded unconservative expectations of strength for 14 of the 16 tests, and the average value of measured strength divided by calculated capacity was 0.85.

2.5.1.12 Kaufmann and Marti (1998)

Kaufmann and Marti analytically developed a cracked membrane model for reinforced concrete. The model requires an iterative solution that proceeds until all equilibrium conditions are met. Each cycle of iteration requires revising the initial assumptions regarding the width of the cracks, slip between the concrete and reinforcement, and overall system displacements. For the complex modeling process the following parabolic compression softening model was used to describe the concrete behavior.

$$v = \frac{1}{(0.4 + 30\varepsilon_1)\sqrt[3]{f'_c}} \le 1 \tag{2-26}$$

Where: f'_c = specified concrete strength

ε_1 = principle strain normal to a strut

The accuracy of the cracked membrane model was evaluated using the data from the reinforced concrete panels tested at the University of Toronto. The proposed membrane model provides good agreement with the experimental data.

Kaufmann and Marti's cracked membrane model is similar in nature to MCFT. The main difference between the two theories lies with the handling of stresses. MCFT relies on average stresses and strains in the cracked concrete, whereas, the cracked membrane model relies on local stress conditions at cracks.

2.5.1.13 Foster and Malik (2002)

Foster and Malik conducted an analytical investigation into the strength of struts for members failing in shear. To that end, they compiled a database of experimental research that contained results 135 tests. The tests consisted of deep beams and corbels. Using the database, Foster and Malik evaluated the validity of several proposed expressions to determine the efficiency factor for a concrete strut. Foster and Malik evaluated the models proposed by Vecchio and Collins (1993), Kaufmann and Marti (1998), Chen (1998), Batchelor, George, and Campbell (1986), Collins and Mitchell (1986), and Foster and Gilbert (1996).

The results of their analysis indicate that the inclination of the strut relative to the axis of the concrete member is the principle variable in determining strut efficiency. Additionally, they reported that the equations based on Modified Compression Field Theory produced the best correlation to the experimental data.

2.5.1.14 Matamoros and Wong (2003)

Matamoros and Wong have recently (2003) proposed a method for determining the capacity of a deep beam based on the strength of a strut. Their proposal includes not only recommendations on predicting the efficiency of a node-strut interface, but also methods by which the presence of vertical and horizontal reinforcement can be utilized in the strut-and-tie model. Matamoros

48

and Wong based their recommendations on a database of 175 published test results as well as their own experimental program and analytical modeling.
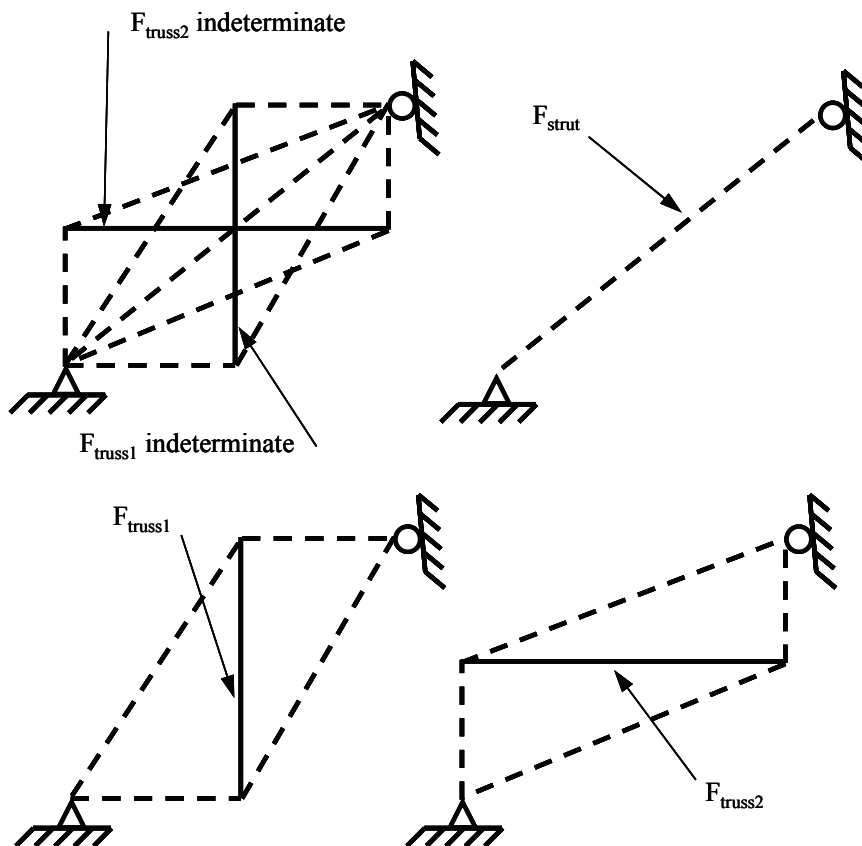
Figure 2-18: Truss models used by Matamoros and Wong

The basis of the Matamoros and Wong model is a statically indeterminate truss (Figure 2-18). The shape of the indeterminate truss is considered to be somewhat inconsistent with the known shape of the stress field present in a deep beam. In the proposed truss the widest points are not at the mid-point of the main compressive strut. Bottle-shaped struts have a different shape, and therefore stress distribution, than what is proposed by Matamoros and Wong. The bottle-shaped dispersion developed by Guyon (1953) (Figure 2-2) shows that the stresses are parallel to the axis of the strut at the midpoint of the strut. However, in the

49

indeterminate truss model proposed by Matamoros and Wong, the struts, and therefore stresses, are not parallel to the axis of the strut.

For the calculation of the forces in the members of the indeterminate truss, Matamoros and Wong assumed "the modulus of elasticity and cross-sectional area were constant and equal for all members." This is analytically equivalent to assuming that the stiffness of all members was assumed inversely proportional to the length of the member. However, the concrete elements (struts) in a strut-and-tie model are likely to be significantly stiffer than the tie elements. While the steel elements have a much higher elastic modulus ($E_{Steel}/E_{Concrete} \approx 5-10$), the struts have enough cross sectional area to result in a stiffness that is much higher than the ties ($A_{Strut}/A_{Tie} \approx 100$).

For an indeterminate structure, the load will follow the stiffest path available. In a traditional STM the struts tend to be the stiffest members and they attract the most force. In the Matamoros and Wong truss model the ties attract a disproportionate fraction of the applied force due to the stiffness assumptions made therein. In Figure 2-19 the indeterminate truss forces are each carrying approximately one-third of the applied load at an a/d of 1.0. In the actual structure, the direct strut between the applied load and the support is the stiffest load-path and should carry the largest fraction of the load.

The increase in tie force significantly increases the strain energy of the ties in the strut-and-tie model. Schlaich, Schäfer, and Jennewein (1987) propose that an optimum model should have the minimum possible strain energy. By increasing the strain energy in the truss model, Matamoros and Wong have moved away from an optimal strut-and-tie model.
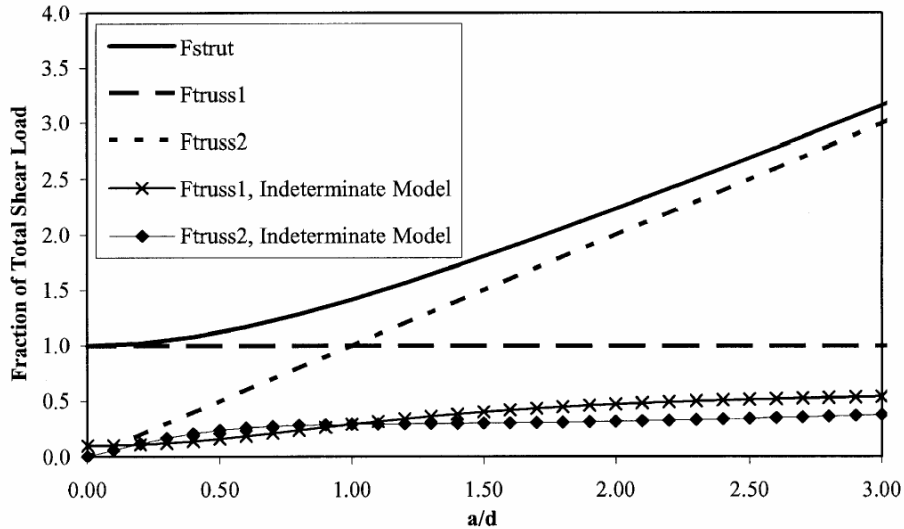
Figure 2-19: Truss forces based on Matamoros and Wong's trusses (from
Matamoros and Wong 2003)

2.5.2   Research Programs Focused on Nodes

The volume of research regarding the strength of behavior of nodes is
much less extensive than that regarding struts. There are two major investigations
into the behavior of nodes both of which were conducted at the University of
Texas at Austin.

2.5.2.1   *Barton, Anderson, Bouadi, Jirsa, and Breen (1991)*

The goal of the study was to describe dapped beams and nodes that were
relevant to those dapped beams. In the first phase of research, four dapped end
beams were tested to failure. All four beams were geometrically identical, only
the reinforcement varied. Two of the beams were detailed using STM, one was
detailed using recommendations by PCI, and the fourth beam was detailed using a
recommendation by Menon and Furlong (1977).

The dapped beams tested were half-scale models of a typical Texas State Department of Highways and Public Transportation (now known as Texas Department of Transportation, TxDOT) beams. All four of the beams safely carried the design load. In the cases of the specimens detailed using a strut-and-tie model procedure, the specimens carried 27% and 42% more load than expected.

As a companion to the dapped beams, two series of node tests were performed. One series focused on CTT nodes, and the other on CCT nodes. Drawings of both types of node specimens, as well as their relation to the dapped beam, are shown in Figure 2-20.

After the dapped beam tests were completed by Barton, Anderson performed 9 tests on isolated CTT nodes. These node tests primarily examined the details necessary for proper anchorage of the ties within the nodal zone. In addition to the steel detailing issues, the concrete strength varied ($f_c' = 5,800$ psi or 3,700 psi) and the allowable bearing area was altered (8 x 12 in. or 4 x 12 in. bearing plates). The results of Anderson's tests indicate that proper detailing is crucial, in some cases 90 degree hooks are unacceptable and 180 degrees bends must be used. The crack patterns of the individual node tests resembled the crack patterns observed in the dapped beam tests.

Concurrent with Anderson, Bouadi conducted tests on CCT nodes. The CCT specimens examined the same variable as the CTT node specimens. In Bouadi's tests, only the specimens constructed of low-strength concrete failed in compression while the specimens constructed of higher-strength material exhibited a loss of anchorage before compression failure. For specimens that failed in compression, the efficiency factors of the struts were very near 1.0.

52
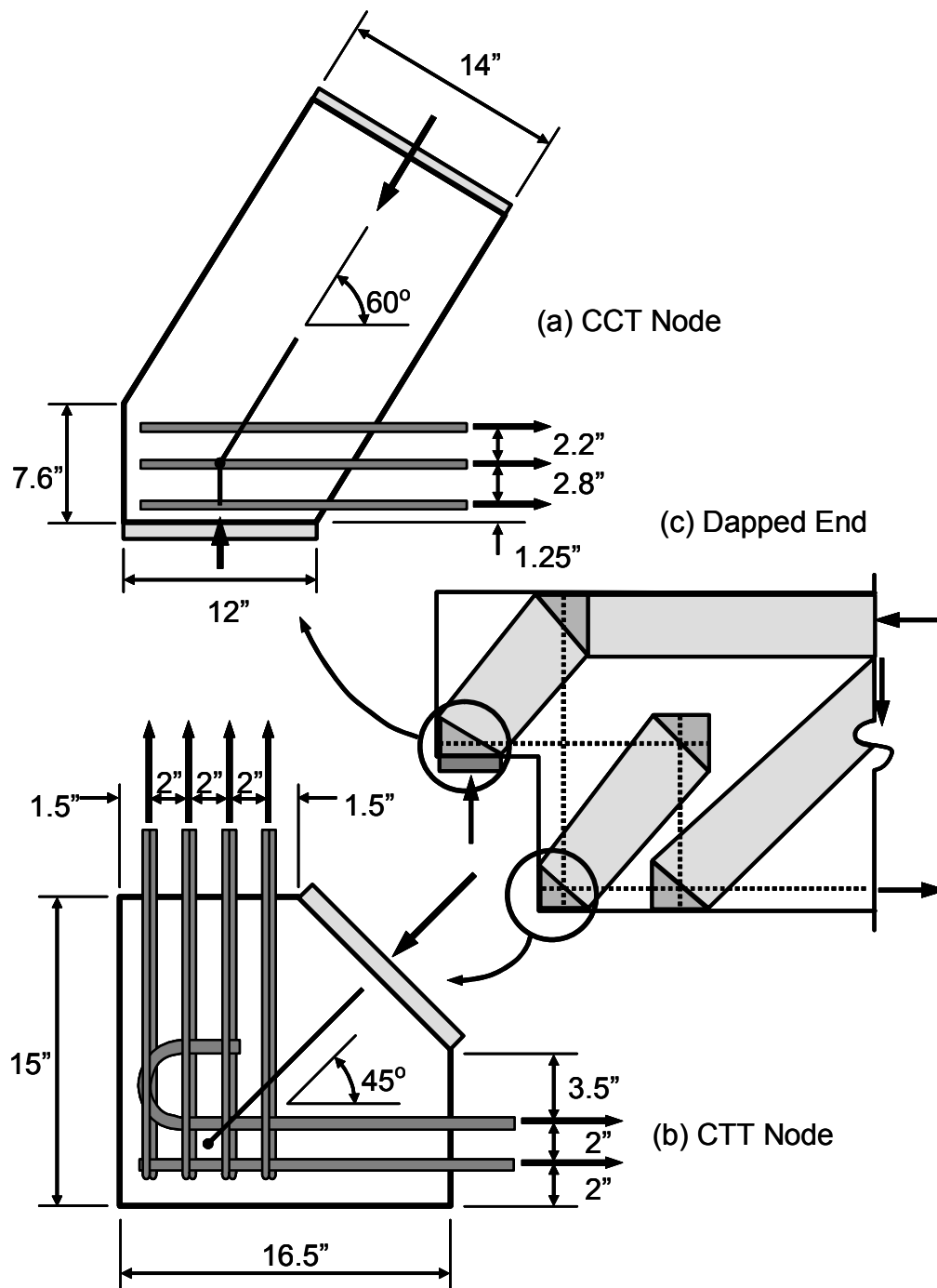
Figure 2-20: Typical isolated node specimens and dapped beam specimen (After Thompson 2002)

2.5.2.2 Thompson, Young, Jirsa, Breen, and Klingner (2003)

The purpose of this study was to examine the behavior of headed reinforcement in concrete structures. To that end, a CCT node was chosen as a typical location where bars may be limited to a very short anchorage length. The specimens for the CCT node tests consisted of deep beams (Figure 2-21). Sixty-four such specimens were tested with concrete strengths ranging from 3,000 to 4,100 psi. The main variables of the study were the strut angle, size of the tie, area of the head of the tie, and confinement.
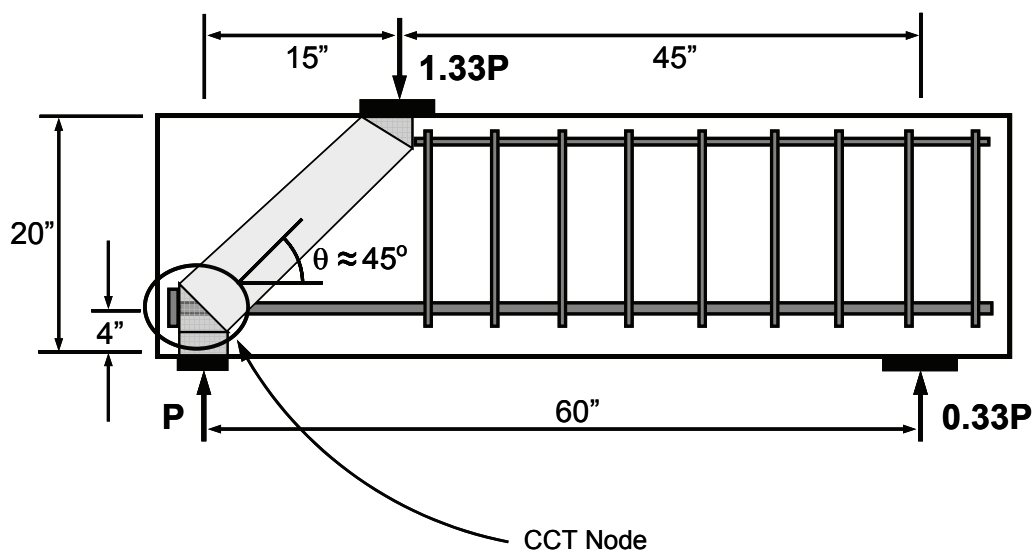
Figure 2-21: Typical Specimen for development of headed bar in CCT node (Thompson 2003)

The conclusions of this research indicate that the mechanisms of force transfer between the concrete and longitudinal steel shifts from bond at low levels of load to bearing of the head at high load levels. Confinement was found to increase the capacity of both mechanisms. Thompson proposed that there was a critical point at which the tie must be developed. That point was where the tie passes beyond the boundary of the strut (Figure 2-22).

54
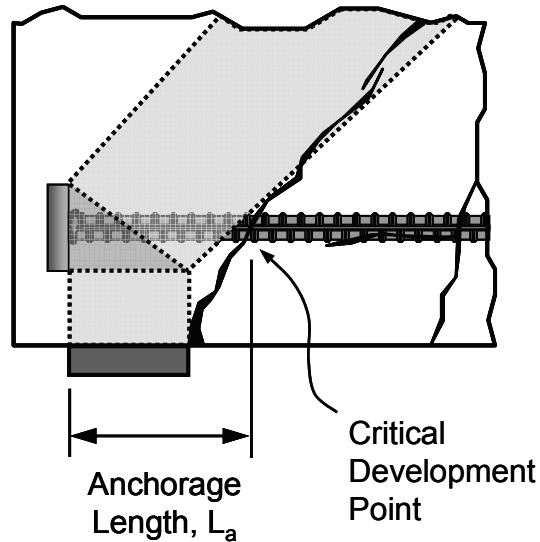
Figure 2-22: Critical anchorage point for CCT node (After Thompson 2003)

In addition to the conclusions regarding headed bar behavior, a number of conclusions about STM in general were presented. The first of these conclusions is that anchorage controls the strength of a CCT node. In the cases of straight bars, the bars pulled out of the node, and in the case of headed bars, the concrete crushed at the face of the head. Both of those mechanisms were considered anchorage failures. For all of the CCT node specimens a minimum amount of anchorage was provided in the specimen by the nature of the tests. If more anchorage was provided for the bars perhaps other limit states could have been observed. Also, the observed stresses on the node faces were much higher than those suggested in ACI 318-05 or AASHTO LRFD recommendations. It is interesting to note that the stresses were significantly higher than allowed by codes, yet the strength of the CCT node specimens were governed by anchorage failures.

2.5.3 Research Programs Focused on Structures with D-Regions

The research that has been conducted regarding the behavior of structures with D-regions varied greatly. While some research has focused on relatively simple structures such as corbel and deep beams, other researchers have examined much more complex structures.

2.5.3.1 Cook and Mitchell (1988)

Cook and Mitchell conducted tests on four components that were significantly affected by the behavior of D-regions: one corbel (f'_c = 4,300 psi), two dapped beams (f'_c = 5,850 psi), and a T-beam with a void in the web (f'_c not reported). In addition to the experimental work, the capacities of those members were predicted using two methods. The first method was a nonlinear FEA that incorporated MCFT into its constitutive laws, and the second method was STM. The STM method used by Cook and Mitchell was also based on MCFT and was identical to AASHTO STM provisions (Equations 2-3 and 2-4). In all three cases the FEA and STM produced safe expectations of strength. For one of the dapped beams, the ratio of measured strength to the calculated capacity was 1.18 based on STM and 1.14 based on nonlinear FEA. For the corbel the ratios were 1.23 and 1.12 for STM and FEA analysis, respectively. The data (both analytical and experimental) for the other dapped-end and the T-beam were not reported in their paper explicitly.

Based on the results of this research program, Cook and Mitchell recommended that any bearing areas be carefully modeled regardless of the analysis technique (FEA or STM). They also recommended that the contribution of any concrete that could potentially spall off of the structure be ignored in the analysis of the bearing areas. Finally, Cook and Mitchell recommended that

careful attention be given to the detailing of nodal regions so that premature anchorage failure could be avoided.

2.5.3.2   *Adebar, Kuchma, and Collins (1990)*

Adebar, Kuchma, and Collins (1990) tested six pile caps. Five of the six pile caps were supported on four piles and the sixth was supported on six piles. The six caps were designed by using Chapter 15 of ACI 318-83, CAN3 A23.3-84, or a STM procedure similar to what is now in the AASHTO LRFD Bridge Design Specifications.

Each of the six caps exhibited nearly linear behavior until failure. Failure was initiated by the splitting of unreinforced struts due to the spreading of compression. Shear failure followed the strut splitting. The pile caps were designed such that yielding of the longitudinal bars should have controlled the strength. However, the minimum efficiency factor for the struts for all six tests was 1.1. Such an efficiency factor demonstrates that the bearing stress at failure was greater than the compressive strength of the concrete by 10 percent. It was also noted that the unreinforced struts continued to carry load beyond that which caused initial splitting cracks. The uncracked body of the pile cap likely created enough confinement to prevent catastrophic failure due to the splitting of a strut which leads to a shear failure.

2.5.3.3   *Breen, Burdet, Roberts, Sanders, and Wollmann (1994)*

Extensive research regarding the behavior of anchorage zones was performed. The focus of this study was to determine if STM could provide an adequate model upon which the design of an anchorage zone can be based rather than to examine the strength of individual strut-and-tie model elements. To that end the anchorage zone was divided into two zones: the local zone and the general zone. The local zone is the region of very high compressive stress directly

influenced by the anchor. The general zone is the region beyond the local zone that is influenced by the spreading of compressive stresses away from the local zone (Figure 2-23).

Based on the division of the anchorage zone, the research project was divided into separate tasks. Roberts (1990) performed tests on isolated local zones, Sanders (1990) performed tests on end-bearing anchorages, Wollmann (1992) performed various tests of typical structures, and Burdet (1990) performed linear FEA.
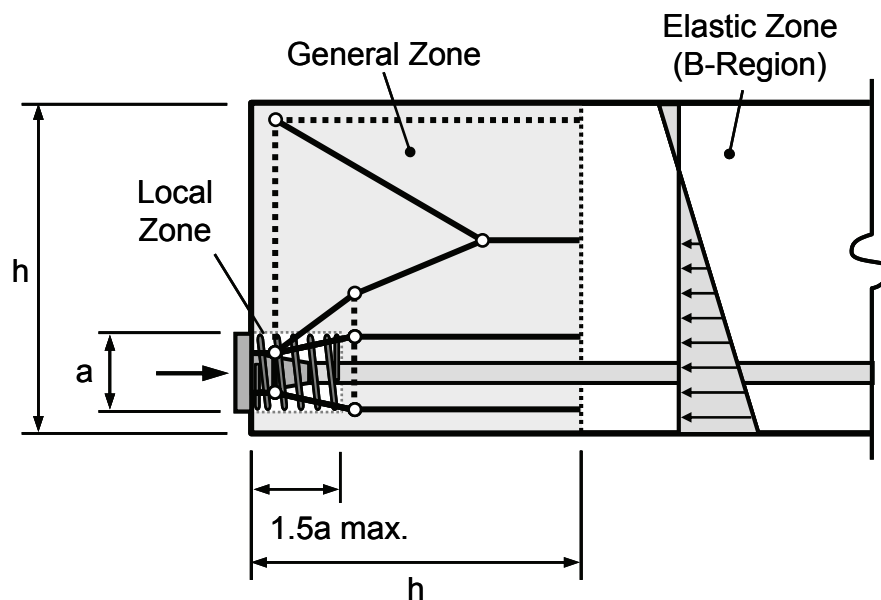
Figure 2-23: Depiction of local and general zones

Roberts (1990) tested 18 isolated local zones and 3 nonisolated local zones (local zones separated from general zones). Her goal was to establish acceptance tests for anchorage devices. The primary variables studied were the type of anchorage device (multi-plane or flat plate), confinement and auxiliary reinforcement, and the type of loading (monotonic, cyclic, or sustained load).

After these tests were performed on isolated specimens, the nonisolated specimens were tested to establish the interaction between zones.

One of the main purposes of Roberts' research was to determine an adequate model for the strength of the local zone. The two primary variables she established were the ratio of A_1/A_2, and the amount of confinement. Of the seven models examined, Roberts found that the following model by Schlaich and Shäfer (1989) best described the data:

$$f_{bearing} = 0.8f_c'\sqrt{\frac{A_2}{A_1}} + 4.1f_{lat}A_{core}\left(1 - \frac{s}{D}\right)^2 \quad (2\text{-}27)$$

$$0.8f_c'\sqrt{\frac{A_2}{A_1}} \leq 3.0f_c' \quad (2\text{-}28)$$

Where: $f_{bearing}$ = bearing stress of supported by the anchorage device (ksi)

f_c' = concrete cylinder strength (ksi)

A_2 = the area of the gross concrete section(in.^{2})

A_1 = the bearing area of the anchorage device (in.^{2})

A_{core} = the area of concrete confined by spirals or ties (in.^{2})

f_{lat} = the lateral confining stress provided by spirals or ties (ksi):

$$\frac{2A_s f_y}{Ds} \quad \text{for spirals}$$

$$\frac{A_s f_y}{Ss} \quad \text{for ties}$$

A_s = the bar area of the spiral or tie confining steel (in.^{2})

s = the pitch of spiral steel or the spacing of tie steel (in.)

59

D = the diameter of spiral confinement (in.)

S = the width tie reinforcement (in.)

The equation proposed by Roberts allows stresses up to $3.0f_c'$ regardless of the amount of reinforcement provided in the local zone. The confining effects of the concrete itself are considered in the A_2/A_1 term, and therefore, higher stresses than f_c' are allowed. If the local zone is viewed as a node, specifically a CCC node, Roberts' work implies that code limits on nodal stress in various codes that were previously discussed are very conservative. When Roberts compared the data from the isolated local zone performance to that of the general zone, it was observed that the cracking and ultimate load data provided a lower bound to the behavior of the general zone.

Following the work by Roberts, Sanders and Wollmann began to experiment with actual anchorage zones rather than isolated local zones. Sanders conducted tests on end-bearing anchorage devices. In his tests, the effects of eccentricity, multiple anchors, and curved or inclined tendons were also examined. These tests provided data regarding the amount and distribution of tie reinforcement, and lateral post-tensioning required for such structures. Wollmann tested still more complex specimens: 3 beams whose general zone was affected by reactions, 8 intermediate anchorage tests (blisters), and 3 anchorage diaphragm tests. For all of these tests, the FEA results produced by Burdet provided guidance to the development strut-and-tie models.

The compressive stress in the struts and nodes was limited to $0.7f_c'$. With such a conservative stress limit the values of measured strength divided by the calculated capacity ranged from 0.95 to 3.33 with an average of 1.40. These numbers indicate that STM is a safe and reliable method to determine the capacity of anchorage zones.

However, the strut-and-tie models produced by Wollmann and Sanders failed to determine the correct failure mechanism for many of the specimens. Typically the strut-and-tie model indicated that failure would be caused by yielding of ties. In the actual experiments the failure was initiated either by compression or bursting in front of the local zone.

The shift in failure mechanism was attributed to the conservative estimate of the compressive strength of nodes and struts. The nodes and struts exhibited much greater strengths than predicted. The higher strength elements failed in a brittle manner. The research was not focused on the strength of nodes and struts. Therefore, the inability to predict the correct failure mode was not viewed as a critical problem by the researchers since safe and reliable capacities of anchorage zones were predicted.

One of the major conclusions of the work had to do with serviceability. If the struts and ties are closely aligned to the elastic principle stress distributions, cracking could be minimized. Also the centroids of the struts and ties should match with the centroids of the resultants of the elastic stress distribution. Based on these ideas, for a complex structure a linear-elastic FEA should be conducted before the STM process begins. The results of the FEA can help lead the designer to an optimal strut-and-tie model.

2.5.3.4 *Maxwell and Breen (2000)*

Maxwell and Breen preformed four tests of wall specimens with an opening. Each specimen had a different layout of reinforcement that was based on a different strut-and-tie model. The wall was based on a detailed example that was published by Schlaich, Schäfer, and Jennewein in 1987. In the design example the wall was detailed using two independent truss models with each model expected to carry half of the total load.

All four specimens safely carried the design load thus demonstrating that there can be multiple truss models with adequate strength. For these four specimens the ratios of actual capacity to predicted capacity were 1.41, 1.50, 1.86, and 1.95.

2.5.3.5   *Chen, Hagenberger, and Breen (2002)*

In a manner similar to that which was taken by Maxwell and Breen (2000), Chen, Hagenberger, and Breen (2002) performed four tests of a dapped beam with a hole in the deeper side. The four specimens were geometrically identical to one another with only the reinforcement layout varied. Each beam was detailed using a different strut-and-tie model. Each of the four specimens carried the design load. The average ratio of measured strength to calculated capacity was 1.21 and the ratio ranged from 1.09 to 1.28.

2.6   FINAL REMARKS

Although STM has been implemented in various building codes throughout the world, there are many details of the process that have yet to be well-documented. Some aspects of STM are not widely understood, such as the relationships between STM and strain energy, while other are fundamental to understanding and applying STM, such as node geometry.

2.6.1   Strength of Struts and Nodes

STM is a very simple idea with wide-ranging applications. The difficulty lies in translating a behavior model into a code specification. The critical part for determining the strength of a truss model is to determine the strength of the individual components (struts, ties, and nodes). STM is governed by the lower-bound theorem of plasticity which requires only static equilibrium and yield conditions be satisfied. Therefore, the appropriate yield condition for struts and

nodes must be identified. The yield conditions for ties are easily quantifiable and readily available to design engineers, but the yield conditions for struts and nodes vary greatly from code to code.

Researchers have indicated that while STM can be used to predict safe estimates of capacity for a structure, often the limit state determined using STM is different than the observed limit state (Adebar et al. (1990); and Breen et al. (1994)). The inability to correctly identify limit states is a result of the inability to determine the strength of struts and nodes.

The lack of knowledge regarding the strength of struts and nodes is evident based on the work presented in this chapter. For a CCC node the specified efficiency factors are 0.85, 0.85, 0.68, and 0.65 in ACI 318-05, AASHTO LRFD, fib, and NZS 3101:1995 respectively. The work done by Roberts (1990) indicates that the efficiency factor for a CCC node can be as high as three even for nodes without confining reinforcement, and Adebar and Zhou allowed the efficiency factor for a CCC node to be as large as 1.8. The simple nodal efficiency factors that are specified in current codes do not attempt to include any behavioral models for determining efficiency factors accurately.

The behavior of struts and nodes are inseparably linked. A strut must abut a node. Therefore, there will be a common plane where the strut and node must have equal stress. The minimum cross-sectional area of a strut, specifically a bottle-shaped strut, occurs where the strut frames into a node. At this location the stresses in the strut will be the greatest. To maintain equilibrium across the plane of intersection of a strut and a node the stresses on opposite sides of the plane must be equal. Therefore, the peak stress in a strut will be equal to the stress at the face of the abutting node. As such, separate specifications for nodal and strut efficiencies may be redundant except in T- or I-sections.

2.6.2 Behavior of Nodes

Research performed by Anderson (1988) (CTT nodes), Bouadi (1989) (CCT nodes), Thompson (2002) (CCT nodes) and Roberts (1990) (CCC nodes) suggests that simple tests on isolated nodes can provide a lower bound estimate of the in-situ strength of nodes. These four series of tests covered basic node geometries of strut-and-tie models.

In most of the analytical literature regarding STM, hydrostatic nodes are recommended. However, each of the code documents described allows, and recommends, the use of non-hydrostatic nodes. The type of node used by the designer affects the geometry of that node, and consequently the geometry of the entire strut-and-tie model. The nature of node behavior, be it hydrostatic or not, must be examined to reconcile the differences in node behavior assumed by analysts and designers.

2.6.3 Detailing of Reinforcement

Detailing is the other crucial element of STM. Typically ties must be anchored over a very short length, or very high stress demands placed on a node may require confinement. Both of the above situations can lead to difficult details. To a large extent the detailing questions about nodes have been addressed. Anderson (1988), Bouadi (1989), Roberts (1990), and Thompson (2002) focused on the details required for proper anchorage and confinement in nodal zones.

Currently both ACI 318-05 and the AASHTO LRFD Bridge Design Specification stipulate a minimum amount of reinforcement that must cross the axis of the struts. AASHTO LRFD requires significantly more reinforcement compared to ACI 318-05 Appendix A. Reinforcement in a strut will not eliminate cracking. Reinforcement is only effective at reducing crack widths once the initial cracking has occurred.

2.6.4   Serviceability

Serviceability in reinforced concrete structures often centers on the reduction, or if possible prevention, of cracking. Once cracks form they create a path for the ingress of water, and other deleterious substances which can affect the service life of the structure.

Schlaich, Schäfer, and Jennewein (1987) state that cracking can be minimized if the axes of the struts and ties within the strut-and-tie model coincide with the directions of the principle stresses within the D-region. The logic behind this statement being that the structure will crack due to the elastic stresses, and if the structure is reinforced according to those stresses, cracking can be minimized. Unfortunately, the elastic stress distribution in a D-region is difficult to determine and changes as cracking progresses, and consequently the associated strut-and-tie model will be difficult to develop.

Schlaich, Schäfer, and Jennewein (1987) also recommend that the strain energy within a strut-and-tie model be minimized so that the truss model will be as efficient as possible. Minimization of strain energy is not necessarily consistent with minimizing cracking. Transverse tensile stresses are often present in an uncracked concrete member. In order to minimize cracking, reinforcement must be placed so that it can resist the tensile stresses. By adding reinforcement, i.e. ties, to carry the tensile stresses, the strain energy of the model will likely be increased, but the crack widths will be reduced due to the presence of the reinforcement. Minimization of strain energy and orientation of the struts and ties with the elastic stresses can be at odds with each other. Current research is inadequate to determine which of the approaches can reduce cracking.

Additionally, to further enhance service life, the structure should remain without shear cracks under its own dead load. If a structure cracks due to shear under its self-weight, the cracks will widen when live loads act on the structure

65

which can, in turn, lead to yielding of the reinforcement in some cases. If the reinforcement has yielded while live loads acted upon the structure, the cracks will not close when the live load is removed. However, if the initial diagonal cracking occurs while the structure is subjected to live and dead loads, it is expected that the reinforcement will not yield and the cracks will close when the live load is removed.

2.6.5   Minimization of Strain Energy

Minimization of strain energy will produce an optimal truss model. An actual structure will seek the stress distribution with the least possible energy, and a design model should also seek this end. Schlaich, Schäfer, and Jennewein (1987) suggest that in order to minimize the energy in a truss, only the energy of the ties must be considered.

However, the concrete elements (struts) in a strut-and-tie model are likely to be significantly stiffer than the tie elements. While the steel elements have a much higher elastic modulus ($E_{Steel}/E_{Concrete} \approx 5-10$) the struts will have enough cross sectional area to result in a stiffness that is much higher than the ties ($A_{Strut}/A_{Tie} \approx 100$). In a traditional STM the struts tend to be the stiffest member and they will develop significant strain energy.

2.6.6   Modeling of Distributed Loads

In a typical reinforced concrete building structure the loads are applied to the beams via a slab or series of joists. In a bridge structure, a large column can produce a near-uniform distribution of load on a pile cap. Either of those two types will be much more similar to a distributed load than a concentrated load. The uniform load acting over a limited length is sufficient to generate D-regions within a beam, and therefore STM may be necessary. In 1986 Batchelor, George,

66

and Campbell concluded that additional research was needed before proper efficiency factor could be determined for beams subject to uniform loads. Alternatively, a transfer girder often has a single column load applied to it, and would not be similar to a distributed load.

Relatively few tests have been conducted on structures subjected to uniform loads (Leonhardt and Walther (1962); Krefeld and Thurston (1966), Uzel (2003)). Leonhardt, Walther, Krefeld, and Thurston compared the shear strength of reinforced concrete beams that were subjected to concentrated or distributed loads to those determined using a sectional design method. Strut-and-tie modeling was not a common practice at the time this work was first published. Marti (1985) proposed methods through which a uniformly distributed load could be modeled using STM. Nevertheless his recommendations were based on analytical models rather than experimental observation.

2.6.7   Concluding Observations

The history of STM dates back to the very beginnings of reinforced concrete construction. It began as a qualitative tool for describing the forces within the simplest concrete members, and has evolved into a quantitative tool for designing the most complex and critical portions of reinforced concrete structural members. In the process of the transformation many additional details (development of ties, strut behavior, node geometry and behavior, etc…) were introduced. Some of the critical elements in these details have yet to be completely verified.

CHAPTER 3

Tests of Isolated Struts

3.1   INTRODUCTION

In order to examine the behavior of bottle-shaped struts, a series of simple experiments were performed. The tests allowed for the observation of the behavior of an isolated bottle-shaped strut. Based on those observations, code provisions and the geometry of the bottle shape could be examined. Additional details of the isolated strut test series can be found in Sankovich (2003).

3.2   EXPERIMENTAL INVESTIGATION

During this phase of the study, 26 concrete panels as shown in Figure 3-1 were tested to failure. The primary variables were the amount and placement of the reinforcing bars. The strength of the strut may be influenced by the amount of reinforcement that crosses the axis of the strut. The amount of reinforcement is calculated based on the size of the bars, the spacing between the bars, and the angle between the strut axis and the bars. Each of these variables was examined in the research presented in this chapter.

The typical specimen consisted of a reinforced or plain concrete panel that measured 36 x 36 x 6 in. and was loaded using steel bearing plates that were 12 x 6 x 2 in. However, in one series of tests the thickness of the panel and the bearing area were altered to examine the effects of the specimen geometry. Each specimen is described in detail in Figure 3-2.

Figure 3-1: Bottle-shaped strut and associated strut-and-tie model

Specimen A
f'$_c$: 3,830 psi
Reinforcement: None
Dimensions: 4 x 36 x 36 in.
Bearing Area: 4 x 12 in.

Specimen H
f'$_c$: 5,290 psi
Reinforcement:
 #3 @ 6 in. θ = 45°
Dimensions: 6 x 36 36 in.
Bearing Area: 6 x 12 in.

Specimen B
f'$_c$: 4,200 psi
Reinforcement: None
Dimensions: 6 x 36 x 36 in.
Bearing Area: 6 x 12 in.

Specimen I
f'$_c$: 5,490 psi
Reinforcement:
#2 @ 6 in. θ = 45°
Dimensions: 6 x 36 x 36 in.
Bearing Area: 6 x 12 in.

Specimen C[1]
f'$_c$: 3,910 psi
Reinforcement: Nodal
Dimensions: 4 x 36 x 36 in.
Bearing Area: 4 x 12 in.

Specimen J
f'$_c$: 5,490 psi
Reinforcement:
#2 @ 6 in. θ = 45°
Dimensions: 6 x 36 x 36 in.
Bearing Area: 6 x 12 in.

Specimen D[1]
f'$_c$: 3,910 psi
Reinforcement: Nodal
Dimensions: 4 x 36 x 36 in.
Bearing Area: 4 x 12 in.

Specimen K
f'$_c$: 4,350 psi
Reinforcement:
#3 @ 6 in. θ = 30°
Dimensions: 6 x 36 x 36 in.
Bearing Area: 6 x 12 in.

Specimen E
f'$_c$: 3,230 psi
Reinforcement: #3 @ 6 in.
Dimensions: 4 x 36 x 36 in.
Bearing Area: 4 x 12 in.

Specimen L
f'$_c$: 5,290 psi
Reinforcement: #3 @ 6 in.
Dimensions: 6 x 36 x 36 in.
Bearing Area: 6 x 12 in.

Specimen F[1]
f'$_c$: 3,910 psi
Reinforcement: #3 @ 6 in.
Dimensions: 4 x 36 x 36 in.
Bearing Area: 4 x 12 in.

Specimen M[2]
f'$_c$: 4,300 psi
Reinforcement: #3 @ 6 in.
Dimensions: 6 x 36 x 36 in.
Bearing Area: 2 - 6 x 6 in.

Specimen G
f'$_c$: 4,300 psi
Reinforcement: #3 @ 6 in.
Dimensions: 6 x 36 x 36 in.
Bearing Area: 6 x 12 in.

Specimen N
f'$_c$: 4,300 psi
Reinforcement: #3 @ 6 in.
Dimensions: 6 x 36 x 36 in.
Bearing Area: 6 x 6 in.

Figure 3-2: Reinforcement layouts for isolated strut tests

Specimen O
f'$_c$: 5,500 psi
Reinforcement: #2 @ 3 in.
Dimensions: 6 x 36 x 36 in.
Bearing Area: 6 x 12 in.

Specimen U
f'$_c$: 4,350 psi
Reinforcement: 6 - #3 (bundled)
Dimensions: 6 x 36 x 36 in.
Bearing Area: 6 x 6 in.

24"

Specimen P
f'$_c$: 5,500 psi
Reinforcement: #3 @ 3 in.
Dimensions: 6 x 36 x 36 in.
Bearing Area: 6 x 12 in.

Specimen V
f'$_c$: 4,350 psi
Reinforcement: H – 3 - #3
V - #3@4in.
Dimensions: 6 x 36 x 36 in.
Bearing Area: 6 x 12 in.

12"

Specimen Q
f'$_c$: 4,200 psi
Reinforcement:
1 - #3 @ middepth
Dimensions: 6 x 36 x 36 in.
Bearing Area: 6 in. x 12 in.

Specimen W
f'$_c$: 4,350 psi
Reinforcement:
#3 @ 6in.
Dim: 6 x 60 x 36 in.
Bearing: 6 x 16 in.

Specimen R
f'$_c$: 3,910 psi
Reinforcement:2-#3
Dimensions: 4 x 36 x 36 in.
Bearing Area: 4 x 12 in.

24"

Specimen X
f'$_c$: 4,350 psi
Reinforcement:
#3 @ 6in.
Dim: 6 x 60 x 36 in.
Bearing: 6 x 12 in.

Specimen S
f'$_c$: 5,290 psi
Reinforcement: 2-#3
Dimensions: 6 x 36 x 36 in.
Bearing Area: 6 x 12 in.

24"

Specimen Y
f'$_c$: 4,350 psi
Reinforcement:
#3 @ 6in. - 2 matts
Dimensions: 10 x 36 x 36 in.
Bearing Area: 4 x 12 in.

Specimen T
f'$_c$: 5,290 psi
Reinforcement:
6 - #3 (bundled)
Dimensions: 6 x 36 x 36 in.
Bearing Area: 6 x 12 in.

12"

Specimen Z
f'$_c$: 4,350 psi
Reinforcement:
#3 @ 6in. -2 matts
Dimensions: 10 x 36 x 36 in.
Bearing Area: 4 x 12 in.

1. Special Nodal Reinforcement

2. Bearing Detail for Specimen M

A
A
Plan View
No. 3 Bars
Section A-A

Steel Bearing Plates
Concrete Panel
Neoprene Pads

Figure 3-2 – continued: Reinforcement layouts for isolated strut tests

71

Five basic reinforcement layouts were used in the 26 isolated strut specimens:

Unreinforced: The first layout consisted of no reinforcement. Four plain concrete panels (specimens A through D) were tested to establish the contribution of the concrete alone. In order to observe a pure strut failure, two of the unreinforced panels and one reinforced panel employed supplemental confinement at the nodes. This confinement consisted of short pieces of reinforcing No. 3 bars welded to a steel plate and surrounded by ties bent from No. 3. bars. (Figure 3-2).

Orthogonal mats: Next was a series of panels reinforced with two orthogonal mats of steel (specimens E through K). This series was reinforced with No. 3 bars as well as 6 mm deformed bars (6 mm bars will be called No. 2 bars). The effect of the angle between the reinforcing steel and the principle compression direction was investigated by rotating the mats 45 or 30 degrees. The yield stress of the bars were 89.9 and 78.1 ksi for the No. 2 and No. 3 reinforcing bars respectively.

Uni-directional mats: The third series of specimens (L through V) consisted of reinforcing bars working in one direction as opposed to the previous mats, which contained steel in two orthogonal directions. In these specimens, the reinforcement was either uniformly distributed or concentrated at locations that correspond to the discrete ties in the STM (Figure 3-1). The STM shown in Figure 3-1 assumes that the ties act at the third-points of the length of the strut, and the dispersion of compression occurs at a 2:1 slope. The final specimen (Specimen V) in series three consisted of horizontal bars placed at the tie locations as well as compression bars that were bundled beneath the loading plate. The arrangement of bearing plates was altered for three specimens (M, N, and U). For specimen M, the bearing plate was split into two bearing plates of half size. These two plates

were in turn supported on neoprene bearing pads (Figure 3-2). The purpose of this arrangement was to limit the amount of restraint against cracking in the vertical direction that was provided by friction at the bearing plate-to-concrete interface. Splitting the bearing plate into two pieces effectively split the CCC node at the panel boundary into two nodes. The split bearing plate boundary conditions are shown in the second note in Figure 3-2. For specimens N and U, only a single half-sized bearing plate was used, to explore the geometry of the bottle shape.

Panel Width: The two specimens in the fourth series were tested to determine effects of the width of the panel on the strength while keeping the reinforcement similar to previous specimens. For these two specimens (W and X), the width of the panel was increased from 36 in. to 60 in. As with specimen N, the ratio of loaded area to total area of a specimen was altered.

Panel Thickness: The fifth series also consisted of two specimens (Y and Z). These specimens were 10 in. thick, and the bearing plates were only 4 in. x 12 in. These were the only panels tested in which the loaded area was narrower than the thickness of the panel.

Each of the panels was tested to failure under a monotonically increasing load. A thin layer of a quick-setting grout was used to create a bedding layer and ensure uniform stress distribution under the bearing plates. The bedding layer also allowed final alignment of the specimen within the test machine. A spherical seat was placed on the bearing plate to eliminate any load eccentricities. A picture of the experimental setup can be seen in Figure 3-3.

Before tests were performed on the panels, standard 6 in. x 12 in. cylinders were tested to determine the concrete strength at the time of testing. During the isolated strut tests, a computer-controlled data acquisition system was used to monitor and record the output of internal (reinforcing bar) and external (concrete surface) strain gages as well as the applied load.

Figure 3-3: Testing of an isolated strut specimen

In each isolated strut test, the same mode of failure was observed. The first indication of distress in a specimen was a vertical crack that formed approximately at the center of the panel. This crack then propagated from mid-height of the panel towards the loading points. However, the crack did not propagate all the way to the loaded surface. Instead, the crack changed direction

as it neared the point of loading. Failure was then initiated by spalling and crushing of the concrete near, but not adjacent to, the bearing plate. The typical failures are illustrated in Figure 3-4 and Figure 3-5.
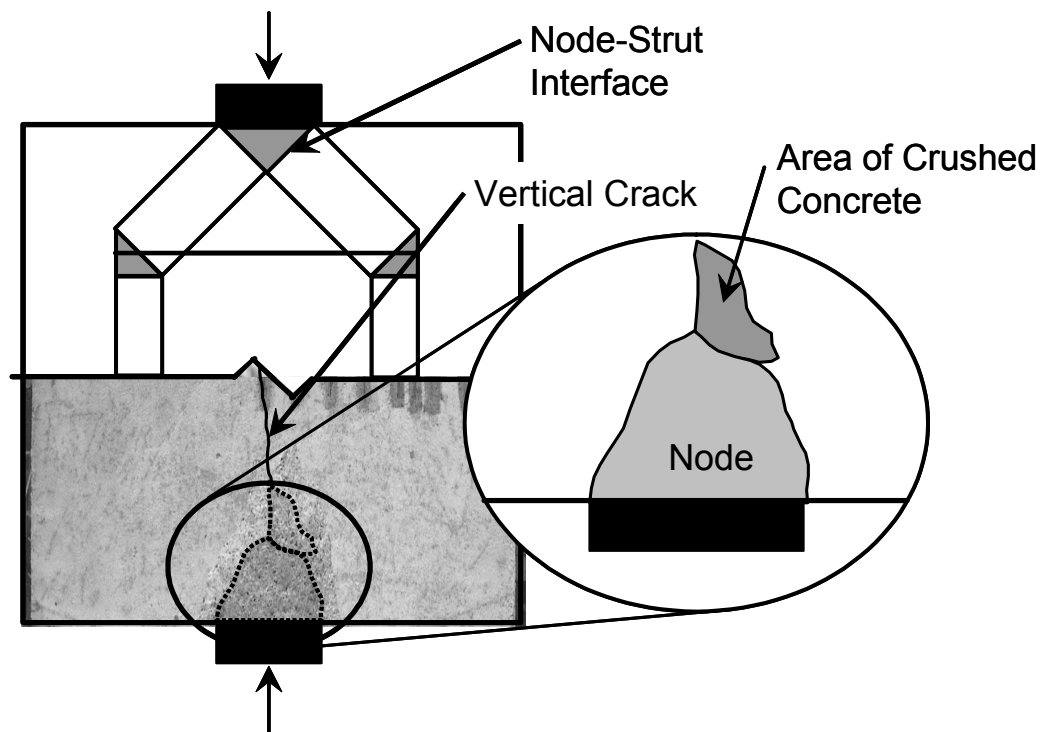
Figure 3-4: Typical failure mode for an isolated strut specimen
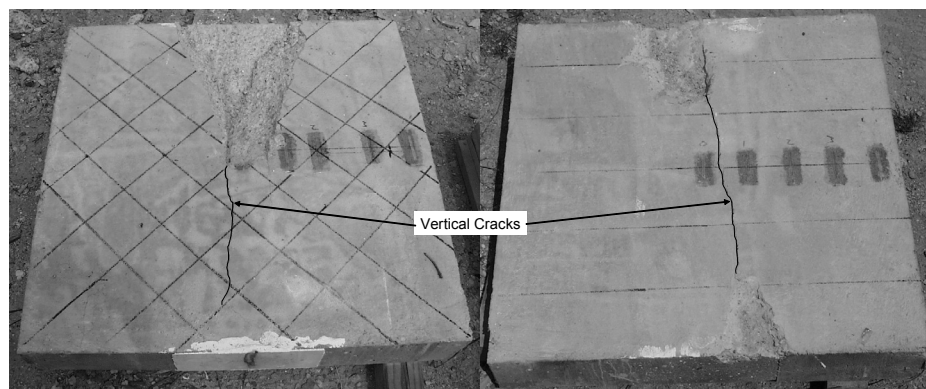
Figure 3-5: Additional photographs of specimens after failure (left: Specimen H; right: Specimen L)

3.3   EXAMINATION OF CODE PROVISIONS

The panels had very well-defined boundary conditions in the isolated strut tests. The measured efficiency factor was calculated with the ultimate load the panel resisted and the area over which the panel was loaded. In each test, the efficiency factor at failure was the efficiency of the CCC node when the strut crushed as seen in Figure 3-4. If the CCC node was hydrostatic, the stress, and efficiency factor, beneath the bearing plate was equal to the stress, and efficiency, along the node-strut interface. Therefore, the strut efficiency could be determined experimentally. The results of those experiments are compared to the values determined using ACI 318-05 and AASHTO LRFD.

3.3.1   Examination of ACI 318-05 Appendix A Provisions

The results of all 26 panel tests are tabulated in Table 3-1. The measured efficiency factor is plotted against $\sum \dfrac{A_{si}}{bs_i} sin\alpha_i$ in Figure 3-6. Recall that ACI 318-05 presented two different efficiency factors for bottle-shaped struts based on the reinforcement within the strut. The reinforcement requirements for ACI 318-05 were discussed in detail in Section 2.3.1 of this dissertation, specifically Eqn. 2-2. The stepped horizontal line in the figure represents the design values for strut strength presented in Appendix A of ACI 318-05. The line is placed at 0.85 times the appropriate efficiency factor to follow the format of ACI 318-05 Appendix A. For a strut that does not meet the requirements of A.3.3.1, the appropriate β_s factor is 0.6, and the line is placed at 0.51, which is equal to $0.85 \cdot 0.60$. For struts that do meet the A.3.3.1 requirements, the line is placed at 0.64 ($= 0.85 \cdot 0.75$).

To calculate the efficiency factor based on the data, the applied load at failure of the specimen was divided by the bearing area of that particular specimen times the compressive strength. The nodes are assumed to be

76

hydrostatic; therefore, the same stress is present on each face of the node. If the stress on each node face is the same, the efficiency factor for each of the node faces is also equal.
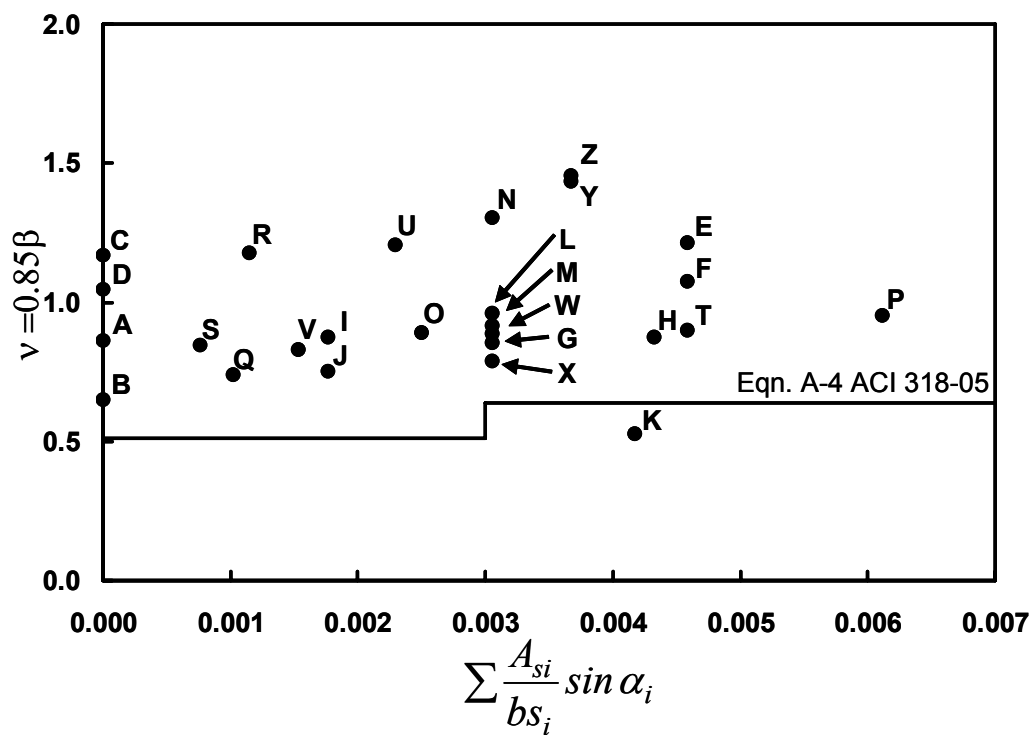
Figure 3-6: Results of isolated strut tests compared to ACI efficiency factors

Table 3-1: Results of isolated strut tests

Specimen	Efficiency Factor, v[†]	$\sum \dfrac{A_{si}}{bs_i} \sin \alpha_i$	ε_1, measured
A	0.86	0.0000	0.0022
B	0.65	0.0000	0.0014
C	1.17	0.0000	0.0021
D	1.05	0.0000	0.0020
E	1.21	0.0046	0.0022
F	1.07	0.0046	0.0020
G	0.85	0.0031	0.0013
H	0.88	0.0043	0.0017
I	0.88	0.0018	0.0017
J	0.75	0.0018	0.0016
K	0.53	0.0042	0.0014
L	0.96	0.0031	0.0018
M	0.91	0.0031	0.0014
N	1.31	0.0031	0.0012
O	0.89	0.0025	0.0016
P	0.95	0.0061	0.0015
Q	0.74	0.0010	0.0014
R	1.18	0.0011	0.0019
S	0.85	0.0008	0.0019
T	0.90	0.0046	0.0018
U	1.21	0.0023	0.0012
V	0.83	0.0015	0.0013
W	0.89	0.0031	0.0009
X	0.79	0.0031	0.0011
Y	1.43	0.0037	0.0009
Z	1.46	0.0037	0.0008

$$^{†}v = \frac{\text{Peak Load}}{f_c' \cdot \text{Bearing Area}} = 0.85\beta$$

3.3.1.1 Effect of Reinforcement Crossing the Strut Axis

Within the 26 tests, three groups of panels had identical (or nearly identical) amounts of steel crossing the strut axis, which coincides with the expected vertical crack location as shown in Figure 3-5. These groups of specimens (Group 1: A, B, C, D ($\sum \frac{A_{si}}{bs_i} \sin\alpha_i = 0.0$); Group 2: G, L, M, N, W, X ($\sum \frac{A_{si}}{bs_i} \sin\alpha_i = 0.003$); and Group 3: E, F, H, K, T ($\sum \frac{A_{si}}{bs_i} \sin\alpha_i \approx 0.0045$)) are shown in Figure 3-6. The third group, Specimens H and K had slightly less reinforcement than Specimens E, F, and T but the amounts of reinforcement are similar enough for comparison. In each group there is considerable variation in the experimental efficiency factors. For the unreinforced specimens (A through D), the efficiency factors ranged from 0.65 to 1.17; for the second group of specimens the efficiency varied from 0.79 to 1.31. In the third group, which had slightly different amounts of reinforcement, the efficiency factor varied from 0.53 to 1.21. This group also contained the only efficiency factor that was unsafe when compared with the code value of 0.64.

79
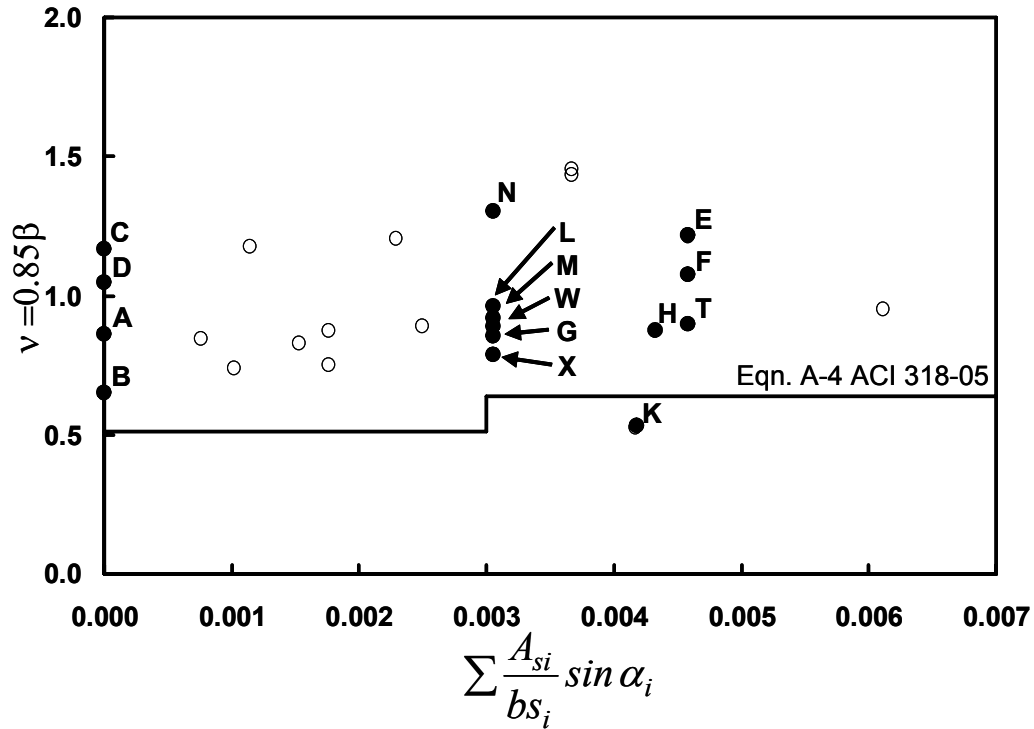
Figure 3-7: Effect of reinforcement crossing the strut axis

Since failure of the panel initiated at the node-strut interface, it is logical that reinforcement within the body of the panel has little effect on the failure. To further illustrate this point, specimen P had the most reinforcement, but had a nodal efficiency of 0.95, which is not significantly different than the average of all tests (0.97). The specimen containing the most reinforcement had a lower efficiency factor than some specimens with no reinforcement at all. Specimen O had the same layout of reinforcement as specimen P, except that No. 3 bars replaced with No. 2 bars. The marked decrease in steel area was not associated with any significant decrease in efficiency of specimen O compared to specimen P.

3.3.1.2 *Effect of Angle between Reinforcing Steel and Strut Axis*

Four specimens contained mats of reinforcement that were rotated such that the reinforcing bars were no longer parallel and perpendicular to the loading axis. In three cases there was an angle of 45 degrees between the load axis and the reinforcing bars (specimens H, I, and J). For the fourth case, specimen K, the angle was 30 degrees. These specimens can be compared with specimen G, which had the same layout of steel without any rotation of the mat. Those results of those tests are highlighted in Figure 3-8.
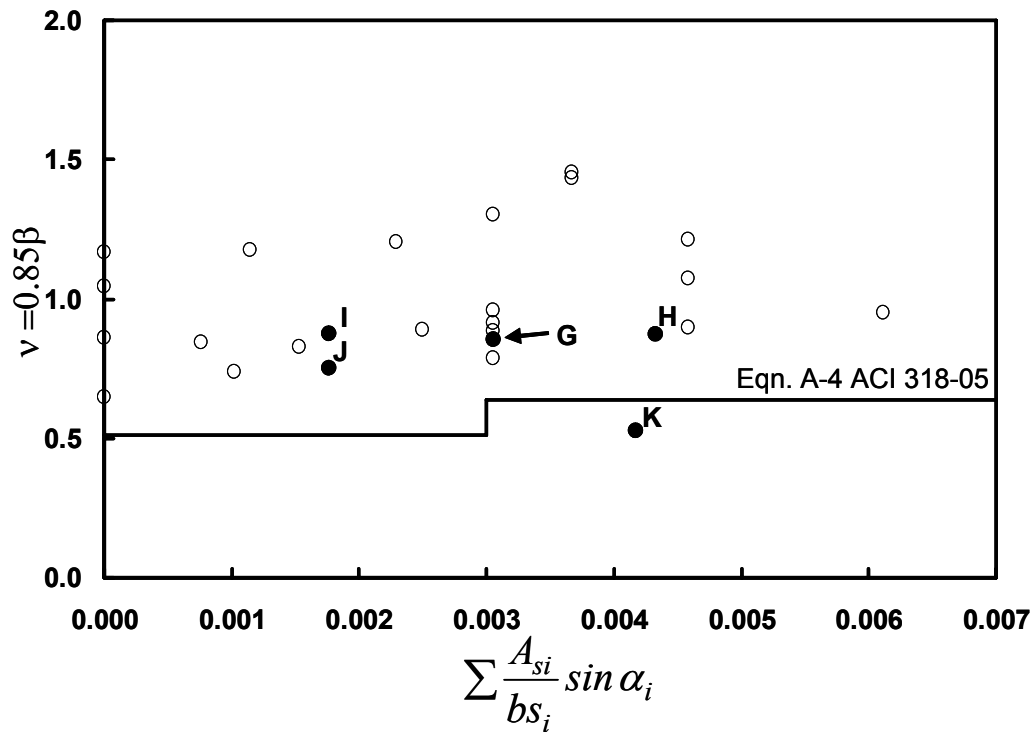
Figure 3-8: Effect of mat rotation

With the exception of specimen K, the angle of the mat did not appear to affect the efficiency factor. Panels H and G were identical, except for the mat rotation, and the respective efficiency factors were 0.88 and 0.85. Panels I and J

contained No. 2 bars rather than the No. 3 bars used in the other specimens. I and J had efficiencies of 0.88 and 0.75. Specimen K had the lowest efficiency factor of any of the test data ($v = 0.53$). Since differences in efficiency were minimal in the previous cases where mat rotation was the primary variable, the low value of efficiency for specimen K is difficult to explain. Specimen K was the only specimen tested with the mat rotated by 30 degrees. The low strength of Specimen K could be due to the mat rotation, variability that is typical of concrete research or a combination of the two.

3.3.1.3   Effect of Specimen Width

In order to examine the geometry of the bottle-shaped strut, the panel width and the width of the bearing plate were carried. By changing these variables, it could be determined if the width of the panels was limiting the lateral spread of the compressive stresses. Of the 26 panels tested, a comparison of specimens L, N, W and X can be used to examine the effect of strut width. Specimens W and X were 60 in. wide as opposed to the standard width of 36 in. Panel X had a 12 in. bearing plate, and panel W had a 16 in. plate. Specimen N was a standard width panel, but the bearing area was only 6 x 6 in. Specimen L could be considered the control specimen for the examination of strut width. It was a standard size panel with a standard size bearing plate (6 x 12 in.). For all four of these specimens, an identical amount of reinforcement was used.

During the tests, concrete surface strain gages were placed on the panels. The gages were oriented vertically and distributed across the mid-height of the panel. The goal was to obtain the distribution of vertical strains (and therefore stresses) across the width of the panel. The vertical strain gage at the extreme edge of the 36 in. panel would typically record a peak compressive strain of 30 to 70 microstrain. Such a low strain implies that there was very little vertical stress

82

acting on the cross-section at the edge of the standard sized panel. Both panels L and N had strains in the same range (30 to 70 microstrain) with different bearing widths.

When panels W and X were tested, concrete surface strain gages were placed at the same location as in the tests involving standard width specimens. The strains measured 16 in. from the centerline for specimens W and X were 60 microstrain for both panels. The vertical strain distributions are discussed in detail in a later section of this chapter. The strain distributions for Specimens L,N, W, and X are shown in Figure 3-9.
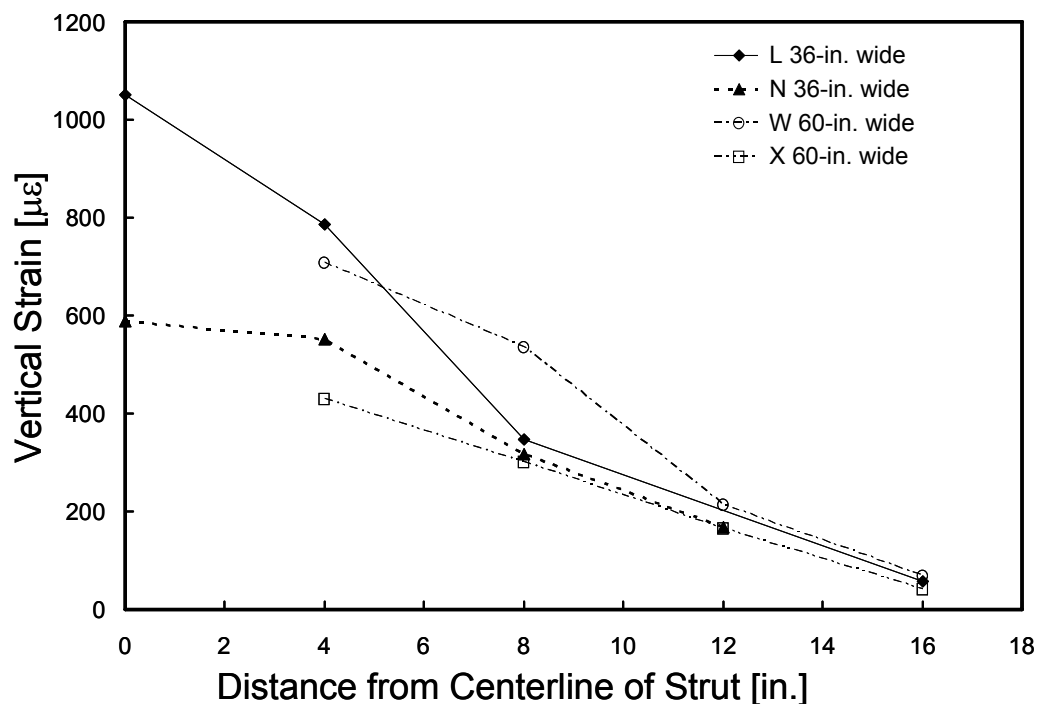
Figure 3-9: Strain distributions for panels of varying widths

Based on the strain measurements, it is apparent that the panel width, and subsequently, bearing width, did not have a significant impact on the geometry of the bottle-shape. The width of the bearing area necessarily affected the stress state

very near the loading points, but had negligible impact on the stress state at midheight of the specimens. Increasing the width of the specimen had minimal impact on the results.

3.3.1.4 Effect of Specimen Thickness

Six specimens were 4 in. thick, 18 specimens were 6 in. thick, and two were 10 in. thick. These variations in thickness provide some information regarding the effect of panel thickness. The 4-in. thick specimens are highlighted in Figure 3-10.
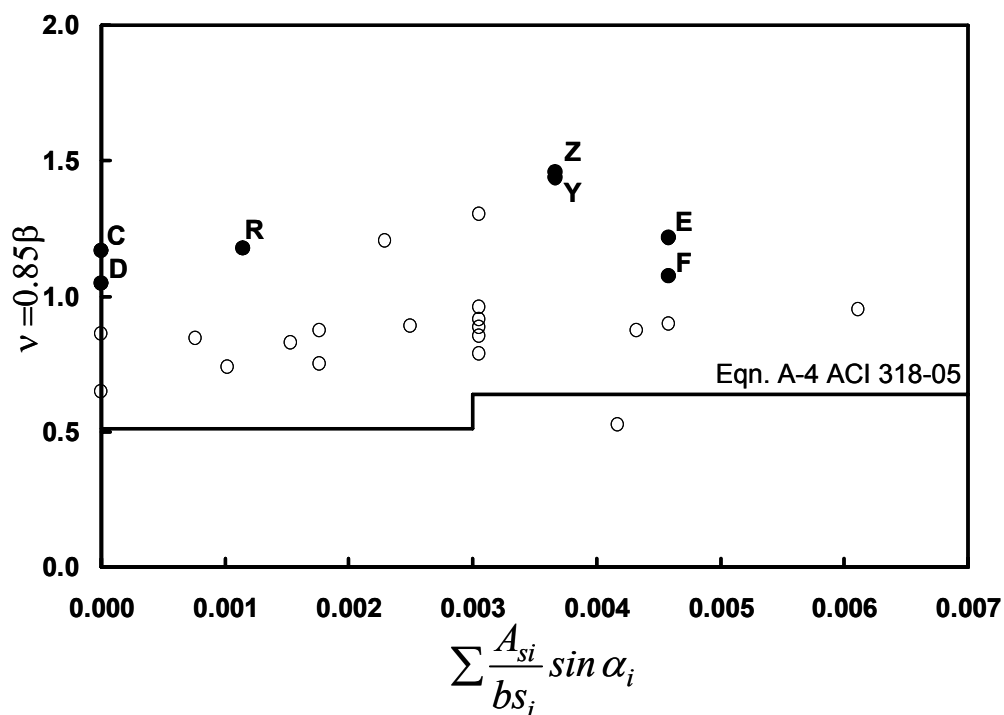
Figure 3-10: Effect of specimen thickness

The 4-in. thick panels had consistently higher efficiency factors than similar specimens that were 6 in. thick. Note that in Figure 3-10, the 4-in. thick panels (C, D, E, F, and R) are near the upper bound of the test data. The 10-in.

84

specimens (Y and Z) resulted in a higher efficiency factors than did the 4-in. thick panels. The 10-in. thick panels were tested using a bearing plate that was 4 x 12 in. For these thicker panels, a more complex stress state was likely present because the bearing plate did not cover the full thickness of the specimen. The results of the 10-in. thick panels will be discussed in detail in the next section.

3.3.1.5 Effect of 3-D Stress State

Specimens Y and Z were the thickest panels. These panels were 10 in. thick; however, they were loaded through a bearing plate that was only 4 in. x 12 in. The bearing plates were placed in the center of the loaded face of the specimen. In doing so, these specimens likely had a three-dimensional bottle-shaped strut similar to that shown in Figure 2-15. The bearing plate did not cover the entire thickness of the panel. The applied compression was therefore able to disperse along the width and along the thickness of the panel.

These two specimens yielded the highest efficiency factors of the test series. The bearing capacity likely benefited from confinement in the direction normal to the surface of the panel when 4 in. bearing plate was placed on a 10 in. thick panel. An increase in the confinement, and therefore strength, of the specimen at the critical location, *i.e.* the node-strut interface, would be expected to increase the specimen strength, as was observed experimentally. This observation agrees with the conclusions presented by Adebar and Zhou (1993). Adebar and Zhou noted in double punch tests, the bearing pressure at failure increased with increasing distance between the edges of the bearing plate and the specimen. The unloaded area of concrete provided small amounts of confinement to the inner core that was subjected to load.

3.3.1.6 *Effect of Concentrated vs. Distributed Reinforcement*

Five specimens (Q, R, S, T, and U) contained reinforcement that was lumped at a location that could correspond to a discrete tie location in an STM. Specimen Q contained only a single bar at the midheight of the specimen. The associated STM for this specimen would contain four diagonal struts that form a diamond shape within the square panel. There would be no vertical struts, as depicted in at left in Figure 3-11. The four remaining specimens with bundled reinforcement conform to the general shape of STM, as depicted in at right Figure 3-11. The four specimens slightly altered that model by forcing the tie location to occur at the location of the steel.

Tie Locations varied by placement of reinforcement
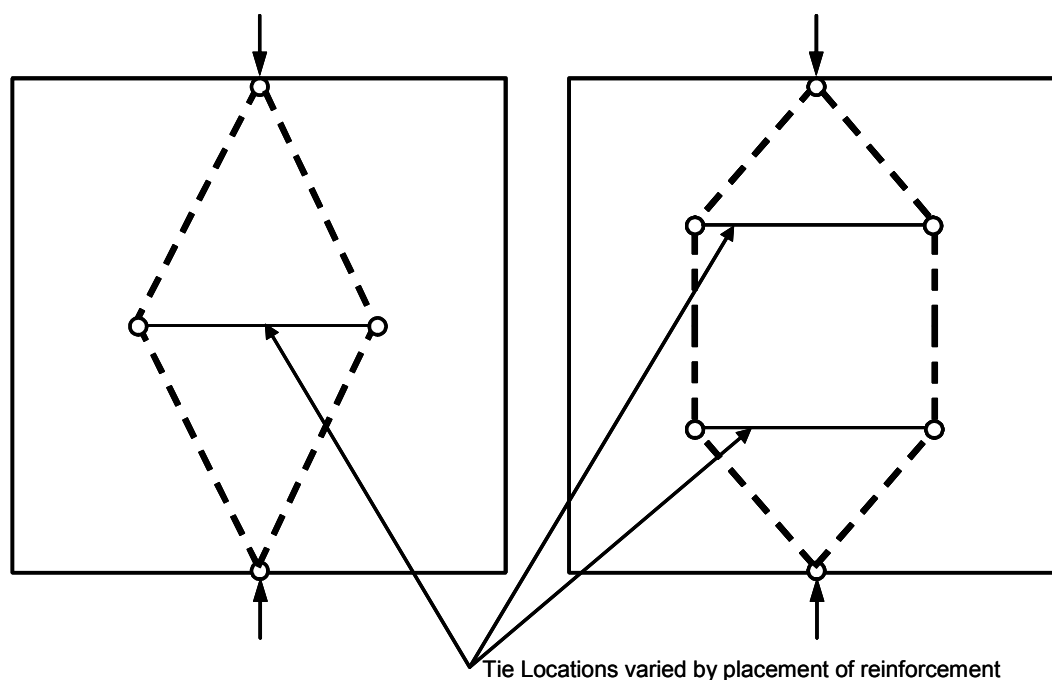
Figure 3-11: Variation in bottle shaped based on placement of reinforcement

As can be seen in Figure 3-6, five specimens (Q, R, S, T, and U) exhibit levels of scatter similar to the entire group of 26 specimens. Specimen Q has one of the lowest efficiency factors; conversely, specimen U has among the highest.

86

The only conclusion that can be drawn from these results is that lumping the reinforcing steel produced similar amounts of scatter as all other variables examined in this testing series. No distinct effect of limiting the reinforcement to discrete tie locations can be discerned from the data set, nor did the amount of reinforcement within the discrete tie locations appear to have a significant effect.
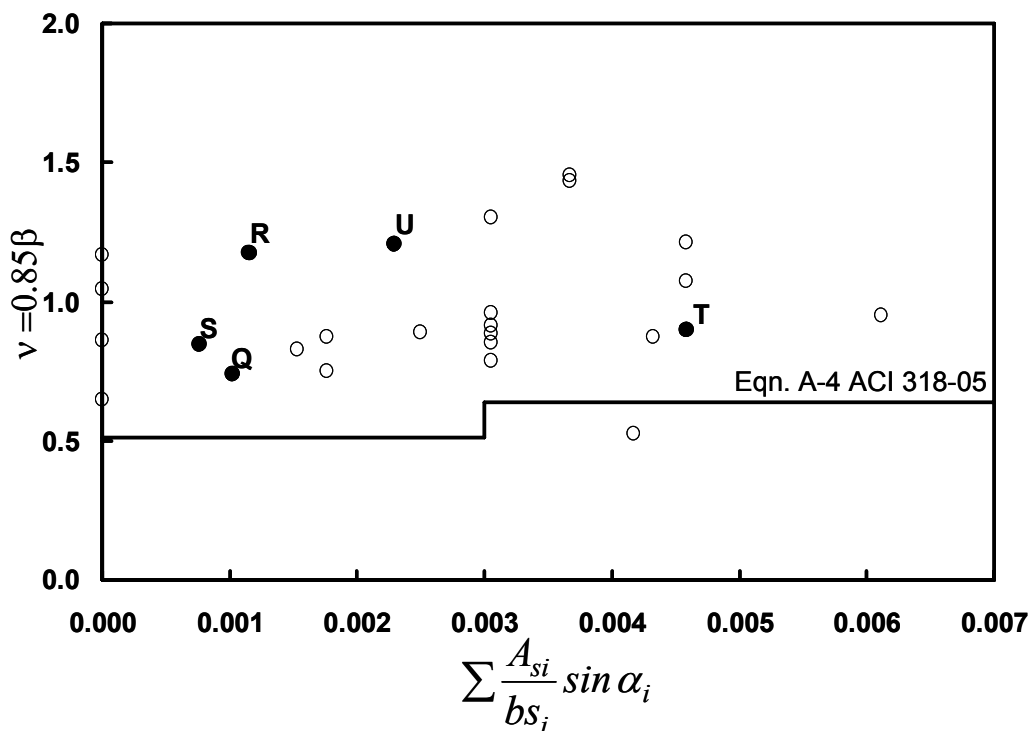
Figure 3-12: Effect of concentrated and distributed reinforcement

3.3.1.7 *Effect of Compression Reinforcement*

Specimen G contained reinforcement parallel to the direction of loading, while specimen L did not. Specimen G had a lower efficiency factor than specimen L despite the presence of reinforcement parallel to the direction of compression.

To further examine the effect of compression steel, specimen V was constructed. This specimen contained reinforcement concentrated under the loading points. Four No. 3 bars were distributed over the bearing length of the panel and were instrumented with strain gages. During the test, all four of these bars yielded. Even with the bars yielding in compression, the nodal efficiency factor does not appear to be increased by the vertical reinforcement. In Equation A-4 of Appendix A of ACI 318-05, bars which are parallel to the anticipated cracking direction are not included for the purposes of reinforcing the strut. For these compression bars, the sine term is zero; thus the compression bars do not affect the efficiency factor. Physically, a bar that is parallel to the expected cracking in a bottle-shaped strut does not restrain that crack. Specimens G, L, and V are highlighted in Figure 3-13.
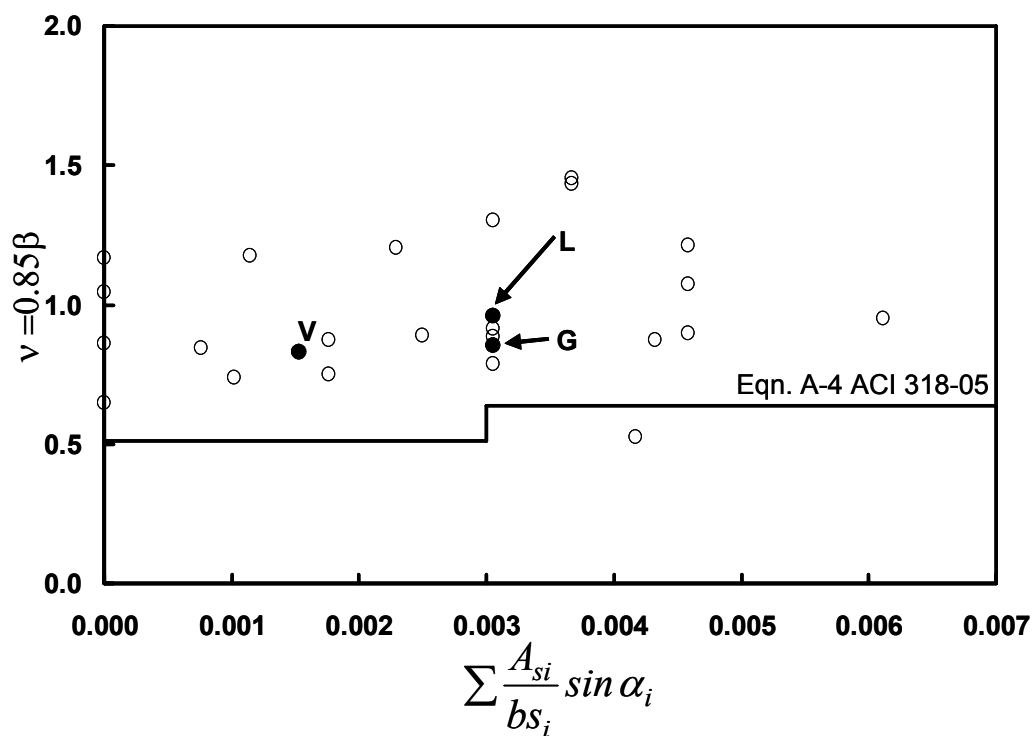
Figure 3-13: Effect of compression reinforcement

3.3.1.8 Effect of Boundary Conditions on the Tests

During the course of testing, all specimens failed at the interface between the node and the strut. In an effort to observe any possible alternate limit states, extra confinement was added to the nodal zones (Figure 3-2). Even with this extra confinement, the same type of failure was observed. The confinement appears to have slightly increased the nodal efficiencies (specimens C, D, and F).

The results of specimen M imply that the friction between the steel bearing plates and the concrete specimen had minimal impact on the results, including those tested with a single bearing plate. Recall that specimen M used a split bearing scheme to limit the confinement due to friction at the node face (Figure 3-2). Specimens C, D, E, and M are highlighted in Figure 3-14.
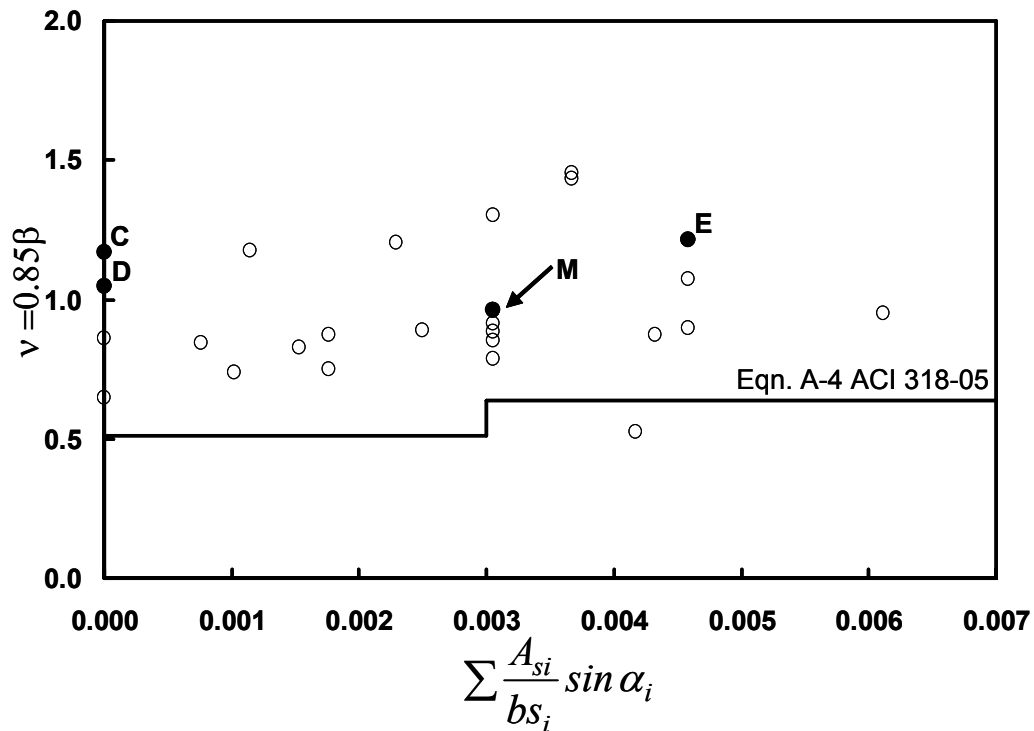
Figure 3-14: Specimens with altered boundary conditions

3.3.2 Examination of AASHTO LRFD STM Provisions

One of the primary inputs into the AASHTO LRFD expressions regarding strut strength is the tensile concrete strain in the direction of the tie. For the isolated strut specimens, this strain was measured by strain gages placed on the reinforcing steel. For specimens without transverse reinforcement, strains were measured by strain gages placed on the surface of the panels. The measured strain was somewhat different than implied by AASHTO. The strains required for input into the AASHTO design procedures should be average strains across cracked concrete. Even though different measures of strain are used in this document and by the authors of the AASHTO LRFD STM provisions, comparisons can be made.

The strain in the reinforcing bars is greatest where the bar crosses the crack. The strain gages were located very near to the cracks that developed in the panels. In general, the cracks in the panels did not cross the reinforcement at the exact location at which the strain gage was applied. Therefore it is unlikely that the strain recorded in Table 2 is the maximum strain in the specimen or the reinforcing bar. However, since the strain gages were very near the cracks, the strain values presented in the table are likely greater in magnitude than the average strain in the bars.

The isolated strut data are displayed in Figure 3-15 and Table 3-1. Steel strains are shown on the horizontal axis, and the vertical axis is the efficiency factor, as in Figure 3-6. The solid line is the design equation given in the AASHTO provisions. The dashed line represents the design equation presented within AASHTO LRFD if the upper limit of $0.85 f_c'$ was removed.
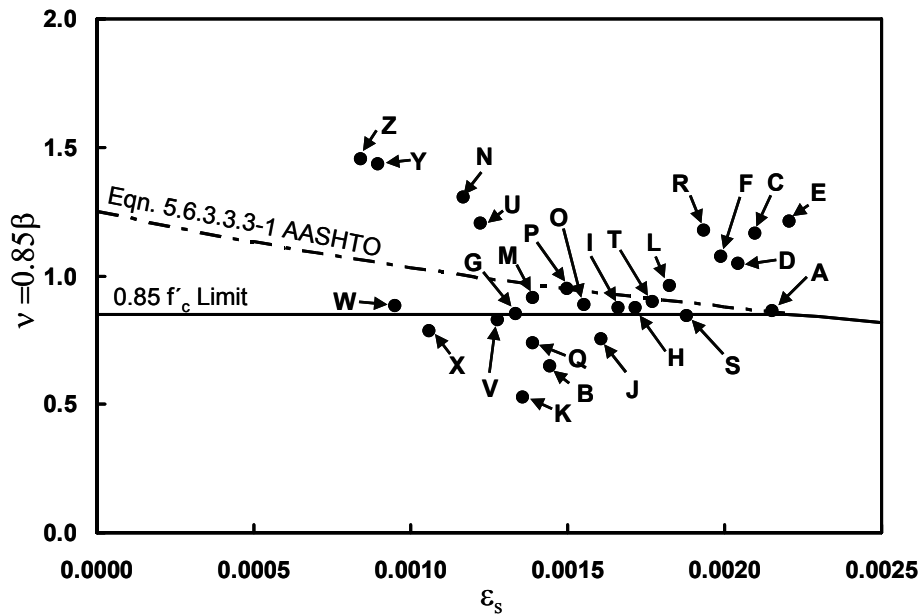
Figure 3-15: Results of isolated strut tests compared to AASHTO LRFD efficiency factors

In Figure 3-15, the data tend to be grouped. For example, all of the panels that were 4 in. thick (A, C, D, E, F, and R) are in a group at strains between 0.002 and 0.0025. Also, each of the pairs of panels with altered boundary conditions (W and X; N and U; Y and Z) are grouped together and lie away from the main cluster of test data. The 14 panels that were geometrically identical (only the reinforcement varied) constitute the main group that is very near or below the AASHTO design value ($0.0013 \leq \varepsilon_s \leq 0.0019$).

Applying the AASHTO STM provisions to the isolated strut test data, the average ratio of measured strength to calculated capacity is equal to 1.14. With the ratio close to one, unconservative test results can be expected as shown in Figure 3-15. In this case, six of the test specimens failed at loads less than those determined using the AASHTO LRFD design expression when using the measured tie strain.

91

For design purposes, the value of strain in the direction of the tensile tie would be calculated rather than measured. Typically, the strain in the tie would be assumed to be equal to the yield strain of the reinforcement comprising the tie. If the yield strain is used for the strain in the direction of the tie, the average ratio of tested strength to predicted strength is 1.21 and the number of unconservative estimates of strength is reduced to three.

3.4   CRACKING LOADS

During the panel tests the load at which the first vertical crack was also recorded. The loads at cracking and failure are tabulated in Table 3-2. The data listed in Table 3-2 are shown graphically in Figure 3-16. In Figure 3-16 efficiency factors at cracking and failure loads are plotted rather than applied loads. The panels had four different thickness, as well as different bearing areas and concrete strength. The use of efficiency factors rather than applied loads helps to address the differences between tests. In each of the three plots in Figure 3-16, the horizontal axis is $\sum \dfrac{A_{si}}{bs_i} \sin\alpha_i$.

Table 3-2: Cracking and failure loads for panel tests

Specimen	Cracking Load [kip]	Failure Load [kip]	Ratio of Cracking Load to Failure Load
A	117.8	158.9	0.74
B	136.8	196.3	0.70
C	101.4	219.2	0.46
D	132.3	196.7	0.67
E	70.5	188.1	0.37
F	153.9	201.7	0.76
G	142.8	264.5	0.54
H	190.0	333.3	0.57
I	187.1	346.4	0.54
J	198.4	298.0	0.67
K	117.4	165.1	0.71
L	192.3	366.8	0.52
M	150.1	283.2	0.53
N	138.4	202.1	0.68
O	195.0	352.4	0.55
P	186.0	377.0	0.49
Q	138.6	224.0	0.62
R	145.1	220.8	0.66
S	170.9	322.5	0.53
T	170.5	343.1	0.50
U	128.6	189.0	0.68
V	139.3	259.7	0.54
W	187.4	370.1	0.51
X	170.3	246.7	0.69
Y	208.4	299.5	0.70
Z	247.6	303.8	0.81
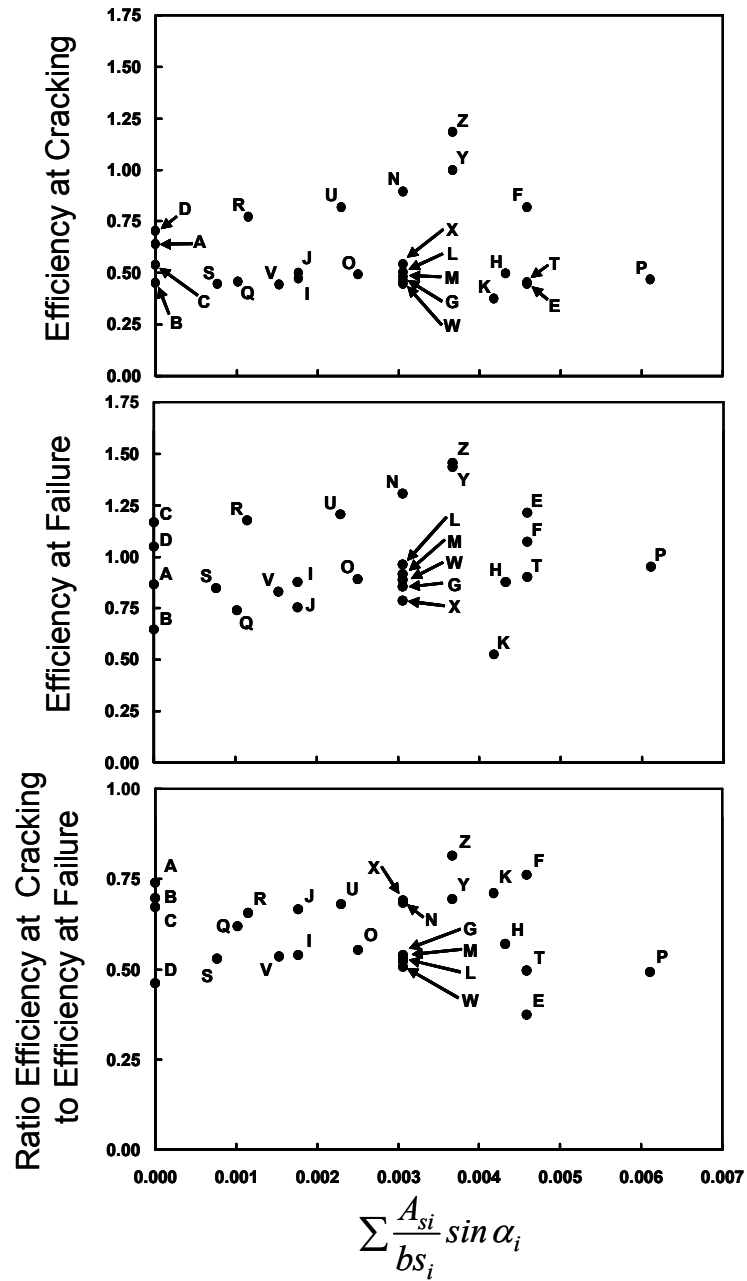
Figure 3-16: Results of isolated strut tests (top: efficiency at cracking; middle: efficiency at ultimate; bottom: ratio of efficiency at cracking to efficiency at ultimate)

Figure 3-16 indicates that there is not a strong correlation between the cracking strength of the isolated struts and the amount of reinforcement crossing the crack. Before cracking the concrete is nearly elastic in tension and largely unaffected by the presence of reinforcement. Just as in flexure of a reinforced concrete beam, reinforcement in the isolated struts is only engaged after cracking occurs and does little to affect the formation of the initial cracks.

The cracking loads ranged from 37 to 81% of the failure loads. The average cracking load was 61% of the ultimate load. The data lie within approximately two standard deviations of the average value ($\sigma = 0.11$).

3.5   STRAIN DISTRIBUTIONS

In addition to the data collected regarding the loads, strain readings in the panels were recorded during the test. The strain gages were located at midheight of the specimen and were distributed across half of the panel as shown in Figure 3-17. The left-most strain gage in Figure 3-17 is located at the center of the panel. The strain distribution across the width of the specimen was expected to be symmetric. In early tests the strain distribution was measured across the full width of the concrete panel to verify the symmetry of strain distributions. After testing approximately six panels, symmetrical strain distributions were observed. Strain gages were only placed on one side of the panel for subsequent specimens to reduce the instrumentation in the tests.

For all panels the strain readings were greatest at the centerline of the panel and decreased for gages nearer the panel edge. The strain distribution for Specimen O is shown in Figure 3-17. This distribution is typical for the panel tests. Some of the strain distributions indicated a tensile strain near the outer edge of the specimen, in addition to the large compressive strain along the centerline.
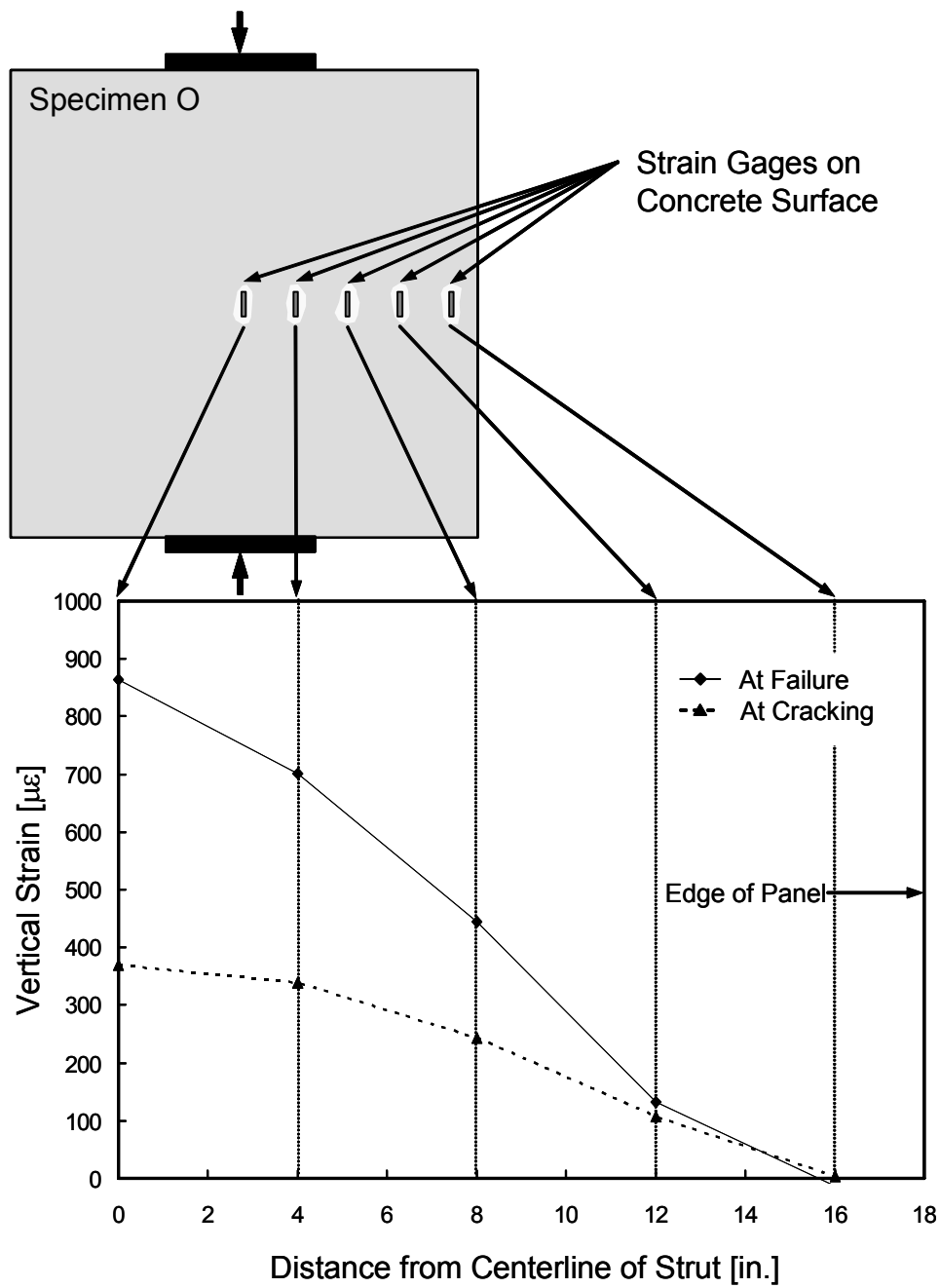
Figure 3-17: Strain gage locations and a typical strain distribution (positive strains are compression)

Figure 3-18 shows a composite of strain distributions for some of the panel tests. Only 14 of the 26 isolated strut specimens had strain gages placed to measure the distribution of strain at midheight. The upper boundary of the grey area on the graph represents the maximum strain readings from the panels. Similarly the lower boundary of the grey portion represents the minimum reading at a given location. All of the strain distributions are contained within the grey portion of Figure 3-18. Note that there are small tensile readings for the outer portions of the panel. For the panels used to develop this composite, a 12 in. wide bearing plate was used, so that the edge of the bearing plate was 6 in. from the centerline of the panel.
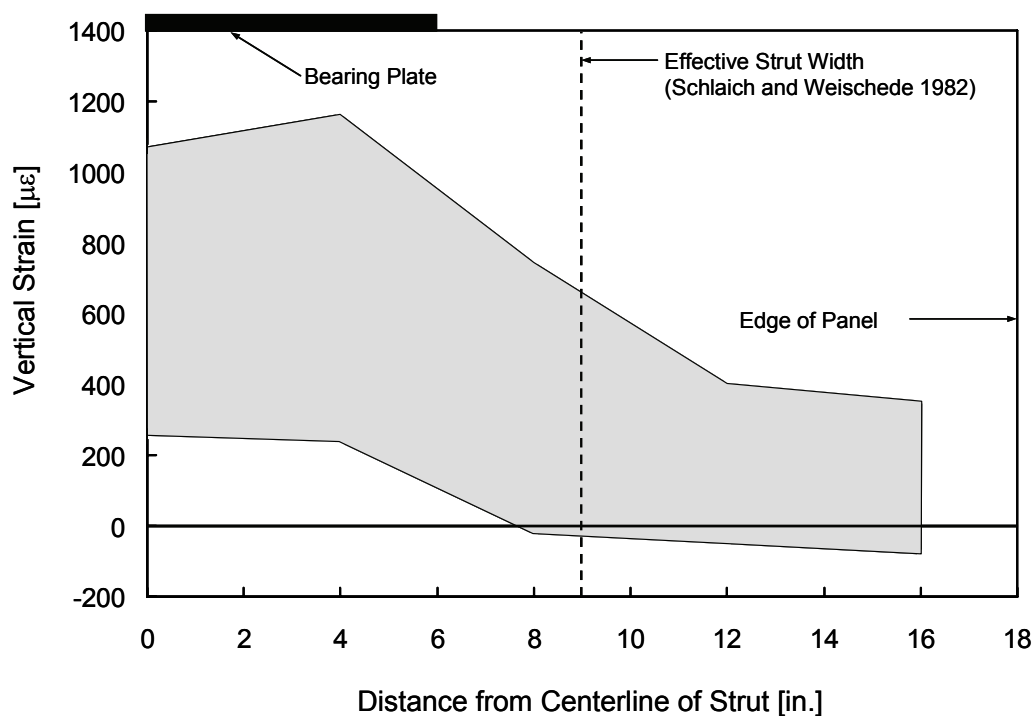
Figure 3-18: Envelope of strain distributions from isolated strut tests at ultimate load (positive strains are compression)

Based on the envelope shown in Figure 3-18, the dispersion of compression in the panels results in a maximum width in the bottle-shaped strut between 8 and 18 in. Small tensile strains were measured at distances of 8 to 18 in. from the center of the panel; therefore there was no compression in that range for some of the panels.

Traditionally, the angle of dispersion is assumed to have a slope of 2:1 ($m = 2$ in Figure 3-19). However, Schlaich and Weischede (1982) presented a simple method for approximating the dispersion of compression in an elastic body. This simple elastic model was applied to bottle-shaped struts along with the assumption that the first crack will occur due to elastic stresses. The Schlaich and Weischede model assumes the bottle geometry as shown at the right in Figure 3-19. The width of the larger end of the bottle is assumed to be equal to one-third of the length of the strut but not less than the width of the bearing. For short struts in which the limit of $b_{ef} > b_{min}$ governs, it is assumed that:

$$b_{ef} = b_{min} + \ell/6 \qquad\qquad (3\text{-}1)$$

Where: ℓ = the length of the strut

b_{min} = the minimum strut width

b_{ef} = the maximum strut width
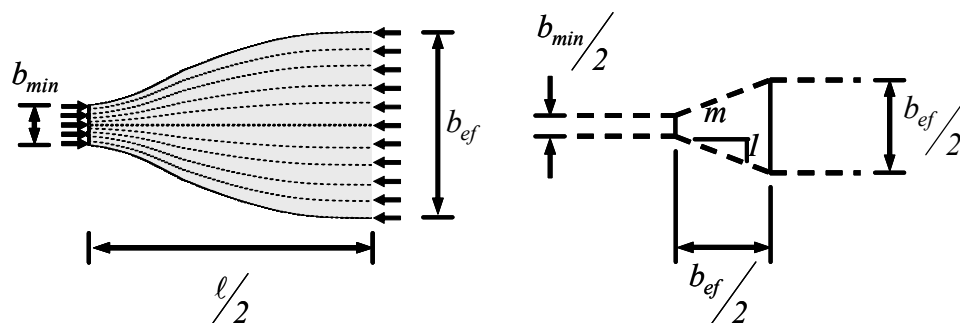
Figure 3-19: Dispersion of compression (Left: elastic distribution; Right: equivalent STM) (Schlaich and Weischede 1982)

When applying the elastic bottle geometry proposed by Schlaich and Weischede, the maximum strut width for the isolated strut tests is 18 in. The effective strut width is indicated by the dashed line in Figure 3-19. The strut width as determined by Schlaich and Weischede seems to be in agreement with the width of the strut for the lower bound of the strain distributions. However, the upper bound of the strain distributions indicates a wider strut.

3.5.1 Effects of Cracking on Strain Distributions

The use of STM implies that a plastic mechanism has developed in the structure. Therefore, all of the discussion in the previous section focused on the strain distribution within the tests specimens at failure load. However, cracks in a bottle-shaped strut form due to elastic stresses. Strain distributions from Specimen L are shown in Figure 3-20. The two strain distributions are determined from approximately the same applied load; however, the post-cracking load was slightly greater than the load prior to cracking. The solid line is the strain distribution immediately prior to the formation of the vertical crack, and the dotted line is just after the crack occurred. The data presented in Figure 3-20 are typical of all panel tests.

99

The data indicate that prior to cracking, the full cross-section of the panel is in compression with the maximum compressive strain occurs at the center of the panel. After cracking, small tensile strains were observed at the outer edges of the panel along with a peak compressive strain at the center of the specimen. The strain distributions in Figure 3-20 have a similar shape, but the post-cracking distribution focuses a larger fraction of the applied load through the center of the panel specimen.
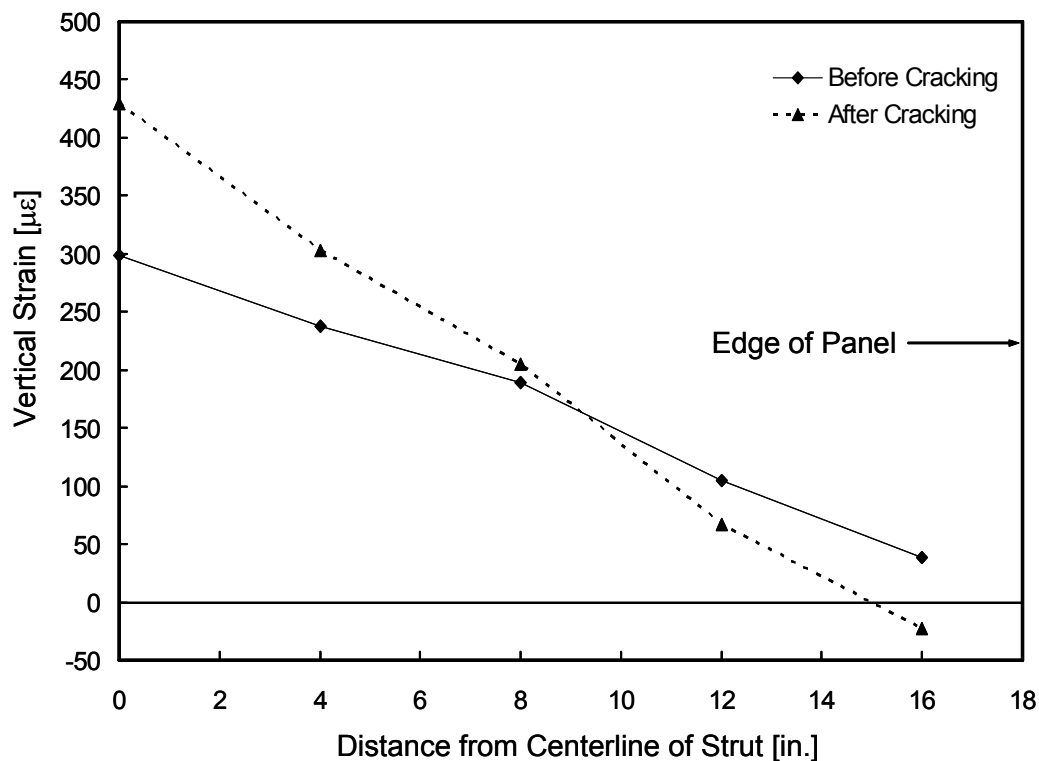
Figure 3-20: Strain distributions before and after cracking

3.6 OBSERVATIONS

Regardless of the boundary conditions, the same failure mode was observed in each test. The failure was caused by crushing of the strut adjacent to

the node while the node remained intact and undamaged (Figure 3-1). Failure initiated at the interface between the node and strut. Reinforcement in the body of the panel had minimal, if any, impact on the strength of that interface and therefore on the strength of the strut. This idea is reinforced by the data plotted in Figure 3-1. The most heavily reinforced strut had an efficiency factor that was not significantly different than the efficiency of unreinforced specimens.

For 25 of 26 tests, the efficiency factors presented in Appendix A of ACI 318-05 resulted in a safe estimate of the isolated strut strength. Nevertheless, the data do not seem to relate to the ACI requirements for reinforcement crossing the strut axis (Equation A-4 of ACI 318-05). The critical value of 0.003 is inconsequential when viewed against the test results. Based on the data presented herein, a constant value of strut efficiency (β_s =0.60) would provide adequate safety and simplify the code. The average value of experimental efficiency factor divided by the efficiency used for design in ACI 318-05 is 1.68.

For 20 of 26 tests, the efficiency factor as determined by AASHTO LRFD produced a safe expectation of the strength of the isolated strut specimens. All of the data presented are governed by the AASHTO LRFD upper limit of $0.85 f_c'$. The average value of experimental efficiency factor divided by the efficiency predicted by AASHTO is 1.14.

Experimental results indicate that the load at which the splitting crack occurs is not affected by the reinforcement in the panel; which is in agreement with general reinforced concrete behavior. Strain distributions across midheight in the specimens yielded results in agreement with expectation: the vertical strain directly beneath the applied loads was the greatest in each test, and the magnitude of the strain decreased close to the edges of the panel. Similar data from deep beam tests are needed to compare with the results of the isolated strut tests. With

such data, the dispersion of compression in more complex members can be compared to the simple tests discussed in this chapter.

CHAPTER 4

Tests of Shear Critical Beams

4.1 INTRODUCTION

The isolated strut tests described in Chapter 3 provided data to evaluate the geometry of a bottle-shaped strut in its simplest form. The stress distribution in isolated strut tests was symmetric. However, the stress conditions in a panel are considerably different than those found in a beam. In more complex structural components, the stress distribution may not be so simple. For a deep beam the stress distribution is affected by normal and shear stresses due to bending.

Three series of beam tests were performed to examine the behavior of struts in the more complex, and hence, more realistic, circumstances of a beam. The first series of beam tests consisted of deep beams that were subjected to various uniform or concentrated loads. These beams contained different configurations of shear reinforcement to examine the effects of horizontal and vertical reinforcing bars. The second series of tests was used to examine the effects of the width as well as the effects of shear span-to-depth ratio on shear strength. Finally, the effects of load distribution were examined in the third test series. The results of each of these series are described in detail in the subsequent portions of this chapter.

4.2 TEST SETUP

All three series of beam tests were conducted in the reaction frame shown in Figure 4-1. The frame consisted of four columns that were connected with heavy steel W-shapes to form the cross-head. Each of the columns was attached to the strong floor. The maximum load the frame could withstand was 480 kip. The

maximum load was limited to the capacity of the anchors in the strong floor. The reaction frame was post-tensioned to the strong floor.
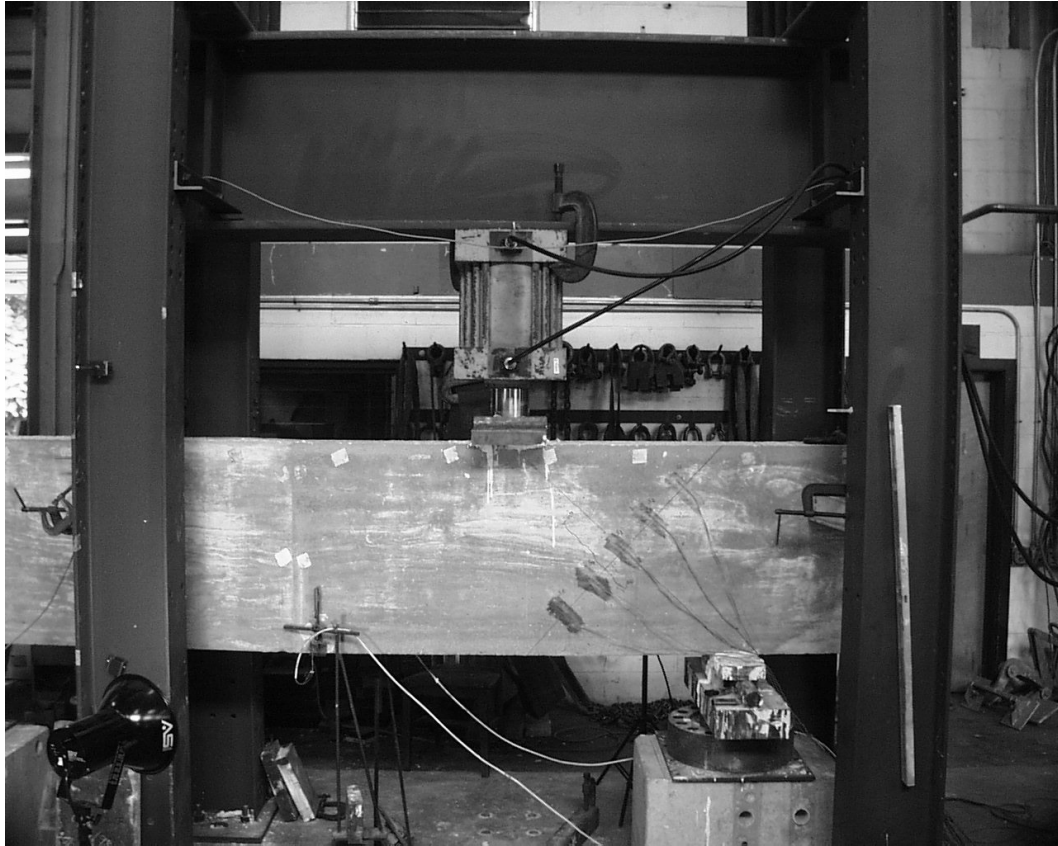
Figure 4-1: Reaction frame used for beam tests

The reaction frame was designed to allow different load applications. In Figure 4-1 the frame is configured to apply a single concentrated load to the specimen. The concentrated loads were produced using hydraulic rams capable of applying 200 kip.

In the cases where specimens were subjected to uniform loads, the load was produced by 30 identical hydraulic rams (10 kip each). A photograph of the uniform load apparatus is shown in Figure 4-2. Each of the rams was connected to the same hydraulic manifold to ensure that the pressure supplied to each ram was

identical. The rams were arranged such that a pair of rams acted on a single bearing plate along the top surface of the beam.
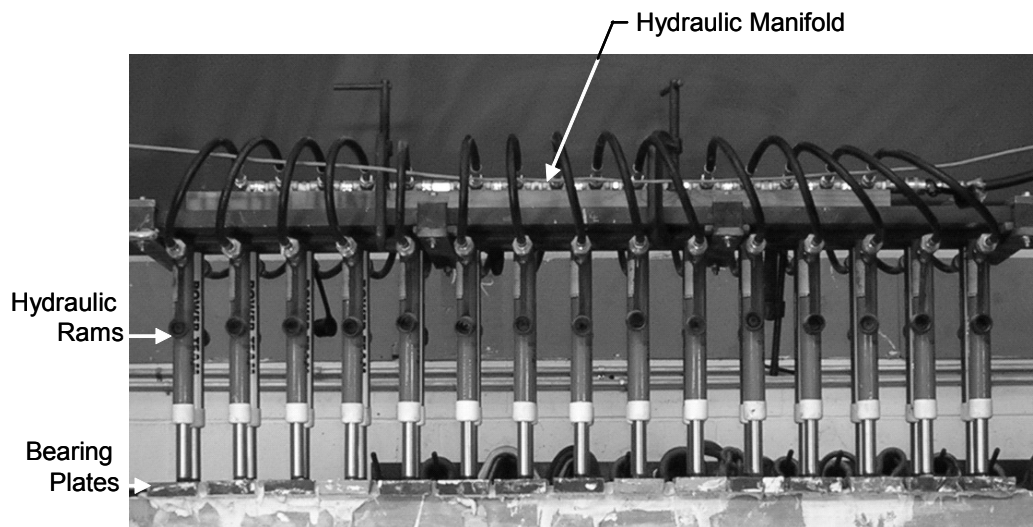
Figure 4-2: Loading apparatus for uniform load tests

4.3   BEAM TEST SERIES I

The first series of tests consisted of narrow ($b = 6in.$), deep ($h = 30in.$) beams subjected to distributed loads, concentrated loads, or pairs of concentrated loads. In each type of loading, the loads were placed asymmetrically on the beam specimens.

4.3.1   Details of Series I Specimens

The basic details of the series I specimens are shown in Figure 4-3. The figure shows only the details that were common to all ten specimens in this series. The beams had a 6 x 30 in. cross-section with an effective depth of 27 in. To prevent anchorage failures, the longitudinal bars were anchored with standard hooks that met ACI 318-05. The hook was positioned such that the bars could be fully developed outside the exterior edge of the bearing plate. In terms of strut-

and-tie modeling, the tie (longitudinal tension reinforcement) could be fully developed at the vertical face of the CCT node (outer face of the bearing plate) at each support.

In each test the load was placed asymmetrically within the 10 ft span. The various load configurations are shown in Figure 4-5. For each of the load configurations, failure was expected near the north support (as shown in Figure 4-3) due to the higher shear force at that section. To further that goal, the bearing plate used at the right support (triangle in Figure 4-5) was smaller than the bearing plate at the left support (circle in Figure 4-5). The smaller bearing plate was 6 x 6 in. and the larger plate was 6 x 8 in.

Notes:
1. 4 – No. 8 (Tension) and 2 – No. 3 bars (Compression)
2. Shear reinforcement varied
3. Longitudinal bars anchored with standard hooks. Hooks were confined with No. 3 stirrups spaced at 3 in.
4. Longitudinal bars: f_y = 68 ksi
5. Stirrups: f_y = 73 ksi
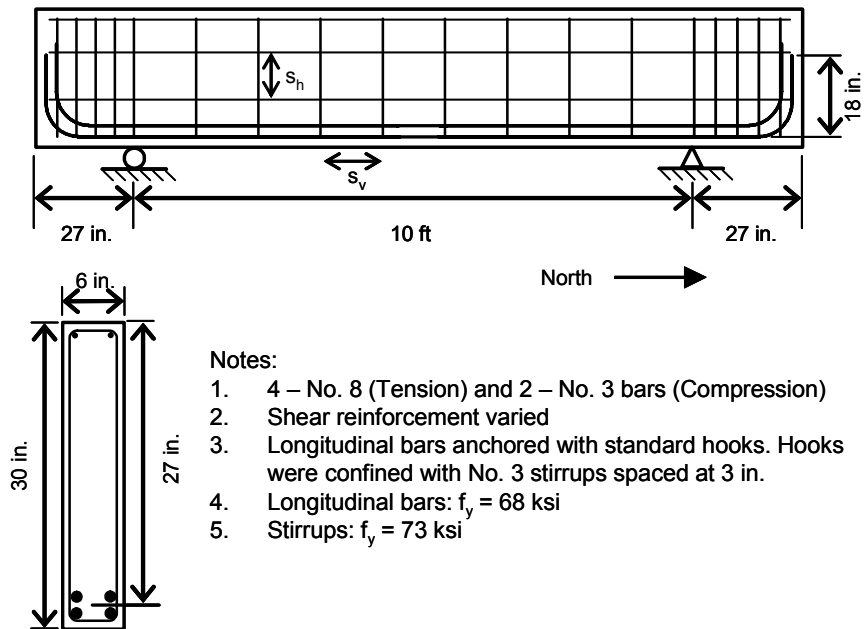
Specimen	Concrete Strength [psi]	Stirrup* Spacing, s_v [in.]	Spacing of Horizontal Shear Reinforcement[†], s_h [in.]
I-UL-8.5-0a	2440	8.5	N/A
I-UL-8.5-0b	2640	8.5	N/A
I-UL-0-0	3230	N/A	N/A
I-UL-0-8.5	2640	N/A	8.5
I-UL-17-17	2660	17	17
I-UL-17-0	2660	17	N/A
I-2C-8.5-0	3210	8.5	N/A
I-2C-0-0	3210	N/A	N/A
I-CL-8.5-0	2580	8.5	N/A
I-CL-0-0	2370	N/A	N/A

* Stirrups were No. 3 closed stirrups with two legs
[†]Horizontal shear reinforcement consisted of pairs of straight No. 3 bars placed inside the stirrups
Figure 4-3: Details of Series I specimens

Each of the ten specimens can be identified by a unique notation. The notations are explained in Figure 4-4. The first number is the series in which the beam was tested. The second set of characters indicates the type of loading that was applied to the beam. The loading configurations are shown in Figure 4-5. The third and fourth numbers are the spacing of the vertical and horizontal shear reinforcement in inches respectively. A value of zero in either placeholder indicates that no such reinforcement was used. Vertical shear reinforcement consisted of No. 3 closed stirrups, and horizontal shear reinforcement consisted of pairs of straight No. 3 bars. For specimens with horizontal shear reinforcement and without stirrups, the horizontal shear reinforcement was held in place with thin wire before concrete was cast so that he horizontal bars were placed in the same positions for all specimens.

Within the ten tests, there were two nominally identical specimens. Those two specimens are distinguished by the letters "a" and "b." Details of the specimens are given in Figure 4-3.

I-UL-8.5-0

— Spacing of horizontal shear reinforcement in in.

— Spacing of vertical shear reinforcement in in.

— Load Configuration:
UL: Uniform load
CL: Concentrated load
2C: Pair of concentrated loads

— Test Series (I, II, or III)
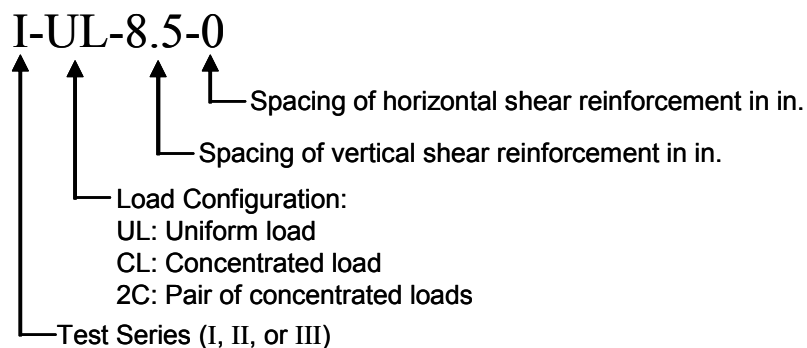
Figure 4-4: Nomenclature for Series I tests

108
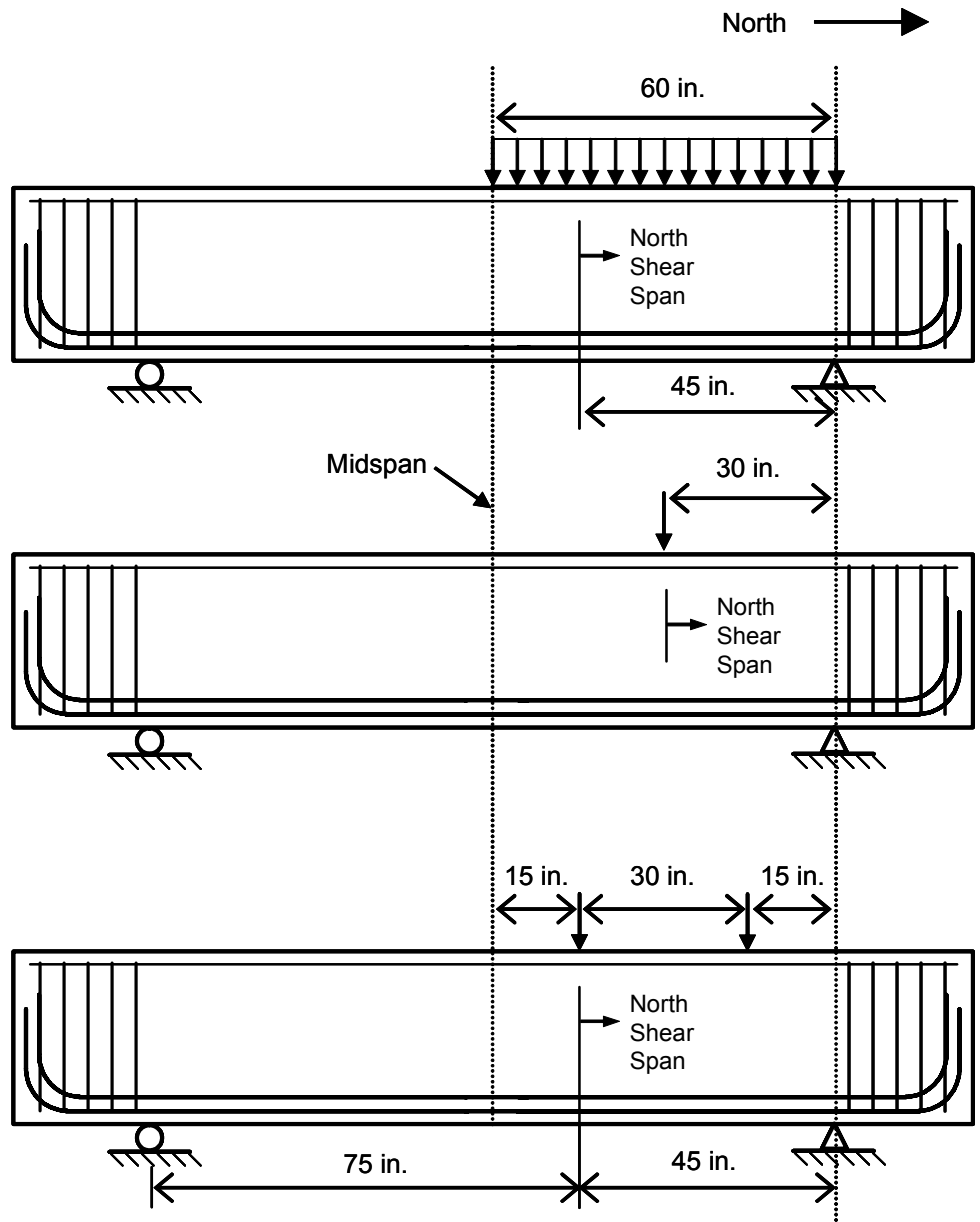
Figure 4-5: Load configurations for Series I tests (top: uniform load; middle: concentrated load; bottom: pair of concentrated loads)

4.3.2 Results of Series I Tests

During the tests a computerized data acquisition system was used to gather and record the data. In each test both of the support reactions were measured with load cells, and the applied load was monitored using a pressure transducer. The beams were tested such that the reaction at the North end of the beam was the greatest. In Figure 4-5 the North support reaction is indicated with a triangle.

For specimens that contained stirrups within the shear span, each stirrup within the shear span was instrumented with electrical resistance-type strain gages at two locations. The gages were placed at mid-height on each leg of the stirrups.

4.3.2.1 *Cracking and Failure Loads*

Periodically during the tests, the load was paused to observe cracks. The load at which cracks occurred was determined by visual inspection. The data from the internal and external strain gages were used to confirm the diagonal cracking load. For all tests, the visual observations regarding the loads at which cracks appeared were in good agreement with the data gathered electronically. The cracking and failure loads are listed in Table 4-1. The cracking loads listed in Table 4-1 are not necessarily the load at which the first crack formed. The cracking loads presented in the Table 4-1 are the loads at which a diagonal shear crack formed. Often small flexural cracks occurred near the location of maximum moment before the diagonal shear cracks; however, the shear cracks are most relevant to these test specimens. All loads listed in Table 4-1 include the shear due to the self-weight of the test specimen.

Table 4-1: Cracking and ultimate loads for Series I Specimens

Specimen	North Reaction [kip]	South Reaction [kip]	Failure Load [kip]	Diagonal Cracking Load [kip]	$\sum \dfrac{A_{si}}{bs_i} \sin \alpha_i$
I-UL-8.5-0a	161.7	59.7	221.4	64.3	0.003
I-UL-8.5-0b	142.5	56.6	199.1	69.9	0.003
I-UL-0-0	135.8	49.6	185.5	83.6	0
I-UL-0-8.5	123.9	48.7	172.6	103.5	0.003
I-UL-17-17[†]	138.5	52.6	191.0	84.1	0.003
I-UL-17-0	143.4	57.5	200.9	82.7	0.0015
I-2C-8.5-0	120.8	45.4	109.1	54.6	0.003
I-2C-0-0	91.1	33.6	125.7	82.6	0
I-CL-8.5-0	79.1	30.0	166.2	41.1	0.003
I-CL-0-0	92.2	33.5	124.6	68.3	0

[†]Specimen I-UL-17-17 failed in shear in the South shear span while all other specimens failed within the North shear span

The final column of Table 4-1 indicates the amount of shear reinforcement the specimen contained. The specimens contained various combinations of horizontal and vertical bars. To compare the various combinations, the equation presented in ACI 318-05 Appendix A (Eqn 4-1) was adopted. That equation is based on the components of the vertical and horizontal shear reinforcement perpendicular to the strut axis. If the value of $\sum \dfrac{A_{si}}{bs_i} \sin \alpha_i$ equals or exceeds

0.003, the strut is considered reinforced as per ACI 318-05 Appendix A provisions.

$$\sum \frac{A_{si}}{bs_i} sin\, \alpha_i \geq 0.003 \qquad (4\text{-}1)$$

Where: A_{si} = area of surface reinforcement in the ith layer crossing a strut

s_i = spacing of reinforcing bars in the ith layer adjacent to the surface of the member

b = the width of the strut perpendicular to the plane of the reinforcing bars

α_i = the angle between the axis of the strut and the bars in the ith layer of reinforcement crossing that strut

Figure 4-6 shows the ratio of shear at which diagonal cracking occurred to shear at the failure load as a function of the shear reinforcement in the beam. As was the case with the isolated strut test data (Chapter 3), there does not appear to be a strong correlation between the diagonal cracking load and the amount of reinforcement crossing the splitting crack. Prior to cracking, reinforcement does little to affect the strength of a reinforced concrete member.
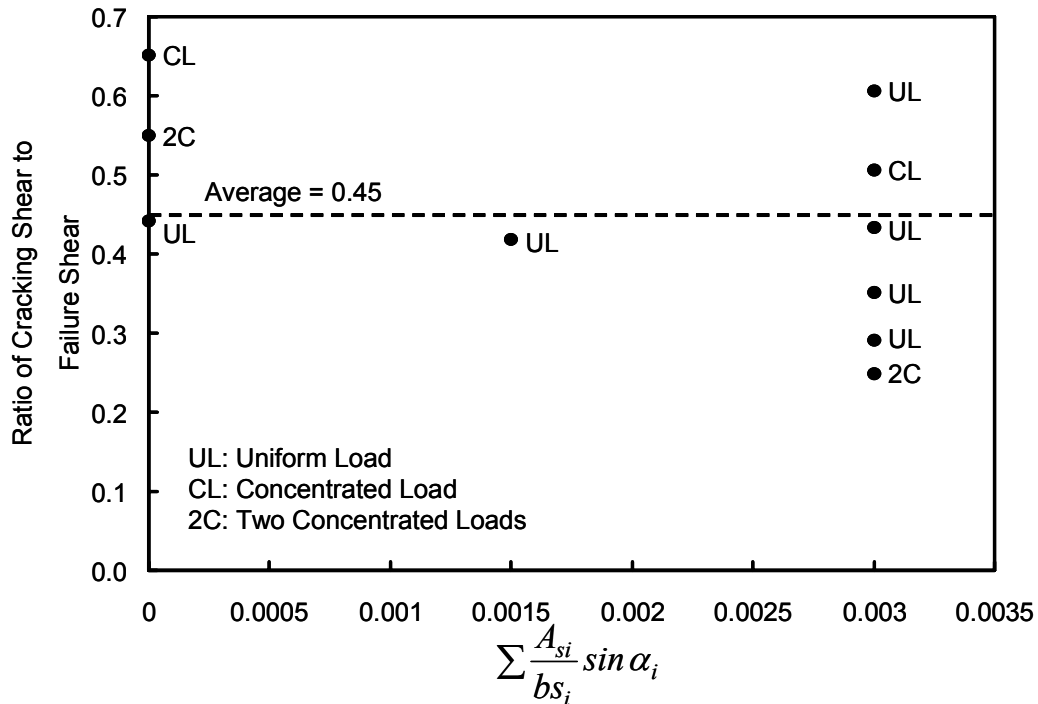
Figure 4-6: Ratio of shear at cracking to shear at ultimate for Series I specimens

4.3.2.2 Effect of Load Distribution

Specimens subjected to uniform loads failed at higher shear forces than the beams with one or two concentrated loads while the diagonal cracking loads remained similar (25% - 66% of the failure load) between load configurations. There does not appear to be a trend between the load distribution and the cracking load.

There were two sets of nominally identical specimens tested in Series I. The first set of beams was I-UL-0-0, I-2C-0-0, and I-CL-0-0 (shown in Figure 4-7). These beams had no shear reinforcement. Of these three beams, the specimen tested under uniform load carried the greatest shear while the remaining two specimens failed at nearly the same shear force.

For Specimen I-UL-0-0 (at bottom in Figure 4-7) the crack along which the shear failure occurred did not propagate towards the centroid of the uniform load. Instead the crack propagated towards the point at which the shear was zero. For the specimens that were subjected to a uniform load, the point of zero shear was located 45 in. from the North reaction. That point is marked in the bottom photograph in Figure 4-7.

In the tests where two concentrated loads were applied, one of the loads (the load nearer midspan) was applied at 45 in. from the North support. That location coincided with the point of zero shear. In Specimen I-2C-0-0, as was the case with Specimen I-UL-0-0, the failure crack propagated towards the point where the applied shear was zero. The shape of the failure cracks in Specimens I-UL-0-0 and I-2C-0-0 are similar while the cracking pattern of Specimen I-CL-0-0 is different. The similar cracking patterns for the specimens with uniform or two concentrated loads indicate that these two load distributions are inducing comparable levels of distress in the specimens.
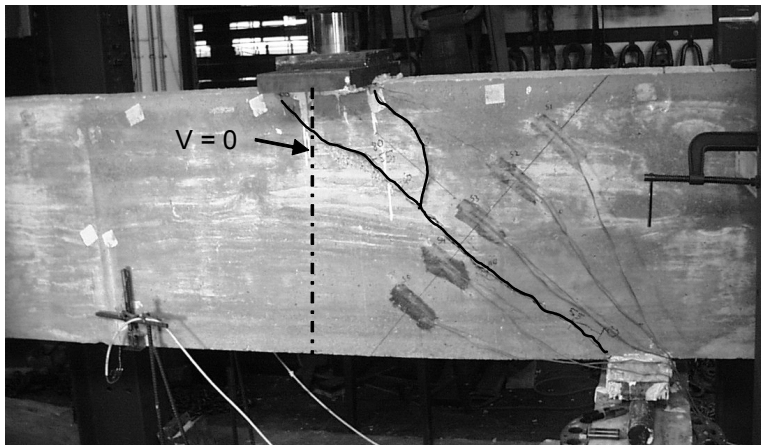
Specimen: I-CL-0-0
V_{cr} = 60.0 kip
V_{Max} = 92.2 kip
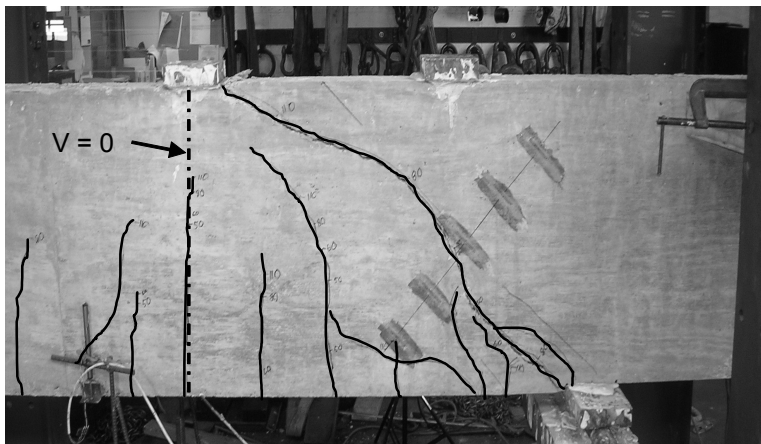
Specimen: I-2C-0-0
V_{cr} = 50.0 kip
V_{Max} = 91.1 kip
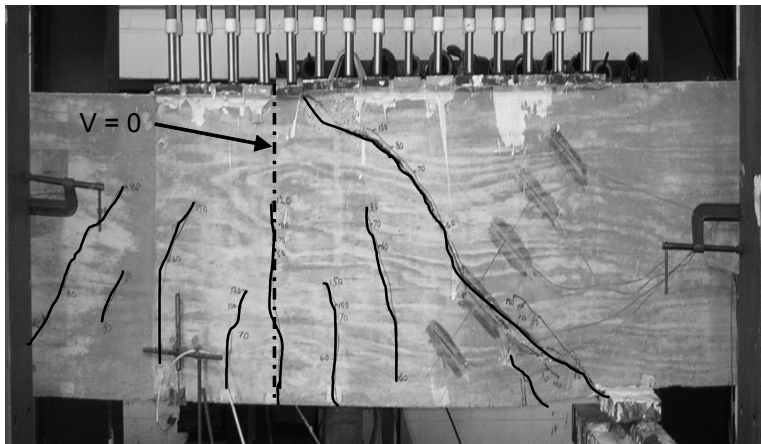
Specimen: I-UL-0-0
V_{cr} = 60.0 kip
V_{Max} = 135.8 kip

Figure 4-7: Comparison of load distributions and cracking patterns (specimens without shear reinforcement)

The other set of nominally identical beams (I-UL-8.5-0a, I-UL-8.5-0b, I-2C-8.5-0, and I-CL-8.5-0) shows a similar trend (Figure 4-8). Specimen I-CL-8.5-0 failed at the lowest shear force of the ten specimens tested in this series, and specimen I-UL-8.5-0a carried the greatest shear force. As the load distribution became more uniform, the shear strength of the beams increased. It is interesting to note that this trend could be observed in beams with (Figure 4-7) and without (Figure 4-8) shear reinforcement.

In Specimens I-UL-8.5-0a and I-UL-8.5-0b all of the cracks propagated towards the point of zero shear as in the companion specimen without shear reinforcement (I-UL-0-0). Also, the crack distributions of Specimens I-CL-8.5-0a and I-UL-8.5-0b are similar to those of companion specimens that contained no shear reinforcement (Specimen I-CL-0-0).

For both sets of nominally identical beams, the cracking pattern was similar for specimens with the same configuration of applied load. The specimens with uniform load or two concentrated loads the cracks were much more distributed. For the specimens with a single concentrated load, the cracking pattern was dominated by a single crack that formed between the load point and the reaction. The differences in cracking pattern may be indicative of different load-carrying mechanisms in the specimens with uniform load or two concentrated loads.
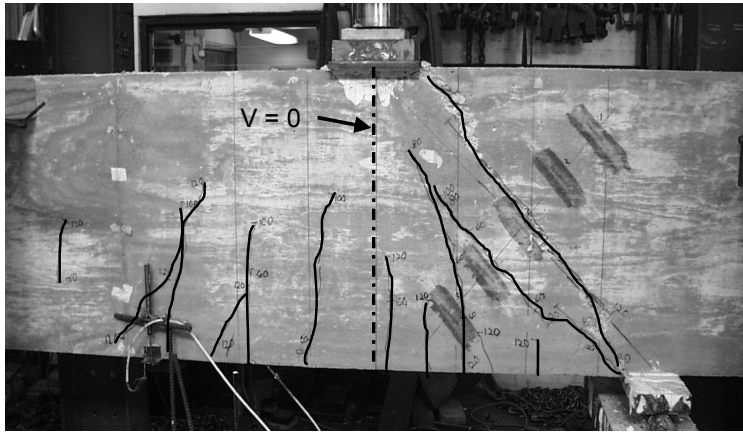
Specimen: I-CL-8.5-0
V_{cr} = 40.0 kip
V_{Max} = 79.1 kip
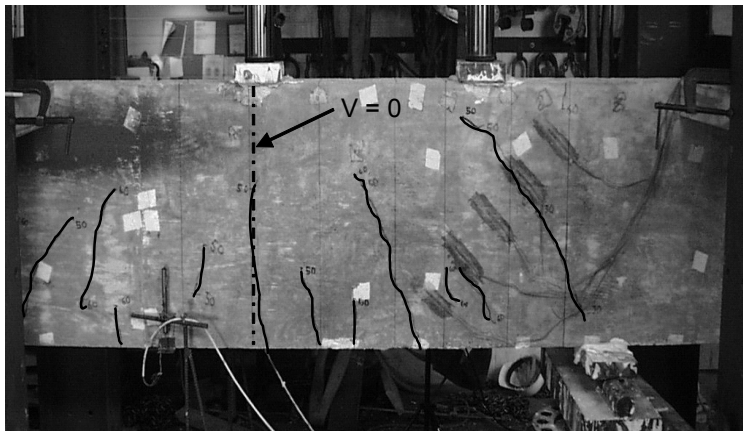
Specimen: I-2C-8.5-0
V_{cr} = 30.0 kip
V_{Max} = 120.8 kip
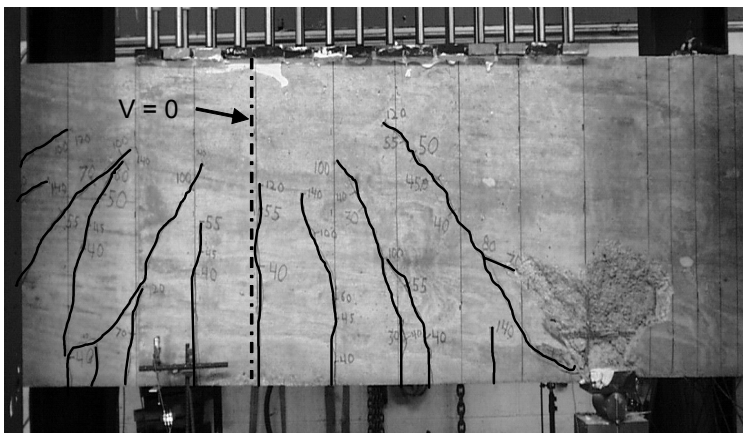
Specimen: I-UL-8.5-0b
V_{cr} = 50.0 kip
V_{Max} = 142.5 kip

Figure 4-8: Comparison of load distributions and cracking patterns (specimens with stirrups spaced at 8.5 in.)

117

4.3.2.3 *Effect of Reinforcement*

Photographs of all the specimens subjected to uniform loads can be seen in Figure 4-9. Those photographs show the specimen after failure. The specimens shown in Figure 4-9 are identical except for the shear reinforcement. The concrete strength within those members was nominally identical. The details of the specimens are given in Figure 4-3.

Of the six specimens loaded with uniform load, only two contained no vertical shear reinforcement. Although the two specimens (I-UL-0-0 and I-UL-0-8.5) carried the least shear of the six beams; the shear strength was only slightly lower than the others. The specimen with only horizontal shear reinforcement carried about 10% less shear than the specimen with no shear reinforcement. Tests I-UL-0-0 and I-UL-0-8.5 indicate that the horizontal shear reinforcement did not improve the shear strength of the specimen. Specimens I-UL-17-0 and I-UL-17-17 had identical vertical shear reinforcement, and one of the two beams had horizontal shear reinforcement. The specimens with both horizontal and vertical reinforcement (I-UL-17-17) carried slightly less shear (5%) than the specimen with vertical stirrups only (I-UL-17-0). However, Specimen I-UL-17-17 failed in the South shear span outside the distributed load. The failure of this specimen is discussed in detail in a later portion of this chapter.

The horizontal shear reinforcement was anchored into the ends of the beam that were overhanging the supports. Each of the horizontal bars had an embedment depth that exceeded the bar development length as determined using ACI 318-05.
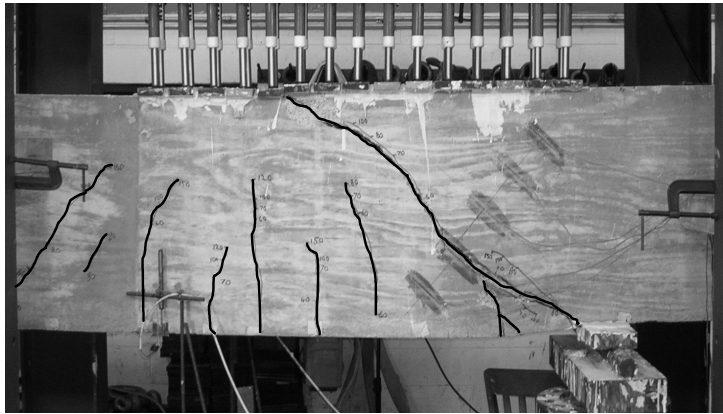
Specimen: I-UL-0-0
V_{Max} = 135.8 kip
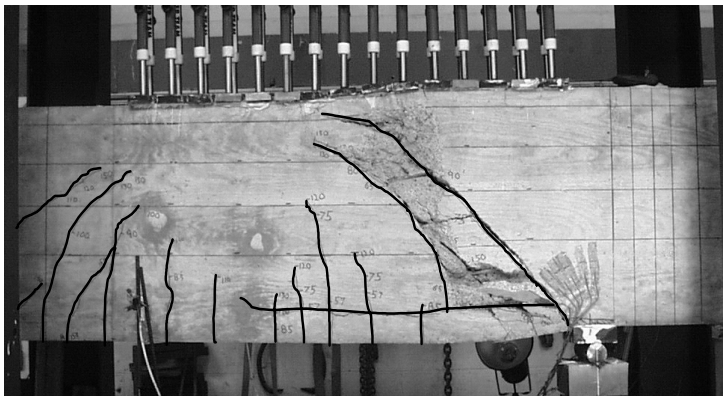
Specimen: I-UL-0-8.5
V_{Max} = 123.9 kip
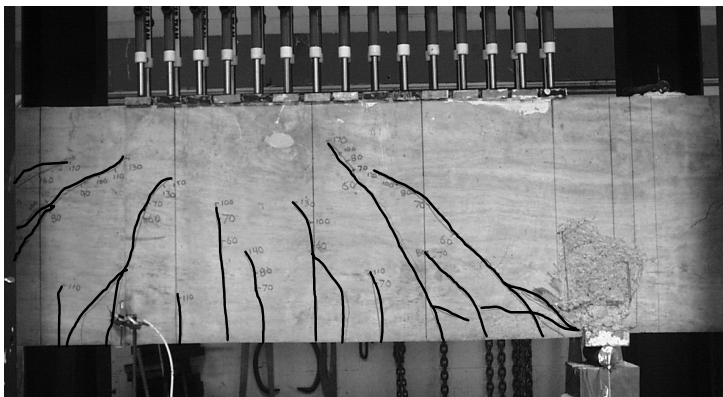
Specimen: I-UL-17-0
V_{Max} = 143.4 kip

Figure 4-9: Photographs of specimens with uniform load

119
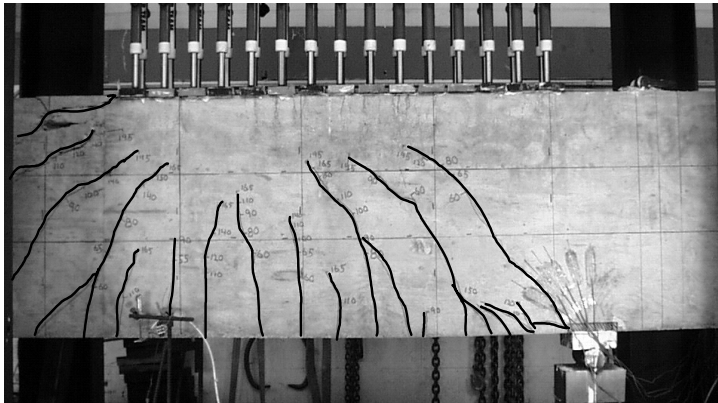
Specimen: I-UL-17-17
V_{Max} = 138.5 kip
V_{South} = 52.6 kip
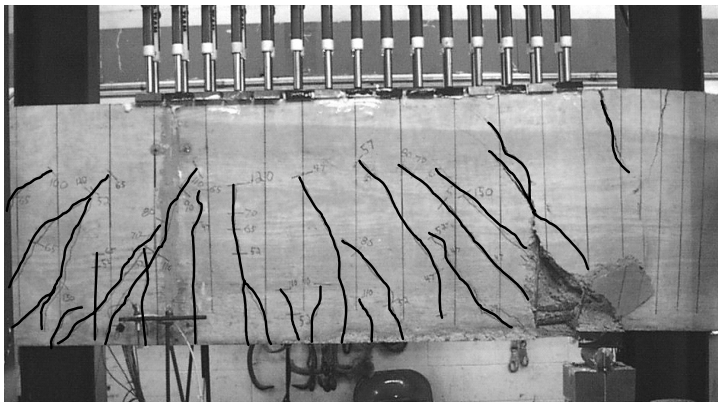
Specimen: I-UL-8.5-0a
V_{Max} = 161.7 kip
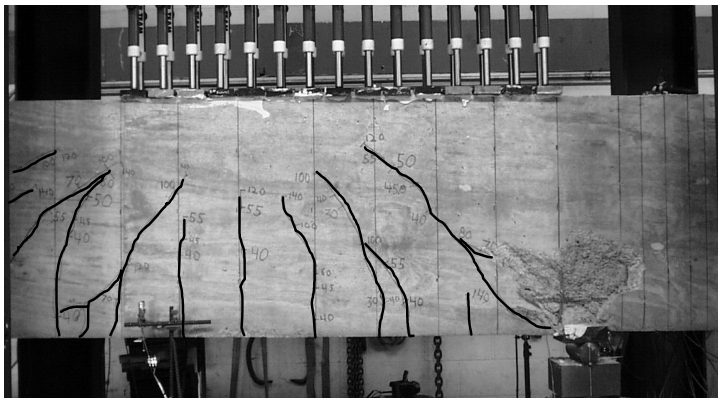
Specimen: I-UL-8.5-0b
V_{Max} = 142.5 kip

Figure 4-9 – continued: Photographs of specimens with uniform load

120

Unlike horizontal shear reinforcement, small amounts of vertical shear reinforcement improved shear strength. Specimens I-UL-17-0, I-UL-8.5-0a, and I-UL-8.5-0b all had similar modes of failure. That mode involved concrete crushing at the North reaction. Those same three specimens also carried the three greatest shear forces. Specimen I-UL-17-0 had only half as much vertical shear reinforcement as Specimen I-UL-8.5-0, but the same mode of failure resulted. These tests indicate that only a small amount of vertical shear reinforcement is necessary to change the mode of failure from diagonal tension (Specimen I-UL-0-0) to concrete crushing adjacent to the node (Specimens I-UL-17-0). Additional increases in shear reinforcement did not seem to produce any additional shear strength. Specimens I-UL-8.5-0a and I-UL-8.5-0b carried peak shear forces of 161.7 kip and 142.5 kip respectively. Specimen I-UL-17-0 carried a peak shear force of 143.4 kip. Reducing the spacing of the shear reinforcement from 17 in. (Specimen I-UL-17-0) to 8.5 in. (Specimens I-UL-8.5-0a and I-UL-8.5-0b) did not result in significant increases in strength.

4.3.2.4   Strain Distributions

In the isolated strut tests (Chapter 3), strain gages were attached to the concrete surface. The gages were aligned with the strut axis and distributed across the half the panel width. The locations of the surface strain gages as well as the range of strain data collected during the isolated strut tests are shown in Figure 4-10. All of the measured strains from the panel tests lie within the grey area of the plot in Figure 4-10. The distribution of strains parallel to the axis of the strut from the isolated strut tests was compared to similar readings from the beams tests of Series I.
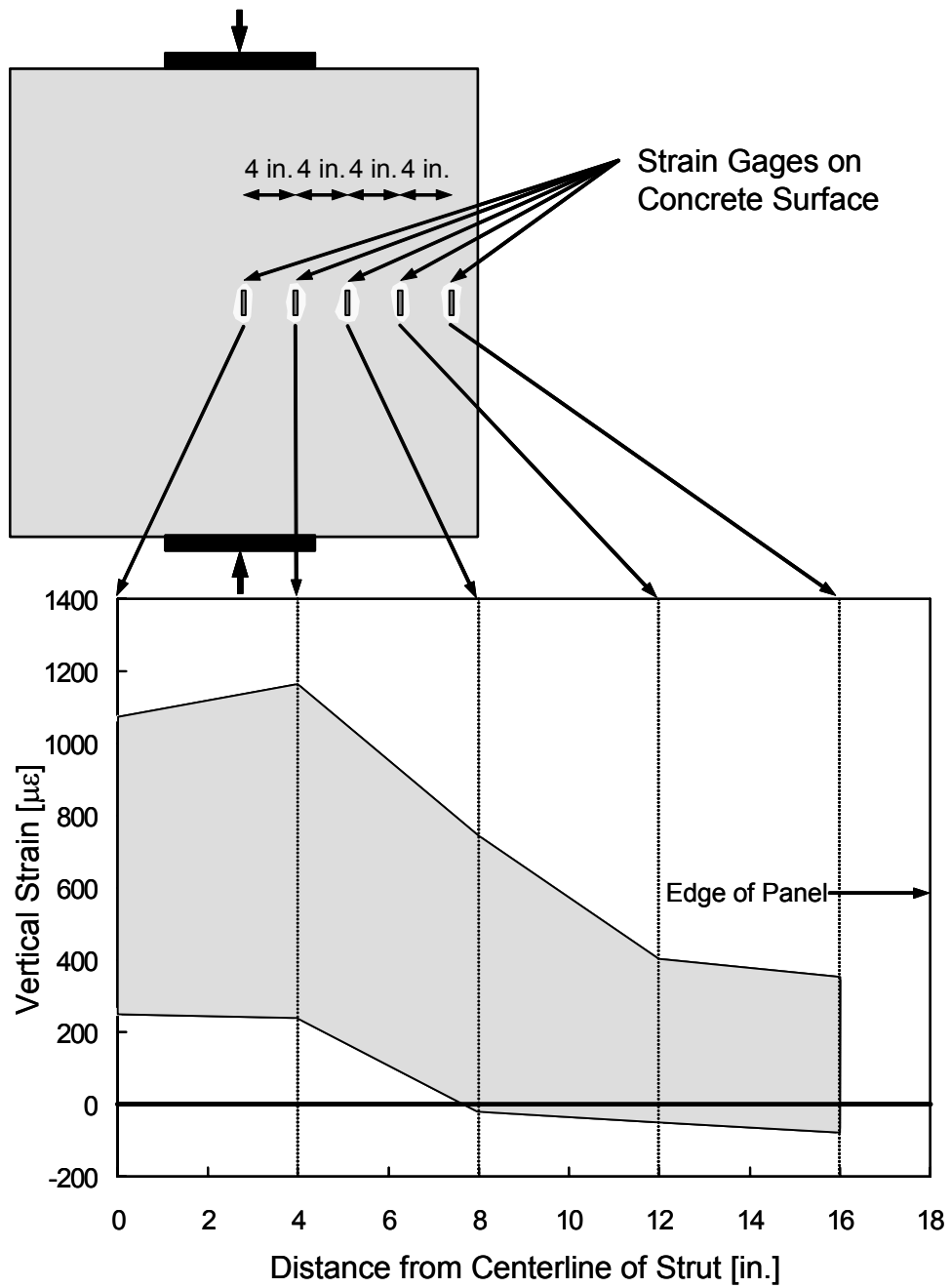
Figure 4-10: Strain distributions from isolated strut tests

The location of the surface strain gages for the beams tests is shown in Figure 4-11. The surface gages were oriented to measure strains that are parallel to the strut axis. The strain distribution in a beam was not expected to be symmetric as in the isolated strut tests. Therefore, gages were placed on both sides of the strut axis as shown in Figure 4-11.
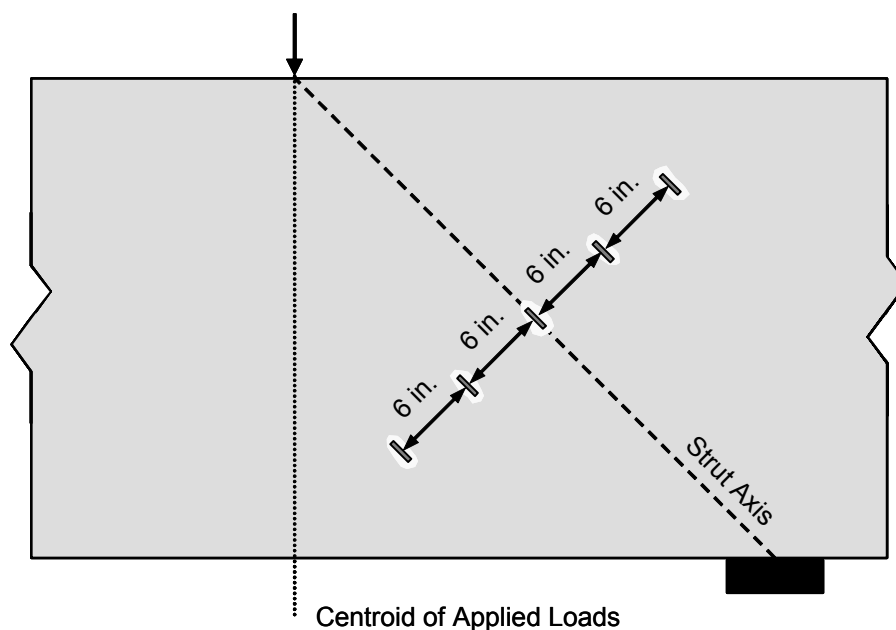
Figure 4-11: Location of surface gages on Series I specimens

The strain distributions from the two specimens with single concentrated loads are shown in Figure 4-12. In Figure 4-12, the negative values of distance from the strut axis correspond with strain gages below and to the left of the strut axis, e.g. strain gages closer to the extreme tension fiber (Figure 4-11). The specimens with single concentrated loads were expected to produce strain distributions that were similar to the isolated strut tests. The strain distributions from Specimens I-CL-0-0 and I-CL-8.5-0 fell within the range of axial strains measured in the isolated struts. Additionally, the distributions of the strains were similar. The peak strain was measured on the strut axis and the magnitude of the

123

strain decreased with distance from the axis. The similarity between the strain distributions measured in the isolated struts and the deep beams with single concentrated loads indicates that a single strut is forming between the reaction and the applied load.

The strain distributions from beams loaded with two concentrated loads or uniform loads (Figure 4-13) were very different from the distributions produced by single loads (Figure 4-12). There was no sharply defined peak in the distributions from beams with multiple loads. Rather, the distributions were largely uniform with the exception of the large tensile strains recorded by the surface strain gages nearest the tension face of the beam. The lack of a distinct peak in the strain distributions shown in Figure 4-13 indicates that a single strut did not form between the centroid of the applied loads and the support. These data suggest different load-carrying mechanisms, or truss models, for beams loaded with single concentrated loads and beams with multiple loads, e.g. two loads or uniform load, are different.
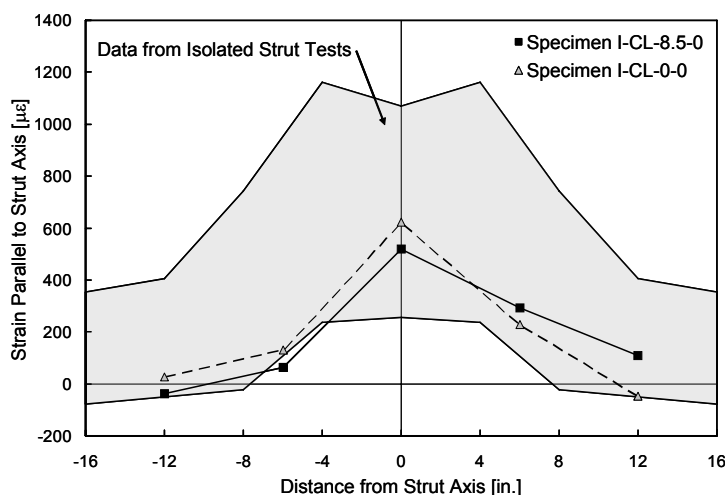
Figure 4-12: Strain distributions from beams with single concentrated loads

124
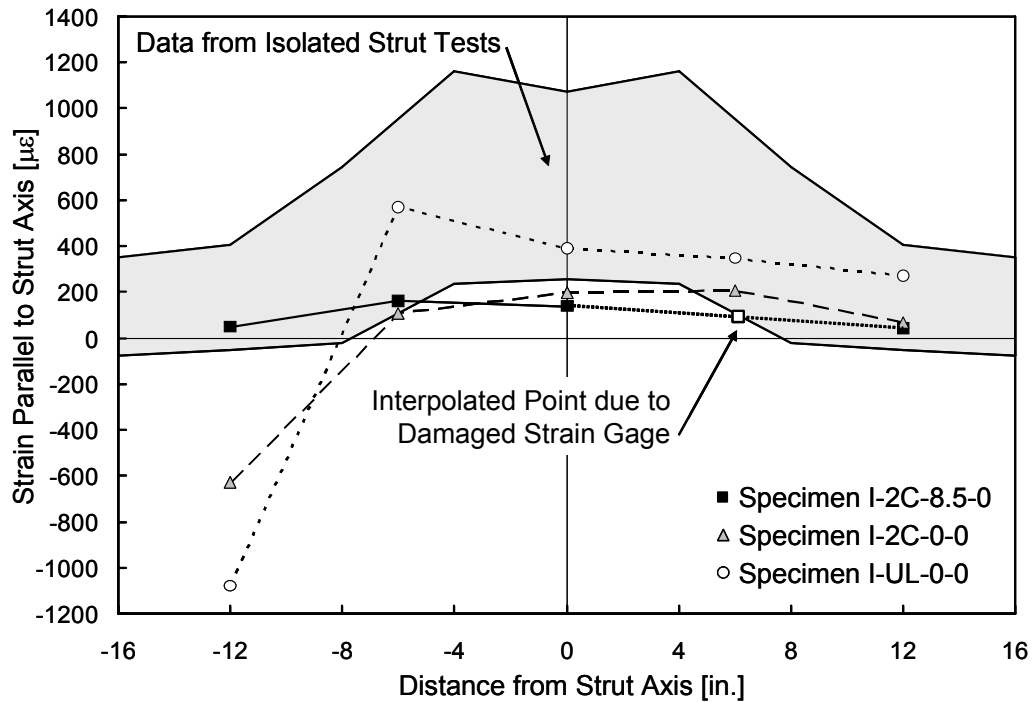
Figure 4-13: Strain distributions from beams with two concentrated loads and uniform loads

4.3.2.5 Observations for Series I Tests

The failure of specimens in Series I involved concrete crushing adjacent to the support. However, before failure occurred, two nearly parallel shear cracks were observed in many of the tests. The formation of the parallel shear cracks occurred between 70 and 80% of the failure load. This type of cracking was indicative of impending shear failure.

The strain distribution in a deep beam subjected to a single concentrated load was similar to that which was observed in the isolated strut tests (Chapter 2). As the load distributions became more uniform, the strain distribution also became more uniform indicating the presence of a different load-carrying mechanism for the uniformly loaded beams.

125

4.3.3 Application of Code STM Provisions to Series I Specimens

All of the specimens tested in Series I fall under the STM provisions of both ACI 318-05 and AASHTO LRFD Bridge Design Specifications. Each of those codes was used to determine the capacity of the Series I specimens. That capacity was then compared with the measured capacity.

The same truss models were used for calculations based on ACI and AASHTO LRFD. Three different truss models were used for the three different load distributions. The trusses are shown in Figure 4-14. In each case the critical element of the various truss models was the interface between the CCT node above the reaction that supports three-quarters of the total applied load and the diagonal strut that abuts that node. That CCT node and strut were designed to be critical regardless of the load distributions. Based on the calculations performed in accordance with code provisions, all of the Series I specimens were expected to have the same mode of failure: crushing in the strut adjacent to the CCT node.
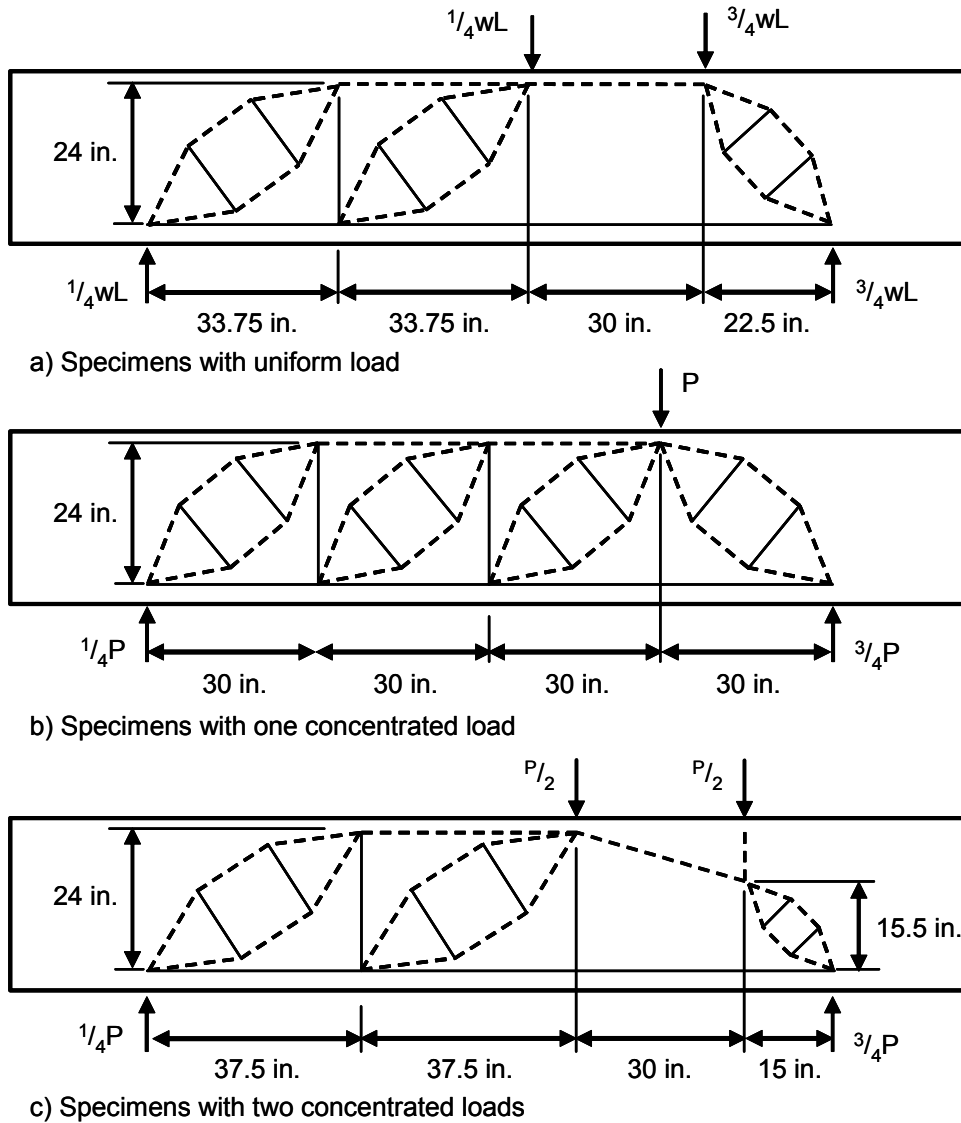
Figure 4-14: Truss models used for code-based calculations

Some explanation of the truss model used for uniformly loaded specimens (Figure 4-14a) is warranted. Based on the strain distributions presented in the preceding section, two concentrated loads were chosen to model the uniformly distributed load. In order to maintain a simple model, the two loads that model the uniform load were not equal to one another. The ratio of the two loads was made

equal to the ratio of the two support reactions. As such, the right-hand point load was set equal to three-quarters of the total applied load and the left-hand load was equal to one-quarter of the total applied load. The concentrated loads were then placed at the centroids of the portions of the uniform load they were intended to model.

Using this load distribution yields the truss model that is the simplest to work with. A truss model similar to that shown in Figure 4-14c could have been used to model the uniform load. However, for that truss model four equations had to be solved simultaneously to determine the proper inclination of the strut that enters the right-hand support. By distributing the loads as described in the previous paragraph for the specimens tested under uniform load, the inclination of the diagonal strut at the right-hand support was known and hence there was no need to solve simultaneous equations.

4.3.3.1 Application of ACI 318-05 STM Provisions

Prior to constructing all of the specimens, a detailed strut-and-tie model was developed for each specimen. Those strut-and-tie models indicated that the capacity of the specimens was limited by the inclined strut that frames into the North reaction. Therefore only the stress check for the strut and the abutting node are presented here.

As per ACI 318-05 the strength of a strut is determined by:

$$f_{ce} = 0.85 \beta_s f_c' \qquad\qquad (4\text{-}2)$$

Where: β_s = the strut efficiency factor

= 0.75 for bottle-shaped struts satisfying Eqn 4-1

= 0.60 for bottle-shaped struts not satisfying Eqn 4-1

f_c' = the concrete compressive strength

f_{ce} = effective compressive strength

128

The effective stress in a strut, f_{cu}, was then multiplied by the area of the end of the strut. The area of the end of the strut is equal to the area of the inclined face of the CCT node. A schematic representation of the CCT node can be seen in Figure 4-15. For all of the specimens tested in Series I $l_b = 6in.$ and $w_t = 6in.$ The angle of inclination, θ, varied based on the load distribution on the specimen in question (Figure 4-14). The node was assumed to act over the full width of the cross-section ($b = 6in.$). Based on the concrete strength, nodal area, and efficiency factor, which was a function of the reinforcement in the strut, the strength of the critical element of the strut-and-tie model could be determined. The nominal capacities of the specimens as per ACI 318-05 are shown in Table 4-2. The measured loads listed in Table 4-2 include the self-weight of the specimen.
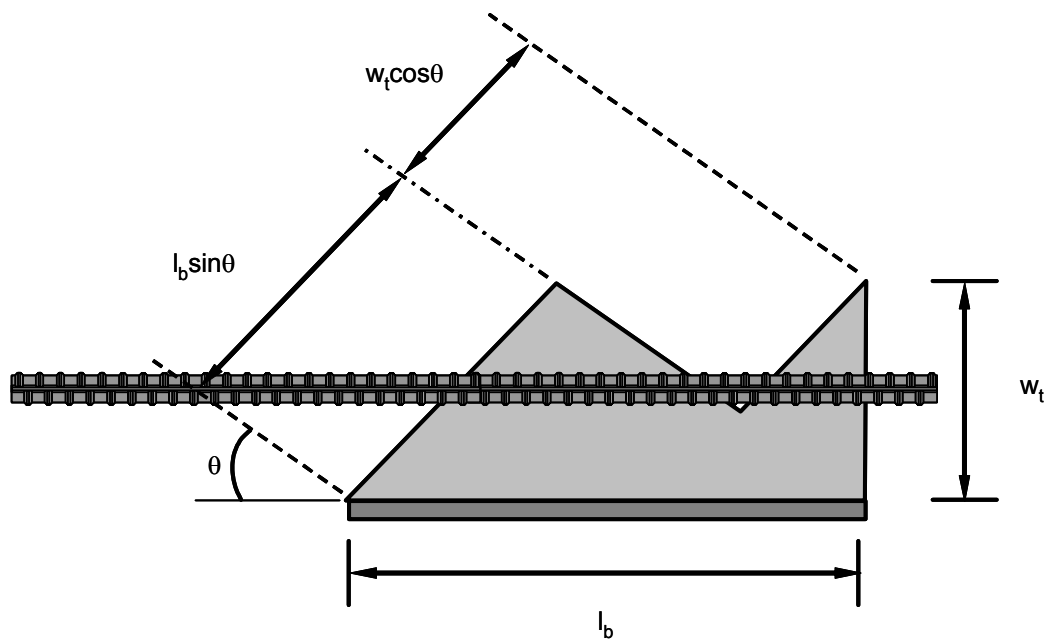
Figure 4-15: Elevation of critical CCT node

Table 4-2: Nominal capacities as per ACI 318-05

Specimen	Nominal Capacities [kip]	Total Measured Load [kip]	Ratio of Measured Load to Nominal Capacity
I-UL-8.5-0a	80.5	221.4	2.75
I-UL-8.5-0b	87.2	199.1	2.28
I-UL-0-0	85.2	185.5	2.18
I-UL-0-8.5	87.2	172.6	1.98
I-UL-17-17	87.6	191.0	2.18
I-UL-17-0	70.1	200.9	2.87
I-2C-8.5-0	74.7	109.1	1.46
I-2C-0-0	54.8	125.7	2.30
I-CL-8.5-0	98.2	166.2	1.69
I-CL-0-0	78.6	124.6	1.59
		Average:	2.13
		Coefficient of Variation:	0.22

The STM provisions of ACI 318-05 yielded conservative estimates of strength for all ten test specimens in Series I. However, the level of conservatism may be excessive. For six of the ten specimens, the nominal capacity calculated using ACI 318-05 Appendix A provisions less than half the measured strength. However, five of those six specimens were subjected to uniformly distributed load. Based on the strain distributions in the previous section, a uniform load is a much less demanding distribution of load than a concentrated load. Therefore, excessive levels of conservatism for the specimens with uniform load were

expected. The two specimens with concentrated loads had ratios of measured strength to nominal capacity that were less than the average value of 2.13.

4.3.3.2 *Application of AASHTO LRFD STM Provisions*

The STM provisions of AASHTO LRFD Bridge Design Specifications are more complex than those in ACI 318-05. The AASHTO provisions were discussed in detail in Chapter 2, and for the reader's convenience the basic equations of the procedure are repeated here:

$$f_{cu} = \frac{f_c'}{0.8 + 170\varepsilon_1} \leq 0.85 f_c' \qquad (4\text{-}3)$$

$$\varepsilon_1 = \varepsilon_s + (\varepsilon_s + 0.002)\cot^2 \alpha_s \qquad (4\text{-}4)$$

Where: α_s = the smallest angle between the compressive strut the adjoining tie

ε_s = the tensile strain in the concrete in the direction of the tension tie

f_c' = specified concrete strength

f_{cu} = effective compressive strength

The two primary inputs into the above equations are the inclination of the strut and the strain in the direction of the tie. The inclination of the strut was based on the truss model used and the tie strains were measured during the test. Tie strains were measured by strain gages that were placed on the longitudinal reinforcing bars at the center of the node. The node geometry used by AASHTO LRFD is identical to that which is used by ACI 318-05 (Figure 4-15). The results of the AASHTO LRFD STM based design calculations are shown in Table 4-3 along with the measured loads which include the specimens self-weight.

131

Table 4-3: Nominal capacities as per AASHTO LRFD (measured strains)

Specimen	Measured Tie Strain	Nominal Capacity [kip]	Total Measured Load [kip]	Ratio of Measured Load to Nominal Capacity
I-UL-8.5-0a	0.0003	89.8	221.4	2.47
I-UL-8.5-0b	0.0004	96.5	199.1	2.06
I-UL-0-0	0.0006	116.0	185.5	1.60
I-UL-0-8.5	0.0008	93.4	172.6	1.85
I-UL-17-17	0.0003	97.7	191.0	1.95
I-UL-17-0	0.0004	96.9	200.9	2.07
I-2C-8.5-0	0.0008	67.9	109.1	1.61
I-2C-0-0	0.0005	64.5	125.7	1.95
I-CL-8.5-0	0.0003	100.6	166.2	1.65
I-CL-0-0	0.0002	101.7	124.6	1.23
			Average:	1.84
			Coefficient of Variation:	0.18

The nominal capacities determined using AASHTO LRFD are slightly less conservative than their ACI 318-05 counterparts. However, there was still a wide margin between the calculated and measured capacities. The coefficients of variation of the ratio of measured to calculated strength for ACI 318-05 and AASHTO LRFD are only slightly different. The increased complexity used in AASHTO LRFD did not result in increased accuracy in predicting the capacity of these ten specimens.

The strain data in the table above was used to calculate the nominal capacities of the tests specimens using the provisions of AASHTO LRFD. However, such data would not be available to a design engineer. A designer would calculate the expected strain in the tie due to the factored force in the tie. Then the capacity of the strut adjoining the tie would be determined. The above procedure was also carried out on the specimens in Series I. The results of those calculations are shown in Table 4-4.

Table 4-4: Nominal capacities as per AASHTO LRFD (calculated strains)

Specimen	Calculated Tie Strain	Nominal Capacity [kip]	Total Measured Load [kip]	Ratio of Measured Load to Nominal Capacity
I-UL-8.5-0a	0.00062	87.4	221.4	2.53
I-UL-8.5-0b	0.00067	94.4	199.1	2.11
I-UL-0-0	0.00081	114.0	185.5	1.63
I-UL-0-8.5	0.00062	94.8	172.6	1.82
I-UL-17-17	0.00067	94.8	191.0	2.02
I-UL-17-0	0.00067	94.8	200.9	2.12
I-2C-8.5-0	0.00065	69.1	109.1	1.58
I-2C-0-0	0.00060	63.7	125.7	1.97
I-CL-8.5-0	0.00081	95.2	166.2	1.75
I-CL-0-0	0.00081	95.2	124.6	1.31
			Average:	1.88
			Coefficient of Variation:	0.18

The calculated values of strain in the direction of the tie are very small in magnitude. These test specimens were intended to fail in shear rather than flexure. To assure the shear failure occurred, the beams contained large amounts of flexural reinforcement. As the amount of flexural reinforcement increased, the amount of steel in the tie also increased. The capacity of the ties was much greater than needed to maintain equilibrium at the node. Therefore the calculated strains in the direction of the tie are rather small.

The use of calculated tie strains (Table 4-4) resulted in similar values as did the use of the measured vales of strain (Table 4-3). The average values of the ratio of measured capacity to nominal capacity were 1.84 and 1.88 for the two methods of determining the strain in the direction of the tie. The coefficients of variation were identical.

It should be noted that none of the ten specimens tested in Series I satisfied the required crack control reinforcement stipulated in Section 5.6.3.6 of AASHTO LRFD. The requirement specifies a reinforcement ratio of 0.003 in the horizontal and vertical directions.

4.4   BEAM TEST SERIES II

The specimens used in the second series of tests had two different cross-sections. The first section was square ($h = b = 18in.$) and the second cross-section had a width greater than the height ($b = 30in.$ and $h = 18in.$). The beam-sections used in Series I were tall and narrow. The specimens in Series II were constructed with cross-sections that were similar to traditional bent caps, which are generally square. The Series II tests were designed to examine the effects of beam width on shear strength.

Test specimens are often loaded using bearing plate widths (perpendicular to the longitudinal axis of the beam) that are equal to the width of the specimen.

However, bent caps may not loaded in the same manner. A single interior bent cap supports the ends of two beams. The ends of the beams are supported on separate bearing pads that cover much less than the full width of the beams. Figure 4-16 shows a plan view of the bearing area used in a typical TxDOT bent cap that supports Type C TxDOT pretensioned girders. The hatched areas represent the locations of the bridge bearings.
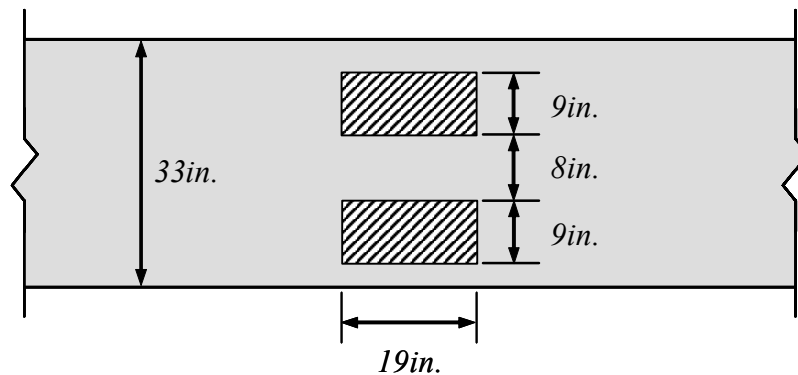
Figure 4-16: Plan view of typical bent cap bearings

The Series II specimens were loaded asymmetrically. These beams were subjected to single concentrated loads that were placed much nearer to one support than the other. Most shear tests have been conducted on symmetric specimens but many bent caps are asymmetrically loaded. The bent cap shown in Figure 4-17 supports the Northbound lanes of US 183 at the intersection with IH 35 in Austin, Texas.
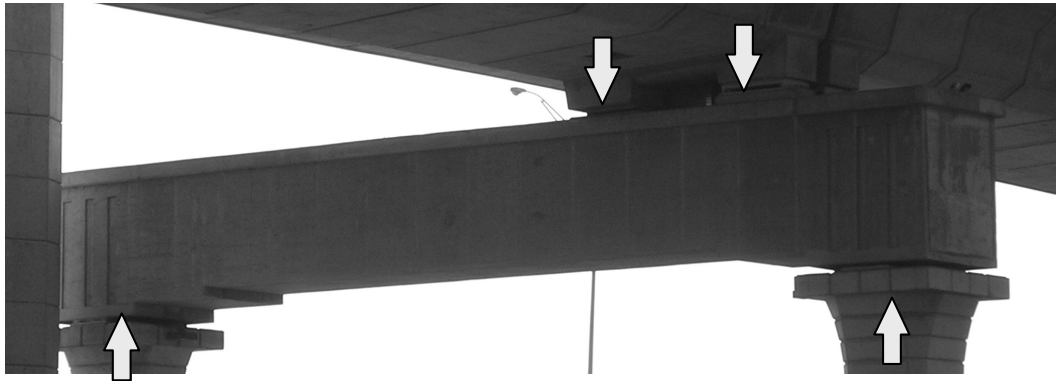
Figure 4-17: Asymmetrically loaded bent cap

4.4.1 Details of Series II Specimens

The two cross-sections used for the specimens in Series II are shown in Figure 4-18. Both sections contained No. 8 bars for the longitudinal reinforcement, No. 3 bars for the compression reinforcement, and No. 3 closed stirrups. Cross-section N had eight No. 8 bars and cross-section W had 15 No. 8 bars. Approximately the same longitudinal reinforcement ratio was present in both cross-sections (2.2% for N and 2.5% for W).
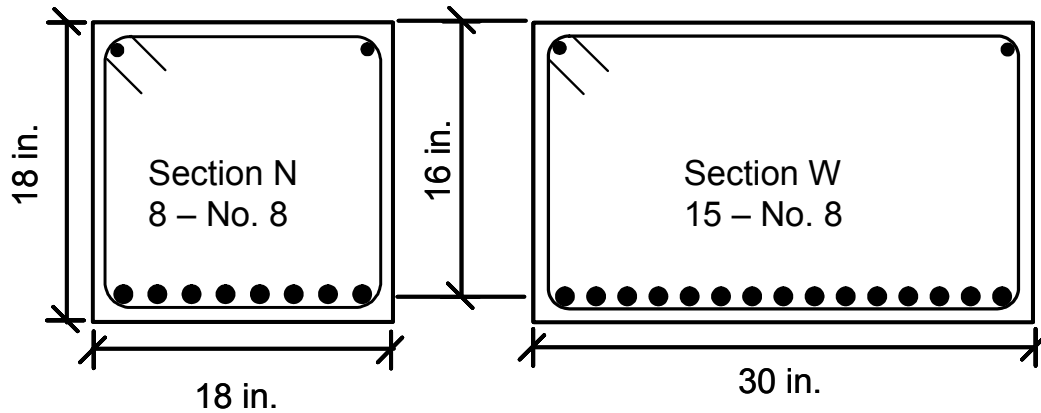
Figure 4-18: Cross-sections N and W

The concentrated load was placed on the beam as shown in Figure 4-19. The center of the concentrated load was located 27 in. away from the center of the North support and the distance to the South support was varied. The shear span-to-depth ratio for the North portion of the span was 1.68. The shear span on the South portion of the beams varied between 48 and 93 in. Accordingly, the shear span-to-depth ratio for the South portion of the span varied between 3.0 and 5.8.
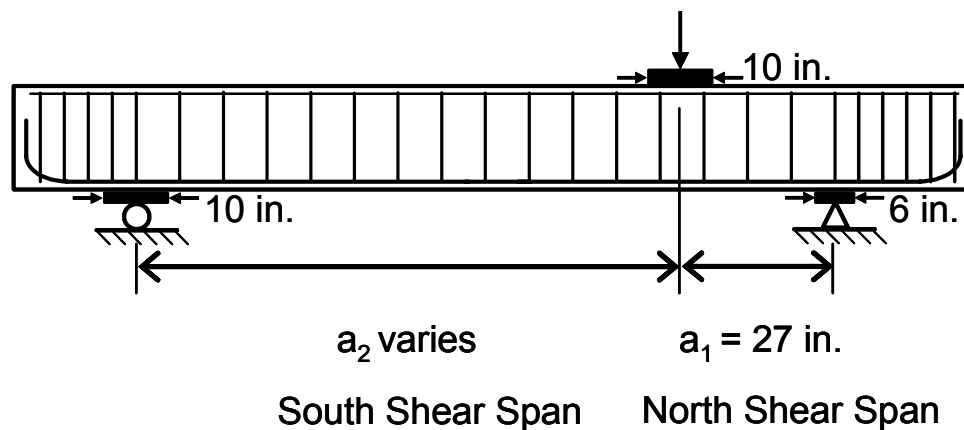
Figure 4-19: Schematic drawing of Series II tests

The bearing plate beneath the load was 10 in. wide (along the length of the beam) and covered the full width of the beam (perpendicular to the span). The bearing plate at the South reaction (the circle in Figure 4-19) had the same size and orientation.

Three different bearing plate arrangements were used for the North reaction (triangle in Figure 4-19). Each of those bearing plates was 6 in. long (parallel to the span). Only the width (perpendicular to the span) varied. All three layouts are shown in Figure 4-20. The E bearing was used to examine the effects of a bearing in which the load was applied through two separate pads. The final bearing (Bearing C) type used a bearing plate that was centered beneath the cross-section. The width of this bearing plate was equal to the combined widths of the

bearing plate for the E-type bearing. This bearing configuration was used to examine the effectiveness of the cover concrete that lies outside the stirrups.
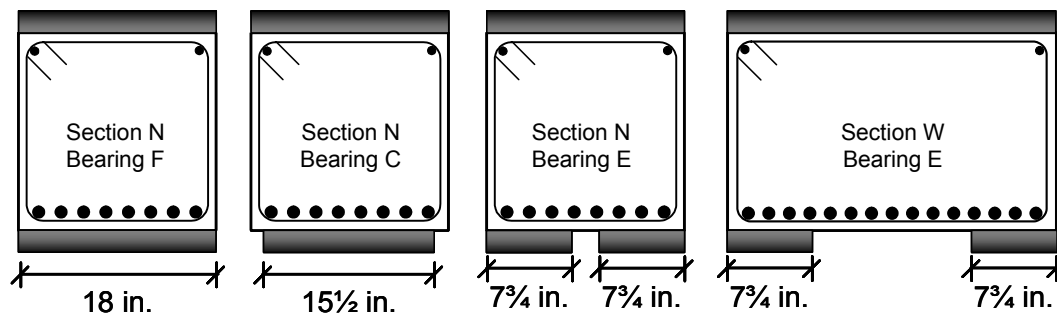
Specimen	Concrete Strength [psi]	North Shear Span, a_1 [in.]	South Shear Span, a_2 [in.]	Stirrup Spacing [in.]	Bearing Area [in.^{2}]
II-N-E-5.8-8	2850	27	93	8	93.0
II-N-F-5.8-8	2850	27	93	8	108.0
II-N-C-5.8-8	2850	27	93	8	93.0
II-N-F-5.8-3	2880	27	93	3	108.0
II-N-C-4.6-8[†]	2880	27	73	8	93.0
II-N-E-4.6-8[†]	2880	27	73	8	93.0
II-N-F-4.6-8[†]	3130	27	73	8	108.0
II-W-E-5.8-8	3110	27	93	8	93.0
II-W-E-4.5-8	3570	27	72	8	93.0
II-W-E-3-8	3650	27	48	8	93.0

[†]These tests were conducted on previously tested specimens. (See Section 4.4.2)

Figure 4-20: Bearings for the North reaction and specimen details for Series II test specimens

Just as in the Series I specimens, in the Series II specimens standard hooks that met ACI 318-05 were used to anchor the longitudinal reinforcement. The

anchorage was such that that full yield strength ($f_y = 68ksi$) of the reinforcement could be developed at the exterior node faces. The hooks were confined with No. 3 stirrups ($f_y = 73ksi$) spaced at 3 in. over the length of the hook.

Each of the ten tests conducted in Series II was given a unique notation based on the details of the test as described in Figure 4-21and Figure 4-20.

II-N-F-4.5-8

Spacing of Stirrups in in.

Shear span-to-depth ratio
for the South portion of span

Bearing Layout

Cross-section
N: 18x18 in. section
W: 18x30 in. section

Test Series (I, II, or III)
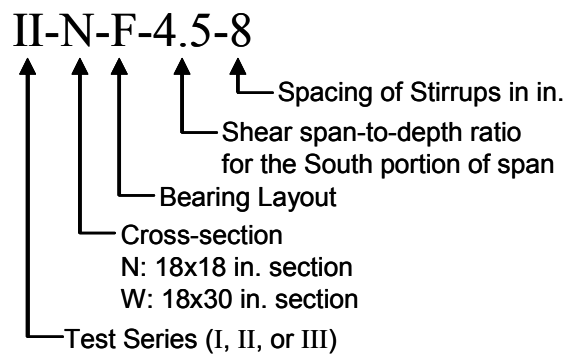
Figure 4-21: Nomenclature for Series II tests

4.4.2 Results of Series II Tests

The data collected for Series II tests were similar to that for Series I. The applied load was measured using load cells placed beneath the beam supports and pressure transducers in the hydraulic lines. Strain gages were placed on the stirrups between the applied load and the North reaction for some tests.

Only seven specimens were used for the ten tests in Series II. Three specimens were tested twice. The load was applied very near one support as can be seen in Figure 4-19. The majority of the damage to the beam was confined to the area between the applied load and the near reaction. Since the damage was confined, the beam could be rotated such that the South reaction in the first test became the North reaction in the second test on the same beam. In the process the

139

span had to be shortened slightly to avoid re-loading the damaged portion of the specimen.

4.4.2.1   *Cracking and Failure Loads*

In each of the Series II tests, the specimens contained two different shear spans. The shear force in each portion of the beam is inversely proportional to the shear span for that portion. Therefore, shear failure was expected in the portion of the beam with the shorter shear span and higher shear force. However, for four of the tests shear failure occurred in the longer shear span. The ultimate and cracking loads can be seen in Table 4-5.

For all of the Series II beams, a diagonal crack formed between the North reaction and the point at which the load was applied. The loads at which that crack first appeared are listed as the cracking load in Table 4-5. The crack extended from the inner edge of the bearing plate at the reaction to the nearest edge of the loading plate. This crack was the first sign of impending failure due to shear. For the beams that failed in the North shear span, failure was caused by concrete crushing along the diagonal shear crack. A typical failure is shown in Figure 4-22. The vertical arrows indicate the centers of the bearing plates.

Table 4-5: Cracking and failure loads for Series II Specimens

Specimen	Diagonal Cracking Load [kip]	Failure Load [kip]	Failure Shear North Shear Span [kip]	Failure Shear South Shear Span [kip]
II-N-E-5.8-8	54.4	132.5	102.8[*]	29.7
II-N-F-5.8-8	59.9	140.3	109.9[*]	30.4
II-N-C-5.8-8	51.5	194.9	152.8	42.1[*]
II-N-F-5.8-3	49.7	226.1	179.3[*]	46.8
II-N-C-4.6-8	65.8	246.4	187.1[*]	59.3
II-N-E-4.6-8	71.6	183.9	138.7[*]	45.2
II-N-F-4.6-8	61.5	146.2	111.1[*]	35.1
II-W-E-5.8-8	106.9	367.7	266.6	101.1[*]
II-W-E-4.5-8	136.3	318.0	235.6	82.4[*]
II-W-E-3-8	159.3	232.6	148.9	83.7[*]

Notes:

1) An asterisk (*) indicates the shear span where shear failure occurred

2) All values in the table include the self-weight of the test specimens

3) Cracking loads indicate the formation of a diagonal crack in the North shear span

Figure 4-22: Typical failure of the North shear span in Series II specimens (Specimen II-N-F-5.8-3)

The observed mode of failure was different for beams that failed in the South shear span. Those beams did exhibit similar crack formation in the North shear span as previously described. However, before failure similar to that shown in Figure 4-22 could occur, a large inclined crack formed in the South shear span and caused failure. This crack was somewhat "S" shaped. The crack followed the longitudinal reinforcement along the bottom of the beam for some distance then turned upwards. The inclined portion of the crack made an angle of approximately 45 degrees with the axis of the beam. Finally the crack turned to follow the compression reinforcement along the top face of the beam.

The following two figures illustrate the formation and orientation of the crack that formed in the South shear span. Figure 4-23 shows the crack at approximately 80% of the failure load the test specimen carried. The photograph was taken such that the inclined portion of the shear crack was in view. Note the

large vertical offset of the beam on opposite sides of the crack. Figure 4-24 shows the entire specimen after failure of the South shear span. Failure occurred after the formation of the shear cracks without any crushing similar to that which was observed in failures of the North shear span.
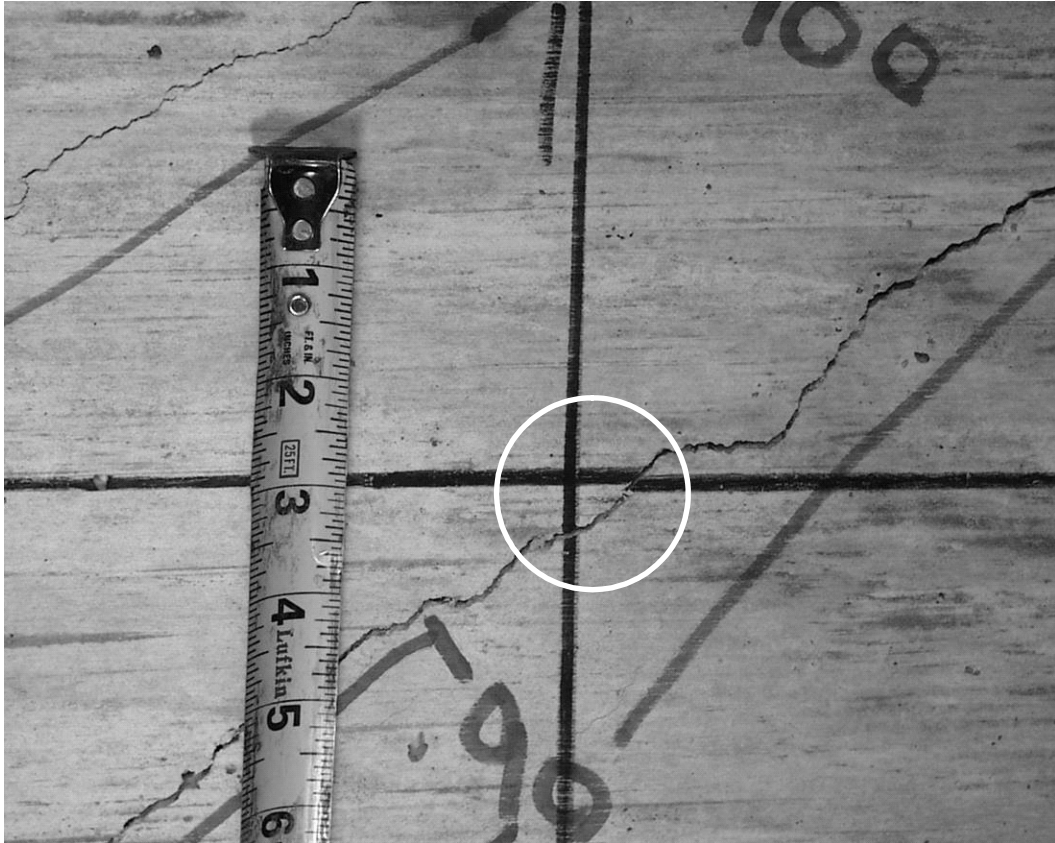
Figure 4-23: Crack in South shear span before failure (II-W-E-5.8-8)
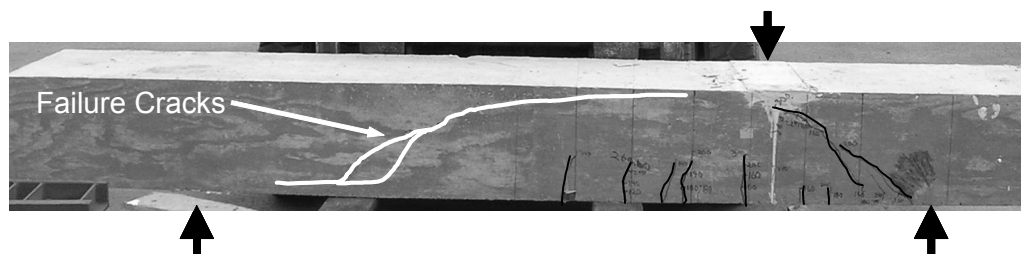
Figure 4-24: Typical failure of South shear span (II-W-E-5.8-8)

The failure cracks shown in Figure 4-24 followed the longitudinal reinforcement along the bottom edge of the beam. Often these cracks are attributed to anchorage failures in the reinforcement. It is doubtful that these cracks are due to insufficient anchorage in the Series II specimens. The South support is indicated by the left-most arrow in Figure 4-24. At that point in the beam, the longitudinal reinforcement is anchored with a standard hook as per ACI 318-05. The cracks that follow the longitudinal reinforcement occurred at a point in the beam where anchorage is considerably more than adequate. Therefore the failure can be attributed to shear. The splitting crack that formed along the longitudinal reinforcement was caused by vertical displacement that forced the bottom reinforcement down.

4.4.2.2   Effect of Shear Span-to-Depth Ratio

The ten specimens in Series II consisted of a beam with two different shear spans. In each test the two portions of the beams were identical except for the shear spans. In four of the ten tests, failure occurred in the longer shear span where the shear was much less than the short shear span. Based on traditional sectional design models, the shear strength of the beam was uniform along its length ($V_c + V_s = $ constant), yet shear failure took place outside the area of maximum shear. Since only the shear span-to-depth ratio varied from the North portion of the beam to the South portion, the reduced strength can be attributed to the shear span-to-depth ratio.

Additionally, one of the specimens in Series I (I-UL-17-17) failed in shear at the South reaction (long shear span). For that specimen, as with the Series II specimens, the section had uniform strength along its length and shear failure occurred outside the region where shear was greatest.

Thompson (2002) observed similar shear failures in asymmetrical test specimens. Thompson's tests were conducted to examine the anchorage of headed reinforcement in CCT nodes. A drawing of the specimens is shown in Figure 4-25. In his first series of tests Thompson chose not to use stirrups in the portion of his specimens with lower shear. All four of those specimens failed in shear in the 45 in. portion of the span where the shear span-to-depth ratio was 3.0. Thompson attributed those failures, in part, to poor development of the tie over the left-hand support. The shear cracks observed by Thompson are similar in shape to those observed in the Series II tests. A photograph of Thompson's specimens can be seen in Figure 4-26. The failure crack in Figure 4-26 follows the longitudinal reinforcement then turns towards the top of the section in a similar manner as shown in Figure 4-24.
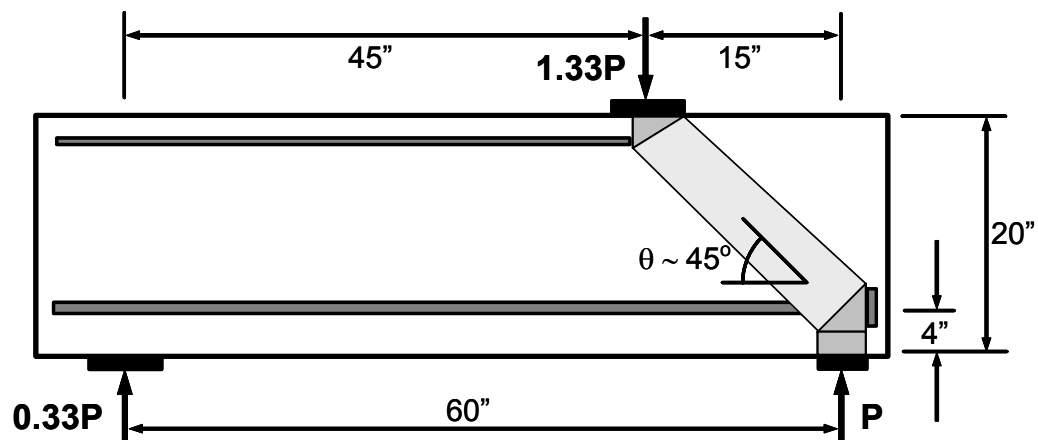
Figure 4-25: Asymmetric specimen (Thompson 2002)
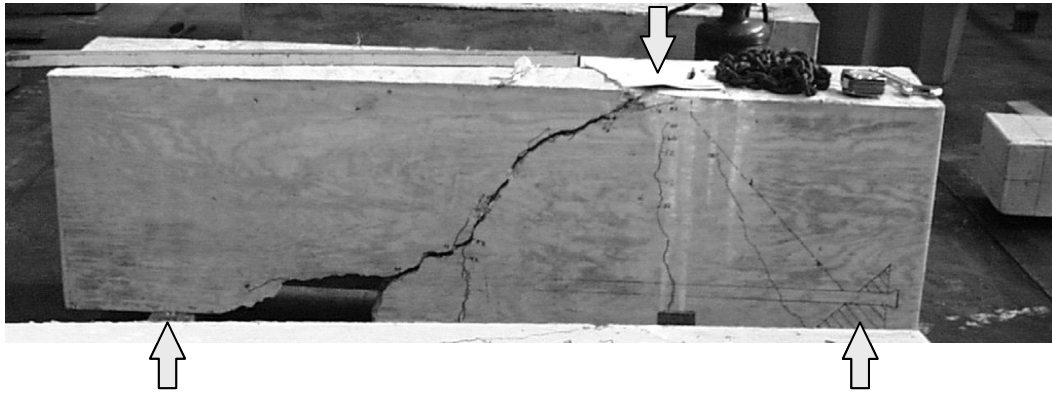
Figure 4-26: Thompson's specimen after failure

Failures of specimens in regions of relatively low shear have been observed in four different cross-sections at various shear span-to-depth ratios. Dating back to Kani (1964), research has shown that beams with different shear span-to-depth ratios developed different shear mechanisms.

The following discussion is quoted from Collins and Mitchell (1997):

…Beams with shear-span-to-depth ratios less then about 2.5 carry the load by strut-and-tie action. In this range the strength of the beams decreases rapidly as the shear span increases. Further, the strength is strongly influenced by details such as the size of the bearing plates supporting the beam. Failure of the beams involves crushing of the concrete. Beams with shear-span-to-depth ratio greater than about 2.5 are governed by conditions away from the disturbed regions adjacent to the supports and the loads…

The findings of this study indicate that beams with a shear span less then approximately two times the effective depth of the section develop a single-strut mechanism. In these cases a single strut forms between the load point and the nearest reaction. This type of failure mechanism can be seen in Figure 4-22 and generally involves crushing of concrete. Failures such as this are heavily

146

dependant on the details of the bearings which support the beam. Beams with shear span-to-depth ratios greater than approximately two are governed by conditions away from the bearings and traditional sectional models should be used. This type of failure can be seen in Figure 4-24. Further discussion of the truss mechanisms present in beams with shear span-to-depth ratios less than 2.0 is presented in Chapter 5.

The results of the tests conducted in this study and those conducted by Thompson indicate that different mechanisms within a single beam have different levels of strength. Additionally, the mechanisms carrying the greatest amount of load may not always be the strength-limiting factor for the beam. The appropriate mechanisms must both be applied to a structure where necessary to determine the capacity.

4.4.2.3 Effect of Strut Width

Two pairs of specimens clearly illustrate the effects of strut width. The first pair consisted of specimens (II-N-E-5.8-8 and II-W-E-5.8-8) that were nominally identical except for the width of the cross-section. Both were supported on the E bearing in which two plates were placed at the outside edges of the cross-section. If those bearing plates accurately reflected the appropriate width of the struts, both specimens would have carried the same load. However, the wide specimen had a maximum load of 367.7 kip and the narrow specimen had an ultimate load of only 132.5 kip. By increasing the width of the cross-section by a factor of 1.67, the strength of the beam was increased nearly three-fold. The other pair of similar specimens (II-N-E-4.6-8 and II-W-E-4.5-8) exhibited the same trend however the wider specimen carried only 70% more load than the narrow specimen (183.9 kip and 318.0 kip for the narrow and wide cross-sections respectively). These results indicate that the center portion of the beam, which

was unsupported by bearings, contributed to the strength of the beam. The failure of these specimens was not caused by bearing failures. If bearing failures had occurred the strengths of the pairs of specimens would have been the same. Shear strength is a direct function of beam width. By increasing the width from 18 in. to 30 in., the shear strength increased accordingly.

Additionally, for the various narrow cross-sections there was no discernable difference in strength between the various bearing arrangements. All seven specimens with the 18x18 in. cross-section failed at similar levels of load.

4.4.2.4 Observations from Series II Tests

The beams with the wider cross-section used in Series II carried higher shear forces than did the beams with the narrow cross-section. Therefore, the additional width in the cross-section had a beneficial effect on shear strength even though the middle portion of the beam was unsupported in the wide beam tests.

As was the case with Series I tests, the failure of specimens in Series II was often preceded by the formation of parallel shear cracks. In Figure 4-22 the concrete crushing that is visible occurred between the parallel shear cracks. Figure 4-24 shows parallel shear cracks in the longer shear span where shear failure took place. The second of the two parallel shear cracks appeared between 65 and 80% of the ultimate load. This type of cracking was observed for failures in both the North and the South shear spans.

The shear span-to-depth ratio, and therefore, strut inclination, plays a significant role in determining the shear strength of the beams. The short and steep strut that formed between the applied load and the North reaction developed strengths that were in excess of those allowed by ACI 318 and AASHTO LRFD. In some cases, the strength of that strut was so great that shear failure happened in the longer shear span where the shear force was much lower.

148

4.4.3 Application of Code STM Provisions to Series II Specimens

The capacities of the specimens tested in Series II were also determined using ACI 318-05 Appendix A and AASHTO LRFD STM procedures. The truss models for the Series II specimens were much simpler than their Series I counterparts. The specimens were modeled with a single strut connecting the load point with the North reaction across the shorter shear span (Figure 4-27). Based on code provisions, in each case the strut that connected the applied load with the nearest reaction was the critical element of the beam.
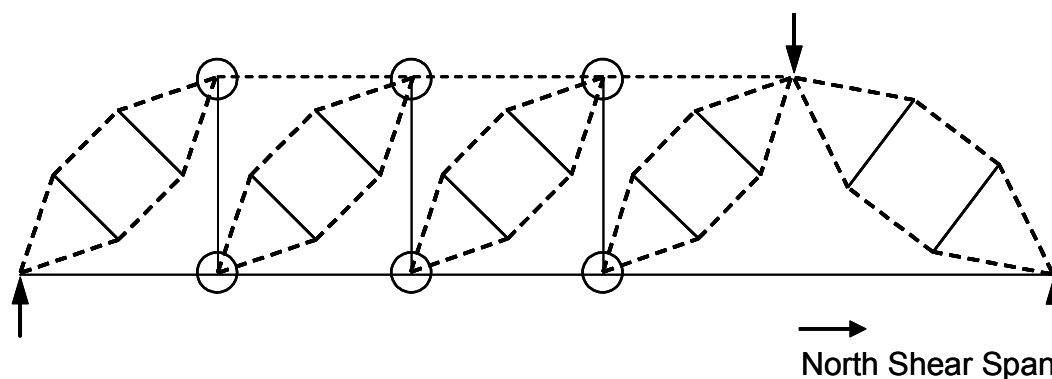
North Shear Span

Figure 4-27: Strut-and-tie model for Series II specimens

The longer shear span of the Series II specimens, varied from 3.0 to 5.8. As such, there would be a small B-Region, where plane sections remain planes, in the South shear span. Therefore STM would not be recommended for use in that portion of the beam. However, STM could be used along with a truss as shown in Figure 4-27. The number of panels on the left portion of the truss could be varied to account for the variable shear span on the South shear span. In the figure six nodes are circled. None of those six nodes abut an external bearing. As such, the geometry of those nodes is largely unknown. Both AASHTO LRFD and the fib provide assumptions for the geometry of such nodes. With those assumptions, the allowable forces at the nodes and strut could be checked. However, such a procedure would be much more complex than sectional design methods. In such

long shear spans ($a/d > 2.0$), sectional design methods can be used. Sectional design methods are discussed in detail in Chapter 6.

4.4.3.1   Application of ACI 318-05 STM Provisions

None of the Series II specimens satisfied the minimum reinforcement based on Section A.3.3.1 of ACI 318-05 (Eqn. 4-1). Therefore the lower strut efficiency factor ($\beta_s = 0.60$) was used for all ten specimens. The capacities of the beams as determined using Appendix A of ACI 318-05 are shown in Table 4-6.

The allowable loads based on Appendix A of ACI 318-05 were conservative for nine of the ten tests. The allowable load was nearly equal to the measured load for the tenth case (Specimen II-N-F-4.6-8). Strut-and-tie modeling should, in theory, provide a lower bound estimate of strength; however, for Specimen II-N-F-4.6-8 this was not the case. In order to be a lower bound approximation, both the yield conditions of the materials and equilibrium of the structure must be satisfied. In the case of this specimen, the yield conditions of the material as defined by ACI 318-05 were not adequate to describe the state of stress at the critical point of this specimen. The nominal capacities were calculated using measured material properties.

On average, the allowable loads for the Series II tests were less conservative than for the Series I tests. However, the ACI STM provisions are still quite conservative. Additionally, the ACI STM provisions indicated that the critical element in all ten of these specimens was the strut that develops between the support and the load. That strut was the critical element for only six of the ten specimens. The other four specimens failed in the region of lower shear. These tests imply that the STM provisions within ACI 318 are very conservative. These tests as they relate to sectional design procedures are discussed in detail in Chapter 6.

Table 4-6 Nominal Capacities as per ACI 318-05

Specimen	Nominal Capacity [kip]	Total Measured Load [kip]	Ratio of Measured Load to Nominal Capacity
II-N-E-5.8-8	109.5	132.5	1.21
II-N-F-5.8-8	127.2	140.3	1.10
II-N-C-5.8-8	109.6	194.9	1.78
II-N-F-5.8-3	128.5	226.1	1.76
II-N-C-4.6-8	117.5	246.4	2.10
II-N-E-4.6-8	117.5	183.9	1.57
II-N-F-4.6-8	148.3	146.2	0.99
II-W-E-5.8-8	119.4	367.7	3.08
II-W-E-4.5-8	146.3	318.0	2.17
II-W-E-3-8	169.7	232.6	1.37
		Average:	1.71
		Coefficient of Variation:	0.37

4.4.3.2 *Application of AASHTO LRFD STM Provisions*

The AASHTO LRFD STM specifications require that the tensile strain in the direction of the tie be input into the mathematical models. That value was measured with strain gages attached to the longitudinal reinforcement at the center of the nodal zone. However, where a specimen was used for two tests the necessary instrumentation was not present for the second test. The value of the tie strain that was used for those three tests was the average of the values measured in the seven tests where the instrumentation was present. The values of the strain

151

in the direction of the tie and the nominal capacities determined using AASHTO LRFD can be seen in Table 4-7.

As with ACI 318-05, the AASHTO LRFD STM specifications result in conservative estimation of the capacities of the Series II beams. The average value of measured strength to allowable strength the coefficient of variation of those values, are nearly the same for ACI 318-05 and AASHTO LRFD. The increase in complexity required for implementation of the AASHTO LRFD STM provisions does not seem to produce any increase in accuracy compared to the ACI 318-05 provisions.

The allowable loads determined by ACI 318-05 and AASHTO LRFD were remarkably similar. The similarity was due to the identical nodal geometry used by the two code documents. Additionally, the inclination of the strut that joins the load and the support and the measured tie strains were such that Eqns 4-3 and 4-4 yielded efficiency factors that are approximately equal to those used by ACI 318-05.

Table 4-7: Nominal Capacities as per AASHTO LRFD (measured strains)

Specimen	Measured Tie Strain	Nominal Capacity [kip]	Total Measured Load [kip]	Ratio of Measured Load to Nominal Capacity
II-N-E-5.8-8	0.0004	106.3	132.5	1.25
II-N-F-5.8-8	0.0005	119.7	140.3	1.17
II-N-C-5.8-8	0.0007	97.1	194.9	2.01
II-N-F-5.8-3	0.0002	133.4	226.1	1.70
II-N-C-4.6-8	0.0004*	114.1	246.4	2.16
II-N-E-4.6-8	0.0004*	114.1	183.9	1.61
II-N-F-4.6-8	0.0004*	144.0	146.2	1.02
II-W-E-5.8-8	0.0005	112.3	367.7	3.27
II-W-E-4.5-8	0.0004	142.0	318.0	2.24
II-W-E-3-8	0.0003	170.2	232.6	1.37
			Average:	1.78
			Coefficient of Variation:	0.38

* Instrumentation to measure tie strain was not present in the test. The value is the average of strains measured in the other tests.

As with the specimens in Series I, the use of measured tie strains would not be possible for a design engineer. A designer must rely on calculated values rather than measured ones. The calculated values of strain in the direction of the tie are shown in Table 4-8. As was the case with Series I, the calculated ties strains are very small in magnitude. The amount of steel in the tie was increased

153

to reduce the likelihood of flexural failure in the specimens. The level of conservatism and the coefficient of variation did not change significantly when the calculated rather than measured strain values were used.

Table 4-8: Nominal Capacities as per AASHTO LRFD (calculated strains)

Specimen	Calculated Tie Strain	Nominal Capacity [kip]	Total Measured Load [kip]	Ratio of Measured Load to Nominal Capacity
II-N-E-5.8-8	0.00069	97.2	132.5	1.36
II-N-F-5.8-8	0.00078	110.0	140.3	1.28
II-N-C-5.8-8	0.00069	97.3	194.9	2.00
II-N-F-5.8-3	0.00079	110.9	226.1	2.04
II-N-C-4.6-8	0.00070	104.1	246.4	2.37
II-N-E-4.6-8	0.00070	104.1	183.9	1.77
II-N-F-4.6-8	0.00084	126.0	146.2	1.16
II-W-E-5.8-8	0.00043	114.6	367.7	3.21
II-W-E-4.5-8	0.00049	138.0	318.0	2.30
II-W-E-3-8	0.00050	159.6	232.6	1.46
			Average:	1.89
			Coefficient of Variation:	0.33

4.5   BEAM TEST SERIES III

The data from Series I of beam tests indicated that there was a significant increase in shear strength if uniform load was applied to a beam. Although past

research (De Cossio and Siess 1960; Krefeld and Thurston 1966; Ramakrishnan and Ananthanarayana 1968; Uzel 2003) has been performed to investigate the effects of loading type on shear strength, none of those studies concluded that specimens with uniform load exhibited increased shear strength compared to specimens with concentrated loads. Since the results of the Series I tests appeared to provide entirely new conclusions that were not reported in the previous research, tests for Series III were undertaken.

4.5.1 Details of Series III Specimens

Series III consisted of four nominally identical specimens. The only variation among the specimens was the strength of the concrete at the time of the test. All four specimens were constructed from a single batch of concrete. Each of the four specimens was subjected to a different type of load. Specimen III-1 ($f_c' = 3,870\,psi$) was subjected to a singe concentrated load at midspan. Specimen III-2 ($f_c' = 3,880\,psi$) was subjected to two concentrated loads at $^L/_4$ and $^{3L}/_4$. Specimen III-4 ($f_c' = 3,900\,psi$) had four loads applied at $^L/_8$, $^{3L}/_8$, $^{5L}/_8$, and $^{7L}/_8$. The final specimen in the series, Specimen III-U ($f_c' = 3,900\,psi$), was subjected to a uniform load that consisted of 24 identical hydraulic rams. The uniformity of the load was maintained by keeping the pressure in all 24 rams equal during the test. The details of the specimens are shown in Figure 4-28. The shear force diagrams for Series III specimens are shown in Figure 4-29.

The specimens contained no stirrups between the supports. Stirrups were used where required as per ACI 318-05 to ensure proper anchorage of the longitudinal reinforcement as shown in Figure 4-28.

155
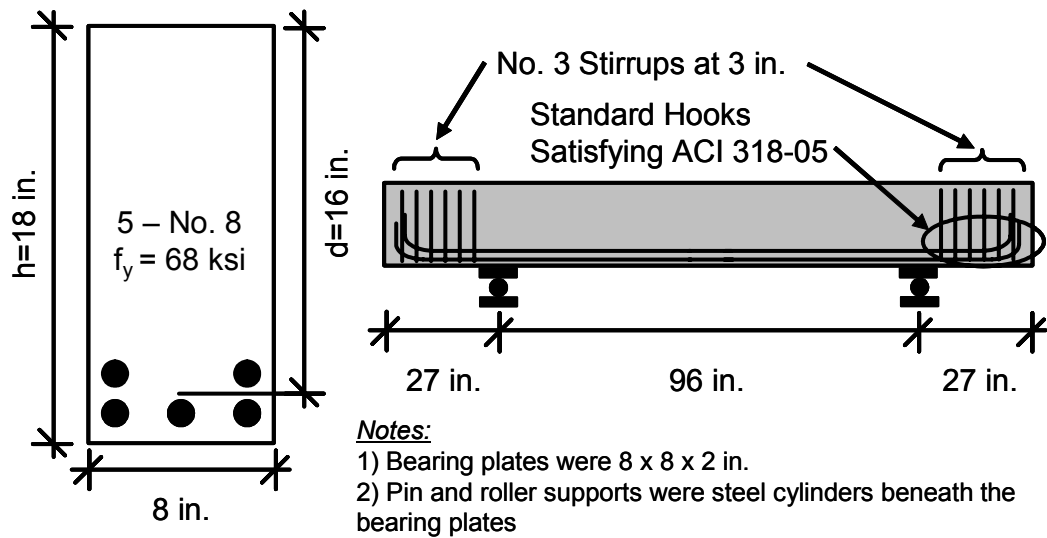
Figure 4-28: Details of Series III specimens
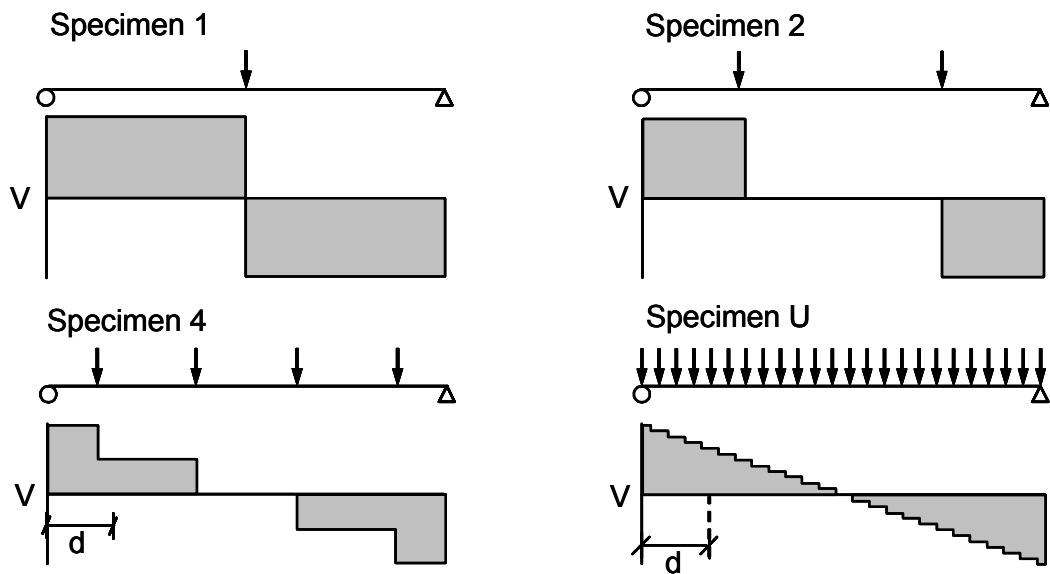
Figure 4-29: Shear diagrams for Series III specimens

4.5.2   Results of Series III Tests

The failure loads for the Series III specimens are presented in Table 4-9 and photographs of the specimens after failure are shown in Figure 4-30. Table

4-9 lists the peak shear carried by each specimen. The tabulated values include the shear due to self-weight of the specimens. For Specimen III-U the failure shear at d away from the support is also listed in the table. For design calculations the shear d away from the support is most relevant.

Table 4-9: Failure loads for Series III specimens

Specimen	Shear at Failure [kip]
III-1	20.4
III-2	64.1
III-4	68.6
III-U	75.8[*]

[*]Peak shear at the face of the support. Shear d away from the support was 50.5 kip

As can be seen in Table 4-9, the capacity of the test specimens increased dramatically as the number of loads was increased from one to two. Further distribution of the load yielded less dramatic increases in shear strength. These data indicate that two concentrated loads more accurately simulate a uniformly distributed load than a single load, and four loads more accurately simulate uniform loads than two.

Additionally the cracking patterns shown in Figure 4-30 are similar for the beams with multiple loads. Specimens III-2, III-4, and III-U exhibited similar cracking at failure. Each of those specimens produced parallel shear cracks at the point where failure occurred. Specimen III-1 developed a crack that was similar in shape and orientation to those produced in the Series II specimens that failed in the long shear span (South shear span). The reinforcing bars were anchored with standard hooks as per ACI 318-05 in all Series III specimens. Therefore, the horizontal portion of the failure crack shown in Specimen III-1 was likely not associated with any deficiencies in anchorage.

157

Strut-and-tie modeling would be applied only Specimen III-2. The other three specimens in Series III are better suited for sectional design methods. The mode of failure exhibited by Specimen III-2 was a strut failure. For Specimen III-2 the capacities determined with ACI 318-05 and AASHTO LRFD were 253.3 kip and 185.7 kip respectively. The measured capacity was 128.2 kip. The use of both ACI 318-05 and AASHTO LRFD produced unconservative capacities for this test specimen. The Series III specimens are discussed in detail in Chapter 6 – Sectional Design Models. Also in Chapter 6, ACI 318-05 and AASHTO LRFD sectional design procedures are applied to these tests specimens.
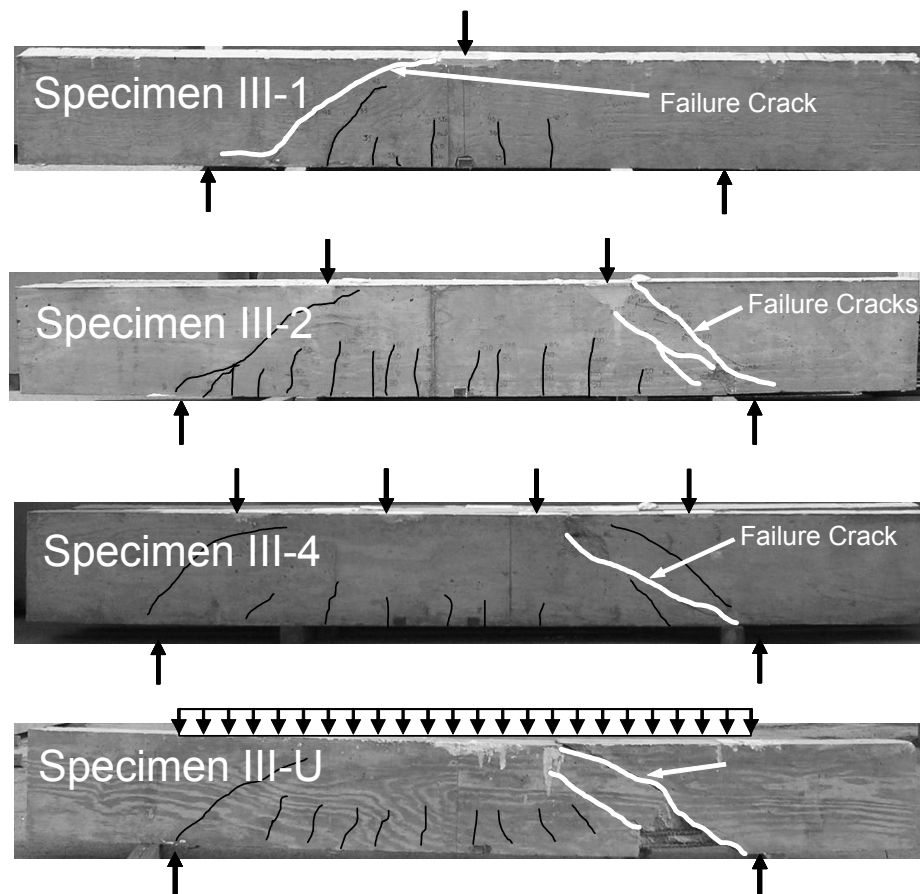
Figure 4-30: Series III specimens after failure

4.6   OBSERVATIONS FROM BEAM TESTS

The specimens in Series I and III indicate that for modeling a uniform load with a strut-and-tie model, two concentrated loads may be adequate. The experimental results indicate that different load carrying mechanisms are present for different load distributions. For both Series I and Series III two concentrated loads appeared to be sufficient to generate the mechanisms present with a true uniform load.

However, the number of loads can not be the only criterion for determining an appropriate model for a uniform load. As the length of the beam increases, two loads become less similar to a uniform load. The spacing of the loads must also be considered. For Specimen III-2, the space between the concentrated loads is three times the effective depth of the member. Based on these test results, it could be concluded that load spacing of less than three times the member depth was sufficient to model a uniform load. Certainly if the spacing of the applied loads is less than the depth of the member, the load is sufficient to be considered uniform.

The shear span-to-depth ratio has significant impact on the shear strength of reinforced concrete beams. The specimens in Series II illustrate the importance of shear span-to-depth ratio on shear strength. There appeared to be two different mechanisms in the two portions of those beams. The two mechanisms had sufficiently different strengths such that failure occurred in the region of least shear.

The two cross-sections used in Series II resulted in very different shear strengths. The increased width appeared to have a beneficial effect on the shear capacity. The strength of the beams increased as the width of the beams increased.

In many of the tests in Series I and II shear failure was preceded by the formation of a shear crack that was nearly parallel to a pre-existing shear crack.

The second of the parallel cracks formed between 60 and 80% of the ultimate capacity of the specimen. Failure of the specimens was the caused by concrete crushing between the two cracks. That type of failure is best illustrated by the photograph of Specimen I-UL-0-8.5 in Figure 4-9 and the photograph of Specimen II-N-F-5.8-3 in Figure 4-22. For specimens with small shear span-to-depth ratios parallel cracking may be an indicator of impending shear failure. This cracking pattern was observed in three very different cross-sections with and without shear reinforcement. Further experimental observations must be made to examine the full meaning of the formation of parallel shear cracks in a specimen. The few tests reported in this chapter are not sufficient to make a firm conclusion regarding the importance of the formation of parallel shear cracks.

CHAPTER 5

Examination of Strut-and-Tie Modeling Specifications and Development of New Design Expressions

5.1 INTRODUCTION

In order to expand the application of the experimental results, a database of beam tests was compiled from data available in the technical literature. Each of the papers whose specimens were added to the database is grouped according to the parameters investigated by the original authors and discussed individually. The research reported in the literature was categorized into the following groups:

- effects of shear span
- effects of transverse reinforcement
- effects of longitudinal reinforcement
- effects of loading type
- size effect.

The database of shear tests was then used to examine ACI and AASHTO STM provisions, and evaluate the levels of conservatism produced when using those code provisions. Finally, a new set of design expressions was developed. The new procedure focuses on improving safety compared to existing code procedures.

5.2 DEVELOPMENT OF THE DATABASE

Combining the results of wide-ranging research into a single database provides the ability to examine current code provisions as well as develop new models for use in design. Each of the papers discussed herein presented the results of experimental investigations.

161

5.2.1 Effects of Shear Span

Typically laboratory investigations concerning the shear strength of reinforced concrete beams use simply supported beams subjected to either one or two concentrated loads placed symmetrically on the span. For tests such as these, there is a region of constant shear adjacent to the support. The length of these regions is called the shear span. As described in Chapter 4, the shear span becomes more difficult to define for beams subjected to distributed loads. For the purposes of this dissertation, the shear span will be defined as the distance from the peak shear, *i.e.* the support, to the point where the shear force diagram is zero. This definition of shear span is implied by the definition of a deep component in AASHTO LRFD Bridge Design Specifications:

> ***Deep Component*** – *Components in which the distance from the point of 0.0 shear to the face of the support is less than 2d or components in which a load causing more that one-third of the shear stress at a support is closer than 2d from the face of the support*

For a beam subjected to one or two concentrated loads, the traditional definition of shear span as the distance between the support and the applied load and the definition of shear span based on the zero-shear point result in the same value. Regardless of the definition of shear span, it is generally believed that shear span has a significant affect on shear strength.

5.2.1.1   Clark (1951)

Clark (1951) tested 62 simply supported beams that were subjected to one or two concentrated loads. The specimens consisted of two different cross-sections (8x18 in. and 6x15 in.) which were designed to fail in diagonal tension. Clark used shear span-to-depth ratios ranging from 1.1 to 2.3 and concrete

strengths ranging from 2,000 to 6,900 psi. He concluded that for a given cross-section and concrete strength, the shear strength of a beam increased as the load was shifted from the center of the span toward the support, i.e. shear strength increased with decreasing shear span-to-depth ratio. His specimens exhibited diagonal tension failure as designed. The majority of the specimens tested by Clark had light vertical shear reinforcement.

5.2.1.2 Laupa, Siess, and Newmark (1953)

The results of the tests conducted by Laupa, Siess, and Newmark (1953), indicated that shear span-to-depth ratio did not affect the shear strength of reinforced concrete beams. However, Laupa, Siess, and Newmark did not use shear span as a primary variable in their tests series. Even though shear span was not the primary variable in these tests, Laupa, Siess, and Newmark developed conclusions regarding the effects of shear span-to-depth ratio on the behavior of reinforced concrete beams. The majority of the beams were tested with the same shear span-to-depth ratio. The few specimens that had a longer shear span than the main series of tests exhibited flexural failure. These results indicate that the shear span can affect, at least, the mode of failure. The tests conducted by Laupa, Siess, and Newmark consisted of beams with a nominal depth of 11 in. and concrete strength ranging from 2,100 to 4,700 psi and no shear reinforcement. The beams were subjected to a single point load that was applied at midspan through a stub column. The beams contained no transverse reinforcement.

5.2.1.3 Morrow and Viest (1957)

Morrow and Viest tested both beams and knee joints. Only the beam tests will be discussed here, and only the beam tests were added to the database. The knee joint specimens were subjected to axial load during the tests; therefore those specimens were not included in the database. The beams tested by Morrow and

Viest had an effective depth of 14 in. with concrete strengths ranging from 1,600 to 6,800 psi. The primary variables in the series of beam tests were shear span and longitudinal reinforcement ratio, which ranged from 0.6% to 3.8%. None of the specimens contained any transverse reinforcement. Their conclusions indicated that shear compression failures occurred in specimens with the shortest shear spans ($a/d < 3.5$). These failures occurred at loads much higher than the loads which caused diagonal tension cracking. For specimens with intermediate shear span-to-depth ratios ($3.5 < a/d < 5.3$) failure was caused by diagonal tension, and for the longest specimens ($a/d = 7.9$) flexural failures occurred. Morrow and Viest suggested that if the shear stress within a concrete beam with no transverse reinforcement was less than $2\sqrt{f_c'}$, shear would not govern the beam strength.

5.2.1.4 *Van den Berg (1962)*

Van den Berg conducted a series of tests on beams with no transverse reinforcement. His goal was to determine the primary factors that affect the diagonal cracking load. The effects of concrete strength, shear span-to-depth ratio, and longitudinal reinforcement were studied. The specimens had concrete strengths which varied from 2,600 to 11,200 psi, and shear span-to-depth ratios ranged from 2.1 to 4.9. All of the specimens had an effective depth of 14.1 in.

Van den Berg concluded that the cracking load was inversely proportional to the shear span-to-depth ratio and directly proportional to the longitudinal reinforcement ratio. Finally, he concluded that there was a "highly significant" correlation between the shear strength of a beam and the tensile strength of the concrete as determined by a split cylinder test.

5.2.1.5 *Kani, Huggins, and Wittkopp (1979)*

G. N. J. Kani conducted several hundred tests of reinforced concrete beams in order to describe shear behavior. The results of his tests were published posthumously by Kani, Huggins, and Wittkopp. Kani's test series consisted of comprehensive examination of the effect of shear span-to-depth ratio. Several groups of nominally identical specimens (without shear reinforcement) were constructed then tested at various shear span-to-depth ratios ($1.0 \leq a/d \leq 10.0$). Each series consisted of a single concrete strength and cross-section.

Based on the observed failures, he developed mechanics-based models to describe failures. More specifically, he quantified a range of shear span-to-depth ratios in which a beam would fail at levels of moment less than the flexural capacity of the beam. The strength envelope Kani developed is shown in Figure 5-1. The vertical axis of Figure 5-1 is the ratio of the measured flexural strength to the calculated flexural strength of the beam. The range where reduced shear strength can occur is shown in Figure 5-1 between $1.1 < a/d < 6.3$. In this range, the measured capacity of the beam is less than the calculated flexural capacity.

Kani defined two critical a/d ratios: a/d_{min} and a/d_{TR}. The first, a/d_{min} is the shear span-to-depth ratio at which the minimum strength of the beam occurs, and a/d_{TR} is the shear span-to-depth ratio at which the full flexural capacity of the beam can be reached. The values of these two critical a/d ratios depend on the material properties and geometry of the cross-section. The data from Kani's shear tests closely correlated with the calculated shear strength envelope.
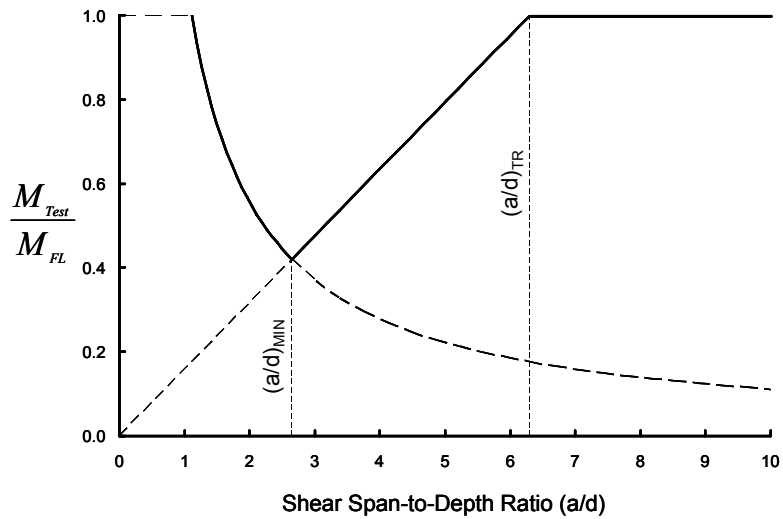
Figure 5-1: Shear strength envelope developed by Kani

5.2.1.6 Subedi, Vardy, and Kubota (1986)

A series of beam tests with small shear span-to-depth ratios ($0.4 < a/d < 1.4$) was conducted by Subedi, Vardy, and Kubota (1986). They concluded that even within such a narrow range of shear span-to-depth ratios different failure modes could be observed. For these tests the longitudinal reinforcement ratio varied from 0.1% to 1.1% and influenced the failure modes. The minimum concrete strength was 4,100 psi and the maximum was 7,500 psi. They also recommended that for beams with very small shear span particular care be taken at the supports and the locations were the loads are applied. Localized crushing under the bearing plates can occur under such conditions. The specimens tested by Subedi, Vardy, and Kubota contained both horizontal and vertical shear reinforcement.

166

5.2.1.7   Ahmad and Lue (1987)

Ahmad and Lue focused on the impact of high-strength concrete on the shear strength of concrete beams. They used concrete strengths from 8,800 to 9,700 psi to construct small beams of approximately 8 in. in overall depth without shear reinforcement. The longitudinal reinforcement ratio ranged from 0.4% to 6.6%. In addition to their experimental work they developed a shear strength envelope that was very similar to that which Kani (1964) developed (Figure 5-1). The similarity extends to the mechanical models used to develop the strength envelope as well as the shape of the envelope.

Based on the experimental and analytical work, they concluded that the minimum of the envelope (Figure 5-1) is much lower for higher strength concrete beams. For beams with very little longitudinal reinforcement the valley of the envelope can disappear entirely because flexure will be the mode of failure rather than shear.

5.2.1.8   Tan, Kong, Teng, and Guan (1995)

Tan et al. used a single cross-section ($d = 18.2 in.$, $\rho = 1.2\%$, and $\rho_v = 0.5\%$) to examine the effects of concrete strength and shear span-to-depth ratio on shear strength. All of the specimens tested contained small amount os vertical shear reinforcement. The shear span-to-depth ratio varied between 0.3 and 2.7 for that cross section. They concluded that the shear span-to-depth ratio had only a marginal effect on the diagonal cracking strength of the beam. For all of their beams the diagonal cracking loads were between 20 and 35% of the ultimate load. For beams with shear span-to-depth ratios less than one, the failure mode was largely determined by the shear span-to-depth ratio.

167

5.2.1.9 *Shin, Lee, Moon and Ghosh (1999)*

In the same manner as Tan et al., Shin et al. used a single cross-section to examine the shear strength of reinforced concrete beams. The cross-section used had an effective depth of 8.5 in. and a longitudinal reinforcement ratio of 3.8%. For their tests the concrete strength, shear span, and transverse reinforcement were varied. The variation in shear span was limited to shear span-to-depth ratios between 1.5 and 2.5. The transverse reinforcement ratio varied from 0 to 1.8%. For this series of tests, the mode of failure was governed by the shear span-to-depth ratio rather than the amount of shear reinforcement. The strain in the transverse reinforcement remained very small until the onset of diagonal cracking. Thereafter strain increased rapidly, and the increase in strain was more pronounced in beams with light shear reinforcement.

5.2.2 Effects of Transverse Reinforcement

Regardless of the design method used (Strut-and-Tie Modeling, Sectional Models, Modified Compression Field Theory, etc.), transverse reinforcement plays a significant role in determining V_n. The transverse reinforcement is intended to maintain the shear strength of the beam after diagonal cracking has occurred. However, the appropriate minimum amount of transverse reinforcement has been debated since the beginnings of reinforced concrete design.

5.2.2.1 *De Paiva and Siess (1965)*

De Paiva and Siess conducted an experimental program using of small beams with effective depth ranging from 6 to 12 in. at small shear span-to-depth ratios (*0.7 < a/d < 1.3*). Transverse reinforcement ratio was the primary variable in these tests. The ratio varied from 0 to 1.4%. They concluded that, for the beams tested, the addition of vertical and/or inclined stirrups had no effect on the

formation of inclined cracks, and seemed to have little effect on the ultimate strength. Additionally specimens with small shear span-to-depth ratios without shear reinforcement were observed to have a "very high load capacity beyond inclined cracking." However, the addition of vertical stirrups reduced deflections at the ultimate load. For such small shear span-to-depth ratios transverse reinforcement does not affect the beam strength because a single direct strut forms between the load point and the reaction. However, increased transverse reinforcement can reduce crack widths.

5.2.2.2   *Bresler and Scordelis (1963)*

Bresler and Scordelis investigated the effects of shear reinforcement on beams with moderate shear span-to-depth ratios ($4 < a/d < 7$). The series of 12 beams contained enough shear reinforcement to resist 0, 50, 75, or 100 psi of shear stress. The amount of shear strength provided by the reinforcement was varied by changing the width of the specimens and keeping all other details constant. The beams were approximately 18 in. deep with concrete strengths from 3,400 to 5,600 psi. Two main conclusions were presented in the paper. The first conclusion was that small amounts of shear reinforcement, as low as 50 psi, effectively increase the shear strength of the beams if the stirrup spacing is less than half the effective beam depth. The second conclusion was that web reinforcement effectively prevents sudden failures due to shear. If enough web reinforcement is provided, the full flexural capacity of the beam can be developed.

Bresler and Scordelis reached different conclusions regarding the importance of shear reinforcement than did de Paiva and Siess (1965). The two pairs of authors tested beams at different shear span-to-depth ratios, and likely observed very different shear failure mechanisms. At small shear span-to-depth

169

ratios ($a/d < 2.0$) transverse reinforcement may be inconsequential to the ultimate strength as concluded by de Paiva and Siess (1965). However at large shear span-to-depth ratios ($4 < a/d < 7$), shear reinforcement is crucial based on the findings of Bresler and Scordelis (1963).

5.2.2.3 *Kong, Robins, and Cole (1970)*

Kong, Robins, and Cole studied the effects of various types of shear reinforcement on shear strength. The shear reinforcement layouts consisted of vertical bars only, horizontal bars only, and orthogonal grids of both types of bars. One of the shear reinforcement layouts consisted of horizontal bars placed in the lower portion of the beam just above the main flexural reinforcement. The beams were between 10 and 30 in. deep with shear spans equal to 10 in. Accordingly, the shear span-to-depth ratios varied from 0.3 to 1.0. Concrete strength of approximately 3,000 psi was used for all the specimens. Kong, Robins, and Cole concluded that the proper shear reinforcement to control cracks and deflections was heavily dependant on the shear span-to-depth ratio. For low values of shear span-to-depth ratio horizontal bars placed near the bottom of the section provided the best results. When the shear span was greater than 35% of the effective depth ($a/d > 0.35$) vertical stirrups were more effective at controlling crack widths. When the shear span was greater than 70% of the effective depth ($a/d > 0.70$) vertical stirrups were more effective than horizontal bars or orthogonal reinforcement placed in two directions. The primary mode of failure observed was diagonal cracking and crushing of the compression strut between the support and the applied load.

5.2.2.4 Smith and Vantsiotis (1982)

Fifty two deep beams were tested to examine the impact of vertical and horizontal shear reinforcement. The beams had a concrete strength of approximately 2,800 psi, and an effective depth of 14 in. The shear span varied from 12 to 25 in. For the beams tested, the observed cracking patterns were essentially the same for beams with and without shear reinforcement. However more damage was observed on beams without web reinforcement. Regardless of web reinforcement, the inclined cracking loads were between 40 and 50% of the ultimate loads. Vertical stirrups were observed to increase the shear strength of the deep beams, but the effectiveness of the stirrup was reduced for beams with shear span-to-depth ratios less than one.

5.2.2.5 Hsiung and Frantz (1985)

Hsiung and Frantz investigated the effect of transverse spacing of shear reinforcement on the shear strength of reinforced concrete beams. For their beam specimens the amount of shear reinforcement was kept constant, but the number of legs of stirrups was varied from 2 to 6. The specimens had 16.5 in. effective depth with a concrete strength of 6,240 psi. Hsiung and Frantz used beam widths of 6, 12, and 18 in. The beams were tested with a shear span-to-depth ratio of 3.0. They observed that the distribution of stirrup legs across the cross-section did not have an effect on the shear capacity. However, if stirrups were distributed across the cross-section, interior stirrup legs carried a higher portion of the shear then exterior legs.

5.2.2.6 Rogowsky, MacGregor, and Ong (1986)

Tests were performed on both continuous and single-span deep beams. At the time the paper was written there was little or no available research regarding the behavior of continuous deep beams. The tests consisted of beams with

effective depths between 20 and 40 in. The concrete strength ranged from 3,800 to 6,300 psi. Based on the tests they concluded that the failure of deep beams with no or minimum transverse reinforcement was sudden and brittle regardless of the amount of horizontal web reinforcement. Conversely, beams with heavy shear reinforcement failed in a more gradual manner. In the beams with light shear reinforcement it was observed that the stirrup yielded at only 50 to 60% of the ultimate load and failure was caused by crushing of the compression strut.

Two simply supported specimens were constructed to examine the effect of anchorage of the flexural reinforcement on the behavior of the beam. The first specimen contained No. 6 longitudinal bars that were anchored with standard hooks (90 degree bends) as per ACI 318-83. The second specimen had No. 6 longitudinal bars that were not hooked, and embedded into the support only 6 in. The failure loads of these two specimens were within 1% of each other, and the flexural steel in the second specimen reached 40.6 ksi. The large bar stresses developed over such a short anchorage length were attributed to high transverse compressive stress introduced by the bearing plates at the reaction points.

5.2.2.7 *Johnson and Ramirez (1989)*

Johnson and Ramirez tested eight reinforced concrete beams ($d = 21.2$ in.) to examine the minimum transverse reinforcement requirements of ACI 318 with high-strength concrete. They used concrete strengths between 5,300 and 10,500 psi. The beams were constructed with transverse reinforcement providing 0, 50, or 100 psi of shear strength. It was concluded that with higher strength concrete, the minimum of 50 psi of shear reinforcement may be insufficient to prevent sudden failure. They observed that as concrete strength increased diagonal tension cracking occurred at higher loads. Increased diagonal tension resulted in fracture of the aggregate within the beam causing reduced shear transfer due to aggregate

172

interlock. The higher cracking load and reduced aggregate interlock caused the stirrups to yield and fracture. Premature yielding and fracture of the stirrups prevented plastic redistribution and reduced the reserve strength. These tests were performed at a shear span-to-depth ratio of 3.1. Johnson and Ramirez recommended that the ACI 318 provisions be altered to include the effect of concrete strength on minimum shear reinforcement. However, they did not present a quantitative recommendation.

5.2.2.8 *Anderson and Ramirez (1989)*

Anderson and Ramirez studied the proper detailing of shear reinforcement. To examine the effects of stirrup detailing they used two cross-sections (8x20 in. and 16x16 in.) to construct 16 different specimens. Each of the beams was constructed with approximately 5,000 psi concrete and tested with a shear span of 36 in. Eight different stirrup details (Figure 5-2) were used in the specimens with narrow cross sections (8 x 20 in.).
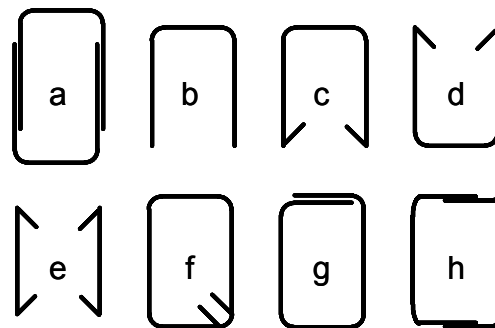
Figure 5-2: Stirrup configurations used by Anderson and Ramirez (1989)

Each of the stirrup configurations was placed at the same spacing so that the percentage of shear reinforcement was the same among test specimens. For the wider cross-section (16x16 in.) only traditional closed stirrups were used, but the number of stirrup legs was varied between tests from 2 to 4. Based on the tests they developed the following design recommendations:

1. Single-legged stirrups should be avoided (Figure 5-2e)

2. Free ends of U-stirrups should be anchored by hooks bent into the confined concrete core

3. In wide beams, stirrup legs should be uniformly distributed transversely across the cross section.

The third conclusion seems to be in conflict with the conclusions produced by Hsiung and Frantz (1985). In examining the effects of transverse stirrup spacing two sets of researchers (Hsiung and Frantz 1985; Anderson and Ramirez 1989) came to opposite conclusions with very similar tests (cross-section geometry, concrete strength, and shear span-to-depth ratio). The conclusions by Hsiung and Frantz were based on the ultimate strengths of the beams. Regardless of the transverse stirrup spacing (the number of stirrup legs was constant among specimens) the beam strength was unchanged. This is also true for the beams tested by Anderson and Ramirez. However, Anderson and Ramirez recommended that stirrups be distributed through the width of a cross-section based on the strains in the longitudinal bars. They observed that strain in the longitudinal bars placed in the corner of a stirrup were greater than other longitudinal bars. In order to prevent premature yielding of the longitudinal bars placed in the corners of stirrups, Anderson and Ramirez recommended uniform transverse distribution of stirrup legs to place more longitudinal bars in the bends of the stirrups.

5.2.2.9   *Roller and Russell (1990)*

Roller and Russell performed an experimental investigation into the shear strength of high strength concrete beams with various amounts of transverse reinforcement. They used concrete strengths of 10,000, 17,000, and 18,000 psi with cross-sections that had effective depths of 22 in. or 30 in. The beams were tested with a shear span-to-depth ratio of 2.5 for the shallower beams and 3.0 for

174

the deeper beams. Their conclusions were in agreement with those produced by Johnson and Ramirez (1989). For high strength concrete, the minimum amount of shear reinforcement, as per ACI 318-83, was inadequate to prevent sudden, brittle failure.

5.2.2.10 Sarsam and Al-Musawi (1992)

Using an experimental program in addition to a small database of tests reported in the literature, Sarsam and Al-Musawi evaluated the safety of the American and Canadian concrete codes. Their specimens were 7x9 in. with concrete strengths of 5,000 or 10,000 psi. The tests were performed at a shear span-to-depth ratio of 2.5 or 4.0. All of the conclusions reported by Sarsam and Al-Musawi were based on as data from of 107 beam tests in addition to the 14 tests performed by the authors. They concluded that both ACI 318-89 and the Canadian code (1984) were conservative, but the Canadian code produced a higher coefficient of variation. The also concluded that that the ACI design provisions for minimum transverse reinforcement were adequate for concrete strengths up to 12,000 psi based on the small database of test data.

5.2.2.11 Xie, Ahmad, Yu, Hino, and Chung (1994)

Xie et al. performed tests of shear critical beams in order to observe the post-peak response of the beams. The specimens had an effective depth of 8.5 in., concrete strengths between 5,800 and 15,800 psi, and shear span-to-depth ratios between 1.0 and 3.0. They concluded that with the proper testing apparatus, a stable and reproducible post-peak response could be observed after a shear failure. Xie et al. also concluded that increased web reinforcement will result in more ductile post-peak response.

5.2.2.12 Yoon, Cook, and Mitchell (1996)

Yoon, Cook and Mitchell performed 12 tests to evaluate the minimum shear reinforcement requirements of ACI 318-83 and the 1994 Canadian Standard. The cross-sections of their tests specimens were 14.8 x 29.2 in. with concrete strengths ranging from 5,200 to 12,600 psi. All 12 beams were tested with a shear span-to-depth ratio of 3.3. The conclusion was that ACI requirements for minimum shear reinforcement, which were not functions of the concrete strength, were not adequate for high strength concrete beams. In the 1994 CSA Standard the minimum shear reinforcement was a function of the concrete strength. The specimens tested indicated that the CSA detailing requirements resulted in greater reserve strengths than the comparable ACI requirements.

5.2.2.13 Tan, Kong, Teng, and Weng (1997)

Tan et al. tested 18 high strength concrete beams with an effective depth of 17.4 in. The beams were tested with shear span-to-depth ratios between 0.85 and 1.7 and concrete strengths ranging from 8,000 to 12,500 psi. Tan et al. concluded that for shear span-to-depth ratios greater than 1.5, an orthogonal mat of reinforcement is more effective at restraining the diagonal tension cracks than vertical or horizontal bars alone. Also for shear span-to-depth ratios greater than 1.0 the vertical web steel has a greater effect on restraining the diagonal crack width and increasing the shear strength of the beam.

5.2.2.14 Additional Studies Regarding High-Strength Concrete

Three additional research papers regarding high-strength concrete were included in the database: Foster and Gilbert (1998), Kong and Rangan (1998), and Ozcebe, Ersoy, and Tankut (1999). These three groups of researchers tested beams with concrete strengths ranging from 8,400 to 17,400 psi. The conclusions were in agreement with the previously described studies regarding the shear

behavior of beams constructed with high strength concrete. Minimum shear reinforcement requirements that were based on data from normal-strength concrete were found to be inadequate when applied to high-strength concrete.

5.2.3 Effects of Longitudinal Reinforcement

The effects of longitudinal reinforcement were discussed in six papers that were included in the database. Those papers are: Moody, Viest, Elstner and Hognestad (1954 and 1955), Watstein and Mathey (1958), Rajagopalan and Ferguson (1968), Tan, Teng, Kong, and Lu (1997), and Oh and Shin (2001). Moody et al. demonstrated that before the formation of diagonal cracks a shear-critical beam would behave in the same manner as a beam that is not shear-critical. After diagonal cracking, a shear-critical beam had decreased stiffness compared to a beam failing in flexure. Sudden shear failures were observed to occur at location where the longitudinal bars had been cutoff. Watstein and Mathey concluded that in a deep beam the strain in the longitudinal reinforcement is approximately uniform along the length; which implies the presence of a tied arch mechanism. They also determined that between 38 and 74 percent of the shear at the ultimate load is carried by dowel action.

Using their own experimental work and results of work performed by other authors, Rajagopalan and Ferguson developed a relationship between the concrete contribution to shear strength and the longitudinal reinforcement ratio. The relationship was linear, and had a maximum value of shear stress equal to $2\sqrt{f_c'}$ at a reinforcement ratio of 1.2%. Based on the experimental evidence, the equation produced by Rajagopalan and Ferguson provided a safe lower bound for the design of beams with shear span-to-depth ratios greater than 2.75. Papers by Oh and Shin (2001) and Tan et al. (1997) agreed with Rajagopalan and Ferguson in that the shear strength of concrete beams is a function of the flexural

177

reinforcement ratio. However, both Oh and Shin (2001) and Tan et al. (1997) concluded that the effects of shear span-to-depth ratio are much more critical than the effects of longitudinal reinforcement ratio.

5.2.4   Effects of Loading Type

A concrete beam can be loaded in various ways that can produce different combinations of shear and moment. Ferguson (1956) examined the effects of load distribution as well as the compression induced by applied loads and reactions. Other authors (De Cossio and Siess 1960; Krefeld and Thurston 1966; Ramakrishnan and Ananthanarayana 1968; Uzel 2003) examined the effects of load distribution on shear strength. Each of these researchers observed behavioral differences between concentrated and distributed loads. Finally, Chang and Kesler (1958) and Uribe and Alcocer (2001) examined the effects of fatigue and reversed-cyclic loads on the shear strength of reinforced concrete beams respectively.

5.2.4.1   Effects of Load Distribution

While none of the researchers specifically concluded that the shear strength of beams subjected to uniform loads was higher than the shear strength of beams subjected to concentrated loads, the data presented supports this hypothesis. Krefeld and Thurston (1966) tested more than 200 simply supported beams under concentrated and uniformly distributed loads. Eighty tests with distributed loads and shear span to depth ratios ranging from two to ten were reported. It was concluded that the beams with uniform load had significantly more reserve strength beyond inclined cracking than beams with concentrated loads, and the level of reserve strength was a function of the shear span-to-depth ratio. De Cossio and Siess (1960) observed that beams with distributed loads exhibited increased yielding of the stirrups before failure than did beams tested

178

using concentrated loads. Additionally, Ramakrishnan and Ananthanarayana (1968) observed that the cracking patterns changed along with the load distribution. For beams with distributed loads the first inclined crack occurred at a one-tenth of the span length from the support, but directly at the support for beams with concentrated loads.

Finally, Uzel (2001) performed a comprehensive experimental program to asses the shear strength of footings. The specimens were subjected to uniformly distributed loads that were reacted by a single concentrated load in the middle of the span. In an attempt to observe reduced shear strength in a beam with distributed loads Uzel tested specimens in which the concentrated load was tensile rather then compressive. The tensile force was produced by embedding large reinforcing bars into the specimen. The bars where then anchored to a steel beam beneath the specimen. A bed of hydraulic rams as placed between the concrete specimen and the steel beam to which the bars were anchored. Even with the tensile load applied, all of the distributed load specimens tested by Uzel resulted in higher shear strength than companion specimens with concentrated loads. Furthermore all of the uniformly loaded specimens tested by Uzel failed at levels of shear greater than the nominal strength indicated in ACI 318-05.

5.2.4.2 *Ferguson (1956)*

Ferguson conducted two series of experiments. The specimens for the first series involved four different distributions of loads. Schematic representations of his test specimens are shown in Figure 5-3. Ferguson observed that Specimen F_2 carried approximately half of the shear that any other specimen carried despite having the highest concrete strength of the group. Specimen F_3 exhibited the greatest shear at failure, and Specimens F_5 and F_7 exhibited approximately the same shear strength. For the two specimens with only two concentrated loads, the

179

shear strength changed by a factor of two simply by moving the loads closer to the support further reinforcing the importance of shear span-to-depth ratio.
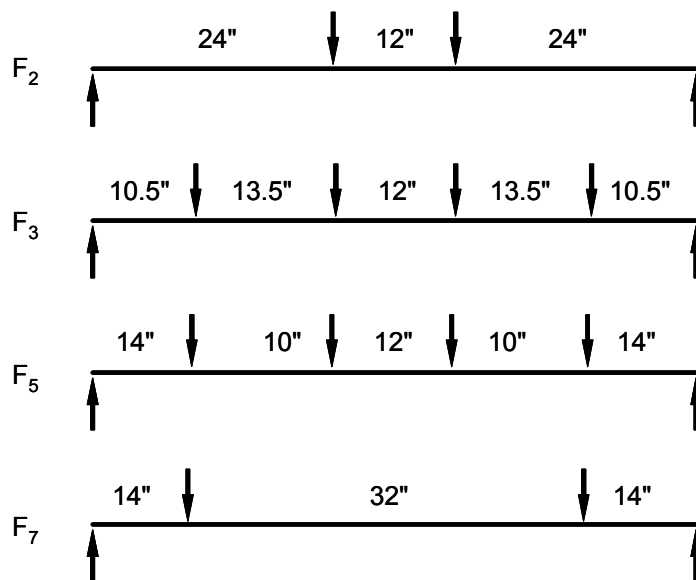
Figure 5-3: Load distribution specimens used by Ferguson (1956)

The second series of specimens tested by Ferguson involved an innovative geometry that allowed examination of the influence of compressive stresses induced by the concentrated loads. The beam geometry is shown in Figure 5-4.
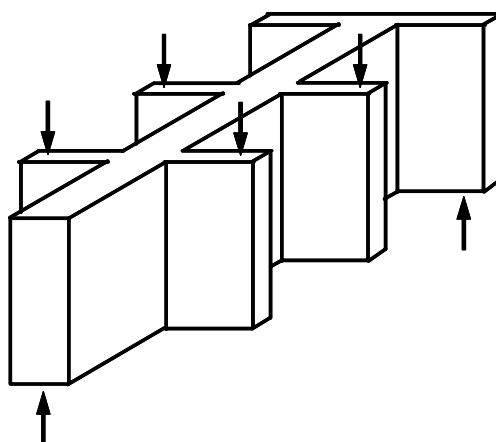
Figure 5-4: Representation of Ferguson's second series of tests.

The geometry shown in Figure 5-4 allowed for the application of loads without inducing compressive stresses into the beam. The loads were applied to small crossbeams rather then the main portion of the specimen. The strength of the beams loaded through the crossbeams was lower than that of the beams loaded traditionally. Ferguson concluded that vertical compression induced by loads or reactions increased the shear capacity of beams.

5.2.5 Fatigue and Cyclic Loading

Chang and Kesler (1958) tested 42 simply supported beams without shear reinforcement. Thirty-nine of the specimens were tested under fatigue loading. It was concluded that the fatigue behavior of beams in shear was affected by concrete strength and longitudinal reinforcement in much the same way as the static strength. Results indicated that if a beam remained uncracked due to fatigue loading, the static strength was unchanged. For fatigue loadings the cracking load was reduced at a higher rate than the ultimate load. Chang and Kesler cite one example in which after 1,000 cycles (stress ranged from 45 to 90% of the expected cracking load) the cracking strength of a beam was reduced to 68% of the static cracking strength, but the ultimate strength was reduced to only 83% of the static value.

Uribe and Alcocer (2001) tested four beams. Two specimens were loaded monotonically to failure, and two companion specimens were loaded cyclically with the loads completely reversing every cycle. The amplitude of each cycle the load was increased over the last cycle until the failure occurred. There was minimal difference between the capacities of the specimens regardless of the load type. However the cyclically loaded specimens exhibited a softer response than the monotonically loaded specimens. The softening, i.e. reduction in stiffness,

181

was attributed to the dramatically increased cracking due to the nature of cyclic loading.

5.2.6 Size Effect

Typically laboratory specimens tend to have relatively small cross-sections, whereas in field conditions the cross-sections of beams can be quite large. Typical bent caps have cross-sections that are on the order of 36x36 in. Code provisions are generally based on laboratory specimens. As such code provisions based on small-scale laboratory specimen may be inadequate for the design of full-scale structural components. Various researchers have examined this effect by testing geometrically similar specimen at various scales.

5.2.6.1 *Shioya (1989)*

The tests conducted by Shioya contain the largest beam tests reported. To examine size effect Shioya tested geometrically similar specimens ranging from 8 to 118 in. deep. The largest beam is shown in Figure 5-5. The Shioya tests consisted of beams with only very light longitudinal reinforcement and no shear reinforcement. For the smaller beams the longitudinal reinforcement varied along the length of the beam. In the middle portion of the beam, the reinforcement ratio was 0.8%, but in the end portions, where shear failure occurred, the reinforcement ratio was 0.4%. In the two largest specimens the longitudinal reinforcement was constant along the length ($\rho = 0.4\%$).

The beams were subjected to uniformly distributed loads. In Figure 5-5 the beam is being tested upside-down. The uniform load is applied at the level of the scaffolding in the picture. The steel beams near the ends on top of the concrete beam are the reaction points. In addition to examining the size effect, Shioya also studied the impact of the maximum aggregate size on shear strength. Shioya concluded that the size effect as it pertains to shear is most significant for beams

182

deeper than 39 in. For beams less than 39 in. deep, shear strength is not affected by increasing beam depth.

Figure 5-5: Photograph of the largest beam test by Shioya (d = 118 in.)

5.2.6.2 Bažant and Kazemi (1991)

Bažant and Kazemi tested a series of simply supported beams with effective depths ranging from 1 to 16 in. The beams were subjected to two point loads with a shear span-to-depth ratio of 3.0. The beams had longitudinal reinforcement only. Among the test results a size effect was observable. However, in some of the specimens, the longitudinal bars were bundled. Bundled bars, in general, have different bond behavior that single bars. Therefore this study combined the effects of bundled bars with size effect. Bažant and Kazemi used fracture mechanics to describe the size effect, and produce analytical models to predict it.

5.2.6.3 Tan and Lu (1999)

Tan and Lu conducted a series of experiments into the size effect using beams with web reinforcement. The specimens ranged from 17 to 61 in. in effective depth with shear span-to-depth ratios ranging from 0.6 to 1.1. It was concluded that the size effect had little effect on the stress which causes diagonal

cracking. Tan and Lu proposed that the critical beam depth beyond which there is no significant size effect is between 20 and 40 in.

5.2.6.4   *Angelakos, Bentz, and Collins (2001)*

Angelakos, Bentz, and Collins tested 21 simply supported beams with 36 in. deep cross-section. The beams were all tested at a shear span-to-depth ratio of 3.0 and had concrete strengths ranging from 3,000 to 14,000 psi. The results indicated that current design procedures are inadequate for members with large effective depths. The beams tested in this series failed at as little as 70% of the load permitted for design using ACI 318-99.

5.2.6.5   *Lubell, Sherwood, Bentz, and Collins (2004)*

Lubell et al. presented the results of a test of a wide and deep beam without shear reinforcement. The beam was 79 in. wide and 36 in. deep. The test was conducted at a shear span-to-depth ratio of 3.0. The beam was intended to model a portion of a slab that supported a column. Because the beam was excessively wide, ACI 318-02 provisions would allow a beam such as this to be designed and built with no transverse reinforcement. Lubell et al. concluded that in order to maintain acceptable levels of safety ACI 318 should reduce the shear strength of beams without shear reinforcement, with excessive member depths or widths, and with light longitudinal reinforcement.

5.2.6.6   *Bentz (2005)*

Bentz developed a series of equations to describe the size effect in shear. To do this he assembled data from past research. He selected series of beam tests from twelve different researchers. Each of the series of tests included geometrically similar beams that were tested at a wide range of effective depths.

The intermediate steps in Bentz' analyses rely on least-squares regressions to various properties of the cross-sections. These least-squares regression resulted in questionable fits to the data. In many cases the regressions yielded values of R^2 that were less than 0.5. Despite the questionable intermediate steps, Bentz was able to produce equations that provide a good fit to each of the test series he included in the analysis. Each of the test series consisted of only a few beams, and no attempt was made to produce an equation that would describe the series of beams tests as a single group of data.

The first conclusion presented in the paper was that the size effect is real and shows decreasing shear stress at shear failure for larger beams without stirrups. Additionally, he concluded that the amount of longitudinal reinforcement and aggregate size are important parameters for accurately determining the shear strength of specimens without shear reinforcement. The remainder of his conclusions discussed the proper coefficients and exponents to be used in the empirical equations presented in the paper.

5.2.7 Anchorage of Longitudinal Reinforcement

For all of the specimens compiled into the database, anchorage of the longitudinal reinforcement at the supports was examined. If a test specimen satisfied the anchorage requirement of the ACI 318 code that was in effect at the time of the test, anchorage was deemed adequate. Early versions of ACI 318 allowed for shorter bar anchorage than currently used. However, several researchers in the 1950s (Clark (1951), Ferguson (1955), and Watstein and Mathey (1958)) welded steel plates onto the reinforcement to increase the anchorage of the bars. Other researchers (Moody et al.(1954), Morrow and Viest (1956), and de Cossio and Siess (1960)) used external "clamp-on" stirrups to

prevent splitting cracks from forming along the longitudinal reinforcement which could induce anchorage failure.

Rogowsky et al. (1986) tested a pair of deep beams to examine the effects of a short longitudinal bar anchorage. Two nominally identical, simply supported specimens were constructed ($a/d = 1.0$). The first had adequate bar anchorage over the supports (standard hooks). In the second specimen the longitudinal bars (No. 6 bars with $f_y = 53.2ksi$) extended only 6 in. into the support. The two nominally identical specimens failed at the same ultimate load, and the poorly anchored bar developed a stress (at the face of the support) of 40.6 ksi (76% of the yield stress) at ultimate load. Rogowsky et al. reported that for beams with small shear span-to-depth ratios, compressive stresses at the supports can greatly reduce the anchorage length of the bars.

For all specimens that were compiled into the database, anchorage within those specimens was examined. All specimens with short anchorages, or that were reported as anchorage failures were not included in the database. Some of the older specimens have less anchorage length than would be required by the current ACI 318 code. The results presented Rogowsky et al. suggest that for beams with small shear span-to-depth ratios (such as those included in the database) anchorage lengths such as those used in the 1950s may be acceptable.

5.2.8   Summary of Database

The results of all the experimental work presented in the above references were compiled into a single database. However additional restrictions were placed on the specimens that were compiled into the database. Only rectangular cross-sections supported on simple spans, without axial loads, were considered. Normal-weight concrete and conventional steel reinforcing bars were used for all beams in the database. These limitations were imposed to assure simple, well-

defined geometry that would permit relatively easy determination of the concrete contribution to shear strength, V_c as well as the parameters necessary for the implementation of STM.

The database comprises tests that represent the last 50 years of research into the shear strength of reinforced concrete beams. Beams that were described by the original authors as having a failure mode other than shear (flexure, anchorage, etc.) were not included in the database. The shear due to the self-weight of the test specimens in the database has been included in the calculation of the failure shear. The details of the specimens which comprise the database are shown in Table 5-1.

5.3 EVALUATION OF STRUT-AND-TIE MODELING SPECIFICATIONS

In AASHTO LRFD Bridge Design Specifications, STM is to be applied only to beams with a shear span-to-depth ratio less than two. The use of ACI 318 does not limit the applicability of STM to beams with a shear span-to-depth ratio of two or less. However in sections 10.7.1 and 11.8.1 of ACI 318-05 a deep beam is defined as a member with a clear span that is less than four times the effective depth of the member. If such a beam is symmetrically loaded, the shear span-to-depth ratio is two. If the shear span-to-depth ratio increases beyond two, a B-Region occurs between two D-Regions and a section model can be used.

However, the shear database contains many specimens with shear span-to-depth ratios greater than two. In order to evaluate STM provisions the subset of the database representing beams with shear span-to-depth ratio less than or equal to two must be used. The shear database contains the results from 494 tests conducted on such beams. All of the statements made regarding STM are based on the set of 494 specimens or a subset of that group based on prescriptive detailing requirements.

187

Table 5-1: Components of the shear database

Reference	No.	f_c' [ksi]	ρ_w [%]	d [in.]	a/d
Ahmad & Lue (1987)	54	9 - 10	0.35 - 6.64	7 - 8	1.0 - 4.0
Angelakos, Bentz, & Collins (2001)	21	3 - 14	0.50 - 2.09	36	2.9
Bažant & Kazemi (1991)	27	7	1.62 - 1.65	1 - 13	3.0
Bresler & Scordelis (1964)	12	3 - 6	1.80 - 3.66	18	3.9 - 7.0
Cao (2001)	4	4 - 5	0.36 - 1.52	74	2.8 - 2.9
Chang & Kesler (1958)	5	2 - 6	1.86 - 2.89	5	1.7 - 3.5
Clark (1951)	2	2 - 7	0.98 - 3.42	13 - 16	1.1 - 2.3
de Paiva & Siess (1965)	9	3 - 6	0.46 - 2.58	6 - 12	0.7 - 1.3
de Cossio & Siess (1960)	7	3 - 5	0.34 - 3.36	10	2.0 - 7.0
Ferguson (1955)	4	4 - 4	2.15	7	1.5 - 3.2
Foster & Gilbert (1998)	16	11 -17	1.25 - 2.15	28 - 47	0.7 - 1.7
Hsiung & Frantz (1985)	4	6	1.82	17	3.0
Johnson & Ramirez (1989)	8	5 - 11	0.25	21	3.1
Kani et al. (1979)	190	2 - 5	0.48 - 2.89	5 - 43	1.0 - 9.1
Kong & Rangan (1998)	48	9 - 13	0.34 - 4.47	8 - 21	1.5 - 3.3
Kong, Robins, & Cole (1970)	35	3 - 4	0.49 - 1.47	10 - 30	0.3 - 1.0
Krefeld & Thurston (1966)	135	2 - 7	0.34 - 5.01	9 - 19	2.3 - 9.7
Laupa, Siess, & Newmark (1953)	13	2 - 5	0.34 - 4.11	10 - 11	5.0 - 5.2
Lubell et al. (2004)	1	9	0.76	36	3.0
Moody et al. (1954)	42	1 - 6	0.80 - 4.25	10 - 21	1.5 - 3.4
Morrow & Viest (1957)	38	2 - 7	0.57 - 3.83	14 - 15	0.9 - 7.9
Oh & Shin (2001)	53	3 - 11	1.29 - 1.56	20	0.5 - 2.0
Ozcebe, Ersoy, & Tankut (1999)	13	8 - 12	1.93 - 4.43	12 - 13	1.9 - 5.0
Rajagopalan & Ferguson (1968)	10	3 - 5	0.25 - 1.73	10 - 11	3.8 - 4.3
Ramakrishnan & Ananthanarayana (1968)	26	2 - 4	0.12 - 0.60	15 - 30	0.2 - 0.9

Table 5-1: Components of the shear database - Continued

Reference	No.	f'_c [ksi]	ρ_w [%]	d [in.]	a/d
Rigotti (2002)	12	2 - 5	4.14	12	1.8 - 2.3
Rogowsky, MacGregor, & Ong (1986)	14	4 - 6	0.40 - 1.80	20 - 39	0.8 -1.6
Roller & Russell (1991)	10	11 - 18	1.64 - 6.97	22 - 30	2.5 - 3.0
Sarsam & Al-Musawi (1992)	14	6 - 12	0.22 - 3.51	9	2.5 - 4.0
Shin, Lee, Moon, & Ghosh (1999)	30	8 - 11	3.77	9	1.5 - 2.5
Shioya (1989)	8	3 - 4	0.39	8 - 118	6.0
Smith & Vantsiotis (1982)	47	2 - 3	1.94	14	0.9 - 1.8
Subedi, Vardy, & Kubota (1986)	13	4 - 8	0.14 - 1.09	18 - 35	0.4 - 1.4
Tan & Lu (1999)	12	5 - 7	0.26	18 - 61	0.6 - 1.1
Tan, Kong, Teng, & Guan (1985)	13	6 - 9	1.23	18	0.3 - 1.1
Tan, Kong, Teng, & Weng (1997)	19	8 - 13	2.58	17	0.9 - 1.7
Tan, Teng, Kong & Lu (1997)	3	9 - 10	2.58 - 4.08	17	0.3 - 0.6
Uribe & Alcocer (2001)	2	5	1.58	43	1.3
Uzel (2003)	14	4 - 6	0.76 - 2.16	9- 36	1.9 - 4.9
Van Den Berg (1962)	44	2 - 11	1.72 - 4.35	14 -18	2.1 - 4.9
Watstein & Mathey (1958)	9	3 - 4	0.75 - 3.05	13 - 16	1.5 - 2.1
Xie et al. (1994)	15	6 - 16	0.21 - 4.54	8 - 9	1.0 - 4.0
Yang, Chung, Lee & Eun (2003)	8	5 - 11	0.90 - 1.00	14 - 37	0.5 - 0.6
Yoon, Cook, & Mitchell (1996)	12	5 - 13	2.49	26	3.3
Yoshida (2000)	4	5	0.74	74	2.9
Brown	24	2 - 4	2.0 - 3.1	16 - 27	1.5 - 6.0
Complete Database	1,194	1 - 18	0.1 - 7.0	1 - 118	0.2 - 9.7

5.3.1 Selection of Appropriate Truss Models

To evaluate the test results contained in the database, standard truss models were developed. Two such models were developed; one model for beams subjected to one concentrated load, and another model for beams subjected to two point loads (Figure 5-6).
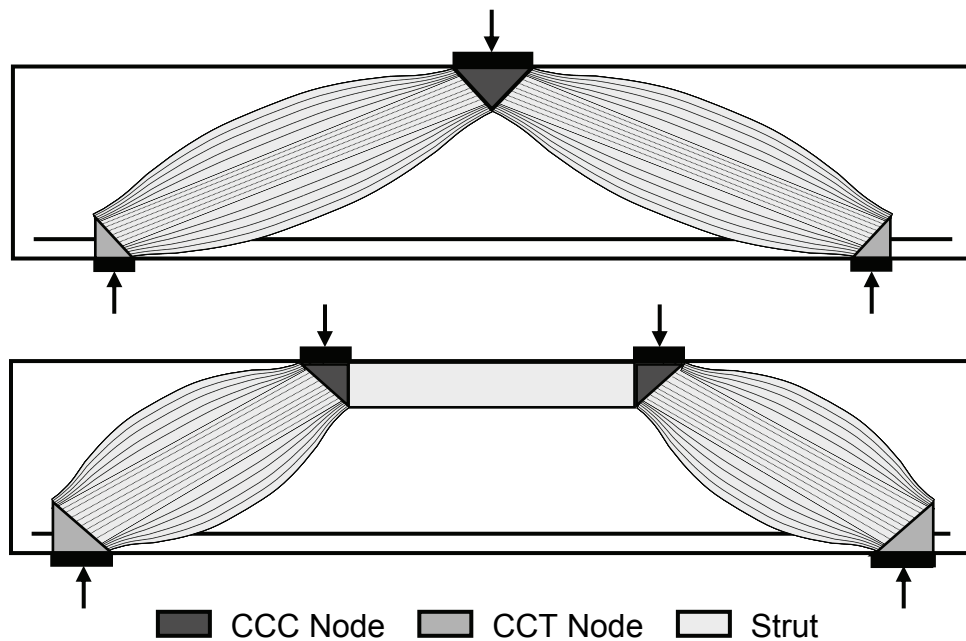
Figure 5-6: Truss models used for specimens in the database

Each of these two truss models (Figure 5-6) represents a tied-arch mechanism that is not affected by the presence or absence of transverse reinforcement. However when transverse reinforcement is present, especially in large quantities, more complicated truss models may be appropriate. Various truss models, some of which include the effects of transverse reinforcement, are shown in Figure 5-7. For specimens with a shear span-to-depth ratio of two or less, the trusses in part a) or b) of Figure 5-7 may both be appropriate. In order to determine which model is most applicable to a given specimen, an energy analysis was performed on the test results in the database.

190
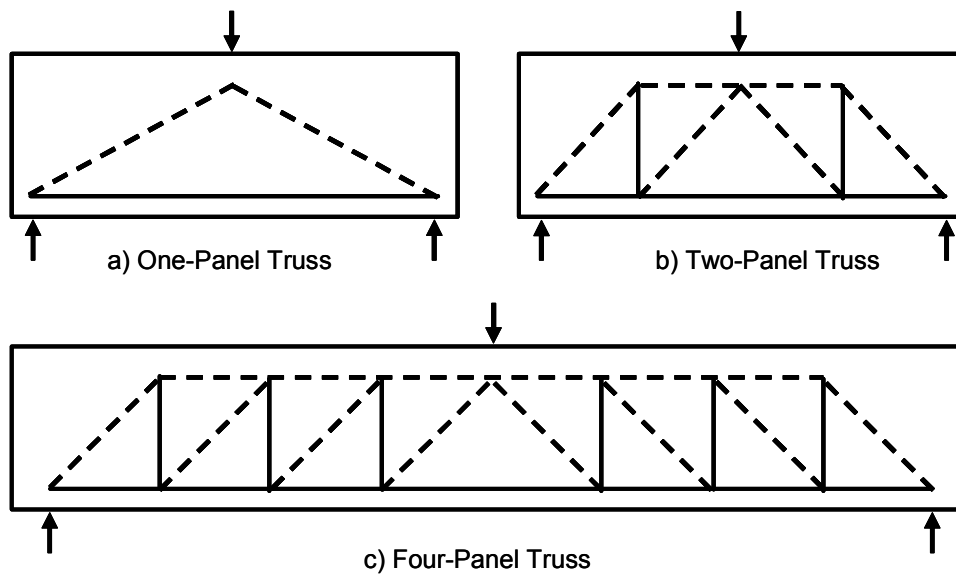
Figure 5-7: Trusses with varying numbers of panels

5.3.1.1 *Strain Energy in a Truss Model*

Based on the recommendations of Schlaich, Jennewein, and Schäfer (1987) the model that contains the least strain energy was determined to be the most appropriate model. For each element in the truss model (struts and ties) the strain energy was calculated then summed to determine the strain energy stored in the truss. For the struts the stress-strain relationship developed by Hognestad (1951) was used. The stress-strain relationship for the steel ties consisted of three piecewise continuous lines. The first portion was the linear elastic range. The second portion was the yield plateau. In this portion the stress was kept constant at the specified yield stress until a strain of 0.01. The third, and final, portion of the stress-strain response of the steel was linear and extended up to a stress that was 50% greater than the yield stress, and a strain of 0.1. Fracture of the steel was assumed to occur at a strain of 0.1. The constitutive laws used for the struts and ties are shown in the lower portion of Figure 5-8.

191
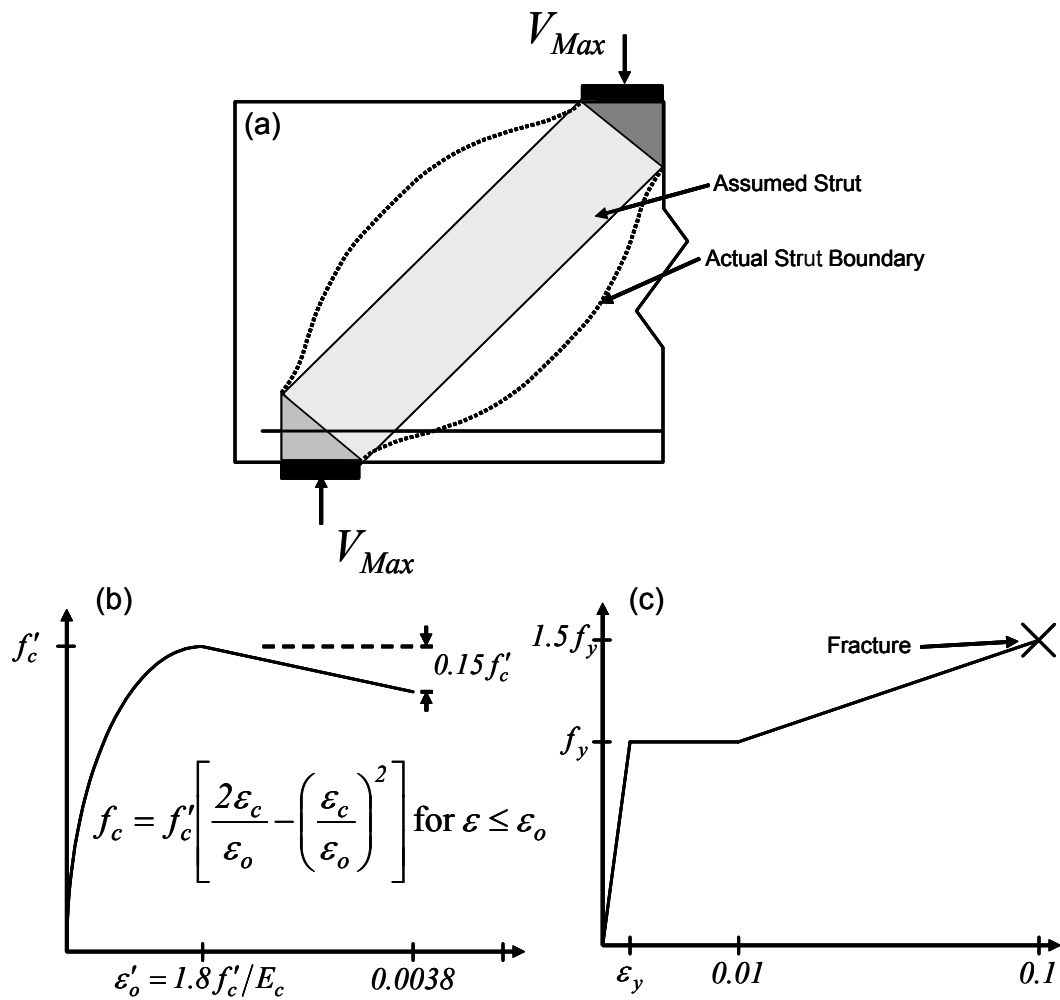
Figure 5-8: Assumptions to strain energy calculations ((a) strut geometry, (b) constitutive relationship for concrete, and (c) constitutive relationship for steel)

Based on the failure load of the truss as reported in the database, the forces in all the truss members were determined. The stresses, and subsequently the strains, in each of the members were based on the geometry of the struts and ties. All of the vertical shear reinforcement within the shear span was included in the area of the tie to determine the stress and strain in the tie. The struts were assumed to be prismatic in order to calculate their volume. The cross-sectional area of the

strut was determined using a hydrostatic node. The size of the bearing plate and the angle of inclination of the strut were used to calculate the area of the end of the strut. That area was assumed to be constant along the length of the strut. In a bottle-shaped strut, the stress at the middle of the strut is less than at the ends of the strut due to the dispersion of compression. However, in the portions of the strut where the stress is less, the cross-sectional area, and hence the volume, is greater. Therefore the use of prismatic struts for the calculations of strain energy should be similar in the assumed strut and the actual bottle-shaped strut.

The area under the stress-strain relationship (Figure 5-8 (b) and (c)) was then multiplied by the volume of the strut or tie to determine the strain energy of that element. The strain energy of the nodes was neglected due to their small volume. Once the strain energy of each element was calculated, the strain energies were summed to determine the strain energy of the entire truss.

The results of the strain energy calculation are heavily dependant on the assumptions used to determine the geometry of the struts and ties. Different, yet equally valid, assumptions would change the numerical results significantly. Therefore, no numerical results of the strain energy calculations are presented herein. The trends observed in the calculations are discussed. Since each calculation was subject to the same set of assumptions, the trends in the results are meaningful.

Based on the results of the energy analysis, the majority of the specimens in the database exhibited the minimum strain energy in a one-panel truss (Figure 5-7a). Only 2% of the 494 specimens contained the minimum strain energy in a two panel solution (Figure 5-7b).

Schlaich, Jennewein, and Schäfer (1987) indicated that when calculating the strain energy of a truss model, the strain energy is concentrated in the ties. They also suggested that the strain energy in the struts can be neglected. Based on

193

the energy analysis conducted this assumption proved to be invalid. For 39% of the 494 records, more than half of the total strain energy was contained in the struts based on the one panel solutions. Based on the two-panel solutions in 5% of the specimens the concrete contribution to the strain energy was more than half of the total energy. Therefore, as a truss model becomes more complex, the concrete contribution to the strain energy is diminished relative to the steel contribution, but for simple models, the strain energy stored in the struts is not likely to be negligible.

5.3.1.2 *Effect of Transverse Reinforcement on Strain Energy*

The one-panel truss does not include any effects of transverse reinforcement, but the two-panel truss does. The vertical ties in Figure 5-7b are representations of the stirrups within the actual beam. The dominant truss mechanism was the one-panel solution. In order to include the effects of stirrups a new model was developed.

The new model consisted of a superposition of one-panel and two-panel trusses. A fraction of the failure load (γ) was applied to a one-panel solution and the remaining fraction ($1-\gamma$) was applied to the two-panel solution. The value of γ was then varied from zero to one, and the value of γ which corresponded to the minimum strain energy was recorded.

194
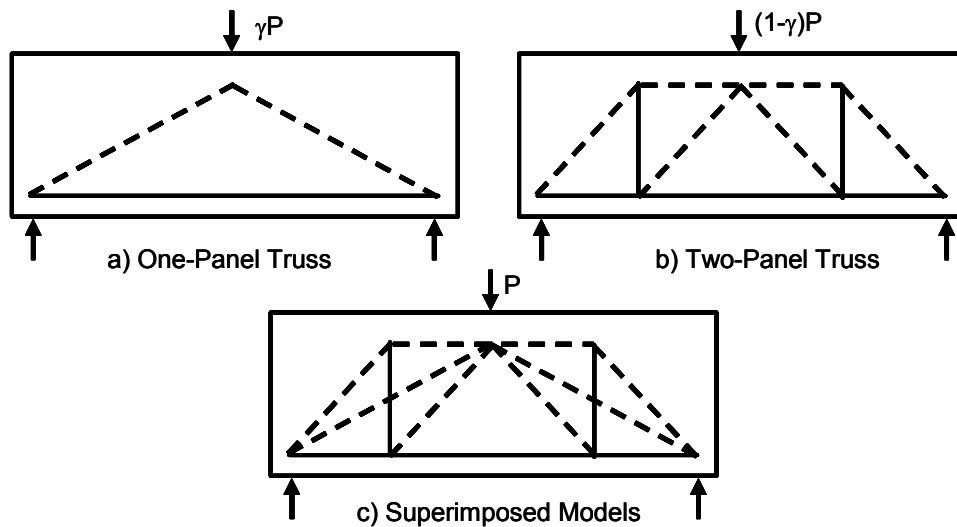
Figure 5-9: Superimposed truss models

Based on γ a representative number of panels (n) was calculated for the superimposed model. The representative number, n, indicated which of the two models (one- or two-panel) was the main load carrying mechanism. For example a value of n equal to 1.5 indicated that half of the load was carried by each of the trusses. A value of n equal to 1.2 indicated that 80% of the load was carried with a one-panel solution and the remaining 20% was carried by the two-panel solution. The value of n as a function of the shear span-to-depth ratio is shown in Figure 5-10. The data in Figure 5-10 indicate that as the shear span-to-depth ratio increases from zero to two, the two-panel truss carried increasing portions of the load. At a shear span-to-depth ratio of 1.7 or greater the two-panel truss is the dominant mechanism ($n > 1.5$) for only 12 specimens.
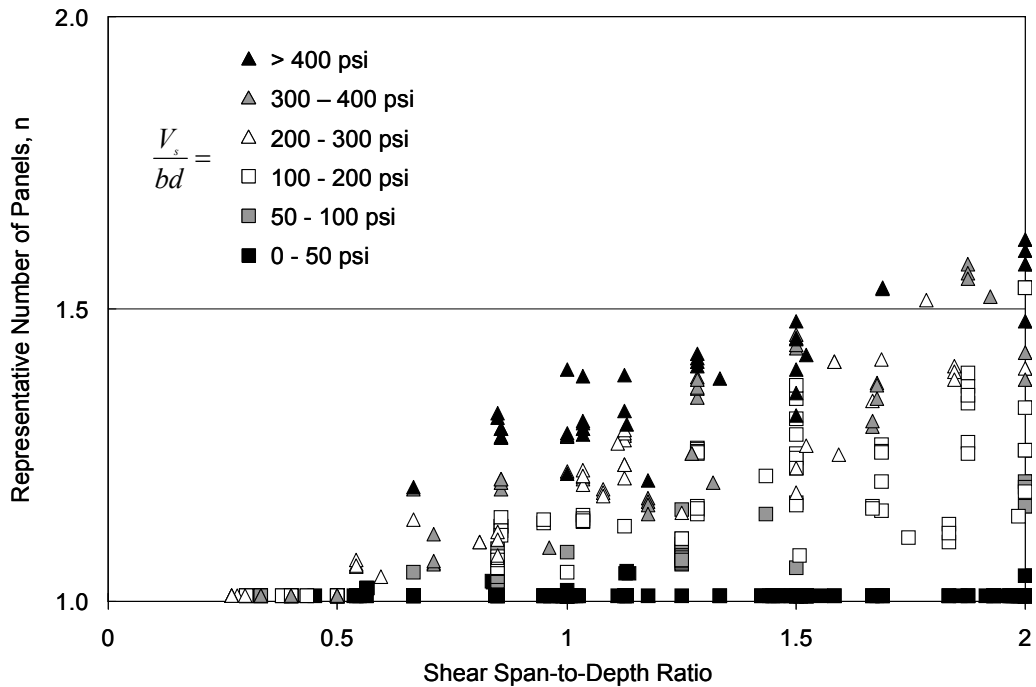
Figure 5-10: Representative number of panels for database specimens

In addition to the trend that exists between shear span-to-depth ratio and n, there is a trend between the transverse reinforcement ratio and n. In Figure 5-10 the specimens without shear reinforcement are plotted on the line n = 1. The points along the upper edge of the cloud of data represent specimens with heavy shear reinforcement. The different symbols within the figure indicate differing amounts of shear reinforcement. The various amounts of shear reinforcement are quantified based on the amount of shear stress that is resisted by the steel contribution to the shear strength of the beam ($V_s/(b_wd)$). For a given shear span-to-depth ratio, more shear reinforcement increased the fraction of the load that was carried by a two-panel solution.

Collins and Mitchell (1997) state that beams with shear span-to-depth ratios less than 2.5 carry the applied load through the formation a direct strut in a

196

manner similar to the one-panel solution in Figure 5-7. Additionally, they conclude that the failure of such beams will involve the crushing of concrete and be heavily influenced by details such as the size of the bearings.

5.3.2 Experimentally Determined Efficiency Factors

As previously described, the efficiency factor is a number, generally less than one, that determines the fraction of the concrete strength to use as the permissible stress on a strut or node. The values of the efficiency factor measured in laboratory investigations will be used to evaluate both ACI and AASHTO STM provisions. To determine the measured efficiency factors only the compressive strength of the concrete, failure shear, and the bearing area at the support need to be known. For 8% of the specimens in the database, the exact sizes of the bearing plates were not presented in the original paper. For approximately half of those specimens (4% of the total database) the size of the bearing plates could be scaled from drawing or photographs within the paper. For the remaining 4% of the specimens, the bearing plates were assumed to be square with the side length equal to the beam width.   Using those values the experimentally determined efficiency is:

$$v_{exp} = \frac{V_{Max}}{A_b f_c'} \qquad\qquad (5\text{-}1)$$

Where: v_{exp} = experimentally determined efficiency factor

V_{Max} = maximum shear (including self-weight)

A_b = bearing area of the reaction or applied load

f_c' = concrete compressive stress

The calculated efficiency factor was based on the maximum stress on the bearing face of the node. However, if the node is hydrostatic, which is a common assumption in STM, the stresses on all node faces will be equal. For the analyses

presented in this chapter, hydrostatic nodes were assumed. At any given node, the node itself and the abutting strut(s) will share a common area at the plane of intersection (Figure 5-11). Therefore the stress on the end of the strut is equal to the stress on the face of the node. In a non-prismatic strut, the maximum stress in the strut will occur at the minimum area. For a bottle-shaped strut the minimum area of the strut occurs where the strut frames into the node. Therefore, for a hydrostatic node with a bottle-shaped strut and uniform beam width, the maximum stress in the strut will be equal to the stress in the node. The calculated value of the efficiency factor can therefore be applied to the adjoining strut.
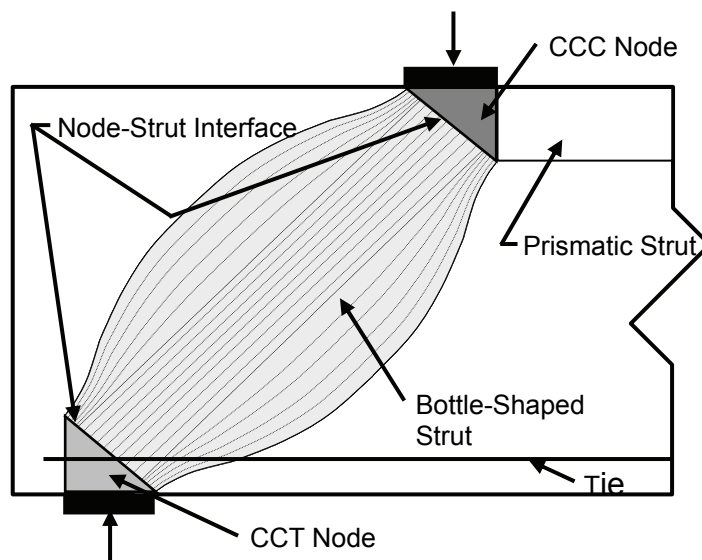
Figure 5-11: Common area at node-strut interface

5.3.3 Examination of STM Specifications

Based on the experimental work described in previous chapters (Chapters 3 and 4), it is believed that for beams with short shear spans failure typically occurs at the interface between a node and a strut with the majority of the damage occurring in the strut. Failures of this type were observed in both the isolated strut tests which involved a CCC node (Chapter 3), and the various beam tests which

involved observed failure at CCT node-to-strut interface (Chapter 4). Similar types of failures were assumed for the tests in the database. Consequently, the efficiency factors calculated using the database are considered to be at failure of the strut at the node-to-strut interface. Specifically, the efficiency factors from the database are based on the nodal stresses present at the time of the strut failure. The measured efficiency factors will therefore be compared to the provisions for strut efficiency factors presented in ACI and AASHTO which are, in general, lower than the nodal efficiency factors. Complete discussions of the ACI 318-05 and AASHTO LRFD Bridge Design Specifications for STM were presented in Chapter 2.

5.3.3.1   Examination of ACI 318-05 Appendix A Provisions

The struts in the beams compiled into the database are bottle-shaped because they are not constrained by the geometry of the beam or the location of the neutral axis. They are inclined and unrestrained by limitations of the beam geometry. ACI 318-05 presents two different efficiency factors for bottle-shaped struts. The provisions of ACI 318-05 Appendix A require that the efficiency factors be applied to $0.85 f'_c$. A higher efficiency factor ($\nu = 0.85 \cdot 0.75 = 0.64$) is reserved for struts that have adequate reinforcement to restrain the splitting crack. A lower efficiency factor ($\nu = 0.85 \cdot 0.60 = 0.51$) is used for struts without sufficient reinforcement. The proper amount of reinforcement can be determined by modeling the spread of compression along the length of the strut or by satisfying Eq. A-4 of ACI 318-05:

$$\sum \frac{A_{si}}{bs_i} sin\,\alpha_i \geq 0.003 \qquad\qquad (5\text{-}2)$$

Where: A_{si} = area of surface reinforcement in the ith layer crossing a strut

199

s_i = spacing of reinforcing bars in the ith layer adjacent to the surface of the member

b = the width of the strut perpendicular to the plane of the reinforcing bars

α_i = the angle between the axis of the strut and the bars in the ith layer of reinforcement crossing that strut

Using the provisions of Appendix A of 318-05, there are no prescriptive requirements for the minimum shear reinforcement. Consequently, the full database of 494 specimens can be used to evaluate the efficiency factors presented in ACI 318-05.

Based on the tests contained in the database, the value of strut efficiencies presented in Appendix A of ACI 318-05 provided unconservative estimates of the measured strut efficiency for 51% of the test data as can be seen in Figure 5-12. The upper portion of Figure 5-12 shows only specimens that do not meet the requirements of Eq. 5-2, and the lower portion shows specimens that do meet the requirements of Eq. 5-2. For both portions of the figure roughly half of the data is on the unconservative side of the line. In the figure, the horizontal lines represent the efficiency factors that are that is permitted for specimens without transverse reinforcement (Figure 5-12a) and specimens with transverse reinforcement (Figure 5-12b). It is important to note that experimental data seem to be evenly distributed throughout Figure 5-12 and the line which represents the design value does not agree with the data.
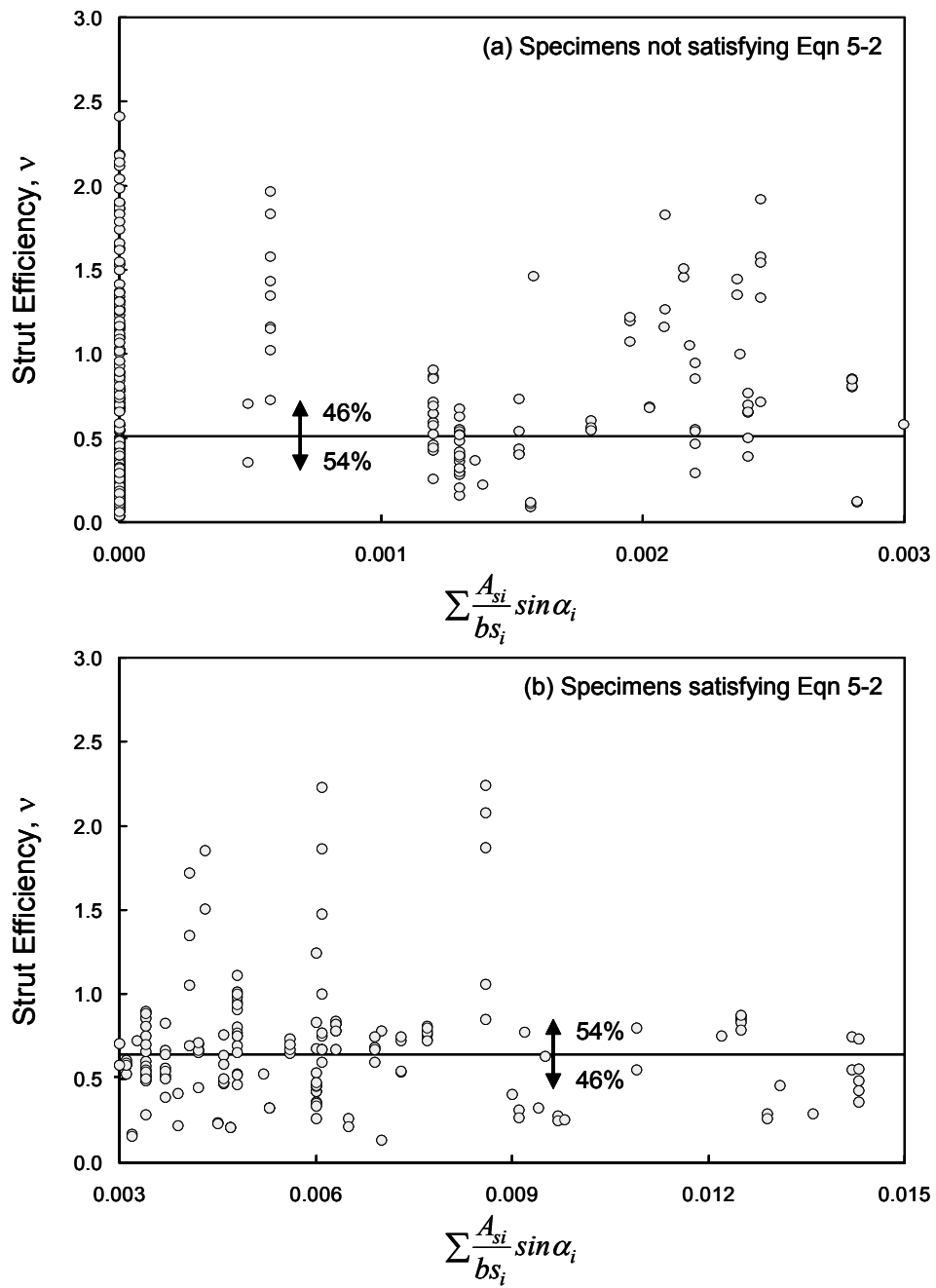
Figure 5-12: Measured strut efficiencies compared with those in ACI 318-05 Appendix A

Comparing the experimentally observed efficiency factors with the design efficiency factor is insufficient to determine the overall conservatism of ACI 318-05 Appendix A. The nominal strength (without load or strength reduction factors) must be compared with the measured load. When comparing the design and measured shear strengths, ACI 318-05 Appendix A results in safe predictions of strength for 73% of the test specimens. For specimens without shear reinforcement, the use of ACI 318-05 Appendix A results in safe predictions of strength for only 66% of the test specimens. The increase in levels of safety based on shear strengths rather than efficiency factors is due to the node and strut geometry.

Appendix A of ACI 318-05 does not specify, or recommend, the use of hydrostatic nodes. Instead the node geometry is determined based on the beam details. A drawing of a typical node defined using ACI Appendix A geometry is shown in Figure 5-13. The inclined face of a CCT node as determined by the geometry in ACI 318-05 has less area than in the hydrostatic case in most cases. The difference between the geometry of a hydrostatic node and a non-hydrostatic node occurs because of differences in the width of the tie (w_t in Figure 5-13). For a non-hydrostatic node the width of the tie, w_t, is limited to twice the distance from the centroid of the tie to the free surface of the beam. For a hydrostatic node w_t can be larger. In turn, the inclined face of the node, and therefore the end of the abutting strut, will be somewhat larger for hydrostatic nodes. In short, the efficiency factors for bottle-shaped struts specified in ACI 318-05 Appendix A are very liberal, but the node geometry can be rather conservative. These two effects partially cancel each other.
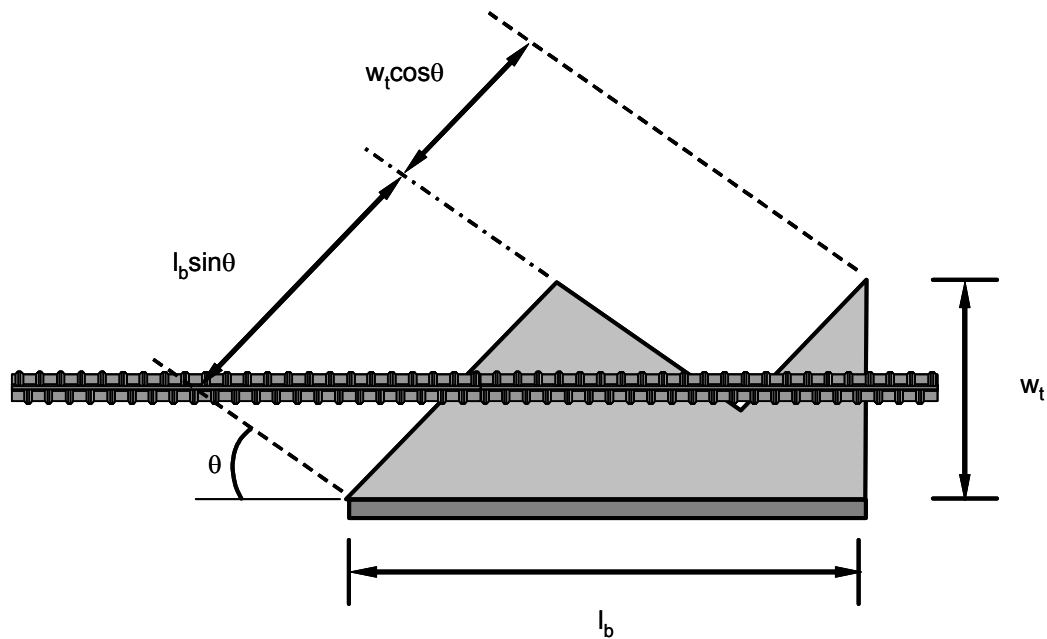
Figure 5-13: CCT node with geometry as defined by ACI 318-05

5.3.3.1.1 Prescriptive Minimum Reinforcement Requirements from ACI 318-99

In ACI 318-99 minimum reinforcement for deep beams were specified in Chapter 11 of the code. The minimum amounts of web reinforcement were:

$$A_v \geq 0.0015 b_w s \qquad\qquad (5\text{-}3)$$

$$A_{vh} \geq 0.0025 b_w s_2 \qquad\qquad (5\text{-}4)$$

Where: A_v = the area of shear reinforcement perpendicular to the span

A_{vh} = the area of shear reinforcement parallel to the span

b_w = width of the web

s = spacing of the vertical shear reinforcement measured parallel to the longitudinal reinforcement

s_2 = spacing of horizontal shear reinforcement in a direction perpendicular to the longitudinal reinforcement.

The above requirements were based, in part, on the recommendations produced by Rogowsky, MacGregor, and Ong (1986).

Many of the specimens in the database described in the previous sections did not meet the minimum reinforcement requirements of ACI 318-99. In order to examine the effect of the minimum shear reinforcement on efficiency factors, a subset of the database described was created to include only specimen that satisfied the ACI 318-99 requirements. Only 81 of the 494 specimens satisfied those reinforcement requirements. Of those 81 test specimens, 66 (82%) exhibited shear strengths that were greater than the design value as determined using ACI 318-02 Appendix A. As mentioned earlier, for the full database (n = 494) 72% of the specimens exhibited failure loads in excess of those determined through implementation of the ACI 318 provisions.

5.3.3.1.2 Prescriptive Requirement from ACI 318-05

In the 2002 version of ACI 318, the prescriptive requirements for minimum shear reinforcement for deep beams were changed from the 1999 edition of the code. Those provisions from ACI 318-02 remain unchanged in ACI 318-05. In the 2002 and 2005 editions, the coefficients in Eqns 5-3 and 5-4 were exchanged. The minimum vertical shear reinforcement ratio increased from 0.0015 to 0.0025. Conversely, the minimum horizontal shear reinforcement ratio reduced from 0.0025 to 0.0015.

Seventy-one specimens in the database satisfied the ACI 318-05 provisions. Of those 71 specimens, 61 (86%) failed at loads greater than the design values determined using Appendix A of ACI 318-05.

5.3.3.1.3 Summary of ACI 318-05 STM Provisions

For a strut at a CCT node, the use of ACI 318-05 results in efficiency factors that exceed values for a majority of the specimens in the database (65% of the data). The high factors are somewhat compensated for by limited node and strut areas. Using ACI 318-05 Appendix A without any additional prescriptive requirements, 72% of the specimens in the database failed above the nominal capacity. Using the minimum shear reinforcement provisions from Chapter 11 of ACI 318-99 and ACI 318-05 increased the percentage of safe specimens to 82% and 86% respectively. Based on these percentages it appears that the minimum shear reinforcement requirements of ACI 318 are affecting the behavior of the specimens in a positive manner.

Here it is important to note that when using the provisions of ACI 318-05 Appendix A, the minimum reinforcement requirement of Chapter 11 can be ignored. Therefore, if a design engineer chooses to use the efficiency associated with an unreinforced bottle-shaped strut, there is no minimum amount of shear reinforcement prescribed for deep beams.

5.3.3.2 Examination of AASHTO LRFD Bridge Design Specifications

The STM provisions of AASHTO LRFD Bridge Design Specifications make no distinction between bottle-shaped and prismatic struts. The strength of struts is based on the following expressions:

$$f_{cu} = \frac{f_c'}{0.8 + 170\varepsilon_1} \leq 0.85 f_c' \qquad (5\text{-}5)$$

$$\varepsilon_1 = \varepsilon_s + (\varepsilon_s + 0.002)\cot^2 \alpha_s \qquad (5\text{-}6)$$

Where: α_s = the smallest angle between the compressive strut the adjoining tie

205

ε_s = the tensile strain in the concrete in the direction of the tension tie

f_c' = specified concrete strength

f_{cu} = usable compressive strength

Unlike ACI 318-05, AASHTO specifies the use of minimum reinforcement for all struts. More specifically, Section 5.6.3.6 of AASHTO requires a shear reinforcement ratio of 0.003 in both the horizontal and vertical directions. The AASHTO minimum reinforcement requirement represents a significant increase in reinforcement compared with ACI 318. Additionally, the commentary of AASHTO section 5.6.3.6 recommends that in wide members the shear reinforcement may need to be distributed throughout the width of a section, resulting in the use of multiple stirrup legs, which can greatly increase congestion.

When the minimum reinforcement requirements are applied to the specimens listed in the database, only 49 specimens meet the AASHTO LRFD requirements. Of the 49 specimens, 92% had measured strengths greater than the nominal capacities determined using the STM provisions.

The measured efficiency factors for the specimens that satisfied the minimum reinforcement requirements are shown in Figure 5-14. The curved line plotted in the figure represents the design value of efficiency that is obtained by using Eqns. 5-5 and 5-6 with a value of 0.002 for the tensile strain in the direction of the tie, ε_s. The principal difficulty in the application of AASHTO STM provisions is the proper selection of the value of ε_s. The value of 0.002 was chosen as a nominal value based on design examples presented in Collins and Mitchell (1997).

In Figure 5-14 only 6 of the measured efficiency factors are below the nominal design value. Also, the data seem to be more closely grouped near the design equation for inclinations less than 60 degrees.
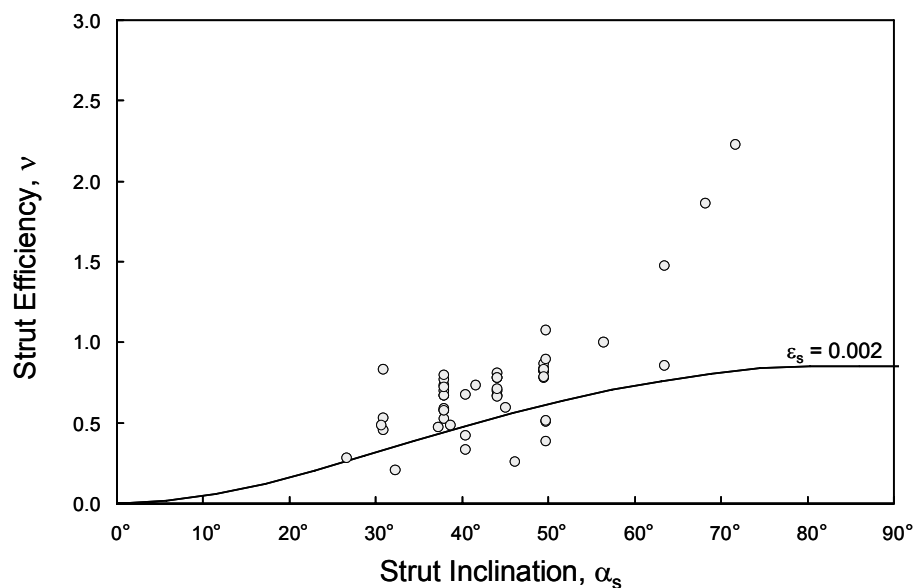
Figure 5-14: Measured strut efficiencies compared to those used in AASHTO STM Provisions (specimens that satisfies minimum reinforcement requirements)

5.3.3.2.1 *Application of AASHTO LRFD STM Provisions to the Full Database*

In order to compare the AASHTO LRFD design expressions with the full database, the AASHTO LRFD minimum reinforcement requirements were ignored. The results of that analysis are shown in Figure 5-15. With the removal of the detailing requirements, the amount of scatter in the data greatly increased, and the number of unconservative test results also increased. Despite the large number of data points below the design equation in Figure 5-15, 84% of the specimens failed at loads greater than the nominal design strength. AASHTO

LRFD provisions, like ACI 318-05 specification, restricted the area of the nodes and struts compared to hydrostatic nodes. The restriction reduces the area, and therefore strengths, of the nodes.
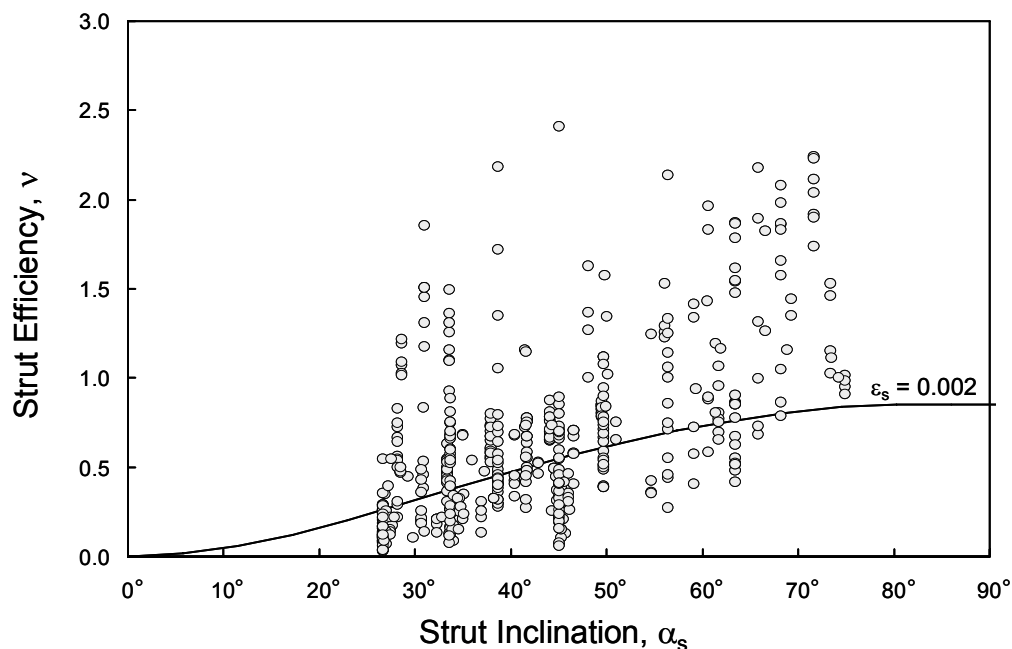
Figure 5-15: Measured strut efficiencies compared to those used in AASHTO STM Provisions (all specimens)

5.3.3.3   *Summary of U.S. Code Provisions for STM*

Both ACI 318-05 and AASHTO LRFD Bridge Design Specifications have some deficiencies in the STM provisions when examined against the database. The ACI STM provisions are very simple to apply, yet they result in unacceptable numbers of test specimens that fail at loads less than the nominal capacity. The levels of conservatism can be improved with the implementation of minimum shear reinforcement for members designed using STM.

The AASHTO STM specifications require large amounts of shear reinforcement to meet the minimum requirements and result in greatly reduced percentage of specimens with low capacities. However, the minimum shear reinforcement requirements in AASHTO LRFD are considerably greater than those presented in CSA A23.3-94 and ACI 318-05. Additionally, the design equation for the efficiency of a strut is based on a tensile concrete strain. The tensile concrete strain in the direction of a tie is easily quantifiable in a laboratory environment, but difficult to determine otherwise.

Traditionally, U.S. codes are based on provisions whose application results in 5% or less unconservative test results. When the current provisions for sectional shear were developed (ACI 326 1962), only 2.5% of the test results available at the time were unconservative. Currently application of the STM provisions of ACI 318-05 and AASHTO LRFD Bridge Design Specifications result in more than 5% unconservative test results. Therefore, a new procedure was developed.

5.4 DEVELOPMENT OF A NEW STM PROCEDURE

Due to the short-comings of the ACI and AASHTO STM provisions, a new method of modeling and design was developed. The new model incorporates the simplicity of the ACI 318 Appendix A STM provisions, with the high levels of safety of the AASHTO LRFD Bridge Design Specifications. Those two ideas, reliability and simplicity, guided the development process.

The newly developed procedure is limited to beams with shear span-to-depth ratios less than two. . If the shear span-to-depth ratio increases beyond two, the direct strut between the support and the load becomes very inefficient. The inefficiency of the strut then induces multiple-panel mechanisms as shown in Figure 5-7. Mechanisms with multiple panels are governed by conditions away

from the disturbed regions and sectional design methods are more appropriate and easier to implement. Additionally, Collins and Mitchell (1997) suggest that as the shear span-to-depth ratio increases beyond 2.5 sectional models are preferable to STM. For the new procedure the shear span-to-depth ratio was limited to two or less to be in agreement with current code practice.

5.4.1   Analysis of the Database

Based on the data shown in Figure 5-12, Figure 5-14, and Figure 5-15, the methods to determine the allowable efficiency factors for both ACI and AASHTO can be considered inadequate based on commonly accepted levels of conservatism. Traditionally, U.S. code authorities seek provisions whose application results in 5% or less unconservative test results. The implementation of both ACI and AASHTO yielded large numbers of specimens with measured strengths less than the nominal capacities. A better method to estimate capacity was sought so that few unconservative estimates of strength would result.

Based on the results of the literature review presented in this chapter along with the experimental results described in Chapter 4, the primary factors affecting strut efficiency can be identified as strut inclination, shear reinforcement, and concrete strength. The relationship between concrete strength and strut strength is intuitive, increased concrete strength results in stronger struts. The correlation between shear strength and shear span-to-depth ratio has been observed by many researchers. Therefore, the strength of a strut is likely to be affected by variations in shear span-to-depth ratio. The role of transverse reinforcement for short shear spans has been investigated by many researchers with varying conclusions.

To develop the new expressions, the effects of shear span-to-depth ratio, transverse reinforcement ratio, and compressive strength were evaluated. Of those three factors, the greatest correlations with efficiency factor were between

210

compressive strength and shear span-to-depth ratio (a/d). The scatter in the data was further reduced by using the square root of the compressive strength as an indicator of efficiency factor. Ultimately the parameter that reduced the scatter the most was a combination of the shear span-to-depth ratio and the square root of the concrete strength. The impact of shear reinforcement on the new procedures is discussed in detail in the next section.

Once the apparent scatter in the data was reduced as much as possible, a least-squares regression was performed. That least-squares regression then served as the basis of the design equations under development. The measured data as well as the least-squares regression are shown in Figure 5-16.
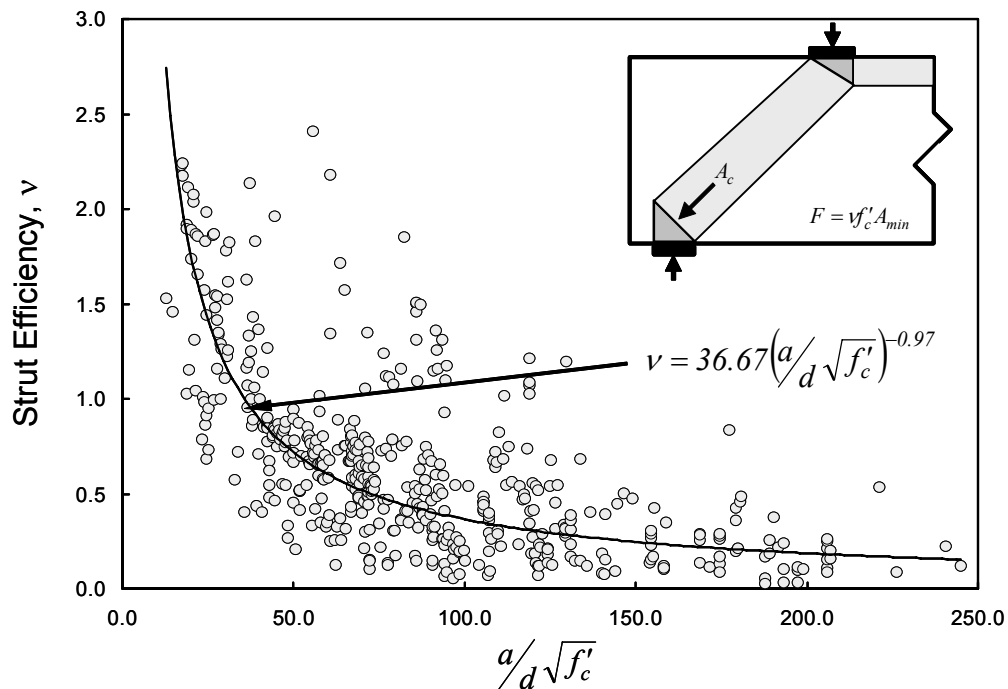
Figure 5-16: Least-squares regression to the data

A design expression resulting from a least-squares regression alone is not acceptable. As can be seen in Figure 5-16, a significant portion of the data lies below the best-fit curve. The best-fit curve must be altered to ensure only a small

fraction of specimens will fail at loads less than that predicted by the design model. To satisfy safety concerns, the leading coefficient (36.67 in Figure 5-16) was varied so that only 5% of the test specimens failed at loads less than predicted by the design model. For the sake of simplicity, the coefficient was rounded from 0.97 to 1.0.

During the process of determining the proper coefficient for the design equation, it was observed that in general the specimens with little or no shear reinforcement produced lower efficiency factors than other specimens with shear reinforcement in significant amounts. Hence, it was decided that two different coefficients would be chosen. The higher of the two coefficients would be used for "sufficiently reinforced" specimens and the lower for "insufficiently reinforced" specimens. For safety purposes both coefficients would need to be less than the value of 36.67 produced by the best-fit regression. Additionally an upper limit on the efficiency would need to be enforced. Clearly a specimen with a shear span-to-depth ratio of zero is not infinitely efficient.

5.4.2 Reinforcement Requirements

The minimum reinforcement requirements in ACI and AASHTO seem to be in disagreement. The AASHTO reinforcement is specifically designated as crack control; whereas there is substantial debate regarding whether the reinforcement required by ACI is for strength or serviceability. For the new model, a solution for the minimum reinforcement required to carry the transverse tension in a bottle shaped strut was developed based solely on strength.

As can be seen in Figure 5-17, the transverse tension in a bottle shaped strut is directly related to the angle at which the compression disperses. Traditionally a 2:1 ($m = 2$) angle of dispersion was used for the purposes of modeling. It has also become standard practice to model the bottle shape with two

212

ties located at third-points of the strut. Therefore the total transverse tension force is twice the individual tie forces. It was assumed that all the reinforcement that crosses the splitting crack contributes to resisting the transverse tension. The traditional strut-and-tie model for a bottle-shaped strut is shown in Figure 5-17.

$$tan\,\phi = \frac{1}{m}$$

$$F/_2 = C\,cos\,\phi$$

$$T = C\,sin\,\phi$$

$$T = F/_2\,tan\,\phi = F/_{2m}$$
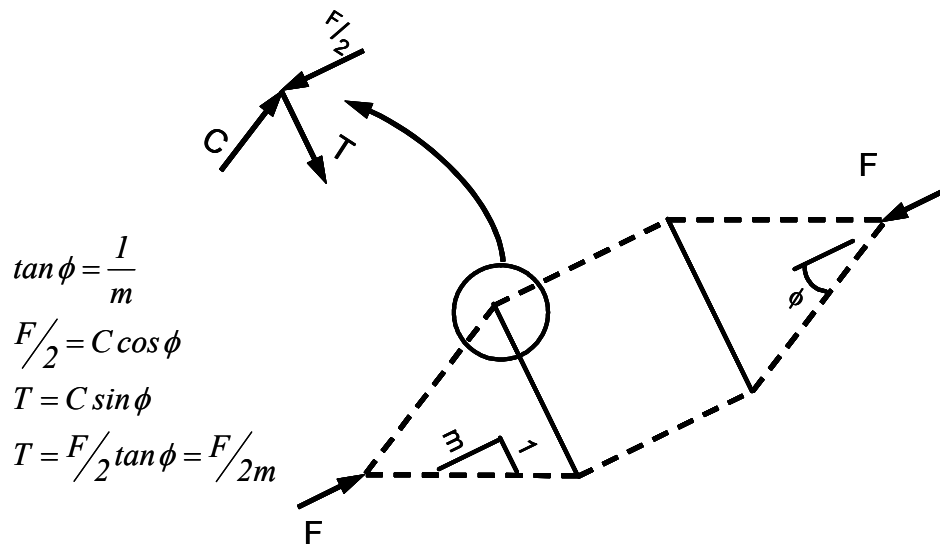
Figure 5-17: Equilibrium of a bottle-shaped strut

The components of the yield force of the vertical and horizontal shear reinforcement perpendicular to the crack must be determined (Figure 5-17). It is this force, F_{Eq}, that must be greater than induced transverse tension. The definition of F_{Eq} is shown in Figure 5-18. However, the force is the resultant of many bars rather than only two bars as shown in the figure. Therefore the tension force across the crack must be based on all the reinforcement that crosses the cracking plane.
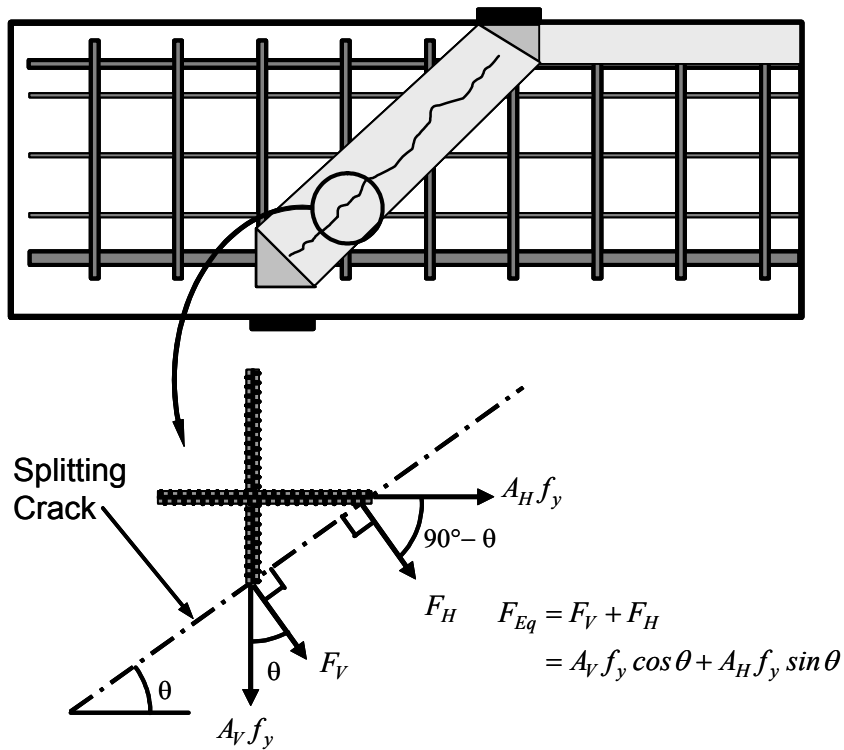
Figure 5-18: Forces in the reinforcement caused by transverse tension

A traditional reinforcement ratio is the ratio of the area of reinforcement to an area of concrete. The perpendicular reinforcement ratio, $\rho_\perp$, is similar except that the area of concrete is not the cross-sectional area in the traditional sense. The area of concrete used in $\rho_\perp$ is the cross-sectional area of the beam along the crack, and the areas of the bars are multiplied by trigonometric functions to include the effects of the angle as shown in Figure 5-18.

$$\rho_\perp \equiv \frac{A_V \cos\theta}{bs_V} + \frac{A_H \sin\theta}{bs_H} \qquad (5\text{-}7)$$

Where: $\rho_\perp$ = reinforcement ratio perpendicular to the splitting crack

A_V = area of vertical shear reinforcement

A_H = area of horizontal shear reinforcement

214

s_V = spacing of vertical shear reinforcement

s_H = spacing of horizontal shear reinforcement

b = beam width

Therefore, the force due to the reinforcement crossing the splitting crack is:

$$F_\perp = \rho_\perp f_y b \frac{d}{sin\,\theta} \qquad\qquad (5\text{-}8)$$

Where: $F_\perp$ = force due to the reinforcement crossing the splitting crack

f_y = yield stress of the web reinforcement

b = width of the beam

$\dfrac{d}{sin\,\theta}$ = approximate length of the splitting crack

In order to maintain equilibrium after cracking has occurred, the force due to the reinforcement, $F_\perp$, must be no less than $F/2m$ (Figure 5-17). The force applied to the strut, F, is a function of the allowable stress on the minimum area of the strut which is based on the efficiency factor.

$$F = \nu f_c' A_c \qquad\qquad (5\text{-}9)$$

Where: F = nominal capacity of a bottle-shaped strut

ν = efficiency factor

f_c' = specified concrete strength

A_c = minimum cross-sectional area of the strut

Therefore the transverse tie force in a bottle-shaped strut is:

$$T = \frac{F}{m} = \frac{\nu f_c' A_c}{m} \qquad\qquad (5\text{-}10)$$

Where: T = total transverse tension force (note that the total tension is twice the force "T" in Figure 5-17)

215

m = slope of the dispersion of compression

The minimum reinforcement ratio required across the crack can be calculated by equating the forces in Eq. 5-8 with Eq. 5-10:

$$\frac{vf_c'A_c}{m} = \rho_\perp f_y b \frac{d}{\sin\theta} \qquad (5\text{-}11)$$

$$\Rightarrow \rho_{\perp,min} \geq \frac{vf_c'A_c \sin\theta}{f_y bdm} \qquad (5\text{-}12)$$

As can be seen the minimum reinforcement across the splitting crack is a function of the force in the strut, and the angle at which the compression disperses.

Equation 5-12 is derived completely on the basis of strength. In other words, additional reinforcement may be required to reduce crack widths. However, the presence or absence of steel will not affect the load at which cracking occurs. Additional reinforcement will not increase the load at which the splitting crack will form.

5.4.2.1   Angle of Dispersion of Compression

If the strut is prismatic, i.e. there is no dispersion of compression, m will be infinite and the minimum reinforcement requirement reduces to zero. Traditionally, the angle of dispersion is assumed to have a slope of 2:1 ($m = 2$). However, Schlaich and Weischede (1982) presented a simple method for approximating the dispersion of compression in an elastic body. This simple elastic model was applied to bottle-shaped struts. The Schlaich and Weischede model assumes the bottle geometry shown at right in Figure 5-19. The larger end of the bottle is assumed to be equal to one-third of the length of the strut but not less than b_{min}. For short struts in which the limit of $b_{ef} > b_{min}$ governs, it is assumed that

$$b_{ef} = b_{min} + \frac{\ell}{6} \qquad (5\text{-}13)$$

216

Where: ℓ = the length of the strut

b_{min} = the minimum strut width

b_{ef} = the maximum strut width
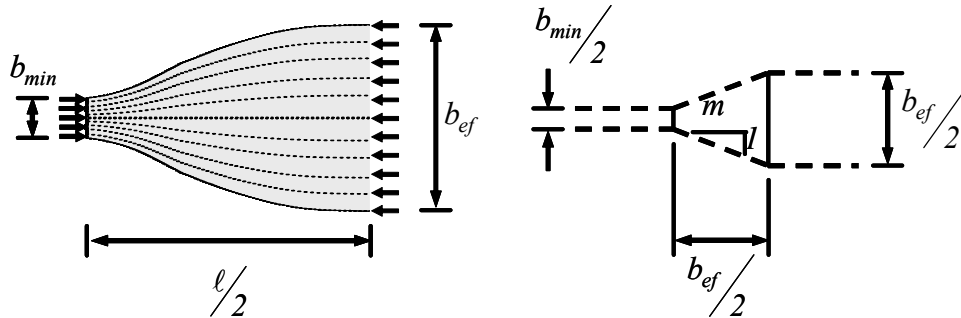
Figure 5-19: Dispersion of compression (Left: elastic distribution; Right: equivalent strut-and-tie model) (Schlaich and Weischede 1982)

When the elastic dispersion model presented by Schlaich and Weischede (1982) was applied to the database of specimens with shear span-to-depth ratios less than two, the average value of m was 8.2, and the minimum value was 2.7. These results indicate that a dispersion angle of 2:1 may be overly conservative, and result in calculated tension forces that are significantly greater than are present in the strut. The amount of reinforcement required to maintain equilibrium after cracking in a bottle-shaped strut is inversely proportional to the slope of the angle of dispersion, m, as determined by Eq. 5-12.

The effects of a variable angle of dispersion as well as the traditional slope of 2:1 will be evaluated using the minimum reinforcement requirements of Eq. 5-12. However, the design expression for the strength of a strut must be developed first since the reinforcement requirement is a function of the strut strength.

217

5.4.3 Development of New Efficiency Factors

For the purposes of the initial development of the new design procedures, the slope of the angle of dispersion as determined using the elastic solution will be used. Afterwards, the traditional value of the slope ($m = 2$) will be examined. The governing equations for the development of the new models were:

$$v_R = \frac{C_R}{a/d \sqrt{f_c'}} \leq 0.85 \qquad (5\text{-}14)$$

$$v_P = \frac{C_P}{a/d \sqrt{f_c'}} \leq 0.85 \qquad (5\text{-}15)$$

$$\rho_{\perp,min} = \frac{v_R f_c' A_c \sin \theta}{f_y bdm} \qquad (5\text{-}16)$$

Where: v_R = efficiency factor for sufficiency reinforced struts

v_P = efficiency factor for insufficiency reinforced struts

C_R = Coefficient for sufficiently reinforced struts

C_P = Coefficient for insufficiently reinforced struts

a/d = shear span-to-depth ratio

With the three above equations there are only two unknown quantities: C_R and C_P. In the above equations the subscript "R" indicates reinforced struts, and "P" indicates insufficiently reinforced, or plain, struts. The value for the minimum perpendicular reinforcement ratio is a function of the efficiency factor for reinforced struts because the minimum amount of reinforcement is that required to increase the efficiency to the "reinforced" value (Eqn. 5-14).

Reinforced struts were of primary concern for the development of the model. Typically deep beams are designed to include some shear reinforcement

for serviceability and crack control. To that end, the value of C_R was examined first (Figure 5-20).
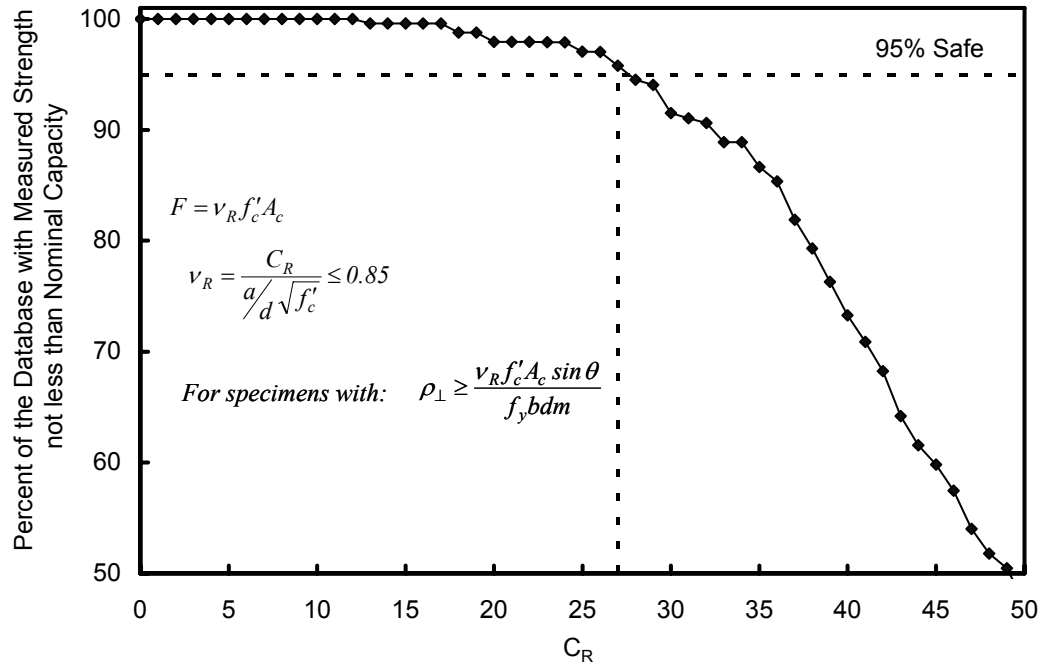
Figure 5-20: Effects of C_R on levels of safety in the database

The amount of reinforcement required within a bottle-shaped strut is a function of the efficiency factor used to determine the strength of the strut based on Eq. 5-16. By changing the value of C_R, the amount of reinforcement needed to maintain equilibrium changes. As C_R changes in Figure 5-20, so does the number of test results in the database used in the analysis. For example, if C_R is equal to 50, 224 test specimens had sufficient reinforcement to satisfied Eq. 5-16. When C_R is equal to 27, 237 test specimens satisfied Eq. 5-16. By changing C_R from 27 to 50, 13 additional specimens satisfied Eq. 5-16 and were considered sufficiently reinforced.

Based on the data shown in Figure 5-20, a value of 27 was chosen for C_R. Based on Eqn. 5-16, choosing the value of the coefficient, C_R, also affects the minimum perpendicular reinforcement ratio, $\rho_{\perp,min}$. For the test specimens listed in the database, the average value of $\rho_{\perp,min}$ was 0.0015 with a maximum and minimum value of 0.0060 and 0.0002 respectively. The preceding values are determined using the elastic dispersion of compression that is shown in Figure 5-19 and are provided to give the reader a sense of the values calculated using Eq. 5-16.

The average value of the reinforcement ratio is one-half of that required by ACI 318-02 Appendix A, and approximately one-third of that required by AASHTO LRFD STM provisions, yet levels of safety are greater using the proposed model than either ACI or AASHTO (95% for the new provisions (Eq. 5-14 to 5-16) versus 86% and 92% for ACI and AASHTO STM design specifications respectively).

If the traditional value of the slope of the angle of compression dispersion of 2 is used, 96% of the tests in the database that meet Eq. 5-16 fail at loads greater than the calculated when using Eq. 5-14. However, the 2:1 slope requires much more reinforcement than the variable-angle elastic slope. For comparison purposes, the average value of $\rho_{\perp,min}$ were 0.0015 and 0.0052 for the variable-angle and 2:1 bottle shapes respectively. On average the use of the variable-angle bottle requires much less reinforcement than the traditional bottle-shaped strut with 2:1 dispersion.

The final parameter to be determined for the new STM design expressions was the coefficient for insufficiently reinforced struts, C_P. A value of 9 was selected for C_P based on the data shown in Figure 5-21. The value was chosen

such that only 5% of the specimens would exhibit unconservative test results based on the new procedures.
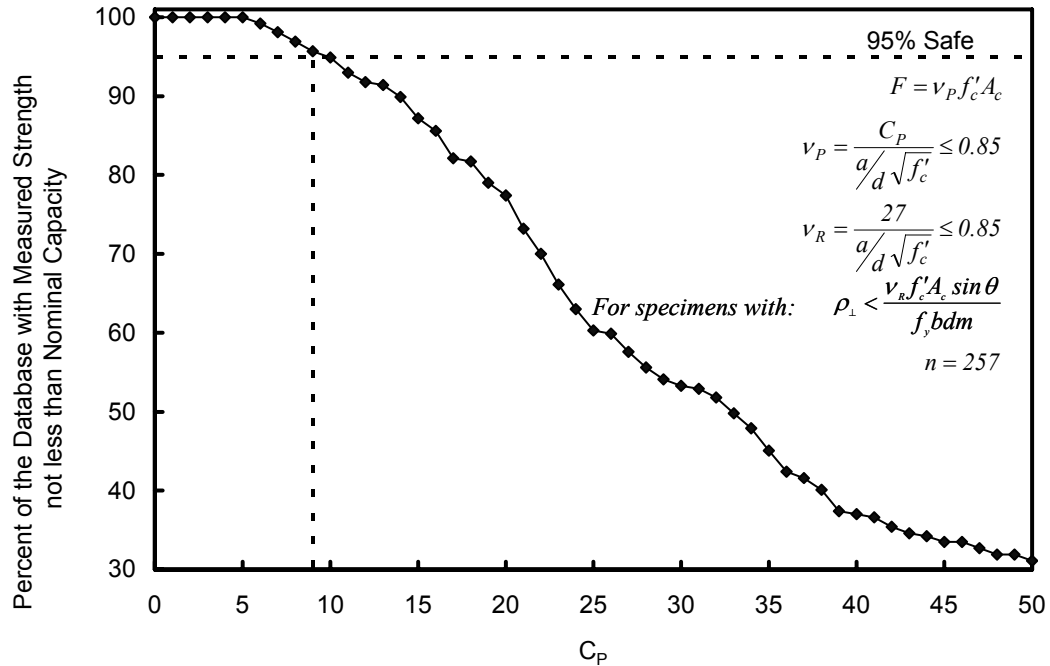
Figure 5-21: Effects of C_p on levels of safety in the database

5.4.4 Summary of Strut Efficiency Expressions

By modifying the coefficient of the best-fit lines design expressions for the efficiency of a strut abutting a hydrostatic node were developed. The new equations are:

$$v_R = \frac{27}{a/d \sqrt{f'_c}} \leq 0.85 \qquad (5\text{-}17)$$

$$v_P = \frac{9}{a/d \sqrt{f'_c}} \leq 0.85 \qquad (5\text{-}18)$$

The higher value of efficiency factor is to be used for struts that are sufficiency reinforced as per Eq. 5-16. When combining the effects of Eqs. 5-17 and 5-18, 95% of the specimens in the database carried loads in excess of the calculated value. The measured data as well as the newly developed expressions are shown in Figure 5-22. In the figure the black diamonds represent the test results of specimens with sufficient reinforcement, and the black curve represents the associated design equation. The gray circles and gray curve represent the insufficiently reinforced specimens and design equation respectively. In both cases the lower bound of the data closely matches the design curve.
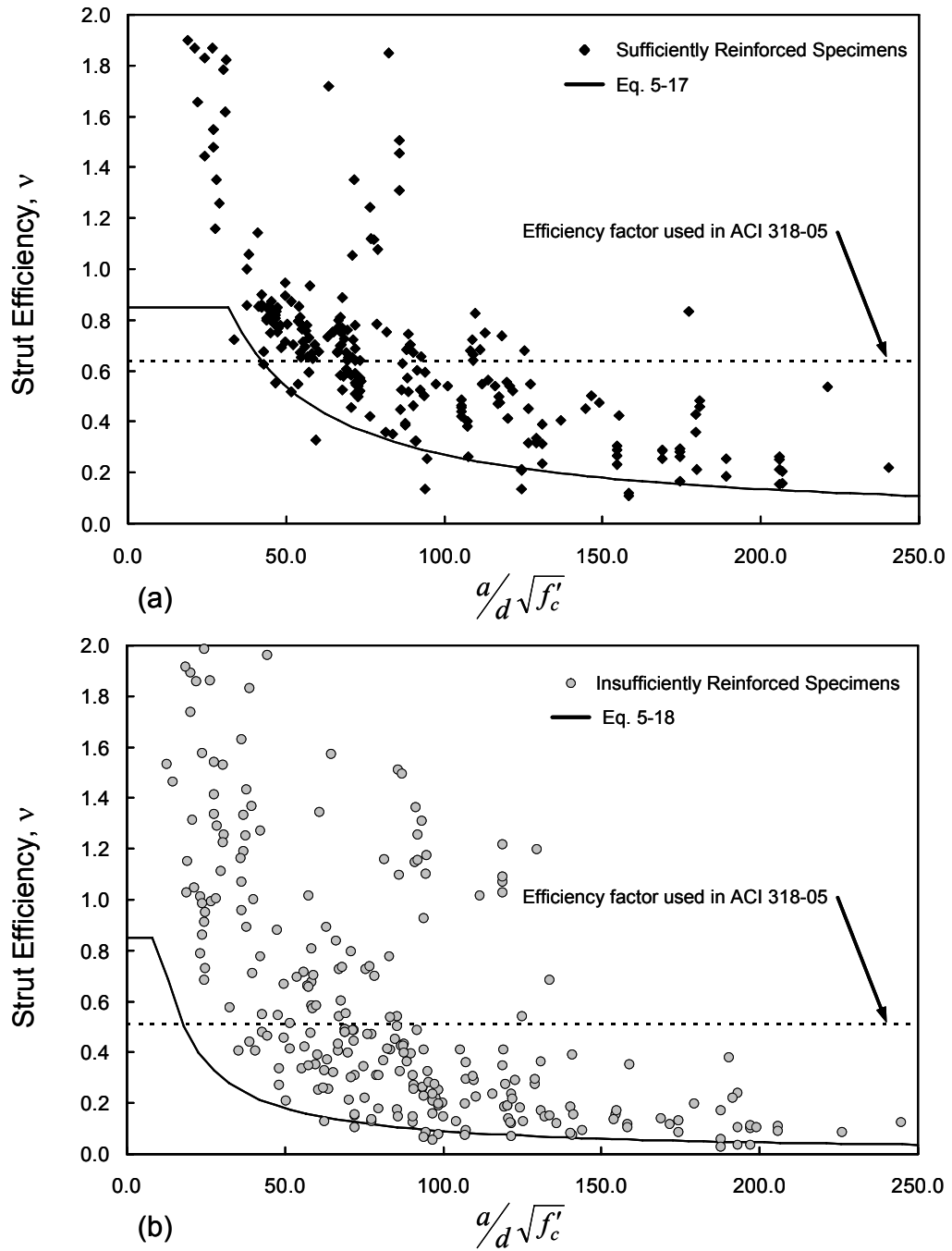
Figure 5-22: Newly developed efficiency factors and experimental data: (a) sufficiently reinforced specimens (b) insufficiently reinforced specimens

5.5 DESIGN PROCEDURE USING THE NEWLY DEVELOPED PROVISIONS

The equations presented in the preceding section were intended for use only on bottle-shaped struts. For a complete design specification additional provisions for the strength of nodal zones and node geometry are required.

5.5.1 Node Geometry

For the development of efficiency factors in the previous section, all nodes were assumed to be hydrostatic. The use of hydrostatic nodes is not always possible. In some cases, the height of a hydrostatic node can be unreasonably large. In cases where hydrostatic nodes may prove to be impractical for design use, it is recommended that the node geometry be carefully and clearly defined as shown in Figure 5-23.

Bottom Face:

$$F_b = v_H f_c' b l_b \qquad\qquad F_b = v_{NH1} f_c' b l_b$$

Left Face:

$$F_t = \frac{v_H f_c' b l_b}{\tan\theta} \qquad\qquad F_t = v_{NH2} f_c' b w_t$$

Inclined Face:

$$F_s = \frac{v_H f_c' b l_b}{\sin\theta} \qquad\qquad F_s = v_{NH3} f_c' b w_s$$
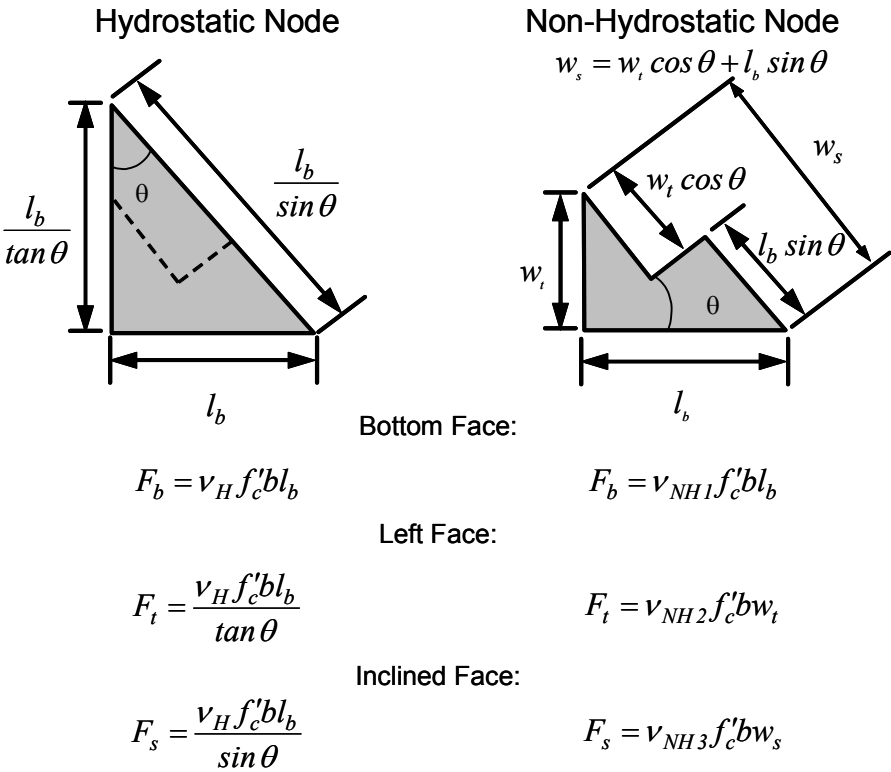
Figure 5-23: Node geometry (hydrostatic at left and nonhydrostatic at right)

The length of the node is often limited to the bearing area. The height of a node can be defined in multiple ways. The most consistent is to limit the height of the node, and therefore the tie, to twice the distance between the centroid of the steel comprising the tie and the bottom edge of the beam (Figure 5-23). The width of the strut is then calculated based on the bearing length (l_b), tie height (w_t), and the angle of inclination (θ) using the equations shown in the figure. Both ACI 318-05 and AASHTO LRFD Bridge Design Specifications use this approach to determine node geometry.

A node with the geometry described in the preceding paragraph will not be hydrostatic and the applied stresses will be different on each face of the node. Schlaich, Schäfer, and Jennewein (1987) recommend that in nonhydrostatic nodes, the ratio of maximum principle stress to minimum principle stress be less than two. A true hydrostatic node has no shear acting within the node itself. For non-hydrostatic nodes shear is present. Limiting the ratio of stresses applied to non-hydrostatic nodes also limits the shear within the node. Currently, neither ACI nor AASHTO LRFD Bridge Design Specifications limit the ratio of stresses applied to a node.

If a non-hydrostatic node is used, the efficiency factors described in Section 5.4 must be modified. The modification is done by examining two different geometries for a single node, and ensuring that each is in equilibrium with the other. The two companion nodes are shown in Figure 5-23.

By equating the forces on each face of each node "conversion factors" between hydrostatic and non-hydrostatic nodes can be calculated so that hydrostatic efficiency factors can be converted to assume higher values before their use on non-hydrostatic nodes. In general, the areas of nonhydrostatic nodes will be less than the hydrostatic counterpart, and to maintain equivalency the efficiency factors will be higher for nonhydrostatic nodes. The conversion factor

225

for the left face of the nodes shown in Figure 5-23 is shown below. The subscripts "H" and "NH" indicate hydrostatic and nonhydrostatic nodes respectively.

$$F_{tH} = F_{tNH}$$

$$\frac{v_H f_c' b l_b}{\tan \theta} = v_{NH} f_c' b w_t$$

$$v_{NH} = k_t v_H$$

$$\therefore k_t = \frac{l_b}{w_t \tan \theta} \tag{5-19}$$

Where: F_t = the force in the tie

k_t = conversion factor for the efficiency of the face of a node anchoring a tie

Similarly the conversion factors for the other faces are:

$$k_b = 1 \tag{5-20}$$

$$k_s = \frac{l_b}{w_s \sin \theta} \tag{5-21}$$

Where: k_b = conversion factor for the efficiency of the face of a node in bearing

k_s = conversion factor for the efficiency of the face of a node abutting a strut

The subscripts "s," "b," and "t" represent the conversion factors for the faces of a nonhydrostatic node acted upon by a strut, bearing, and a tie respectively.

For a CCC node there is no tie height that can be specified to help define the geometry of the node. Instead, there is a compression force due to bending of the beam. In such a case, the use of the rectangular stress block may be overly conservative, particularly if the beam is far from flexural failure. If the applied moment is between the moment that causes flexural cracking and the moment

226

causing yield of the longitudinal reinforcement, the neutral axis depth can be assumed equal to kd. For a singly reinforce cross section k can be calculated as:

$$k = \sqrt{2\rho n + (\rho n)^2} - \rho n \qquad (5\text{-}22)$$

Where: ρ = longitudinal reinforcement ratio

n = ratio of modulus of elasticity of steel to modulus of elasticity of concrete

Alternatively, the depth of the neutral axis can be approximated as:

$$c_a = \frac{c - d/2}{M_n} M + d/2 \qquad (5\text{-}23)$$

Where: c_a = approximate neutral axis depth

c = neutral axis depth at ultimate moment capacity

Equation 5-23 is a straight line interpolation function. The equation assumes the neutral axis depth varies from $d/2$ with no applied moment to c at the maximum moment capacity. Equation 5-23 results in slightly more conservative estimates of neutral axis depth than Eq. 5-22.

Additionally, the conversion factors can also be used for a CCC node. The factors k_b and k_s are unchanged from CCT nodes. However, the definition of k_t must change slightly, but not its mathematical derivation. In a CCC node there are no ties, and therefore no node faces corresponding to ties. As such the definition of k_t must be altered. The appropriate definition of k_t for a CCC node is, "the conversion factor for the face of the node not affected by bearing or an inclined strut." However, Eq. 5-19 should still be used to determine the value of k_t for a CCC node.

5.5.2 Limits on Nodal Stresses

The equations for efficiency factor that were derived for hydrostatic nodes had an upper limit of 0.85. With the conversion factors (k_b, k_s, and k_t), the efficiency factor for nonhydrostatic nodes can in some cases exceed the limit of 0.85. Therefore, additional limits must be placed on the allowable stresses on the faces of nodes. Since this study did not specifically address allowable stresses on the faces of the nodes, pre-existing limits were adopted. The nodal stress limits of both ACI and AASHTO STM provisions were examined using the database. The limits are shown in Table 5-2. It was observed that there was no difference in the percentage of specimens that failed at loads less than that determined using the newly developed model whether the newly developed model adopted ACI or AASHTO nodal stress limits. Therefore, the stress limits presented in AASHTO LRFD are recommended because they are more generous than ACI STM provisions without any reduction in levels of safety.

Table 5-2: Stress limits for the faces of nodes

	CCC Nodes	CCT Nodes
ACI 318-05 Appendix A	0.85	0.68
AASHTO LRFD Bridge Design Specifications	0.85	0.75

The use of the conversion factors (k_b, k_s, and k_t) can limit stresses on node faces to less than the values listed in Table 5-2. Both ACI 318-05 and AASHTO LRFD present flat factors for nodal stresses. The new procedures present equations that determine stress limits based on strut inclination, concrete strength, and shear reinforcement. In some cases the limits on nodal stresses in the new procedures are less than those allowed by current codes. Therefore, application of the new model results in more conservative estimates of strength.

228

5.5.3   Minimum Reinforcement

The derivation of the minimum reinforcement required for a bottle-shaped strut was based entirely on strength. In the derivation, the full yield strength of the reinforcement was used. If high stress levels in the reinforcement were present in a structure, wide cracks would be expected. Therefore, additional reinforcement may be required for serviceability reasons. Examination of the reinforcement requirements for serviceability was beyond the scope of this research.

ACI 318-05 (Section 11.8), ACI 318-05 Appendix A (Section A.3), and CSA A23.2-94 (Section 11.5.5) all require approximately the same amount of reinforcement. Using the notation of this chapter that limit is $\rho_{\perp,min} \geq 0.003$. This amount of reinforcement is significantly greater than that required by Eq. 5-16 for the vast majority of the specimens in the database (91%). Considering that serviceability and crack control was beyond the scope of the current study and recognizing that current code provisions (ACI 318-05 and CSA A23.2-94) provided similar guidance to the proper amount of crack control reinforcement, the minimum reinforcement ratio along a crack surface should be 0.003 (based on the requirements of ACI 318-05):

If hydrostatic nodes are used:

$$\rho_{\perp,min} = \frac{v_R f_c' A_c \sin\theta}{f_y bdm} \geq 0.003 \qquad (5\text{-}24)$$

If nonhydrostatic nodes are used:

$$\rho_{\perp,min} = \frac{k_s v_R f_c' A_c \sin\theta}{f_y bdm} \geq 0.003 \qquad (5\text{-}25)$$

However, for a majority of the specimens in the database, $\rho_{\perp} \approx 0.0015$ was adequate for strength purposes. Any increase in reinforcement beyond that amount does not seem to produce any additional strength in the specimens.

229

However, both ACI and CSA have adopted more stringent reinforcement requirements ($\rho_{\perp,min} \approx 0.003$). In order to reduce crack widths under service loads, the newly developed procedure set the minimum perpendicular reinforcement ratio at 0.003.

The new procedure described above allows the use of the bottle-shaped struts without reinforcement. Those provisions were created to mimic the current provisions of Appendix A of ACI 318. However, the use of bottle-shaped struts without transverse reinforcement is not recommended. Bottle-shaped struts develop tensile stresses perpendicular to their axes. Reinforcement should be provided to carry that tension after splitting cracks have formed. Without reinforcement transverse to the strut axis, the splitting crack could result in failure of the strut. Even if the splitting crack does not result in failure of the strut, serviceability problems could appear due to the presence of wide cracks under service level loads.

5.5.4 Summary of Design Procedure

The newly developed design procedure is summarized with a flowchart in Figure 5-24. The truss model must be developed based on the forces applied to the member, and the internal flow of forces. The amount of steel reinforcement should then be determined based on the tie forces. After the proper amount of reinforcement has been determined for the tie, that reinforcement should be placed in the structure such that the centroid of the reinforcement coincides with the centroid of the tie. Once the tie sizes and locations have been determined, the geometry of the node can be determined.

$vA_sf'_c$

$vA_tf'_c$

$vA_bf'_c$

Determine Truss Member Forces

Size Steel Reinforcement Based on Tie Forces

$v_sA_sf'_c$

$v_tA_tf'_c$

$v_bA_bf'_c$

Determine Geometry of Nodes

Hydrostatic Nodes

Nonhydrostatic Nodes

Calculate Efficiency Factors:

$$v_R = \frac{27}{a/d\sqrt{f'_c}} \leq 0.85 \qquad v_P = \frac{9}{a/d\sqrt{f'_c}} \leq 0.85$$

Check Allowable Stress Levels on One Node Face or Strut per Node

$$v = v_R \qquad \text{or} \qquad v = v_P$$

Strut Reinforcement if v_R Used:

$$\rho_\perp = \frac{v_R f'_c A_c \sin\theta}{f_y bdm} \geq 0.003$$

Calculate Efficiency Factors:

$$v_R = \frac{27}{a/d\sqrt{f'_c}} \leq 0.85 \qquad v_P = \frac{0.1}{a/d\sqrt{f'_c}} \leq 0.85$$

Calculate Conversion Factors:

$$k_b = 1.0 \qquad k_s = \frac{l_b}{w_s \sin\theta} \qquad k_t = \frac{l_b}{w_t \tan\theta}$$

Check Allowable Stress Levels on all Node Faces[*]:

$$v_b = k_b v_R \qquad v_b = k_b v_P$$
$$v_t = k_t v_R \qquad \text{or} \qquad v_t = k_t v_P$$
$$v_s = k_s v_R \qquad v_s = k_s v_P$$

Strut Reinforcement if v_R Used:

$$\rho_\perp = \frac{k_s v_R f'_c A_c \sin\theta}{f_y bdm} \geq 0.003$$

Detail Reinforcement and Tie Anchorage

[*]$v \leq v_{Max}$

$v_{Max} = 0.85$ for CCC Nodes $v_{Max} = 0.75$ for CCT Nodes $v_{Max} = 0.65$ for CTT Nodes

Figure 5-24: Flowchart for the newly developed procedure

231

The designer must choose whether hydrostatic or nonhydrostatic nodes are to be used. The efficiency factor is then calculated using Eqn. 5-17 and 5-18. Equation 5-17 should be used if the struts are to be reinforced as per Eq. 5-24 or Eq. 5-18 should be used if the strut is not reinforced. After the proper efficiency factor is chosen, the allowable force on one face of the node or the end of the strut must be compared to the calculated member force. Clearly the calculated member force should be no greater than the allowable member force. Only one node face needs to be checked because the node is hydrostatic. All three faces of the hydrostatic node have equal stress so that if any one face has adequate strength, all faces have adequate strength. If Eq. 5-17 was used to determine the efficiency factors reinforcement in the strut must be provided according to Eq. 5-24. The final step in the process (if hydrostatic nodes are used) is to detail the reinforcement in the strut and ensure that proper anchorage has been provided for all the ties.

If nonhydrostatic nodes are used, the process is slightly different. The basic efficiency factor for a nonhydrostatic node is calculated using the same equations as in the hydrostatic case (Eqs. 5-17 and 5-18). However, since different faces of the nonhydrostatic node have different stresses, each node face has a unique efficiency factor. The unique efficiency factors are calculated using Eqs. 5-19, 5-20, and 5-21. The basic efficiency factor determined by Eq. 5-17 (for reinforced struts) or Eq. 5-18 (for unreinforced struts) is then multiplied by k_b, k_s, and k_t to obtain the three efficiency factors for the three faces of the nonhydrostatic node. In a nonhydrostatic node any one of the three faces can be the critical element that limits the strength of the node. The maximum efficiency factors for the various typed of Nodes (CCC, CCT, and CTT) have been adopted from AASHTO LRFD (Table 5-2). The strength of a strut framing into a nonhydrostatic node need not be checked because the strength of the node is

232

always less than or equal to the strength of a strut using this procedure. If the efficiency factor for the nodes was based on Eq. 5-17, reinforcement must be provided in the struts as per Eq. 5-24. Just as in the procedure for hydrostatic nodes, the reinforcement within the struts and the tension ties must be detailed.

The new design procedure includes two newly developed equations for determination of the strut efficiency (Eq 5-17 and 5-18). Additionally, it is expected that the minimum values of Eqs. 5-24 and 5-25 will provide some assistance in reducing crack widths under service loads. The upper limits on nodal stresses are adopted from AASHTO LRFD. If the procedure outlined in Figure 5-24 is carried out on the specimens that form the database, estimates of strength are conservative for 473 of the 494 specimens.

The newly developed design procedure blends together elements from ACI and AASHTO STM provisions along with new empirical equations for efficiency factors. The new procedures strike a balance between safety and simplicity, and combines ideas presented by ACI and AASHTO in regards to STM.

Equations 5-17 and 5-18 are shown in Figure 5-25 along with the efficiency factors from both ACI 318-05 and AASHTO LRFD Bridge Design Specifications. The uppers to plots ((a) and (c) in Figure 5-25) in the figure contain Eqs. 5-17 and 5-18 with a concrete strength of 4,000 psi. The shape of the curves for the new equations is quite similar to that used by AASHTO LRFD. The new equations lie slightly below the AASHTO LRFD expression, and are slightly more conservative.

(a) Eq. 5-17, Eq. 5-18, and ACI 318-05

(b) Eq. 5-17 and ACI 318-05 (effect of f'c)

(c) Eq. 5-17, Eq. 5-18, and AASHTO LRFD

(d) Eq. 5-17 and AASHTO LRFD (effect of f'c)
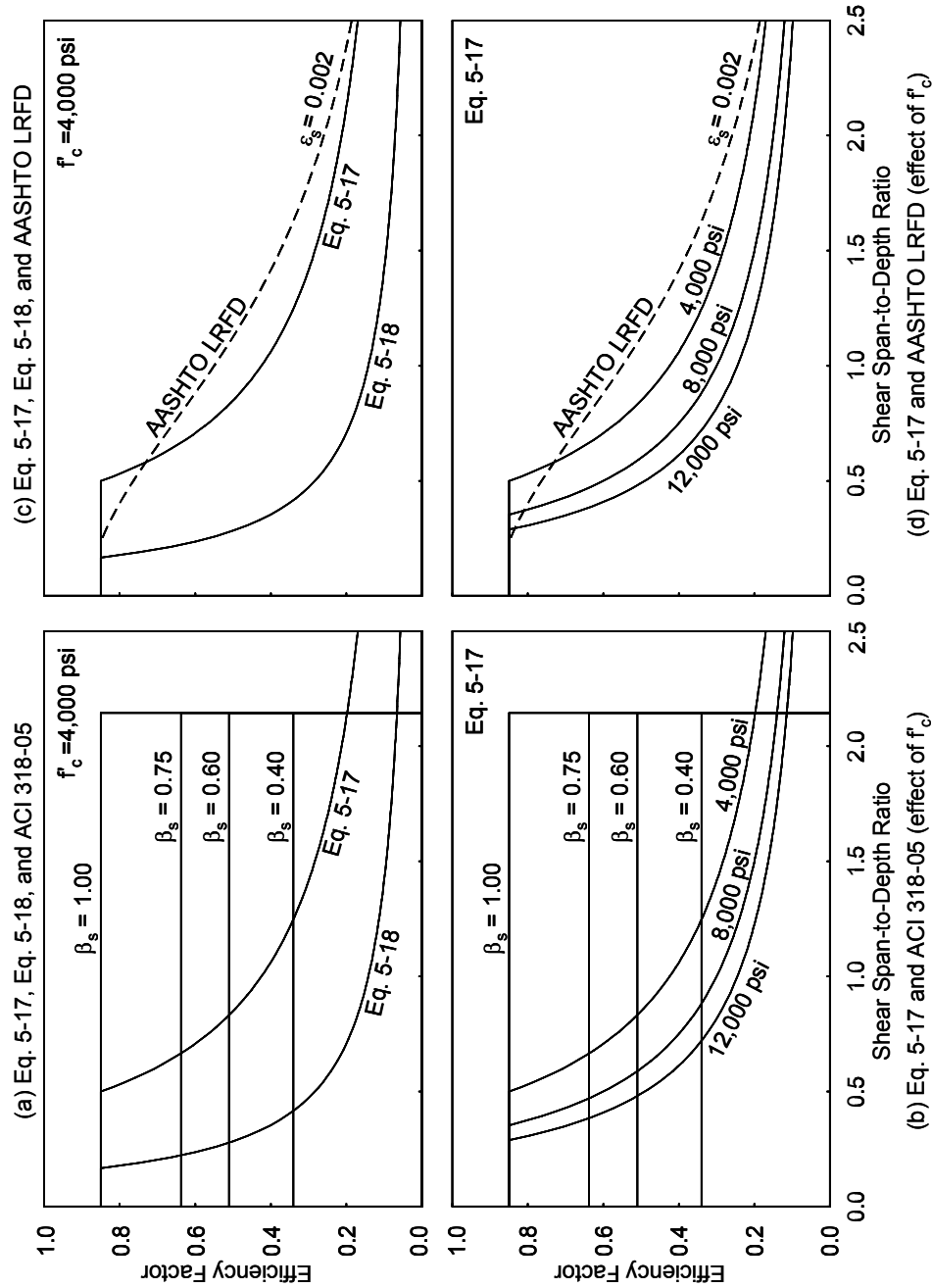
Figure 5-25: Comparison of Eqs. 5-17 and 5-18 with ACI 318-05 and AASHTO LRFD efficiency factors

234

The efficiency factors specified in ACI 318-05 are not a function of shear span-to-depth ratio as indicated by the horizontal lines in Figure 5-25. The use of ACI 318-05 does not allow the angle between struts and ties to be less than 25 degrees (shear span-to-depth ratio = 2.15). The vertical lines in Figure 5-25a and Figure 5-25b indicates that limit. For most of parts (a) and (b) the lines indicating the efficiency factor used in ACI 318-05 Appendix A are above the new equations (Eqs. 5-17 and 5-18). Compared to the new efficiency factors, the factors used by ACI 318 are quite unconservative.

The lower portions of Figure 5-25 (parts (b) and (d)) show the variations in Eq. 5-17 that are produced by varying the concrete strength. Increased concrete strength results in reduced efficiency factors with the newly developed procedures. The reduction in efficiency is due to the decreased plastic deformation capacity of high-strength concrete.

5.6 APPLICATION OF NEW DESIGN PROCEDURES TO SPECIMENS TESTED AS PART OF THIS INVESTIGATION

The newly developed design expressions were calibrated independently of the experimental program described in Chapter 4. In this section, the newly developed design procedures are applied to Series I and Series II of beam tests. The tests comprising Series III relate more closely to sectional design models than strut-and-tie models due to the longer shear span. Hence, Series III specimens are discussed in Chapter 6 which focuses on sectional shear design methods.

5.6.1 Series I Test Specimens

The specimens in Series I consisted of beams with a cross-section that was 6x30 in. Three different load distributions were used: uniform load over half the span, a single concentrated load, and two concentrated loads. A complete discussion of the Series I tests was presented in Chapter 4.

5.6.1.1 Truss Models for Series I Specimens

Three different truss models were used for the specimens in Series I (Figure 5-26). The same trusses were used to apply the newly developed procedures as were used for the application of ACI 318-05 and AASHTL LRFD Bridge Design Specifications.

The first model, used for the specimens with uniform load, discretized the uniform load into two concentrated loads. The results of Chapter 4 indicate that two loads may be adequate to properly model a uniform load. To simplify the truss geometry, the loads were not made equal to each other. Instead the loads were proportioned based on the reactions. The loads were then placed at the centroids of the portion of the uniform load they replaced. Placing the loads in this manner simplified the truss geometry by creating a horizontal strut along the top of the beam between the loads. The two truss models used for the specimens with concentrated loads are much more intuitive. The locations of the loads in the truss model coincide with the locations at which load was applied in the actual test.
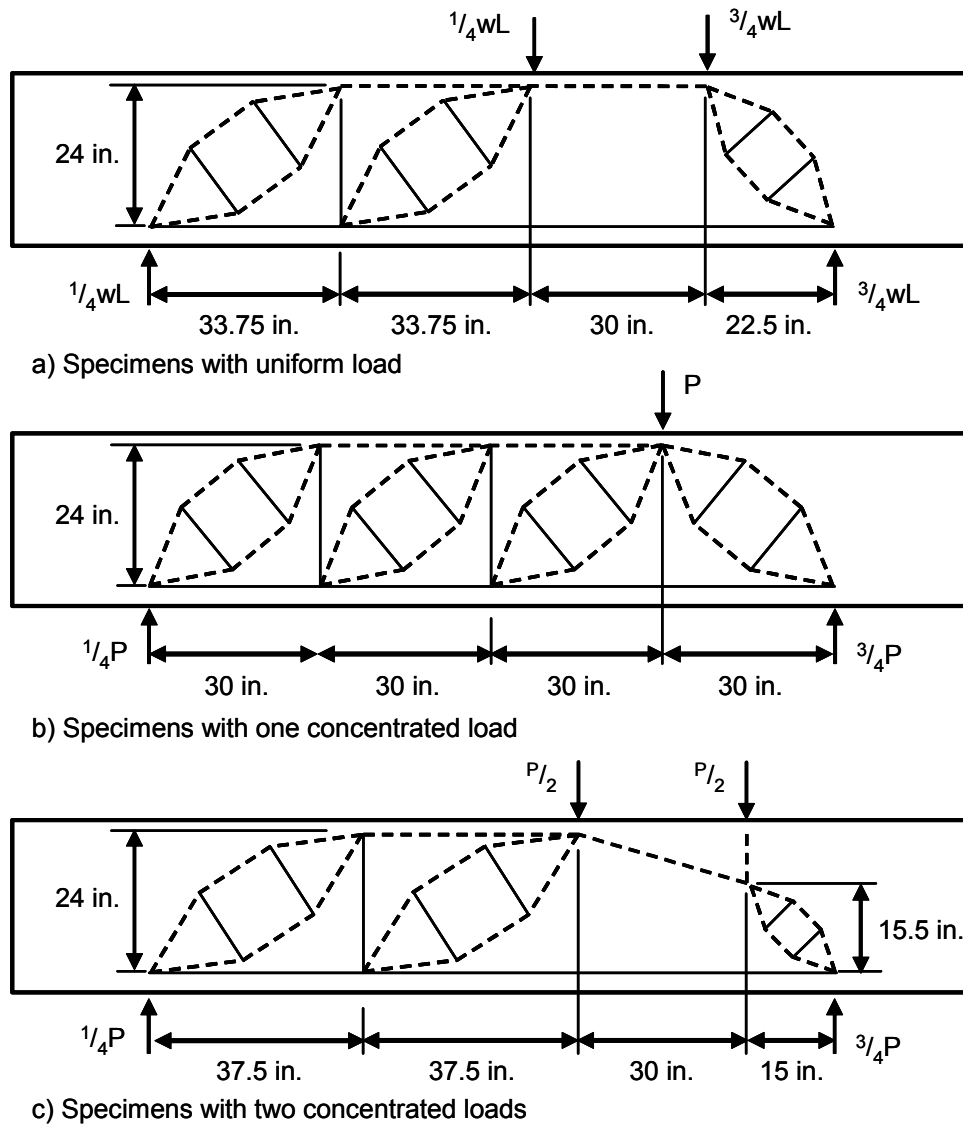
Figure 5-26: Truss models used for Series I Specimens

5.6.1.2 Minimum Reinforcement Requirement

Minimum reinforcement for the newly developed procedure is given by Eq. 5-24. The main portion of that equation was derived based strength, and the lower limit of 0.003 was adopted from existing code standards based on

serviceability. For examination of the Series I specimens, only the portion of the requirement dealing with strength is used.

$$\rho_{\perp,min} = \frac{\nu_R f_c' A_c \sin\theta}{f_y bdm} \geq 0.003 \qquad (5\text{-}24)$$

The application of Eq. 5-24 is very simple for the specimens with concentrated loads. However, for the specimens with distributed loads the proper value of the angle of dispersion of compression, m, requires some discussion.

The bottle geometry presented by Schlaich and Weischede (1982) (Figure 5-19) was developed for struts supporting concentrated loads and some modification is necessary for distributed loading. The strut geometry shown in Figure 5-19 was developed for use when the dimensions of the narrow and wide sections of a strut are unknown. In the case of a beam with distributed load, those dimensions are known as shown in Figure 5-27. The equation for determining m is the same as that presented for traditional struts; however, the definitions of b_{ef} and b_{min} have been adapted for the known geometry in the specimens.

$$m = \frac{d}{\frac{1}{4}b_{ef} - \frac{1}{4}b_{min}}$$
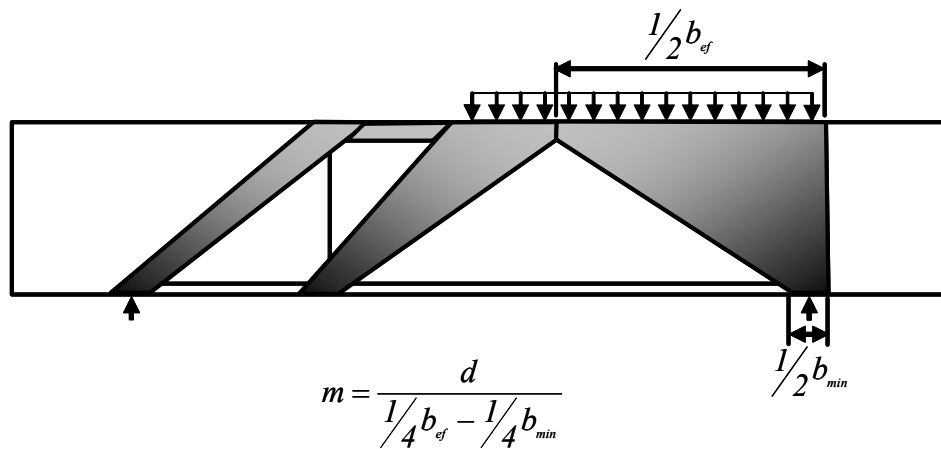
Figure 5-27: Strut geometry from Series I specimens with distributed load

The perpendicular reinforcement ratios and angles of dispersion based on the geometry of the struts in the three different load distributions are shown in

238

Table 5-3. For the specimens with concentrated loads, the required reinforcement ratio is very low; it is only one-tenth of that recommended for serviceability purposes (0.0003). For the specimens with uniform load, the required reinforcement ratio is 0.0016. The increase in required reinforcement for the specimen with uniform load is due to the presence of the uniform load. The widest point in the strut supporting the uniform load, at the top of the beam in Figure 5-27, is much wider than that calculated for the specimens carrying other load distributions. The increase in strut width induces additional tension transverse to the principle compressive direction.

Table 5-3: Minimum reinforcement for Series I Specimens

Loading Type	m	$\rho_{\perp,min}^{*}$
Distributed Load	1.4	0.0016
Single Concentrated Load	6.0	0.0003
Double Concentrated Loads	6.3	0.0003

*Minimum reinforcement for strength only.

The reinforcement required for strength in the specimen that support single or double concentrated loads is so little, that it is almost negligible. The presence or absence of 0.03% reinforcement across the expected shear crack is not likely to affect the strength of the beam. However, for the specimens that support uniform loads, 0.16% reinforcement is significant. The results of the tests appear to agree with the previous statements: for the specimens with concentrated loads shear reinforcement had minimal effect on the strength, and for the specimens with uniform load shear reinforcement affected the mode of failure.

There were four beams loaded with concentrated loads:

1. Single concentrated load and $\rho_\perp = 0.0$ (Specimen I-CL-0-0) (Total applied load at failure was 125.7 kip)

2. Single concentrated load and $\rho_\perp = 0.003$ (Specimen I-CL-8.5-0) (Total applied load at failure was 109.1 kip)

3. Double concentrated loads and $\rho_\perp = 0.0$ (Specimen I-2C-0-0) (Total applied load at failure was 124.6 kip)

4. Double concentrated loads and $\rho_\perp = 0.003$ (Specimen I-2C-8.5-0) (Total applied load at failure was 166.2 kip)

All four of these specimen exhibited similar failure modes. The failure caused sliding along a shear crack that extended over the entire depth of the section. Additionally, Specimen I-CL-8.5-0 carried the least load of the four, and Specimen I-2C-8.5-0 carried the most load. The two specimens without shear reinforcement had a measured strength between the two specimens with significant amounts of shear reinforcement. Therefore, the presence of shear reinforcement did not appear to be sufficient to alter the failure mode or ultimate strength of the beams.

There were also two beams subjected to uniform loads. The first beam had no shear reinforcement and the second had $\rho_{\perp,min} = 0.003$. For these two beams, the failure loads were nominally the same. However, the specimen with shear reinforcement exhibited a mode failure that involved crushing of concrete. The uniformly loaded specimen without shear reinforcement had a mode of failure identical to that described for the specimens subjected to concentrated loads, e.g. sliding along a shear crack. Furthermore, all specimens subjected to uniform load with $\rho_{\perp,min} \geq 0.0015$ had modes of failure that involved concrete crushing. For strength purposes, Series I specimens with uniform load appeared to need only $\rho_{\perp,min} \geq 0.0016$.

These few tests are not sufficient to make a firm conclusion regarding the validity of Eq. 5-24. However, these tests indicate that the use of Eq. 5-24 results in amounts of shear reinforcement that are in accord with observed beam failure modes.

5.6.1.3 *Comparison of Design Capacities and Measured Capacities*

The capacities of all ten specimens in Series I were determined using the newly developed procedures described in the previous portions of this chapter. In each case, the application of the newly developed procedures indicated the Series I specimens would fail due to crushing of the inclined strut adjacent to the CCT node at the North reaction. The estimation of specimen capacities based on the new procedure and the measured capacities are given in Table 5-4. The table is divided into two sections. The upper section contains data regarding the specimens that satisfied the minimum reinforcement specified by Eq. 5-24. The lower section contains data for the specimens that did not satisfy that requirement.

Table 5-4: Nominal Capacities as per the newly developed procedure

Specimens Satisfying Minimum Reinforcement as per Eq. 5-24					
Specimen	Nominal Capacity [kip]	Total Measured Load [kip]	Ratio of Measured Load to Nominal Capacity	Ratio of Measured Load to Nominal Capacity as per ACI 318-05	Ratio of Measured Load to Nominal Capacity as per AASHTO LRFD
I-UL-8.5-0a	76.3	221.4	2.90	2.75	2.47
I-UL-8.5-0b	79.5	199.1	2.50	2.28	2.06
I-UL-0-8.5	79.5	191.0	2.40	1.98	1.85
I-UL-17-17	79.7	200.9	2.52	2.18	1.95
I-2C-8.5-0	72.9	125.7	1.72	1.46	1.61
I-CL-8.5-0	58.9	124.6	2.11	1.69	1.65
Specimens Not Satisfying Minimum Reinforcement as per Eq. 5-24					
Specimen	Nominal Capacity [kip]	Total Measured Load [kip]	Ratio of Measured Load to Nominal Capacity	Ratio of Measured Load to Nominal Capacity as per ACI 318-05	Ratio of Measured Load to Nominal Capacity as per AASHTO LRFD
I-UL-0-0	29.3	172.6	5.90	2.18	1.60
I-UL-17-0	26.6	109.1	4.11	2.87	2.07
I-2C-0-0	24.3	166.2	6.84	2.30	1.95
I-CL-0-0	18.8	185.5	9.86	1.59	1.23

For the six specimens satisfying the requirement of Eq. 5-24 the average ratio of measured strength to predicted strength was 2.36 with a coefficient of variation of 0.17. For the same six specimens the average ratios of measured

strength to predicted strength were 2.06 (C.O.V. = 0.22) when applying ACI 318-05 STM provisions and 1.93 (C.O.V. = 0.16) when applying AASHTO LRFD STM provisions. The minimum shear reinforcement requirement presented in AASHTO LRFD was ignored in calculating the preceding numbers. The minimum shear reinforcement required by AASHTO LRFD is roughly 50% greater than the minimum value presented in this chapter. For these six specimens, the results produced using the new provisions are similar to those produced when applying existing code provisions. However, the new provisions were developed based on a lower bound to the experimental data in the database. The application of existing code provisions resulted in large amounts of unconservative test results in that same database. Given the large amount of scatter, the use of a lower bound method seems prudent. Moving from a "best-fit" type equation to a lower bound equation in the newly developed procedures only increased the average ratio of tested strength to predicted strength slightly while ensuring safety for 96% of the test results in the database.

The average ratio of measured strength to predicted strength for the remaining four specimens in Series I was 6.68 (C.O.V. = 0.36). Since these specimens did not satisfy the reinforcement requirement of Eq. 5-24, a reduced efficiency factor was used (Eq. 5-18). The use of Eq. 5-18 places a large penalty on the strength of a strut without the necessary reinforcement. That penalty is apparent in the large ratios of tested strength to predicted strength listed in the lower portion of Table 5-4. The test results of the insufficiently reinforced specimens in the database displayed significantly more scatter than the results for the reinforced specimens. In order to maintain acceptable levels of safety under increasing scatter, more conservative estimates of strength had to be made. The average value of tested strength to predicted strength of 6.68 reflects that increased conservatism.

For all practical purposes and for reasons of safety and serviceability, some transverse reinforcement should be present in deep beams. The method presented here requires very little reinforcement to use the higher efficiency factors. The large increase in efficiency factor that can be gained through the use of rather small amounts of reinforcement is meant to encourage the use of shear reinforcement in deep beams.

5.6.1.4 Mode of Failure

For the specimens in Series I, applying ACI 318-05, AASHTO LRFD, and the newly developed procedures indicated that failure of the beams would occur due to concrete crushing at the CCT node-to-strut interface. However, that mode of failure was observed in only five of the ten tests. Breen, Burdet, Roberts, Sanders, and Wollmann (1994) had similar difficulties in using STM to determine failure modes of post-tensioned anchorage zones. Breen et al.(1994) concluded that the inability to ascertain the proper failure mode was not critical since safe estimates of strength were obtained regardless of the mode of failure. The same reasoning can be applied to the newly developed procedure. The use of the new procedure failed to indicate the correct failure mode for half of the specimens in this series; however, the use of the new procedure resulted in safe expectations of strength.

5.6.2 Series II Test Specimens

The specimens in Series II were constructed to evaluate the effects of cross-section width. It is important to note that the ten specimens used for Series II were supported by three different layouts of bearing plates with two different cross-sections. One bearing extends across the full width of the beam, the second bearing supported only the exterior edges of the beam as per the CTT node width

244

limitations of AASHTO, and the final arrangement supported the middle portion of the beam. All three bearing arrangements are shown in Figure 5-28.
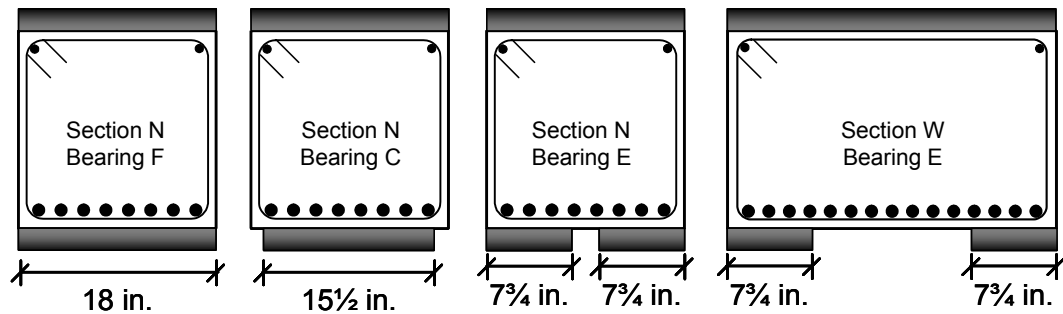
Figure 5-28: Bearing layouts used for Series II tests

For all of the specimens in Series II, the minimum perpendicular reinforcement ratio was 0.0002 based on strength and not serviceability. All ten specimens in the series satisfied that minimum reinforcement requirement. For the purposes of evaluating the specimens in terms of measured strength, the greater efficiency factor (Eq. 5-17) was used to calculate the strength of these specimens. The results are shown in Table 5-5.

Table 5-5: Nominal capacities as per the newly developed procedure

Specimen	Nominal Capacity as per New Procedures [kip]	Total Measured Load [kip]	Ratio of Measured Load to Nominal Capacity	Ratio of Measured Load to Nominal Capacity as per ACI 318-05	Ratio of Measured Load to Nominal Capacity as per AASHTO LRFD
II-N-E-5.8-8	118.2	132.5	1.12	1.21	1.25
II-N-F-5.8-8	117.1	140.3	1.20	1.10	1.17
II-N-C-5.8-8	117.0	194.9	1.67	1.78	2.01
II-N-F-5.8-3	116.2	226.1	1.95	1.76	1.70
II-N-C-4.6-8	121.4	246.4	2.03	2.10	2.16
II-N-E-4.6-8	122.2	183.9	1.50	1.57	1.61
II-N-F-4.6-8	126.4	146.2	1.16	0.99	1.02
II-W-E-5.8-8	220.0	367.7	1.67	3.08	3.27
II-W-E-4.5-8	230.9	318.0	1.38	2.17	2.24
II-W-E-3-8	270.0	232.6	0.86	1.37	1.37
		Average:	1.45	1.71	1.78
		Coefficient of Variation:	0.26	0.37	0.38

For the application of the new procedures, the full width of the cross-section was used to determine the allowable strut force regardless of the support conditions. For the specimens with the "W" cross-section only 15½ in. of the width of the beam was supported and the full width of 30 in. was used for the width of the strut. Specimen II-W-E-3.8 was the only beam specimen tested with the measured strength less than the strength determined with the new procedures.

However, based on Eq. 5-24, all of the specimens in Series II would require that the lower efficiency factor (Eq. 5-18) due to the serviceability requirement ($\rho_{\perp,min} = 0.003$). None of the specimens in Series II satisfied the serviceability requirement of Eq. 5-24.

Just as with the specimens of Series I, the newly developed procedure was unable to correctly identify the failure mode. Based on the new procedures, all of the specimens in Series II should have failed due to crushing of the strut at the CCT node-to-strut interface. Six of the ten specimens failed in that manner. The remaining four specimens failed due to shear in a region where the applied shear force was relatively low. Those failures are more typical of failures observed in longer shear spans where sectional models should be used. Therefore, the four specimens from Series II that failed in the long shear span will be discussed in the Chapter 6 which focuses on sectional design methods.

Based on the strength alone, the required reinforcement crossing the expected shear crack was 0.0002. All of the specimens in Series II satisfied that limit. For the specimens that failed in the short shear span, failure was accompanied by concrete crushing. One specimen (II-N-F-5.8-3) had significantly more shear reinforcement than any other specimen but exhibited the same failure mode.

5.6.3 Bent Caps

In order to further examine the validity of the newly developed design procedures, they were applied to three different bent caps. The full details of the application of the newly developed procedures to the bent caps are given in Appendix A – Design Examples along with examples using ACI 318-05 and AASHTO LRFD strut-and-tie specifications.

For the examples presented in Appendix A, the designs have been carried out using load and strength reduction factors from the same code. For example, all calculations done using ACI 318-05 provisions used the load and strength reduction factors from ACI 318-05. Load factors and strength reduction factors are determined in pairs. A strength reduction factor from one code is not necessarily compatible with a load factor from another code. Alternatively, the design could have been performed using a common set of load factors along with strength reduction factors from he various codes. However, such designs would results in an unfair assessment of the code provisions. The decision to use load and strength reduction factors in pairs from a single code was done so for the sake of consistency.

The main difference between the design examples presented in Appendix A is the load factors. ACI 318-05 is intended for use in the design of buildings and does not have an impact factor, but AASHTO LRFD (intended for use in designing bridges) does have an impact factor. Due to the impact factor, the design loads for use with AASHTO are greater than the design loads for use with ACI 318-05. The designs produced through the use of ACI 318-05 and AASHTO LRFD can not be directly compared. The newly developed provisions use the load and resistance factors from AASHTO LRFD. Therefore, the designs developed with AASHTO LRFD and the newly developed procedures are comparable.

The first two bent caps presented in Appendix A were standard bent caps used by the Texas Department of Transportation (TxDOT) for bridges supporting pretensioned girders. Bent caps such as this are in use throughout the state, and are in general exhibiting good performance under field conditions. In short, the current standard designs are not believed to be deficient.

If AASHTO LRFD Bridge Design Specifications for STM are applied to the current design, significant changes are called for. The main factor reducing the

248

design strength of the standard caps is the required crack control reinforcement. The current cap standard uses No. 5 closed stirrups with two legs each. The AASHTO LRFD STM provisions require a ratio of shear reinforcement to gross concrete area of at least 0.003 in each direction (horizontal and vertical). Since there are no stirrup legs distributed thought the width of the section, the interior portions of the cross-section can not be used for the strut and the capacity of the cap is reduced accordingly (Figure 5-29). Such in increase in the amount of shear reinforcement would approximately double the current amount of shear reinforcement.
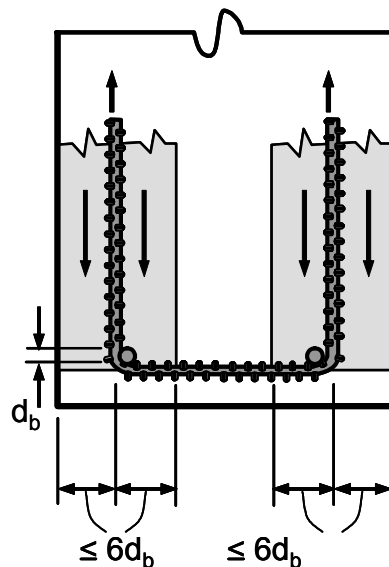
Figure 5-29: CTT node and abutting strut width limitations in AASHTO LRFD Bridge Design Specifications

To gain adequate strength in the caps as per the AASHTO specifications, additional shear reinforcement must be added to the current design. The additional reinforcement consists of internal stirrups legs and horizontal bars placed alongside the internal stirrup legs. In effect, the AASHTO LRFD STM provisions require twice the shear reinforcement currently used in the standard design. Field

performance of the caps does not indicate any need for such drastic increases in shear reinforcement. Application of the ACI 318-05 Appendix A provisions indicates that the current cap design is adequate in all respects (strength and detailing).

The newly developed provisions indicate that minor changes should be made to the bent caps. Currently the caps are constructed with concrete strength equal to 3,600 psi. The new procedure suggests that the concrete strength should be increased to 4,500 psi. It is not unreasonable to expect the in situ concrete strength of the bent caps exceeds 4,500 psi.

Alternatively, the bearing area beneath the pretensioned beams could be increased to gain the needed capacity when using the new procedures. The bearing area covers only about 40% of the available width of the top of the caps. An increase in bearing pad size is an easy and practical solution. Interaction with TxDOT bridge engineers suggests that bearing pads used in Texas are among the smallest in the nation.

The three cross-sections required using AASHTO LRFD, ACI 318-05 and the newly developed procedures are shown in Figure 5-30. Each of the section is the critical section of the cap and was designed to resist the factored shear at that section. The cross-section required to satisfy the AASHTO LRFD provisions has more shear reinforcement than the other two design methods require. The cross-section required by the new procedures is identical to that required to satisfy ACI 318-05. Only the concrete strength changes between the two designs.

No. 11 top

2 – No. 5

2 legs of No. 5
closed stirrups at
10-12 in.

$f_c' = 3,600\,psi$

No. 11 bottom

(a) Current TxDOT Design

No. 11 top

4 – No. 5

4 legs of No. 5
closed stirrups at
12 in.

$f_c' = 3,600\,psi$

No. 11 bottom
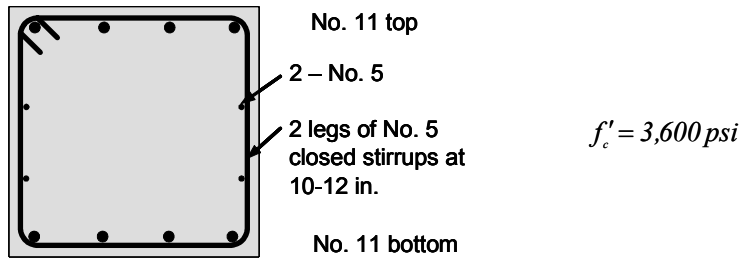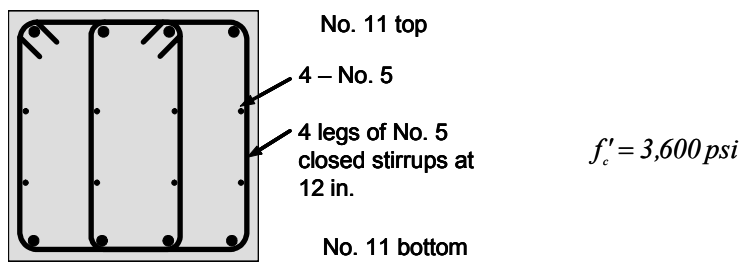
(b) Bent cap section satisfying AASHTO LRFD

No. 11 top

2 – No. 5

2 legs of No. 5
closed stirrups at
7 in.

$f_c' = 3,600\,psi$

No. 11 bottom

(c) Bent cap section satisfying ACI 318-05

No. 11 top

2 – No. 5

2 legs of No. 5
closed stirrups at
7 in.

$f_c' = 4,500\,psi$

No. 11 bottom
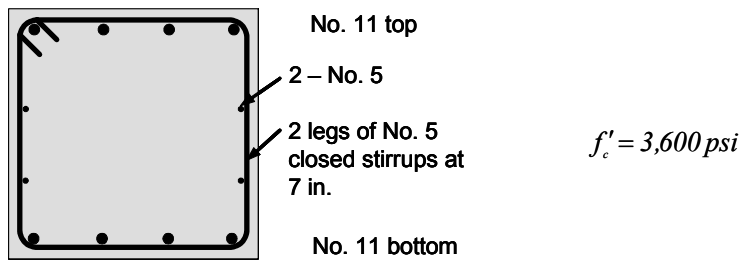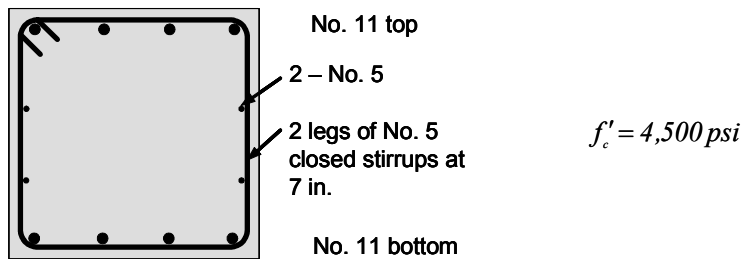
(d) Bent cap section satisfying newly developed procedures

Figure 5-30: Bent cap cross-sections

The third structure presented in Appendix A is also a bent cap. This structure is a hammerhead-type bent cap i.e. a cap supported on a single column. The application of AASHTO LRFD provisions for STM indicate that is cap is grossly undersized and in need of major design changes. The cap was designed in accordance with the AASHTO standard specification rather than the LRFD specification. When the new procedures were applied to this cap, only a small increase in concrete strength was required, and some of the shear reinforcement could actually be removed.

5.7 SUMMARY

A database of experimental research into the shear strength of reinforced concrete was compiled. That database was used to evaluate the levels of safety when applying the strut-and-tie procedures from ACI 318-05 and AASHTO LRFD Bridge Design Specifications. Results indicate that the use of both ACI 318-05 and AASHTO LRFD Bridge Design Specifications results in unacceptable numbers of unconservative test results when specimen without web reinforcement are included in the analysis.

In order to increase levels of conservatism, a new procedure was developed. The new procedure was developed such that its use would result in less than 5% unconservative predictions of capacity for the specimens included in the database. The new procedure required new equations for the determination of efficiency factor (Eqs. 5-17 and 5-18) as well as a new method for determining the appropriate amount of reinforcement that crosses the strut axis (Eqs. 5-24 and 5-25). Based on the derivation of Eqs. 5-24 and 5-25 and the observed failure modes, there appeared to be a critical value of reinforcement crossing the expected shear crack. Any additional reinforcement beyond that critical amount does not increase the shear strength or alter the mode of failure.

252

Finally, the new procedure was applied to the test specimens. The application of the new procedures results in safe predictions of strength for 19 of 20 specimens. The only test specimen that failed at a load less than the nominal capacity calculated using the new procedure reached an ultimate load of 86% of that capacity.

CHAPTER 6

Sectional Design Models

6.1 INTRODUCTION TO SECTIONAL DESIGN PROCEDURES

In 1962 ACI-ASCE Committee 326 published a report regarding the design and behavior of beams failing due to shear and diagonal tension. In order to develop safe design recommendations, a database of 194 beam tests without shear reinforcement was compiled. The database consisted of 130 laboratory specimens tested under single- and double-point loads and 64 beams subjected to uniformly distributed loads. Based on those data the following design equation was developed (Figure 6-1) and is included in ACI 318-05 as Eq. 11-5:

$$V_c = \left(1.9\sqrt{f'_c} + 2500\rho_w \frac{V_u d}{M_u} \right) b_w d \le 3.5\sqrt{f'_c} b_w d \quad (6\text{-}1)$$

Where: V_c = nominal shear strength provided by concrete

f'_c = specified compressive strength of concrete

$\rho_w = A_s / b_w d$

V_u = factored shear force at section

M_u = factored moment at section

b_w = web width

d = effective depth of section

A_s = area of nonprestressed tension reinforcement

As the distance between a concentrated load and the support decreases, the ratio Vd/M increases and the allowable shear strength of the member increases.

For a simply-supported member with a single concentrated load at midspan, the quantity Vd/M varies from infinity at the supports to zero at midspan. In order to circumvent any problems, Committee 326 calculated Vd/M at the section where shear failure occurred in the laboratory specimen. Because the location of shear failure is unknown to the designer, the correct value of Vd/M is also unknown. By neglecting the term involving Vd/M, a simplified, and conservative, version of Eq. 6-1 could be derived (Eq. 6-2).

$$V_c = 2\sqrt{f_c'}b_w d \qquad\qquad (6\text{-}2)$$

Using Eq. 6-2, 2.5% of the test specimens in the 1962 database failed at shear values less than those computed as can be seen in Figure 6-1.
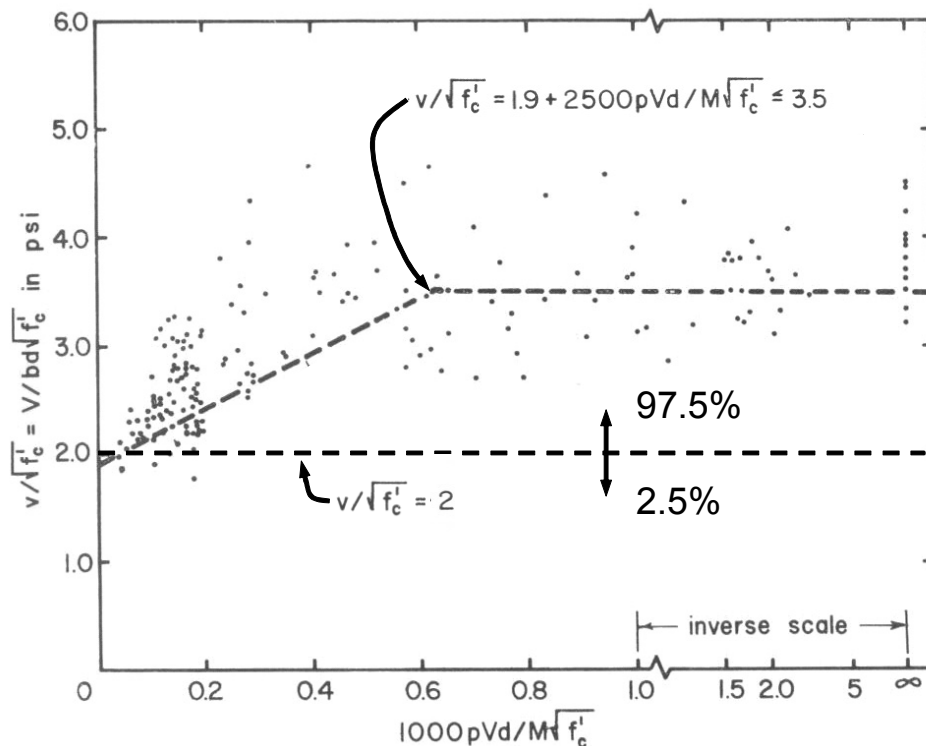
Figure 6-1: Database of shear tests used by ACI-ASCE Committee 326

The concrete contribution to the shear strength members is often only a portion of the shear strength of reinforced concrete members. Most reinforced concrete beams contain shear reinforcement. The contribution to shear strength provided by the shear reinforcement is:

$$V_s = \frac{A_v f_y d}{s} \qquad (6\text{-}3)$$

Where: V_s = nominal shear strength provided by shear

reinforcement

A_v = area of shear reinforcement with a spacing, s

f_y = specified yield strength of reinforcement

s = center-to-center spacing of transverse reinforcement

The additional shear strength provided by transverse reinforcement must also be examined.

It has been evident for over 40 years that the type of loading (concentrated or distributed loads) and the location of the loads have an influence on the shear capacity of reinforced concrete beams. However, no simple method to include these parameters in design equations in the ACI code has been adopted. With the increase in test data reported since 1962, it seems an opportune time to examine those data.

6.2   DEFINITION OF SHEAR SPAN

For a laboratory specimen subjected to one or two point loads, the shear span is simple to define. As defined by ACI 326 in 1962, the shear span is the distance between the support and the point where the load is applied. For more complex load cases, the shear span is more difficult to define. Leonhardt and Walther (1962) chose to define the shear span of a beam with uniform load over its entire length as one-fourth of the span. If a uniform load is replaced by

statically equivalent concentrated loads at $^L/_4$ and $^{3L}/_4$, the maximum moment of the two load cases will be equal. Their definition is practical only if the uniform load is applied symmetrically to the entire span. If uniform load is applied only to a portion of a span Leonhardt and Walther's definition is inadequate.

The AASHTO LRFD Bridge Design Specification defines a deep component as:

[a component] in which the distance from the point of 0.0 shear to the face of the support is less than 2d or components in which a load causing more than one-third of the shear at the support is closer than 2d from the face of the support.

The first clause of the AASHTO definition implies that the shear span is related to the distance between the point of maximum shear and the point of zero shear. The definition implied by AASHTO will be used in the remainder of this chapter for comparing the behavior of all the specimens included in the database. It should be noted that the definition of shear span implied by AASHTO results in the same shear span as that given in the ACI Committee 326 (1962) report for beams subjected to one or two concentrated loads. The implications of the definition of shear span for other load configurations will be discussed in Section 6.4.1.

6.3   EXPERIMENTAL INVESTIGATION

The majority of published shear tests consist of beams with one or two concentrated loads placed symmetrically on the specimens as mentioned in the previous chapter. The 24 specimens that were described in Chapter 4 will also be used to investigate sectional models. In Chapter 4 the results of the experiments were discussed as they pertain to STM. In Chapter 6 those same tests will be re-examined considering sectional shear design models. Eight tests are discussed in

detail in this chapter to describe the effects of loading type and shear span-to-depth ratio on shear strength of reinforced concrete beams. Data from the 24 tests conducted in this study and 1,170 tests extracted from the literature are used in evaluating the current ACI 318 provisions for shear strength.

6.3.1   Effects of Loading Type

To study the effects of loading type, four nominally identical beams were constructed. The details of the test specimens are shown in Figure 6-2. Each of the beams was subjected to a different type of load (Figure 6-3 through Figure 6-6). Specimen 1 had a single point load at midspan, Specimen 2 had two point loads applied at $^L/_4$ and $^{3L}/_4$, Specimen 4 had four point loads applied at $^L/_8$, $^{3L}/_8$, $^{5L}/_8$, and $^{7L}/_8$; and Specimen U was subjected to a uniform load. The uniform load for Specimen U was produced with 24 hydraulic rams connected to a single hydraulic manifold and acting on 24 identical bearing plates. All four beams were constructed without stirrups between the supports. The compressive strength of the concrete was slightly less than 4,000 psi when the beams were tested.

The single concentrated load applied to Specimen 1 created equal shear span-to-depth ratios on either side of the load (Figure 6-3). The shear span-to-depth ratio for Specimen 1 was 3.0 which is near the minimum point of Kani's shear strength envelope. Therefore, the relatively low shear strength (20.4 kip or $2.6\sqrt{f_c'}bd$) of this beam should not be surprising. The peak shear carried by Specimens 2, 4, and U increased as the load distribution became more uniform. However, the increase in strength was most dramatic between Specimens 1 and 2 (for Specimen 2 the ultimate shear strength was 64.1 kip or $8.0\sqrt{f_c'}bd$). Specimen U carried the greatest peak shear (75.8 kip or $9.5\sqrt{f_c'}bd$) of the four tests. However, in accordance with ACI 318 procedures the shear force on the

258

beam should be calculated at a distance d away from the face of the support (50.5 kip) for design purposes. It is important to note that the reported shear strengths of all four beams include the shear due to self-weight which is small in magnitude.
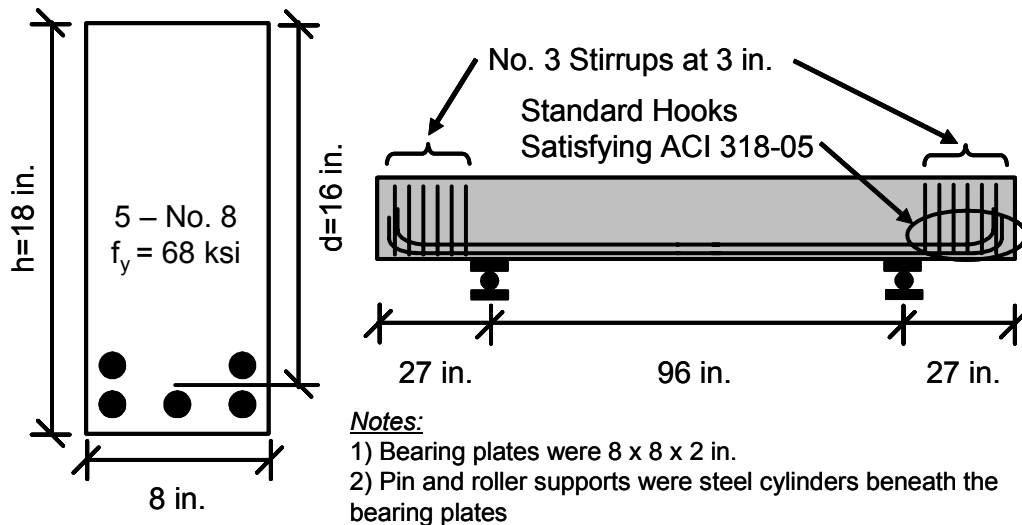
Figure 6-2: Details of Specimens 1, 2, 4, and U

Specimens 4 and U had similar shear strengths and failure crack orientations. The similarity in cracking reflects the fact that four point loads distribute load nearly uniformly along the span. As a result Specimens 4 and U, had greater shear strength than Specimen 1. Specimens 1 and U had the same shear span (a = $^L/_2$), so the greater strength of Specimen U can be attributed entirely to load distribution.

The results of these four tests agree with the results reported by Ferguson (1956). He also tested four beams to examine load distribution, and observed a significant increase in shear strength when the beam was loaded with four loads rather than two. A further increase in shear capacity was observed when the two concentrated loads were shifted closer to the supports.

$$f'_c = 3,870\,psi$$

$$V_{Test} = 20.4\,kip$$

$$V_{test} = 2.6\sqrt{f'_c}bd$$
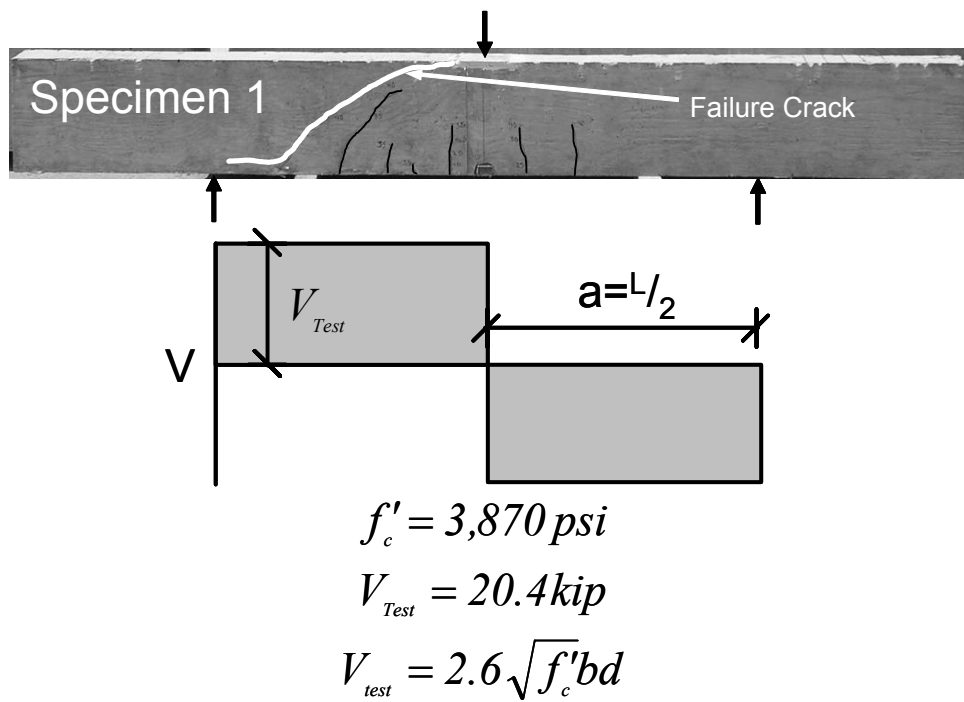
Figure 6-3: Failure conditions of Specimen 1

$$f'_c = 3,880\,psi$$

$$V_{Test} = 64.1\,kip$$

$$V_{test} = 8.0\sqrt{f'_c}bd$$
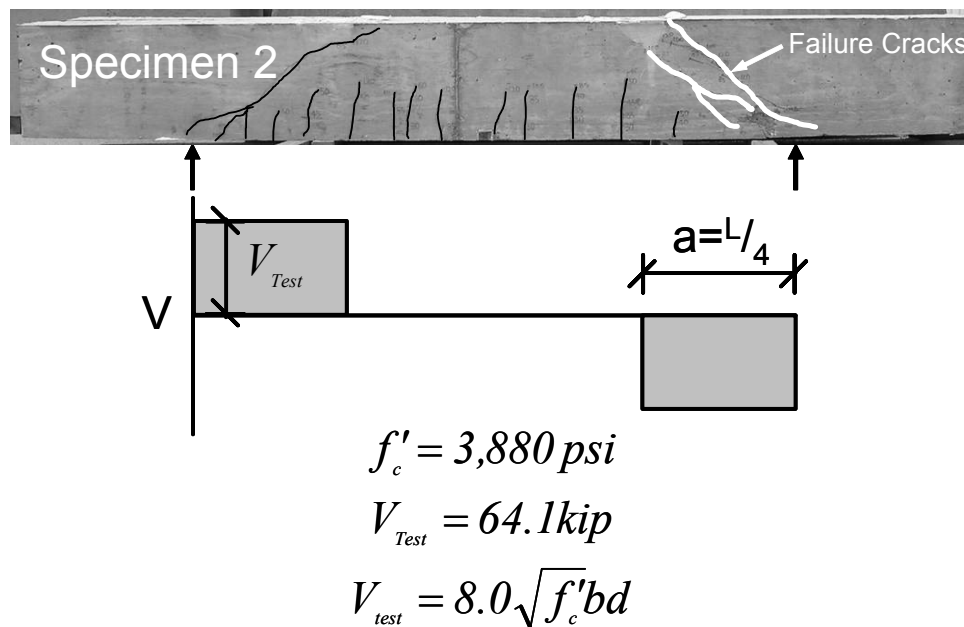
Figure 6-4: Failure conditions of Specimen 2

$$f'_c = 3,900\, psi$$

$$V_{Test} = 68.6\, kip$$

$$V_{Test} = 8.6\sqrt{f'_c}bd$$
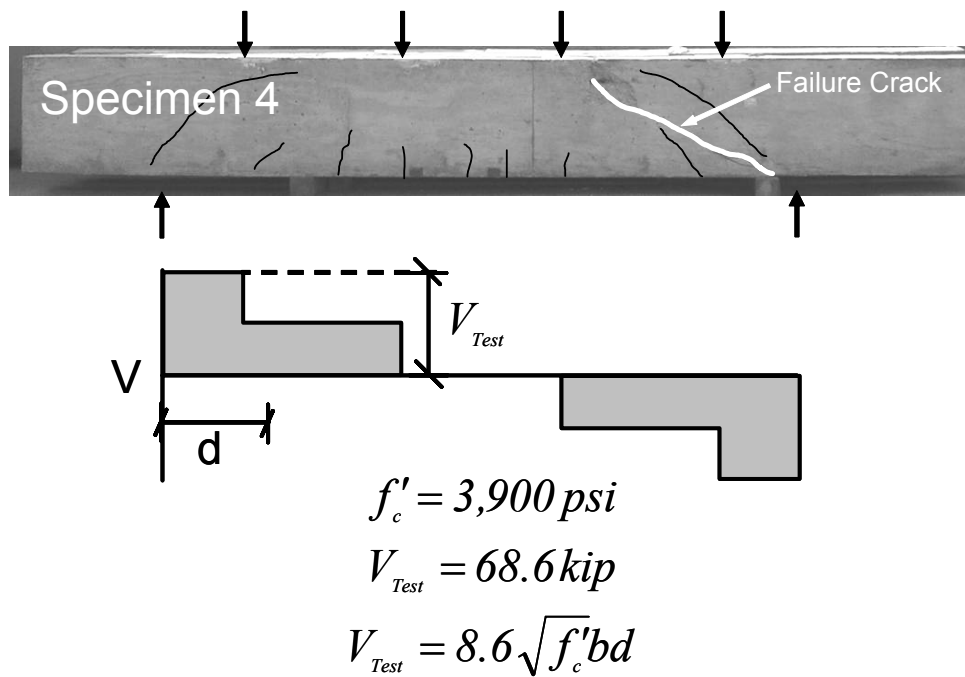
Figure 6-5: Failure conditions of Specimen 4

$$f'_c = 3,900\, psi$$

$$V_{Code} = 50.5 kip \qquad\qquad V_{Test} = 75.8 kip$$

$$V_{Code} = 6.3\sqrt{f'_c}\text{bd} \qquad\qquad V_{Code} = 9.5\sqrt{f'_c}\text{bd}$$
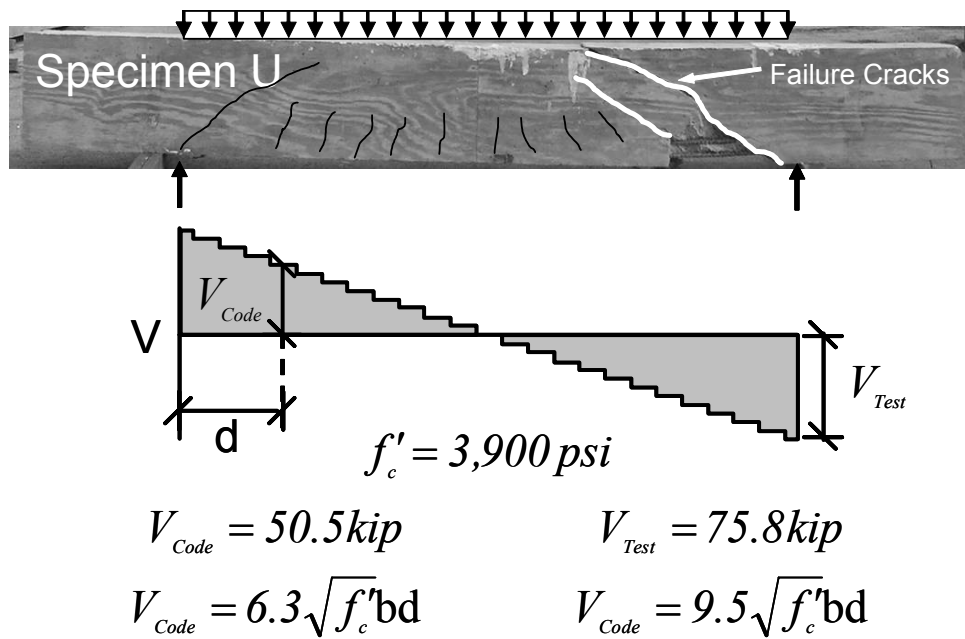
Figure 6-6: Failure conditions of Specimen U

6.3.2 Asymmetric Concentrated Load Tests

Ten tests were conducted with a single concentrated load applied asymmetrically with respect to the supports as described in Chapter 4. Four of those tests are discussed in detail in this chapter. The segment of the beams with smaller shear span was subjected to higher shear force than that with a larger shear span. Other variables (concrete strength and longitudinal reinforcement) were kept constant. Stirrup spacing was constant along the length of the beam.

Two different cross-sections were used in this stage of testing (Figure 6-7). Before Specimen N-1 was tested, it was expected that shear failure would occur in the segment of the specimen with the greater shear force, i.e. the end with the smaller shear span. However, failure occurred on the side of the beam with the longer shear span and smaller shear force. With a/d ratios of 1.7 and 5.8, the applied shear force on the short span was 3.4 times that on the long span, yet shear failure occurred on the longer portion of the span. Failure of all four specimens occurred in the region of lower shear. Photographs of the specimens after failure are shown in Figure 6-8. Only a portion of Specimen N-1 is visible in Figure 6-8. The left reaction is not shown in the photograph, because it is blocked by the loading apparatus. The results of all four asymmetric tests are summarized in Table 6-1. All four specimens had a shear span-to-depth ratio of 1.7 on the right portion of the span, and the shear span-to-depth ratios listed in the figure are for the left portion of the span.

Specimens N-1, W-1, and W-2 failed in shear at a shear force lower than that determined using the provisions for V_c in ACI 318-05. Since these specimens contained shear reinforcement, the concrete contribution was calculated as $V_c = V_u - V_s$. Only Specimen W-3 reached shear strength in excess of the design shear strength of the beam. The long shear span of all four beams was

262

within the limits of Kani's shear strength envelope, thus low strengths are not surprising. These tests suggest that the shear span-to-depth ratio is an important parameter in determining concrete contribution to shear strength.
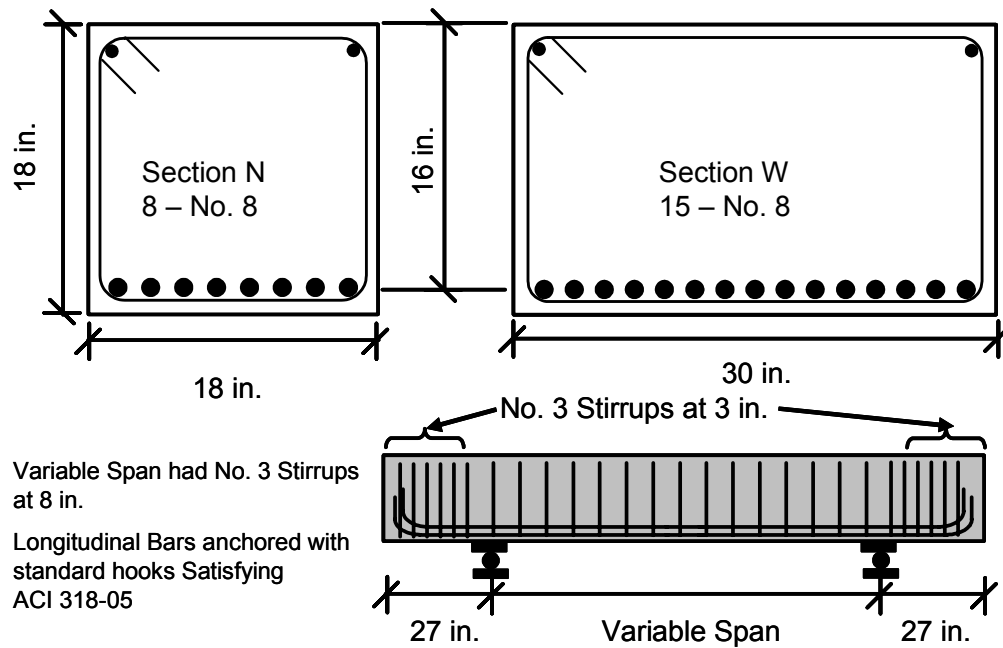
Figure 6-7: Details of symmetric concentrated load specimens

Table 6-1: Results of asymmetric concentrated load tests

Test	f_c' [ksi]	Span [in.]	V_s** [kip]	South Portion of Span*			North Portion of Span	
				Distance from Support to Load [in d]	V_{Test} [kip]	$\dfrac{V_{Test} - V_s}{\sqrt{f_c'}bd}$	Distance from Support to Load [in d]	V_{Test} [kip]
N – 1	2.85	120	32	5.8	42	0.64	1.7	153
W – 1	3.65	75	32	3.0	84	1.78	1.7	149
W – 2	3.57	99	32	4.5	82	1.75	1.7	236
W – 3	3.11	120	32	5.8	101	2.58	1.7	266

Notes:

* Failures occurred on the South portion of the span (Left end in Figure 6-8)

** $V_s = \dfrac{A_v f_y d}{s}$

Specimens N-1, W-1, W-2, and W-3 are identified in Chapter 4 as II-N-C-5.8-8, II-W-E-3-8, II-W-E-4.5-8, and II-W-E-5.8-8 respectively.
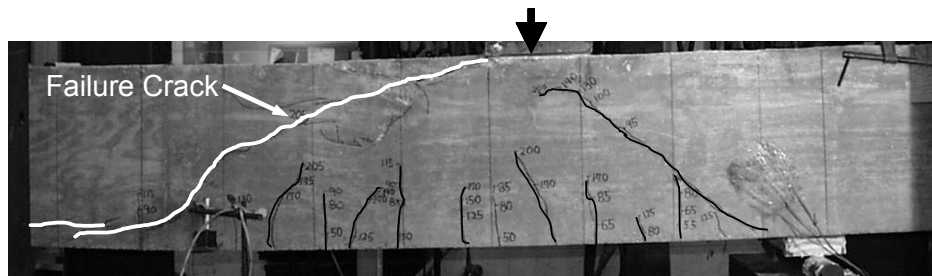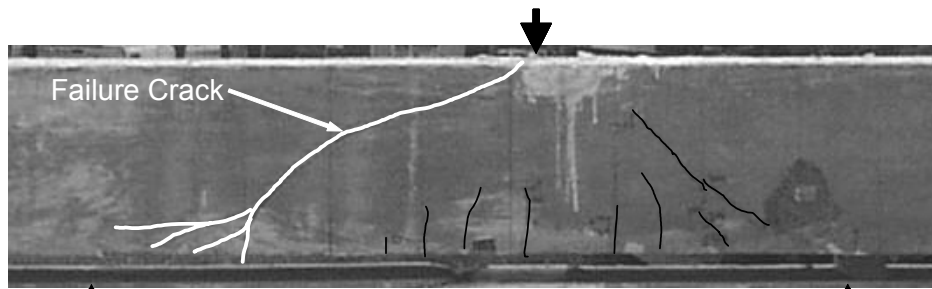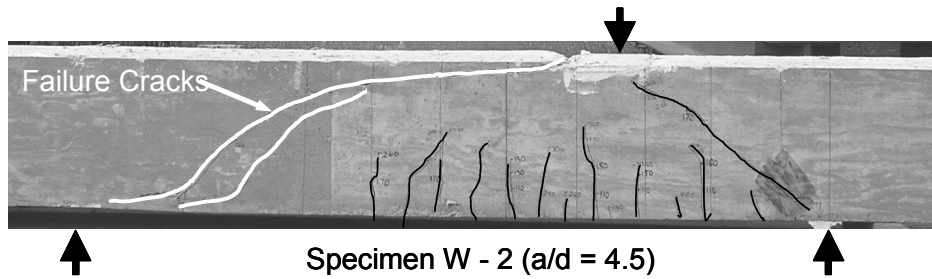
Figure 6-8: Photographs of asymmetrically loaded test specimens after failure

265

6.4 DATABASE OF SHEAR TESTS

In order to examine the differences in the measured shear strengths of beams subjected to concentrated loads and beams subjected to uniform loads, the database of published test results described in Chapter 5 was employed. A full description of the beams compiled into the database can be found in Chapter 5.

Of the 1,194 tests which comprise the database, 104 were beams subjected to uniform load. For the cases of beams subjected to uniform load, the measured shear capacity, V_{Test}, is taken as the shear occurring at a distance d away from the face of the support in accordance with ACI 318 design procedures.

6.4.1 Nominal Shear Strength Provided by Concrete, V_c

For evaluating the concrete contribution to the shear strength in the database, only beams without shear reinforcement were considered. Of the 1,194 tests, 793 beams had no web reinforcement. In order to determine the shear strength provided by web reinforcement, the stirrups must be instrumented. By and large, the test specimens included in the database did not contain such instrumentation or strain measurements were not reported in the papers. For the relatively few tests where strain instrumentation was present, not all stirrups were instrumented so that an accurate estimate of the steel contribution to the shear strength is difficult to determine. Consequently only beams without transverse reinforcement were considered in evaluating V_c. Specimens that included transverse reinforcement will be discussed in a later section in order to evaluate the nominal shear capacity ($V_n = V_c + V_s$).

Of the 793 specimens without web reinforcement, 82 failed at loads less than that given by Eq. 11-3 of ACI 318-05 (Eq. 6-2). The shear provisions of the AASHTO LRFD Bridge Design specifications allow the same value for concrete contribution to shear strength as ACI 318-05. The current strength reduction

factors of ACI 318-05 and AASHTO LRFD (ϕ) are not intended to address the number of unconservative predictions but rather variability in material properties and member dimensions. The test specimens that failed below the strength allowed by ACI 318 were confined to tests of beams with a concentrated load acted between 2d and 6d from the support (Figure 6-9).
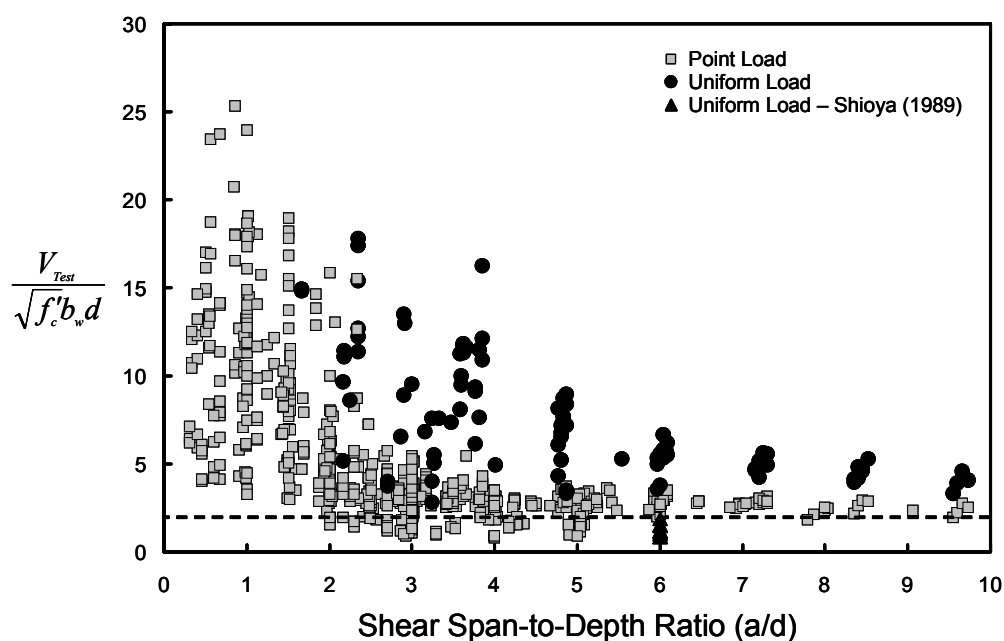
Figure 6-9: Shear strength of specimens without shear reinforcement
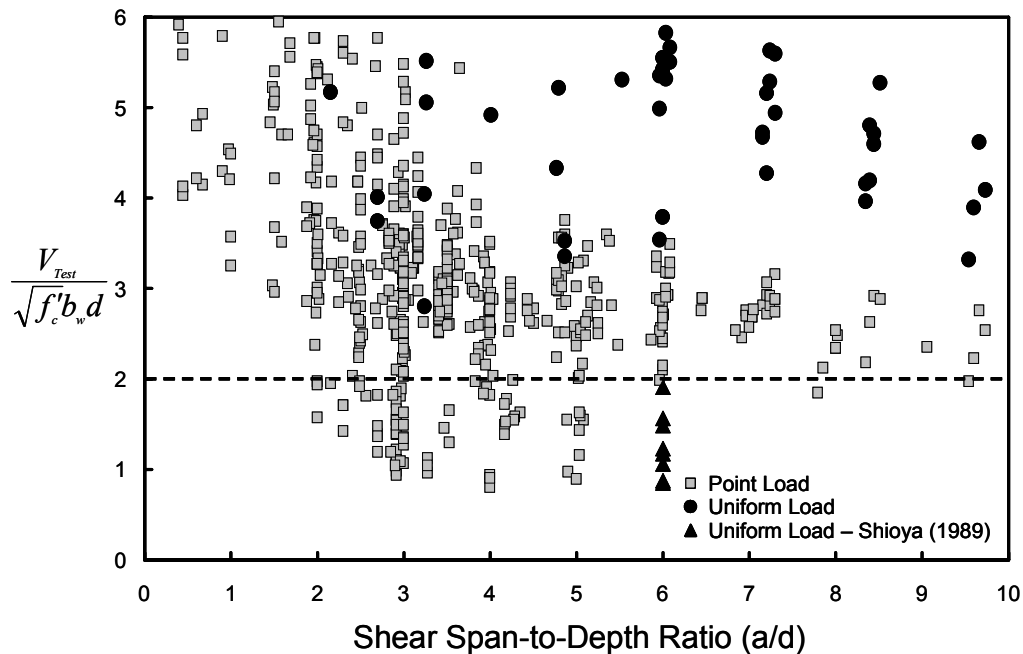
Figure 6-10: Shear strength of specimens without shear reinforcement (expanded scale for region of unconservative tests)

In Figure 6-9 and Figure 6-10, the difference between the response of beams subjected to uniform loads and concentrated loads is apparent. The vertical scale of Figure 6-9 has been changed in Figure 6-10 to better illustrate specimens with low strengths. The use of the ACI 318 provisions for the concrete contribution to shear strength result in conservative estimates of strength for all of the uniform load tests with the exception of the tests conducted by Shioya (1989). Those tests will be discussed in detail later. The only factors common to the tests that failed at $V_c < 2\sqrt{f_c'}b_w d$ are a/d ratios and the loading type, i.e. concentrated loads.

For beams with uniform load, the shear span was defined as the distance from the support to the point of zero shear based on the definition implied by the AASHTO LRFD Bridge Specification. For the tests with concentrated loads, only

268

one or two concentrated were used. For such tests, the definitions of shear span previously discussed converge to a single value. For these cases the shear span is simply the distance between the support and the load. However, if the definition of shear span, as implied by AASHTO, for a uniformly loaded beam or the definition proposed by Leonhardt and Walther (1962) is used, the conclusions regarding the strength of members subject to uniform loads are the same. Changing the definition of the shear span is equivalent to changing the x-coordinate of the points that represent uniform loads in Figure 6-10. A change in the definition of shear span does not change the measured strength of the beams making precise definitions of shear span unnecessary. Beams under uniform loads fail at higher loads than those under point loads as can be seen in the segregation of the data from distributed loads (black symbols of Figure 6-9) relative to the data for concentrated loads (grey symbols of Figure 6-9).

6.4.1.1   *Uniform Load Tests by Shioya (1989)*

The thirteen tests conducted by Shioya (1989) constitute a series of carefully conducted large-scale tests intended to examine size effect and the influence of maximum aggregate size on overall strength. The results were thoroughly analyzed and reasons for the low capacities can be explained. Three of the beams failed in flexure, and are not included in the database. Two of the remaining beams failed due to "abnormal diagonal tension" as per Shioya. These beams have no apparent diagonal or shear cracks, but the flexural reinforcement did not yield during the test, hence they are referenced as "abnormal." These two beams were also omitted from the database.

For six of the eight remaining specimens that failed in shear, the longitudinal reinforcement was not constant along the length of the beam. The location where the longitudinal bars were cut was 1.5d from the support. Six

beams failed at a shear crack that initiated at that cut-off point. It has been established that shear strength may be reduced at the location of a longitudinal bar cut-off. The factored self-weight ($1.4M_{selfweight}$) of the largest beam in the series produced a moment greater than the factored moment capacity (ϕM_n) using the design provisions in ACI 318-05. Therefore, the beam did not have sufficient capacity to carry its self-weight. All of the beams in the test series had minimal longitudinal reinforcement. The beams tested by Shioya had longitudinal reinforcement ratios ($\rho_w = 0.4\%$) that were only slightly greater than the minimum allowed by Section 10.5.1 of ACI 318-05 ($\rho_{min} = 0.33\%$). For the strengths of concrete used by Shioya the minimum reinforcement ratio is governed by $\dfrac{200 b_w d}{f_y}$ rather than:

$$A_{s,min} = \frac{3\sqrt{f_c'}}{f_y} b_w d \tag{6-4}$$

Where: f_y = specified yield strength on nonprestressed reinforcement

The minimum longitudinal reinforcement ratio required by AASHTO LRFD for the largest of the Shioya tests is 0.2%.

The link between longitudinal reinforcement ratio and shear strength can be seen in Figure 6-11. Therefore the parameters of the Shioya tests were considered to be near the limits for reinforcement details given in ACI 318 and less than the minimum capacity required by the code.
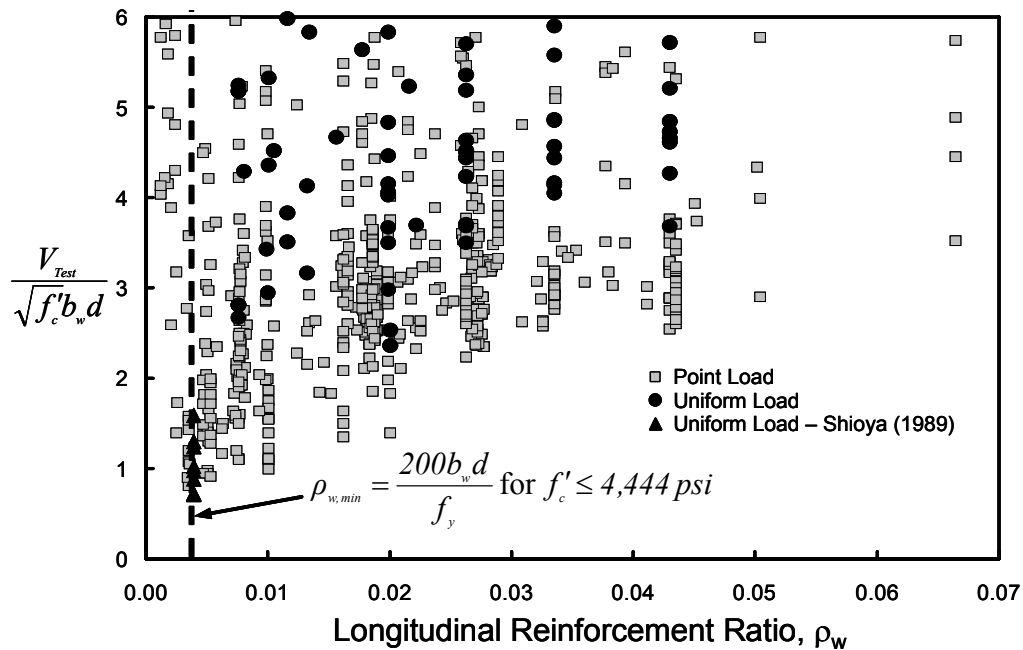
Figure 6-11: Concrete contribution to shear strength vs. longitudinal reinforcement ratio

6.4.2 Size Effect in Shear Strength

Recently a large amount of work regarding the size effect has been published. Proponents of the size effect state that large concrete elements have lower strength than small specimens that are commonly tested in laboratories. Research focusing on size effect (Shioya 1989; Bažant and Kazemi 1991; Tan and Lu 1999; Angelakos, Bentz, and Collins 2001; Lubell, Sherwood, Bentz, Collins 2004) is also included in the database of beams without reinforcement. Figure 6-12 shows the influence of the effective depth on shear strength, and Figure 6-13 shows the effects of beam width on shear strength. In both figures, the lower bound to shear strength is roughly $0.75\sqrt{f_c'}b_w d$ regardless of the cross-sectional dimensions.

271
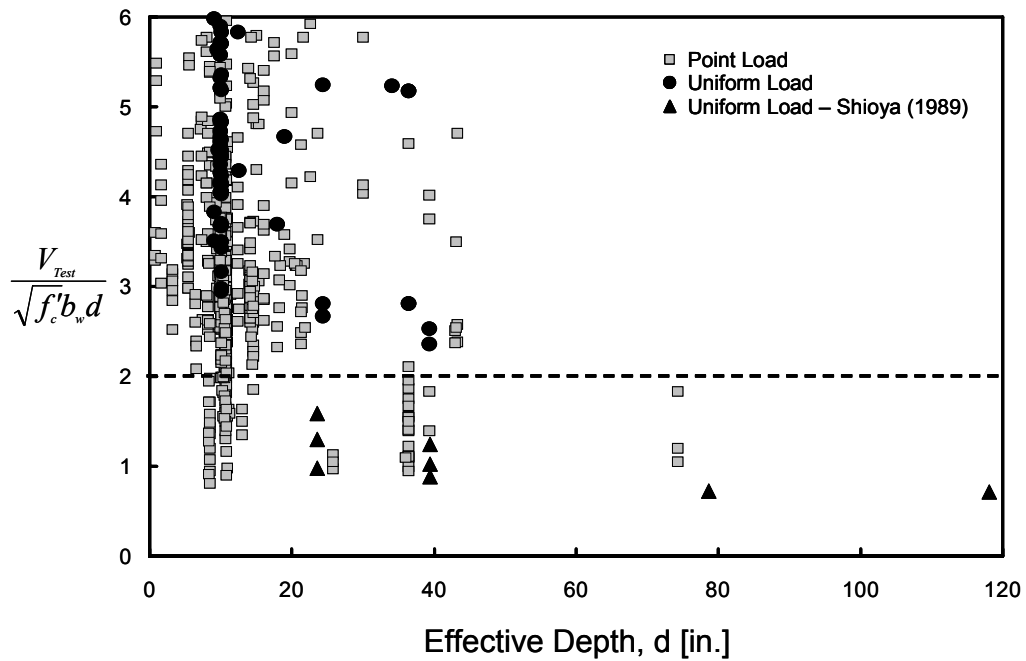
Figure 6-12: Concrete contribution to shear strength vs. effective depth

Two possible conclusions can be drawn from Figure 6-12 and Figure 6-13. The first is that the size effect is evident only in the upper bound or the best-fit of the data; the lower bound is unaffected. Another likely possibility is that there are insufficient data from large specimens to determine whether similar scatter will occur with large beams as has been observed for small and moderately size beams.
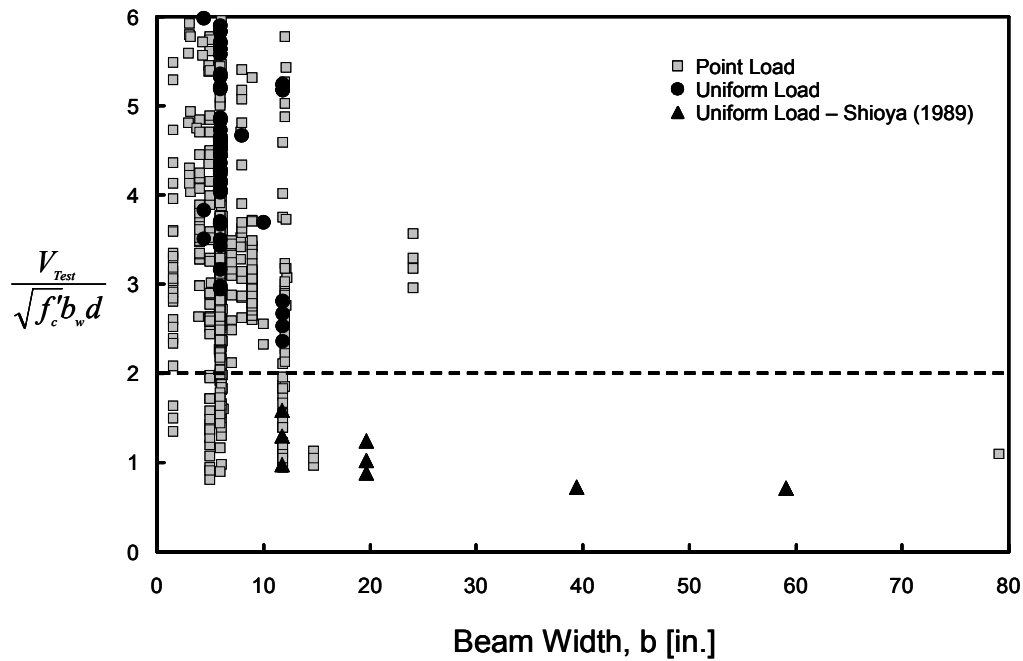
Figure 6-13: Concrete contribution to shear strength vs. beam width

6.4.3 Effect of Transverse Reinforcement

In Figure 6-14, the capacities of 401 test specimens with shear reinforcement are plotted. From this figure it is apparent that the conclusions regarding specimens without web reinforcement hold for specimens with web reinforcement. In Figure 6-10 and Figure 6-14 the majority of unconservative test results are confined to specimens subjected to points loads applied between 2 and 6 d from the support. This similarity between Figure 6-10 and Figure 6-14 implies that unconservative estimates of the concrete contribution to shear strength (V_c) are the primary cause of low strength of beams subjected to concentrated loads.

273
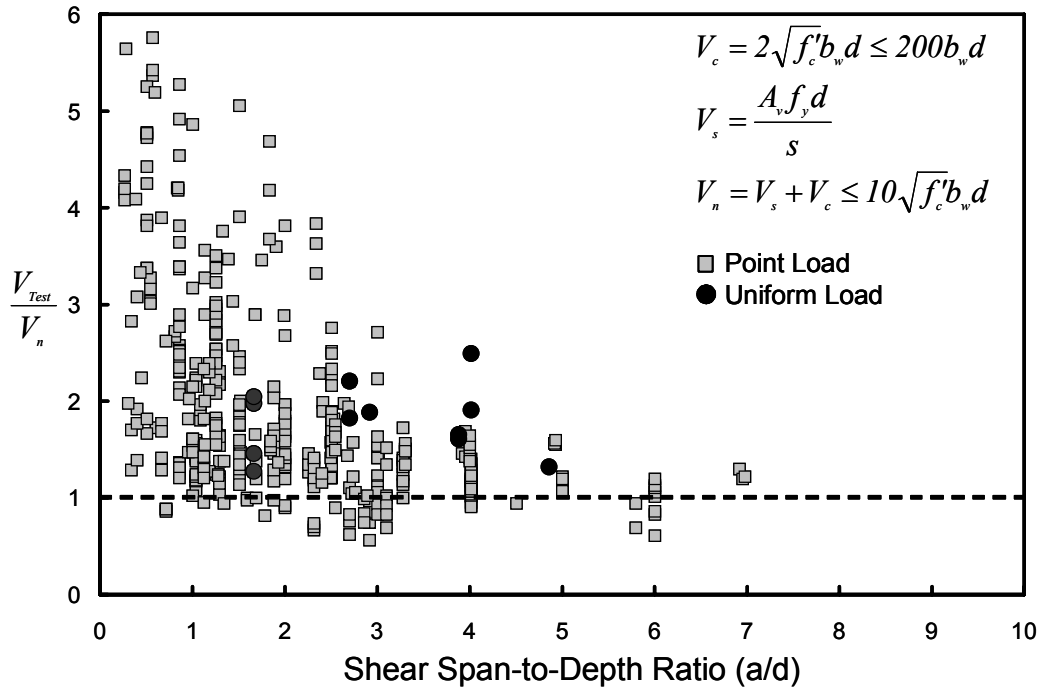
Figure 6-14: Shear strength of specimens with web reinforcement

In Figure 6-14 low strength values for tests with a shear span-to-depth ratio less than 2.0, are in the range that according to ACI 318-05 provisions must be designed using Appendix A – Strut-and-Tie Models. AASHTO LRFD also requires that specimens with shear span-to-depth ratios less than two be designed using STM. Consequently, the shear strength of specimens with shear span-to-depth ratios between 2.0 and 6.0 are of importance for a sectional shear model $(V_n = V_c + V_s)$.

The number of unconservative test results for specimens with shear reinforcement is 43 of 466 such specimens. The corresponding number of unconservative test results for specimens without shear reinforcement is 80 (of 793 tests). If only specimens that satisfy the maximum spacing requirement for

shear reinforcement are considered, the number of results that are unconservative are reduced from 43 (of 466 tests) to 21 (of 278 tests).

In Figure 6-15, the strength of the specimens is plotted as a function of the ratio of V_s to V_c. The majority of unconservative results are from tests with low levels of shear reinforcement ($V_s/V_c < 1$). For specimens that satisfy the transverse spacing requirements of ACI 318-05 (Figure 6-16) many unconservative test results are still present. In both figures the vertical line at $V_s/V_c = 4$ represents the maximum steel contribution to shear strength allowed by ACI 318. Using maximum allowable shear strength of a beam as and $V_c = 2\sqrt{f_c'}b_w d$ the steel contribution is equal to four times the concrete contribution. For the data in these figures, the upper limit of shear strength has been used in determining the nominal shear capacity.
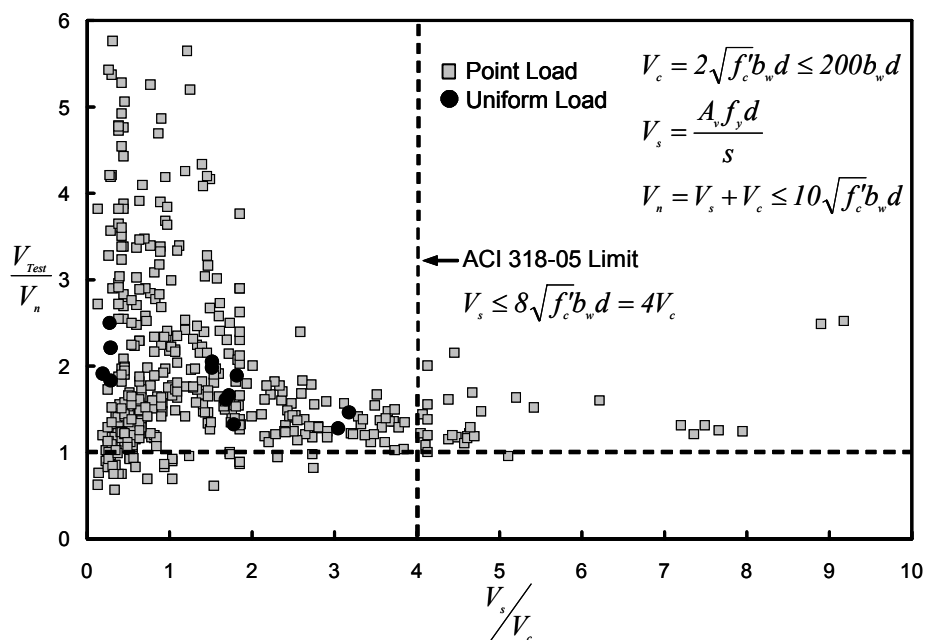
Figure 6-15: Effect of transverse reinforcement for all specimens with $V_s > 0$

275
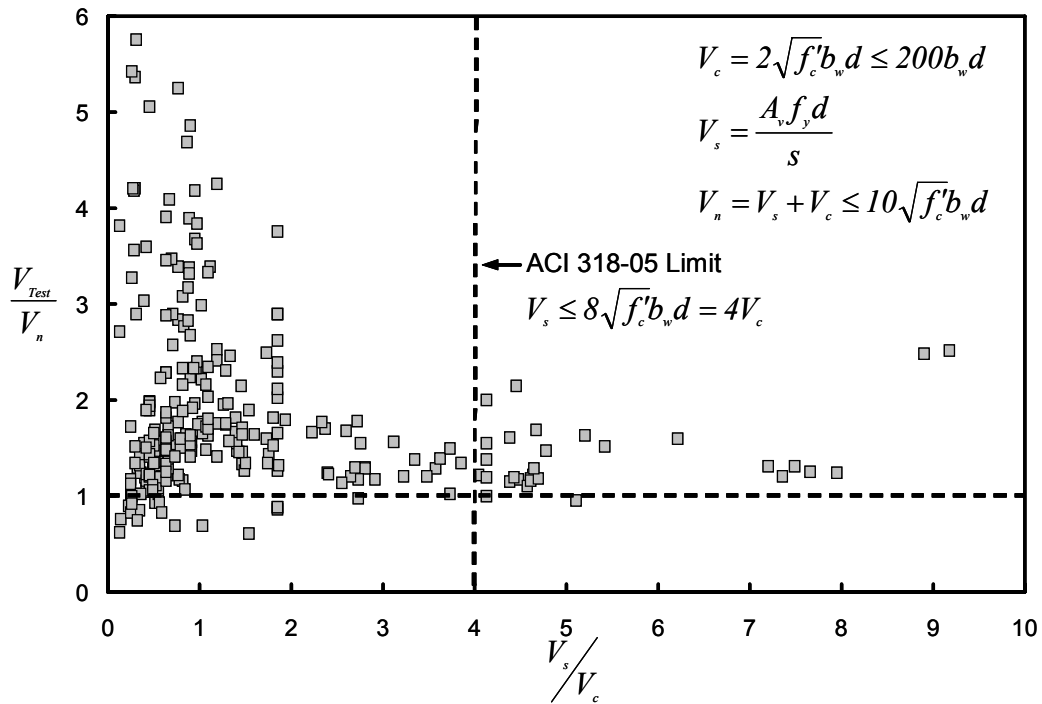
Figure 6-16: Effect of transverse reinforcement for specimens with point loads and satisfying ACI 318-05 spacing requirements and minimum shear reinforcement requirements

In Figure 6-15 and Figure 6-16 the unconservative test results are largely confined to the portion of the plots where the steel contributions to shear strength (V_s) is less than the concrete contribution (V_c). Historically minimum shear reinforcement provisions require enough shear reinforcement to develop 50 psi of shear stress on the section. Recently the requirements for minimum shear reinforcement have been altered to include the effects of concrete strength as seen in Eqn (6-5) below:

$$A_{v,min} = 0.75\sqrt{f_c'}\,\frac{b_w s}{f_{yt}} \qquad (6\text{-}5)$$

Where: $A_{v,min}$ = minimum area of shear reinforcement

276

By modifying Eqn. 6-5, Eqn 6-6 can be developed:

$$\frac{A_{v,min} f_{yt} d}{s} = 0.75\sqrt{f_c'} b_w d \qquad (6\text{-}6)$$

Equation 6-6 requires that the minimum shear reinforcement provide a shear strength of at least $0.75\sqrt{f_c'} b_w d$. If the minimum shear reinforcement requirements were altered such that the minimum steel contribution to shear strength was equal to the concrete contribution, increases in safety would result. However, such changes would require a significant increase in shear reinforcement in typical beams.

6.5 DESIGN RECOMMENDATIONS

The current ACI 318-05 and AASHTO LRFD code provisions for shear yield unconservative strength estimates only for beams subjected to concentrated loads applied between 2d and 6d from the support. From Section 11.3.1.1 of ACI 318-05:

For members subject to shear and flexure only,

$$V_c = 2\sqrt{f_c'} b_w d \qquad (6\text{-}2)$$

To include the effects of loading type and shear span to depth ratio into the current code provisions, the following statement should be added to that provision:

For members in which more than one-third of the factored shear at the critical section results from a concentrated load located between 2d and 6d of the face of the support:

$$V_c = 1\sqrt{f_c'} b_w d \qquad (6\text{-}7)$$

Similar changes could be applied to the ASAHTO LRFD shear provisions for conventionally reinforced concrete structures. The "one-third" that is

277

presented in the proposed changes stems from the AASHTO LRFD definition of a deep component. That definition can be seen in Section 6.2.

Such a reduction in shear strength will substantially reduce the number of tests that fall below code values (Table 6-2 and Figure 6-17). By implementing the proposed provision only 3 test results in the database are unconservative (of 278 specimens that satisfy transverse spacing requirements) compared with 21 (of 278 specimens) using the current provisions. Similar changes result for specimens with no transverse reinforcement.

Additionally, if the concrete contribution to shear strength were reduced to $1\sqrt{f_c'}b_w d$, the alterations to the minimum shear reinforcement requirements that were discussed in Section 6.4.3 become plausible. The strength provided by the minimum shear reinforcement would only increase from $0.75\sqrt{f_c'}b_w d$ to $1\sqrt{f_c'}b_w d$. The represents a 33% increase in the minimum shear reinforcement requirements. Such an increase is somewhat large, but given the scatter and undesirable nature of shear failures increases in detailing requirements may be justified.

Table 6-2: Number of unconservative test results

	Number of Unconservative Tests Results	
	ACI 318-05 Provisions	Proposed Provisions
Specimens without Shear Reinforcement (Vs = 0) 793 Total Tests	80	11
Specimens with Shear Reinforcement (Vs > 0) 466 Total Tests	43	8
Specimens with Shear Reinforcement and satisfy ACI 318-05 Transverse Spacing Requirements 278 Total Tests	21	3

The maximum shear strength allowed by ACI 318-05 is $10\sqrt{f_c'}b_w d$. The data plotted in Figure 6-18 are from test specimens with concentrated loads located between 2d and 6d of the support. Additionally the data shown in Figure 6-18 are from test specimens that satisfy the current limits for the maximum spacing of transverse reinforcement and minimum amount of shear reinforcement in ACI 318-05. Using the proposed shear provisions for V_c, the maximum allowable steel contribution, V_s, is nine times that of V_c so that the maximum shear strength remains at $10\sqrt{f_c'}b_w d$ as indicated by the vertical line in Figure 6-18. Nearly all data in Figure 6-18 exhibits strengths greater than that indicated by ACI 318-05, even for specimens with large amounts of transverse reinforcement.
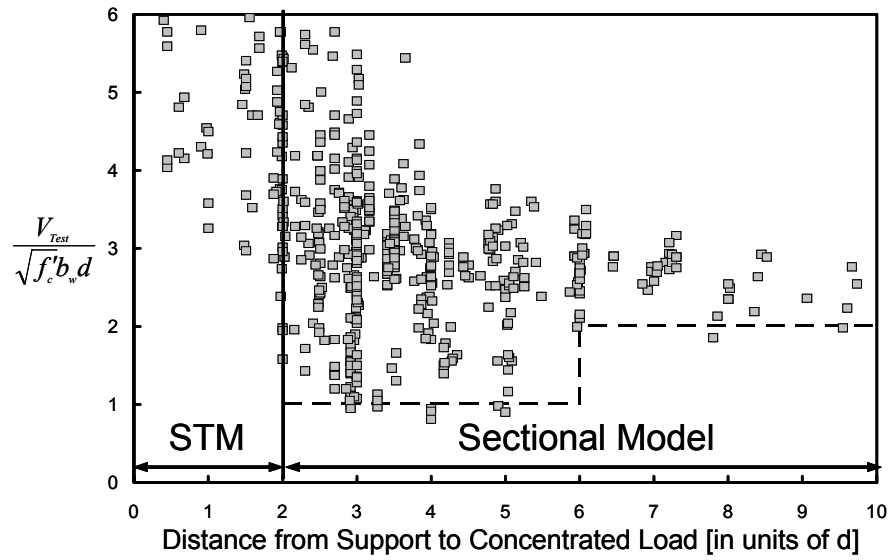
Figure 6-17: Proposed shear strength provisions for sectional models for members subjected to concentrated loads
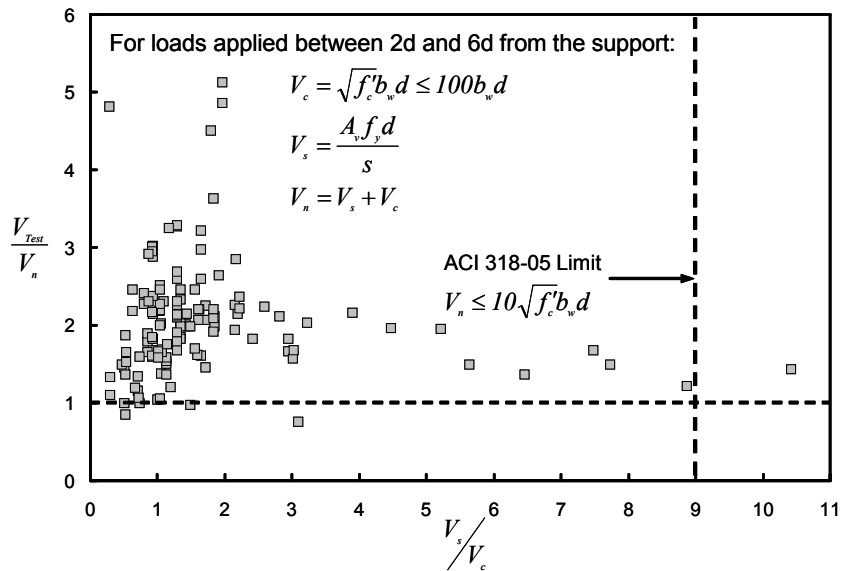
Figure 6-18: Maximum shear strength using proposed shear provisions for specimens that satisfy ACI 318-05 spacing requirements and minimum shear reinforcement requirements and subjected to concentrated loads

280

CHAPTER 7

Summary and Conclusions

7.1 SUMMARY

The research conducted in this study was performed to examine the behavior of shear-critical reinforced concrete beams. The first series of experiments consisted of 26 concrete panels with and without reinforcement. The panels were used to examine the geometry of bottle-shaped struts in the simplest form as well as the impact of reinforcement on that geometry.

Based on the findings from the isolated struts, three series of beam tests were performed. The first series (ten tests) consisted of deep beams. The primary variables within this series of beams were the type of loading applied to the beams and the shear reinforcement (horizontal and vertical) within the beams. The second series of tests also consisted of deep beams. For the second series the primary variables were beam width and shear span-to-depth ratio. Each of these beams was subjected to a single concentrated load placed asymmetrically within the span. The final series of beams tests consisted of nominally identical beams that were subjected to a single concentrated load, multiple concentrated loads, or a uniform load.

In addition to the experimental program a large database of published test results was assembled (approximately 1,200 tests). The tests comprising this database were used to examine the effects of many different parameters on the shear strength of reinforced concrete beams. By carefully examining the data within the database, a new design procedure for use with strut-and-tie modeling was developed. The new procedure increases levels of conservatism compared to existing U.S. code provisions regarding STM (ACI 318-05 and AASHTO LRFD

281

Bridge Design Specifications). The new procedure includes provisions for the required reinforcement within a bottle-shaped strut, efficiency factors for bottle-shaped struts, and guidelines for the use of hydrostatic and nonhydrostatic nodes. Additionally, the database was used to develop recommendations for use in design for shear using sectional models. The recommendations for improvements to the current ACI 318-05 sectional design provisions, like those for STM, were intended to increase conservatism compared to existing provisions.

7.2 CONCLUSIONS

The following conclusions were drawn from the experimental and analytical research conducted in this study:

- **Both ACI 318-05 and AASHTO LRFD Bridge Design Specifications STM provisions provide unconservative estimates of strength for a large portion of the test results in the database.** When ACI 318 and AASHTO LRFD STM provisions are applied to specimens in the database (all specimens with shear span-to-depth ratio not greater than two), 72% and 84% of the test results respectively are conservative. The use of either code does not result in acceptable levels of conservatism. The application of the current shear design provisions ($V_c = 2\sqrt{f_c'}b_w d$) to the database developed by ACI-ASCE Committee 326 in 1962 produces conservative capacities for 98% of those test specimens.

- **The use of the newly developed procedure increases conservatism to more desirable levels.** A new design procedure that consists of new equations to determine the efficiency of a bottle-shaped strut and the reinforcement required for that strut was developed. Application of the new procedure along with the

282

new provisions for reinforcement within a bottle-shaped strut results in conservative estimates of strength for 96% of the specimens in the database. Additionally, the new provisions indicate that the amount of reinforcement necessary for the strength of a bottle-shaped strut can be much less than ACI 318-05 code requires. The new procedure recommends the use of significantly less reinforcement than the current AASHTO LRFD Bridge Design Specifications.

- **Beams subjected to uniform loads exhibit increased shear strength compared with beams with concentrated loads.** The experimental results of the beam tests as well as the results compiled in the database support this conclusion. Also the measured strain distributions within the beams suggest different load carrying mechanisms for beams with concentrated or distributed loads. Beams subjected to closely spaced concentrated loads exhibited shear strength similar to beams with uniform loads.

- **Current ACI 318 provisions for sectional design result in unconservative estimates of strength for beams with concentrated loads between 2 and 6 times the effective depth from the support.** The results from the database indicate that such beams have reduced shear strength. A reduction in the concrete contribution to shear strength for members with concentrated loads applied between 2d and 6d from the support can greatly reduce the number of unconservative estimates without any changes to reinforcement detailing provisions. The use of the AASHTO LRFD Bridge Design Specifications for sectional design reinforced

283

concrete produces unconservative results similar to the ACI 318-05 provisions.

- **Shear span-to-depth ratio has a large effect on shear strength.** The second series of beams tests consisted of beams with two different shear span-to-depth ratios within a single specimen. In four of the ten tests, shear failure occurred in the longer shear span where applied shear was much less than the peak shear. A similar type of failure occurred in one of the ten tests from the first series. Results from the database substantiate the relationship between shear strength and shear span-to-depth ratio.

- **The strength of beams with shear span-to-depth ratios less than two are better represented by a direct strut mechanism.** The energy analysis indicates that a direct strut between the load point and the support carries most of the load for beams with small shear span-to-depth ratios. Increased shear reinforcement can shift portions of the load to multiple panel mechanisms; however a single panel mechanism dominates the behavior.

- **Loads at which cracking occurred are unaffected by reinforcement.** In both the isolated strut tests and the beams tests, the cracking loads were not affected by reinforcement that bridged the splitting crack(s). This observation is consistent with theory of reinforced concrete structures. In the elastic realm (prior to cracking) reinforcement is not influential, only after cracking are significant forces transferred to the reinforcement.

- **Nearly parallel shear cracks were observed just prior to failure of the beam specimens.** In all three series of beam tests, a second shear crack nearly parallel to the first shear crack was observed at

approximately 80% of the ultimate load. Cracking behavior such as this could be indicative of impending failure due to shear.

- **Failure occurs due to crushing of the strut at node-strut interfaces.** In the isolated strut tests (Chapter 3) and the beam tests (Chapter 4), crushing failure was observed. In general, a node is subjected to a multi-axial state of compressive stress. Therefore the node benefits from increased strength due to confinement. This mode of failure can be prevented through the use of additional confinement at the node-strut interface.

7.3 SUGGESTIONS FOR FUTURE RESEARCH

During the course of this research, the need for future research was encountered:

- **How does STM address serviceability of structures?** Strut-and-tie modeling is governed by the lower bound theory of plasticity. As such the method does not allow for computation of deflections or crack widths under service loads. Perhaps serviceability concerns can be handled by limiting stresses within the strut and nodes. Preventing cracks under dead load and some fraction of the live load might also solve serviceability problems.

- **How many reinforcing bars comprise a tie?** In a strut-and-tie model a tie is intended to approximate a reinforcing bar or a group of bars. If a bar is located a great distance from the assumed tie location, can that bar be included in the area of the tie?

- **How does confinement affect the strength of a node?** The beneficial effects of confinement have been well-documented in

the literature. However, in a typical beam a node is subjected to confinement within the plane of the beam (biaxial confinement) rather than in three dimensions as in true confined conditions (triaxial confinement). The effects of confinement have been observed experimentally, but currently there are no methods to determine the capacity of a node with planar confinement.

- **What is the actual geometry of a node?** Often nodes are assumed to be hydrostatic. With that assumption the geometry of a node is simple to determine. However, in the elastic region the nodes are almost certainly not hydrostatic. At failure load (where STM is valid), the nodes may be hydrostatic. Current thoughts on the matter present much conjecture and little empirical evidence. If a node is not directly influenced by the presence of a bearing, the geometry becomes even more difficult to define.

- **What is the acceptable minimum amount of shear reinforcement for use in sectional design methods?** Recently there has been much debate over the minimum shear reinforcement requirements. Traditionally the minimum shear reinforcement was enough steel reinforcement to resist 50 psi of shear stress within the section. With high strength concrete, that traditional limit has become inadequate. However, if the minimum shear reinforcement were such that the steel contribution to shear strength was at least equal to the concrete contribution ($V_s \geq V_c$) adequate safety would be present regardless of concrete strengths. The minimum reinforcement required for flexure is based on that which is required to maintain strength after cracking. The requirement that $V_s \geq V_c$ is similar in nature.

286

- **What is the geometry of a bottle-shaped strut after cracking?** Traditionally the geometry of a bottle-shaped strut is based on elastic stress distributions. After cracking, the stress distribution can change significantly and affect the reinforcement required to maintain equilibrium within the strut.

- **Why is there a single strength reduction factor for all elements of a STM?** The philosophy of modern concrete codes has been to favor ductile modes of failure. This philosophy is implemented throughout strength reduction factors. Strength reduction factors closer to 1.0 are used for ductile failure modes (i.e. flexure). If this same philosophy is applied to STM, different strength reduction factors should be used for ties, which are ductile, and for struts, which are brittle.

APPENDIX A

Design Examples

A.1 INTRODUCTION

A series of four design examples are presented. The STM provisions of
AASHTO LRFD Bridge Design Specifications, ACI 318-05 Appendix A, and the
newly developed procedures for STM are used for the design calculations. In
some of the examples sectional shear models are also be needed. The sectional
shear models from AASHTO, ACI, and Chapter 6 of this dissertation are used in
concert with the companion STM procedures where applicable.

The example problems in this chapter represent the design procedures for
shear strength only. Two of the four examples are continuous bent caps. The
continuity requires additional load combinations to determine the most extreme
load cases for flexure. Those load cases are not presented herein. Traditional
methods for determining the flexural design that include the effects of continuity
should be used for determining the amount of longitudinal steel.

A.2 BASIC BENT CAPS

The design examples in this section focus on bent caps. The basis for the
examples is the Texas Department of Transportation (TxDOT) standard cap
design. The standard design supports either Type C or Type IV pretensioned
girders. For each example, the girders are assumed to be at their maximum usable
span to generate the greatest loads in the bent cap. The spacing of the girders on
the cap and the columns supporting the cap are varied in accordance with standard
design details. The limits of the dimensions used in the standard caps are shown
in Figure A-1 and Table A-1.

The loads listed in Table A-1 are unfactored. For the examples using ACI and AASHTO the load factors and strength reduction factors from the respective codes will be used. As for the newly developed model, the load factors and strength reduction factors from AASHTO have been adopted.
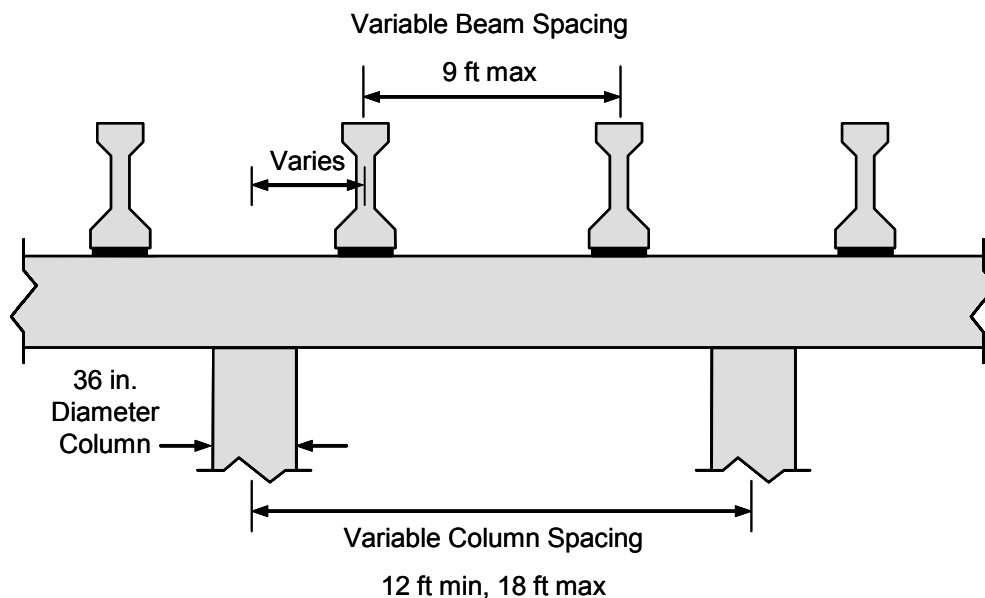
Figure A-1: Typical bent cap beam and column spacings

Table A-1: Details of typical bent caps

	Effective Depth [in.]	Width [in.]	Unfactored Live Load [kip]	Unfactored Dead Load [kip]	Bearing Length [in.]
Cap Supporting Type C Beams	30	33	61	120	19
Cap Supporting Type IV Beams	36	39	79	210	22

For the examples presented in Appendix A, the designs have been carried out using load and strength reduction factors from the same code. For example, all calculations done using ACI 318-05 provisions used the load and strength reduction factors from ACI 318-05. Load factors and strength reduction factors are determined in pairs. A strength reduction factor from one code is not necessarily compatible with a load factor from another code. Alternatively, the design could have been performed using a common set of load factors along with strength reduction factors from he various codes. However, such designs would results in an unfair assessment of the code provisions. The decision to use load and strength reduction factors in pairs from a single code was done so for the sake of consistency.

The main difference between the design examples presented in Appendix A is the load factors. ACI 318-05 is intended for use in the design of buildings and does not have an impact factor, but AASHTO LRFD (intended for use in designing bridges) does have an impact factor. Due to the impact factor, the design loads for use with AASHTO are greater than the design loads for use with ACI 318-05. The designs produced through the use of ACI 318-05 and AASHTO LRFD can not be directly compared. The newly developed provisions use the load and resistance factors from AASHTO LRFD. Therefore, the designs developed with AASHTO LRFD and the newly developed procedures are comparable.

A.2.1 Effect of Continuity on Shear in Bent Caps

If the behavior of a bent cap is considered to be linear and elastic, a small error in the calculated shear force would result from neglecting the continuity. As can be seen in the influence lines shown in Figure A-2, the maximum error is 11% (for a load located at a quarter-point of the span). However, if a fully plastic mechanism forms, the end moments are equal (Figure A-3). If the end moments

are equal in magnitude and opposite in direction, and the shear forces are distributed just as in a simply supported beam. So there would be no error in the calculated shear force if a simple support was assumed rather than a continuous beam at the support.
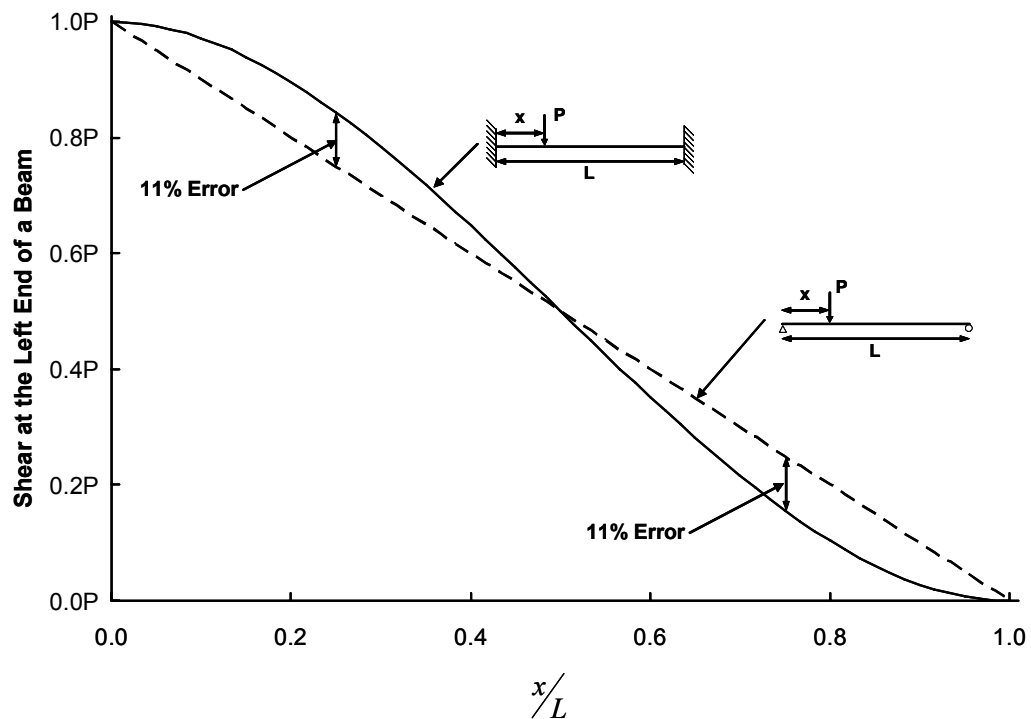
Figure A-2: Influence lines for simple and continuous beams
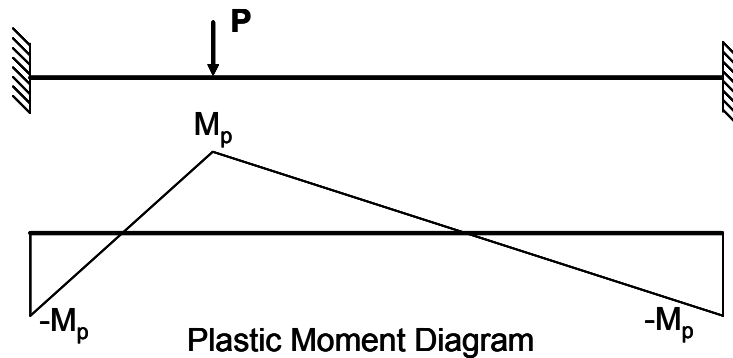
Figure A-3: Plastic moment diagram for a fixed-fixed beam

If a truss model was developed to explicitly model the effects of continuity, the truss over the column would consist of a single tie at the top of the section and a node directly above the column. The moment would then be calculated as the force in either the tie or the node times the distance between their centroids, or in other words the plastic moment of the section. The actual behavior of a bent cap at capacity will likely not be linear. However, the three plastic hinge mechanism may or may not form depending on the geometry. The error in calculated shear forces would be between 0 and 11% depending on the behavior of the cap near ultimate capacity. Near ultimate load the cap would likely be nearer to fully plastic than linear elastic. Therefore it is not believed that significant error arises from neglecting the effects of continuity on shear in the following examples.

The design method presented here is not the only possible solution. There are multiple trusses that could be used for any cap.

A.2.2 Cap Supporting Type C Beams

This example is intended to represent a single span in a multiple span, continuous beam. To simulate the continuity Node A will only use half of the available area on top of the column. The remaining half of the column is reserved

292

for any necessary nodes from the neighboring span. The reaction is assumed to be located at the center of the node which occurs at a quarter point of the column thickness.

The first design example is the simplest of the structures examined. It consists of a cap supporting a single Type C beam. The column spacing is 12 ft, and the center beam is located 30 in. from the center of the column. The shear span-to-depth ratio is 1.0. The structure and the associated STM are shown in Figure A-4.
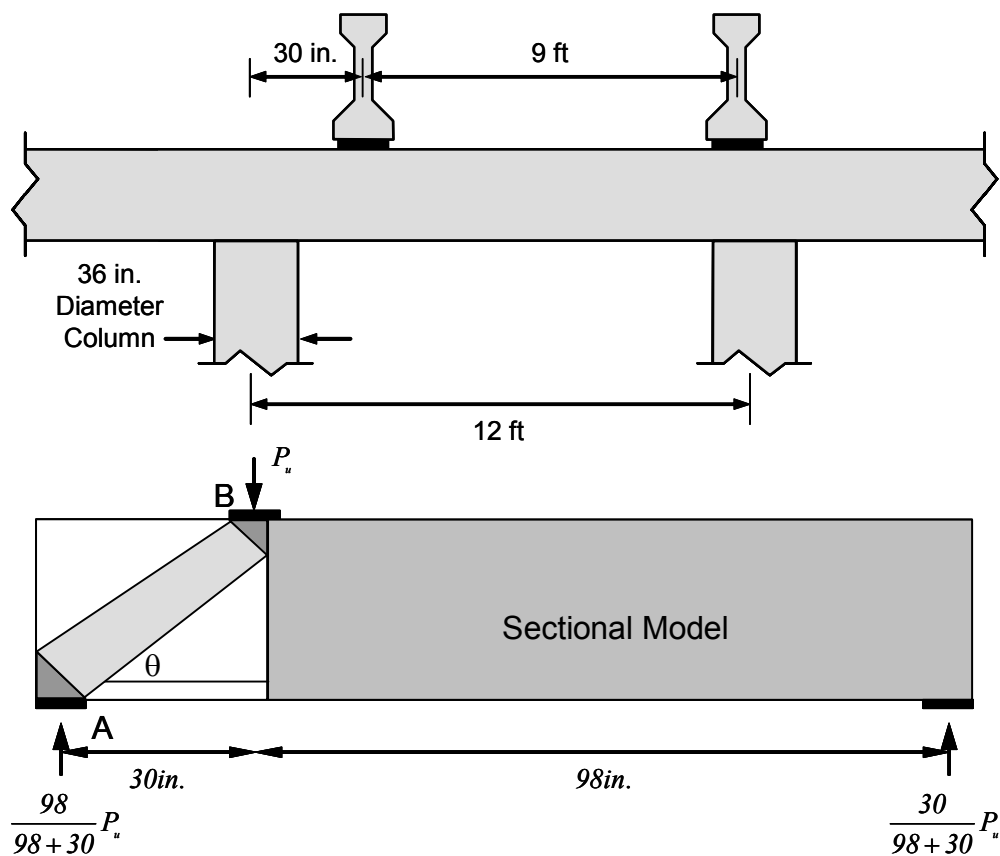
Figure A-4: Details for Example 1

In this example both sectional shear models and STM are needed. Both ACI and AASHTO require STM only if a concentrated load is located within

twice the effective depth of the member from the support. To the left of the load a single direct strut will form. To the right of the load a multiple-panel truss mechanism is likely. When multiple-panel solutions are expected, sectional shear models should be used as shown in Figure A-4. For this example, the pretensioned girder on the right side of the span is directly on top of a column. Therefore, the load in this beam induces no shear in the bent cap. As such, the beam on the right side of the span is neglected in the example.

A.2.2.1 Standard Bent Cap Design

The standard bent cap used to support TxDOT Type C girders is 2 ft 9 in. wide by 2 ft 9 in. deep with an effective depth of 2 ft 6 in. The caps are constructed with concrete that has a specified compressive strength of 3,600 psi.

The longitudinal reinforcement within the cap varies based on the continuity of the cap. However, the longitudinal reinforcement always consists of a single layer of No. 11 bars at the top and bottom of the cross section. The number of bars in the layer varies between four and eight.

The shear reinforcement consists of closed stirrups and longitudinal bars near the vertical faces of the cap. The stirrups are No. 5 bars. For narrow bridges (roadway width equal to 24 ft) the stirrups are spaced at approximately 6 in. For wider bridges, the stirrups are spaced at 10 to 12 in. The tighter stirrup spacing in narrow bridges stems from those caps being supported by only two columns, whereas three columns are used for wider bridges. The skin reinforcement is also comprised of No. 5 bars. The skin reinforcement is placed such that there are two longitudinal bars along each vertical face of the cap. The spacing between the skin reinforcement and the longitudinal bars is 8 in. A cross-section of the standard bent cap is shown in Figure A-5.

No. 11 top

2 – No. 5

2 legs of No. 5
closed stirrups at
10 to 12 in.

No. 11 bottom
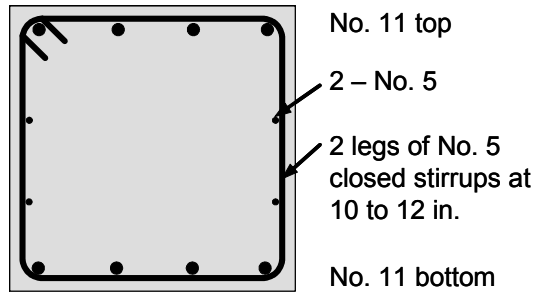
Figure A-5: Standard cap that supports Type C beams

A.2.2.2 Design Based on AASHTO LRFD STM Provisions

Based on the unfactored loads presented Table A-1 and the appropriate load factors for use by AASHTO LRFD, the maximum expected factored beam load is 320 kip. The reaction at Node A is therefore 245 kip. The height of the truss model is assumed to be equal to the internal lever arm, jd, which is approximately 28 in. The angle between Strut AB and the tie is therefore:

$$\theta = a\,tan\left(\frac{28in.}{30in.}\right) = 43.0°$$

Based on static equilibrium of Node A, the force in Strut AB is:

$$F_{AB} = \frac{245^k}{sin\,43.0°} = 359.2^k$$

The force in the Tie is:

$$F_{Tie} = \frac{F_{AB}}{tan\,43.0°} = 262.7^k$$

A.2.2.2.1 Node A

Node A is at the top of a round column. For simplicity an equivalent square column is used. The equivalent square for a 36 in. diameter column is 32x32 in. Therefore the bottom face of node is 16x32 in. The elevation of Node A

is show in Figure A-6. As per the AASHTO LRFD STM recommendations the height of node A is limited to twice the distance from the centroid of the tie to the free surface of the beam. For a typical cap supporting Type C beams that dimension is 6 in.
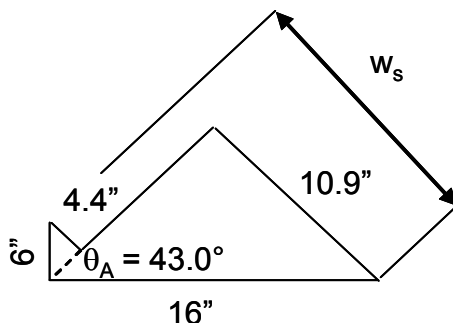
Figure A-6: Elevation of Node A

Using the geometry for Node A shown in Figure A-6, the width of the strut at the node face can be calculated as:

$$w_s = l_b \sin\theta + w_t \cos\theta$$
$$= 16in.\cdot\sin 43.0° + 6in.\cdot\cos 43.0°$$
$$= 10.9in. + 4.4in. = 15.3in.$$

Where: w_s = width of the strut (along the inclined node face)

l_b = length of the bearing (parallel to the span)

w_t = height of the tie

Stresses acting on all faces of Node A must be checked. Node A is a CCT node. Using AASHTO STM provisions the allowable stress on a CCT node is $0.75\phi f'_c$. For the bottom face of the node the allowable force is:

$$\phi P_n = 0.7\cdot 0.75\cdot 3.6ksi\cdot 16in.\cdot 32in.$$
$$= 967.7^k > 245^k - OK$$

For the left face of the node (Figure A-6):

$$\phi P_n = 0.7 \cdot 0.75 \cdot 3.6\,ksi \cdot 6in. \cdot 32in.$$
$$= 326.9^k > 262.7^k - OK$$

For the inclined face (Figure A-6):

$$\phi P_n = 0.7 \cdot 0.75 \cdot 3.6\,ksi \cdot 15.3in. \cdot 32in.$$
$$= 925.3^k > F_{AB}(= 359.2^k) - OK$$

The forces applied to Node A are less than that allowed by the code.

A.2.2.2.2 Node B

Similar calculations must be performed at Node B. Node B serves as the intersection point between the STM and the sectional model. The entire width of the bearing area should not be used for the node. Only a portion of the load applied at Node B flows toward Node A, the remaining portion flows to the right reaction and sectional methods are to be used to design for that portion of the applied force. The fraction of the bearing area that acts as Node B is equal to the fraction of the load that flows to the right support. The width of Node B (parallel to the span) is $\dfrac{245^k}{320^k} \cdot 19in. = 14.5in.$ The length of the beam bearings are given in Table A-1. The geometry of Node B is shown in Figure A-7.
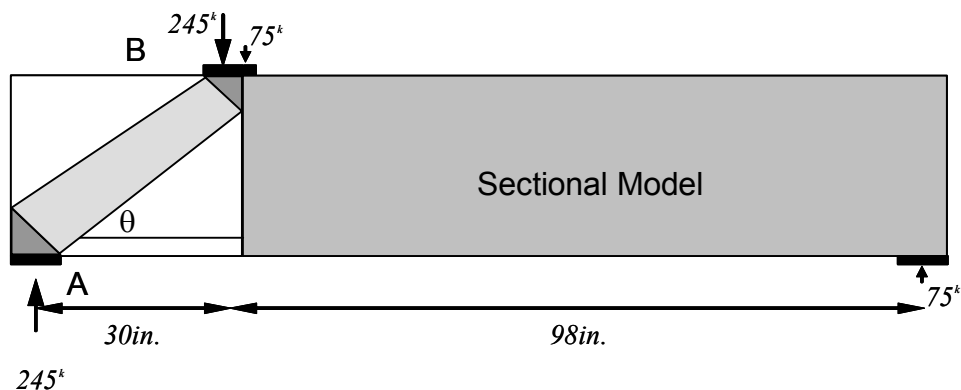
Figure A-7: Portion of applied loads for STM and sectional design

To determine the vertical face of Node B, it was necessary to determine the depth of the neutral axis. It is common to assume that a CCC node at the top of a section has the same size as the compressive stress block. Typical flexural reinforcement for a bent cap such as this is a single layer of No. 11 bars with yield strength equal to 60 ksi. For this particular section the depth of the neutral axis at the ultimate load was determined to be 4.4 in. Based on all the information regarding Node B, the rest of the node geometry can be calculated as shown below:

$$w_s = l_b \sin\theta + w_t \cos\theta$$
$$= 14.5in. \cdot \sin 43.0° + 4.4in. \cdot \cos 43.0°$$
$$= 9.9in. + 3.2in. = 13.1in.$$

θ = 43.0°

14.5"

θ

4.4"

9.9"

3.2"
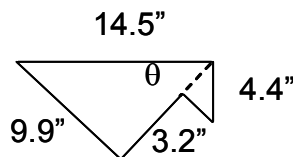
Figure A-8: Elevation of Node B

Node B is a CCC node and as such the allowable stress on the node is $0.85\phi f_c'$ rather than $0.75\phi f_c'$ for a CCT node as per the AASHTO LRFD Specifications. The bearing area on the top face of Node B is slightly more complex than the bearing area associated with Node A. The pretensioned beams are supported on two bearing pads (each 9x19 in.) that do not cover the entire width of the cap. A plan view of the beam bearings is shown in Figure A-9. It was assumed that the area between the bearing pads would also be included in the node based on the results of the wide beams tests described in Chapter 4. Therefore the bearing area for Node B was assumed to be 19x26 in.
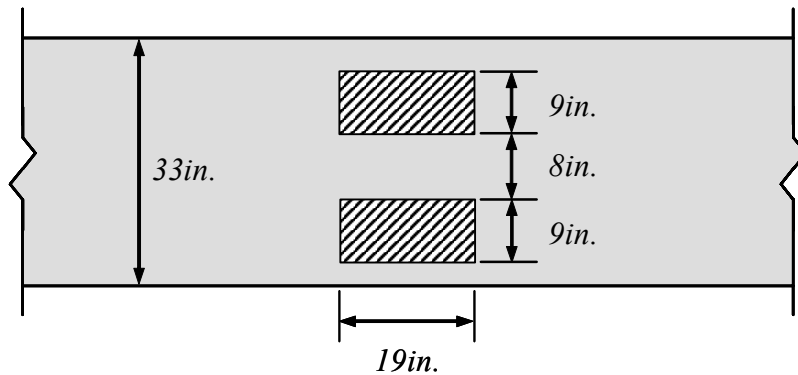
Figure A-9: Plan view of bearing area for Type C beams

Since the complete geometry of Node B has been determined, the allowable forces can be calculated. For the top face of the node:

$$\phi P_n = 0.7 \cdot 0.85 \cdot 3.6\,ksi \cdot 14.5\,in. \cdot 26\,in.$$
$$= 807.5^k > 245^k - OK$$

For the right face of the node:

$$\phi P_n = 0.7 \cdot 0.85 \cdot 3.6\,ksi \cdot 4.4\,in. \cdot 26\,in.$$
$$= 245.0^k < 262.7^k - NG$$

For the inclined face:

$$\phi P_n = 0.7 \cdot 0.85 \cdot 3.6\,ksi \cdot 13.1\,in. \cdot 26\,in.$$
$$= 729.6^k > F_{AB}(= 359.2^k) - OK$$

The right face of Node B is inadequate to carry the design loads applied to it. The inadequacy is rather small, only about 7%. The assumption that the node height is equal to the neutral axis depth is very conservative. As a beam approaches failure, the neutral axis depth reduces very sharply. The moment on the bent cap due to the applied loads is approximately one-half of the nominal moment capacity. Unless this bent cap is near flexural failure, the neutral axis depth, and therefore the node height, will be much larger than 4.4 in. and hence the node should be adequate to carry the design loads. The neutral axis depth can be approximated using Eq. 5-22 or 5-23.

299

A.2.2.2.3 Strut AB

The strut efficiency is determined using Eqns 5.6.3.3.3-1 and 5.6.3.3.3-2 of AASHTO LRFD Bridge Design Specifications (Eqns A-1 and A-2 below):

$$v = \frac{1}{0.8 + 170\varepsilon_1} \leq 0.85_c \qquad \text{(A-1)}$$

$$\varepsilon_1 = \varepsilon_s + (\varepsilon_s + 0.002)\cot^2 \alpha_s \qquad \text{(A-2)}$$

Where: α_s = the smallest angle between the compressive strut the adjoining tie

ε_s = the tensile strain in the concrete in the direction of the tension tie

v = efficiency factor

AASHTO recommends that the value of ε_s be determined from the stresses in the tie due to the factored loads. However, this determination is difficult. If STM is to be used for design, the strain profile is necessarily nonlinear due to the presence of significant shear strains. The influence of shear makes accurate determinations of strain impracticable. To be consistent with the analysis methods used in Chapter 5, the value of ε_s was set equal to 0.002. Consequently the strut strength is determined as:

$$\begin{aligned}
\varepsilon_1 &= \varepsilon_s + (\varepsilon_s + 0.002)\cot^2 \alpha_s \\
&= 0.002 + (0.002 + 0.002)\cot^2 43.0° \\
&= 0.0066
\end{aligned}$$

$$\begin{aligned}
v &= \frac{1}{0.8 + 170\varepsilon_1} \leq 0.85 \\
&= \frac{1}{0.8 + 170 \cdot 0.0066} \leq 0.85 \\
&= 0.52 \leq 0.85
\end{aligned}$$

The efficiency factor is the same on both ends of the strut. Therefore the strength of the strut need only be determined at the minimum cross-section. For Strut AB, the minimum area occurs at the plane of intersection with Node B. The nominal strength of the strut is:

$$P_n = 0.7 \cdot 0.52 \cdot 3.6ksi \cdot 26in. \cdot 13.1in.$$
$$= 466.3^k > F_{AB}(359.2^k) - OK$$

Section 5.6.3.6 of the AASHTO STM provisions stipulates minimum reinforcement for a strut. Specifically, the ratio of reinforcement area to gross concrete area shall not be less than 0.003 in each direction. This requirement includes both transverse shear reinforcement and horizontal shear reinforcement.

If the transverse reinforcement is spaced at 12 in., the area of steel is:

$$A_s = 0.003 \cdot 12in. \cdot 26in.$$
$$= 0.94in.^2$$

Where: A_s = the area of transverse reinforcement

The area of steel can be obtained by using 4 No. 5 horizontal bars at 12 in. spacing for the horizontal bars of the web reinforcement and 4 legs of No. 5 stirrups spaced at 12 in.

A.2.2.2.4 Sectional Shear Design

The general provisions for determining shear strength using AASHTO LRFD rely on Modified Compression Field Theory. However, for conventionally reinforced beams the traditional value of $2\sqrt{f_c'}b_w d$ (f_c' in psi) can be used to determine the concrete contribution to shear strength as per Section 5.8.3.4.1. The concrete and transverse reinforcement contributions to shear strength are shown in Eqns A-3 and A-4 respectively.

$$V_c = 0.0316\beta\sqrt{f_c'}b_w d \qquad \qquad (A-3)$$

$$V_s = \frac{A_v f_y d \cot \theta}{s} \qquad (A\text{-}4)$$

Where: V_c = concrete contribution to shear strength

β = factor indicating the ability of diagonally cracked concrete to transmit tension. For conventionally reinforced concrete $\beta = 2.0$

f'_c = specified concrete strength in ksi

b_w = width of the web

d = effective depth of the section

V_s = transverse reinforcement contribution to shear strength

A_v = area of shear reinforcement

f_y = yield strength of the transverse reinforcement

θ = angle of inclination of diagonal compressive stresses. For conventionally reinforced concrete $\theta = 45°$

s = spacing of stirrups

For this example, $V_u = 75^k$. As per Eqn A-3, the concrete contribution to shear strength is $0.0316 \cdot 2 \cdot \sqrt{3.6ksi} \cdot 33in. \cdot 30in. = 118.7^k$. The factored concrete contribution to shear strength ($\phi = 0.9$) is greater than the applied shear. The applied shear is greater than one-half the factored concrete contribution to shear strength, therefore minimum stirrups are needed.

When using a sectional model in AASHTO, there are two different minimum shear reinforcement requirements that must be satisfied. The first is in Section 5.8.2.5:

$$A_{v,min} = 0.0316 \sqrt{f'_c} \frac{b_w s}{f_y} \qquad (A\text{-}5)$$

The second minimum shear reinforcement requirement is in Section 5.13.2.3. This requirement is used for deep flexural members. The bent cap in this example falls under the AASHTO definition of such a member. The minimum reinforcement requirement of Section 5.13.2.3 (Eqn A-6) applies to both stirrups and horizontal shear reinforcement.

$$\phi f_y A_v \geq 0.12 b_w s \qquad \text{(A-6)}$$

Where: s = spacing of stirrups and shall not exceed $d/4$ or 12 in.

Eqn. A-6 can be rearranged to determine the maximum reinforcement spacing as follows:

$$s \leq \frac{\phi f_y A_v}{0.12 b_w} \leq \frac{d}{4} \text{ and } 12in. \qquad \text{(A-7)}$$

The shear reinforcement for the portion of the beam design with STM consisted of No. 5 bars, and bars of the same size will be used for the portion of the beams designed using sectional models. However, the maximum spacing must be calculated. The spacing requirements of Eqn A-7 are much more stringent than Eqn A-6; hence Eqn A-7 is evaluated first:

$$s \leq \frac{\phi f_y A_v}{0.12 b_w} \leq \frac{d}{4} \text{ and } 12in.$$
$$\leq \frac{0.9 \cdot 60ksi \cdot 2 \cdot 0.31in.^2}{0.12 \cdot 33in.} \leq \frac{30in.}{4}$$
$$\leq 8.5in. \leq 7.5in.$$

For this section the maximum spacing as 7.5 in. The maximum spacing given by Eqn. A-5 is 9.1 in. The minimum shear reinforcement for the portion of the beam design with sectional models consists of No. 5 stirrups spaced at 7.5 in. and pairs of No. 5 horizontal bars spaced at 7.5 in. near the vertical faces of the member.

A.2.2.2.5 Summary

The cross-sections of the cap beams are shown in Figure A-10. The design using AASHTO LRFD requires a large volume of shear reinforcement (both transverse and longitudinal) so that the design strength is adequate using STM provisions. For the portion of the cap design using the sectional model, the minimum reinforcement requirement dictated that stirrups be spaced at less than $d/4$. The reinforcement required using AASHTO LRFD is much higher than currently used by TxDOT in caps of this size. Typically this cap would have No. 5 stirrups spaced at 12 in. and two No. 5 horizontal bars near each vertical face.

Standard Design:

No. 11 top

2 – No. 5

2 legs of No. 5
closed stirrups at
10 - 12 in.

No. 11 bottom
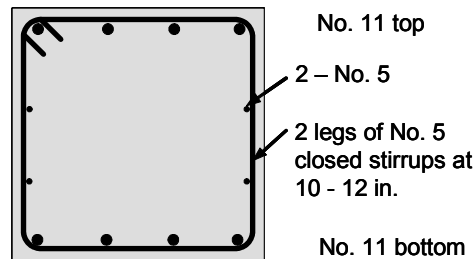
Design Based on AASHTO LRFD:

Section to the Left of the Beam Load:

No. 11 top

4 – No. 5

4 legs of No. 5
closed stirrups at
12 in.

No. 11 bottom
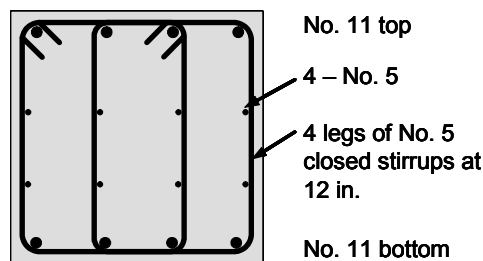
Section to the Right of the Beam load:

No. 11 top

2 – No. 5

2 legs of No. 5
closed stirrups at
7.5 in.

No. 11 bottom
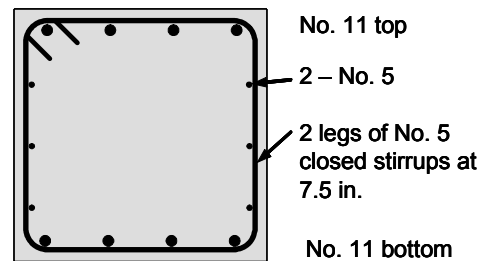
Figure A-10: Cross-sections of bent cap based on standard and AASHTO LRFD

A.2.2.3 Design Based on ACI 318-05 STM Provisions

ACI 318-05 uses different load factors than AASHTO LRFD. For design using he ACI procedures the factored design load is 242 kip as compared to 320 kip for AASHTO. The majority of the discrepancy between these two design loads stems from the impact factor used in AASHTO LRFD. Due to the differences in design loads, the left reaction is 185.3 kip, the right reaction is 56.7 kip, the force in the strut is 271.7 kip, and the force in the tie is 198.7 kip (Figure A-11). These values are determined using the details shown in Figure A-4.
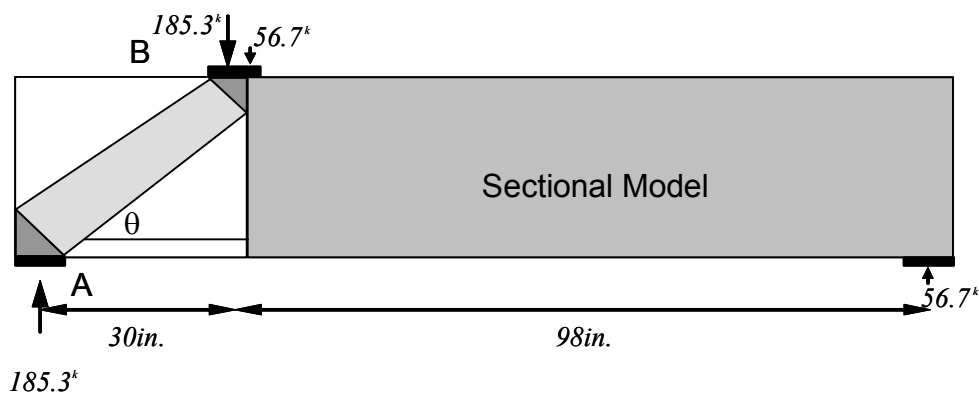
Figure A-11: Loading for bent cap based on the load factors used in ACI 318-05

The same design models are used for the application of ACI STM procedures as were used for the AASHTO procedures. A single strut is used to the left of the load, and sectional models are used to the right.

A.2.2.3.1 Node A

The node geometry used by ACI 318-05 is identical to that used by AASHTO LRFD (Figure A-6). For a CCT node, such as Node A, the allowable stress on any of the faces is $0.75 \cdot 0.85 \cdot 0.80 \cdot f_c'$ using ACI 318-05 Appendix A provisions (including the strength reduction factor).

The allowable forces on the faces of Node A respectively are:

305

Bottom Face:

$$\phi F_{nn} = 0.75 \cdot 0.85 \cdot 0.80 \cdot 3.6\,ksi \cdot 16\,in. \cdot 32\,in.$$
$$= 940.0^k > 185.3^k - OK$$

Left Face:

$$F_{nn} = 0.75 \cdot 0.85 \cdot 0.80 \cdot 3.6\,ksi \cdot 6\,in. \cdot 32\,in.$$
$$= 352.5^k > F_{Tie}(=198.7^k) - OK$$

Inclined Face:

$$F_{nn} = 0.75 \cdot 0.85 \cdot 0.80 \cdot 3.6\,ksi \cdot 15.3\,in. \cdot 32\,in.$$
$$= 899.0^k > F_{AB}(=271.7^k) - OK$$

A.2.2.3.2 Node B

As in Node A, the geometry of Node B is identical to that used by AASHTO (Figure A-8). Node B is a CCC node, and the efficiency factor, as per ACI 318-05, is $0.85 \cdot 1.0 = 0.85$. The allowable forces on the faces of Node B are:

Top Face:

$$\phi F_{nn} = 0.75 \cdot 0.85 \cdot 1.0 \cdot 3.6\,ksi \cdot 14.5\,in. \cdot 26\,in.$$
$$= 865.2^k > 185.3^k - OK$$

Right Face:

$$F_{nn} = 0.75 \cdot 0.85 \cdot 1.0 \cdot 3.6\,ksi \cdot 4.4\,in. \cdot 26\,in.$$
$$= 262.5^k > F_{Tie}(=198.7^k) - OK$$

Inclined Face:

$$F_{nn} = 0.75 \cdot 0.85 \cdot 1.0 \cdot 3.6\,ksi \cdot 13.1\,in. \cdot 26\,in.$$
$$= 781.7^k > F_{AB}(=271.7^k) - OK$$

A.2.2.3.3 Strut AB

Just as with AASHTO STM procedures, the allowable force on Strut AB is determined using the efficiency factor and the minimum cross-sectional area of

the strut. For Strut AB the minimum area occurs at the inclined face of Node B. The strut will be detailed as to satisfy the minimum strut reinforcement requirements. Therefore the higher efficiency factor ($0.75 \cdot 0.85 = 0.64$) can be used. The strength of the strut is:

$$F_{ns} = 0.75 \cdot 0.85 \cdot 0.75 \cdot 3.6\,ksi \cdot 13.1\,in. \cdot 26\,in.$$
$$= 586.3^k > F_{AB}(= 271.7\ ) - OK$$

The strut must meet the requirement of Section A.3.3 to justify the higher efficiency factor. The minimum reinforcement required by A.3.3.1 is:

$$\sum \frac{A_{si}}{bs_i} \sin \alpha_i \geq 0.003 \qquad\qquad \text{(A-8)}$$

Where: A_{si} = area of surface reinforcement in the ith layer crossing

a strut

s_i = spacing of reinforcing bars in the ith layer adjacent to

the surface of the member

b = the width of the strut perpendicular to the plane of the

reinforcing bars

α_i = the angle between the axis of the strut and the bars in

the ith layer of reinforcement crossing that strut

Assuming that No. 5 bars are to be used for the stirrups and skin reinforcement Eqn A-8 yields:

$$\sum \frac{A_{si}}{bs_i} \sin \alpha_i = \frac{0.62in.^2}{33in. \cdot 8.5in.} \sin 43.0° + \frac{0.62in.^2}{33in. \cdot 8.5in.} \sin 47.0°$$
$$= 0.0031 > 0.003 - OK$$

For the portion of the cap designed using STM, No. 5 closed stirrups must be spaced at 8.5 in. or less. Pairs of horizontal No. 5 bars must meet the same spacing limitation.

A.2.2.3.4 Sectional Shear Design

The sectional shear provisions in ACI 31-05 are very similar to those in AASHTO LRFD. The nominal strength is determined as:

$$V_c = 2\sqrt{f_c'}b_w d \qquad\qquad (A\text{-}9)$$

$$V_s = \frac{A_v f_y d}{s} \qquad\qquad (A\text{-}10)$$

The design shear for the right side of the cap is $56.7^k/0.75 = 75.6^k$, and $V_c = 2\cdot\sqrt{3600\,psi}\cdot 33in.\cdot 30in. = 118.8kip$. Since the concrete contribution to shear strength is greater than the applied shear, and the applied shear is greater than half the factored concrete contributions to shear strength, only the minimum amount of shear reinforcement is necessary.

The maximum stirrup spacing is given as $d/2$ in Section 11.5.4.1 of ACI 318-05, and the minimum shear reinforcement requirements are given in 11.5.5.3 as:

$$A_{v,min} = 0.75\sqrt{f_c'}\,\frac{b_w s}{f_y}\text{ but not less than } 50\frac{b_w s}{f_y} \qquad (A\text{-}11)$$

For concrete strength of 3,600 psi, the second portion of Eqn A-11 controls the requirement. If the reinforcement consists of No. 5 close stirrups, the maximum spacing as per Eqn A-11 is 22.5 in. The maximum spacing is therefore limited to 15 in. ($d/2$) by Section 11.5.4.1.

Section 11.8 of ACI 318-05 specifies additional minimum shear reinforcement requirement for use in deep beams. Those requirements stipulate a minimum shear reinforcement ratios of 0.0025 and 0.0015 in the vertical and horizontal directions respectively. Again assuming No. 5 bars:

In the vertical direction:

$$\frac{0.62in.^2}{33in. \cdot s} \geq 0.0025 \rightarrow s \leq 7.5in.$$

In the horizontal direction:

$$\frac{0.62in.^2}{33in. \cdot s} \geq 0.0015 \rightarrow s \leq 12.5in.$$

A.2.2.3.5 Summary

If the spacing of the stirrups is reduced to 7 in. and the spacing of the horizontal shear reinforcement is reduced to 12 in., the requirements of the STM provisions would be satisfied in addition to the deep beams requirements. Therefore a single shear reinforcement layout could be used along the entire length of the beam. The cross-section is shown in Figure A-12.
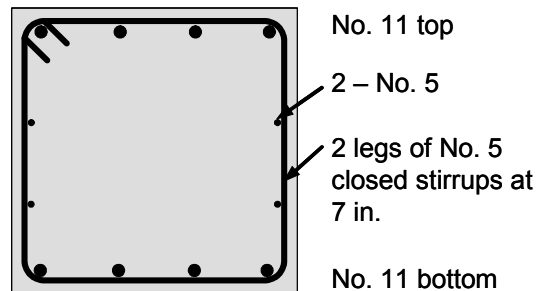
Figure A-12: Cross-section of bent cap based on ACI provisions

A.2.2.4 Design Based on Newly Developed Procedures

This example problem is solved using the newly developed models in two different ways. This first method uses hydrostatic nodes, and the second uses nonhydrostatic nodes. The newly developed models are intended for use with the AASHTO LRFD load and resistance factors rather than the factors from ACI 318-05.

A.2.2.4.1 Design Based on the Newly Developed Provisions with Hydrostatic Nodes

The solution method using hydrostatic nodes is presented first. The equations for efficiency factor described in Chapter 5 were developed using such nodes. Additionally, hydrostatic nodes are simpler and should help facilitate understanding of the application of the new procedures.

A.2.2.4.1.1 Node A – Hydrostatic Conditions

The node geometry used by AASHTO and ACI are identical, but are not hydrostatic. The node geometry for this solution is therefore be different than was what used for the AASHTO and ACI based calculations. Node A is shown in Figure A-13. For the hydrostatic node, the ratio of the height of the node to the width of the node is equal to the ratio of shear span to internal lever arm (jd). The length of the diagonal face of the node is determined using the Pythagorean Theorem rather then components of the length of the bearing or the height of the tie.
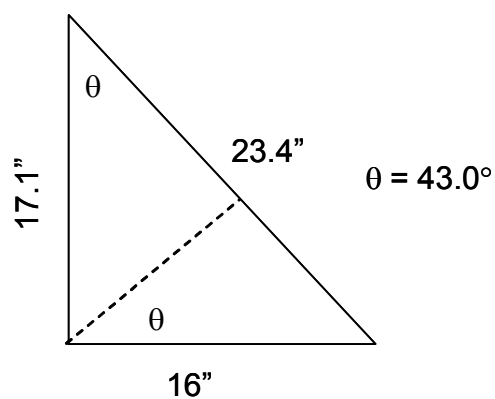
Figure A-13: Hydrostatic geometry of Node A

When using the newly-developed procedure, the efficiency of a node is determined based the abutting strut using Eqn A-12. For shear span-to-depth

ratios less than two (where STM is to be used) failure at the interface between the node and the strut was observed and it is believed that the same efficiency factor should apply to both sides of the node-strut interface. Note that the efficiency factor being calculated for this example assumes a sufficiently reinforced strut.

$$v = \frac{27}{a/_d \sqrt{f'_c}} \leq 0.85 \qquad\qquad (A\text{-}12)$$

Where: a = the shear span

Using the parameter of this example, the efficiency for the node is:

$$v = \frac{27}{30/_{30} \sqrt{3600}}$$
$$= 0.45$$

The above efficiency factor is intended for use on all three faces of the node as shown below:

For the bottom face of the node:

$$\phi P_n = 0.7 \cdot 0.45 \cdot 3.6 ksi \cdot 16 in. \cdot 32 in.$$
$$= 580.6^k > 245^k - OK$$

For the left face of the node:

$$\phi P_n = 0.7 \cdot 0.45 \cdot 3.6 ksi \cdot 17.1 in. \cdot 32 in.$$
$$= 620.5^k > 262.7^k - OK$$

For the inclined face:

$$\phi P_n = 0.7 \cdot 0.45 \cdot 3.6 ksi \cdot 23.4 in. \cdot 32 in.$$
$$= 849.1^k > F_{AB}(= 359.2^k) - OK$$

For a hydrostatic node, the allowable forces are in the same proportion as the applied forces $\left(\dfrac{580.6^k}{245.0^k} = \dfrac{620.5^k}{262.7^k} = \dfrac{849.1^k}{359.2^k} \right)$. All faces of a hydrostatic node are equally critical. If one face has insufficient strength, all faces will have insufficient strength. The inverse is also true.

311

The allowable force on the inclined face of the node is 620.5 kip which is oriented at 43 degrees to the horizontal. The vertical component of the force on the inclined face is

$$620.5 \cdot sin\,43.0° = 580.6^k$$

The vertical component of the allowable force on the inclined face is equal to the allowable force on the bottom face. The same is true for the vertical face of the node. Therefore, if one face of a hydrostatic node has adequate strength, all aces have adequate strength. The converse of the previous statement is also true.

A.2.2.4.1.2 Node B – Hydrostatic Conditions

The geometry of Node B when using hydrostatic geometry is also different than that used for AASHTO and ACI procedures. The node can be seen in Figure A-14.
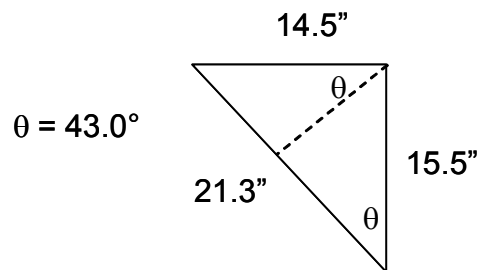
Figure A-14: Hydrostatic geometry of Node B

Based on the calculations shown for Node A, only one face of the node must be checked. For simplicity the top face is used here:

$$\phi P_n = 0.7 \cdot 0.45 \cdot 3.6\,ksi \cdot 14.5in. \cdot 26in.$$
$$= 427.5^k > 245.0^k - OK$$

The same efficiency factor is used to Node B because it is based on Strut AB. The strut is equally efficient at both ends. Since one face of Node B has adequate strength, all faces of Node B are adequate.

312

A.2.2.4.1.3 Strut AB

The strength of Strut AB has already been checked at the faces of the nodes. However, the appropriate reinforcement must be determined. Using the elastic bottle-shaped geometry described in Chapter 5 (Figure A-15), the widest portion of the bottle is equal to one-third of the length of the strut but not less than b_{min}. For struts in which the limit of $b_{ef} \geq b_{min}$ governs, it is assumed that

$$b_{ef} = b_{min} + \frac{\ell}{6} \qquad\qquad (A\text{-}13)$$

Where: l = the length of the strut

b_{min} = the minimum strut width

b_{ef} = the maximum strut width
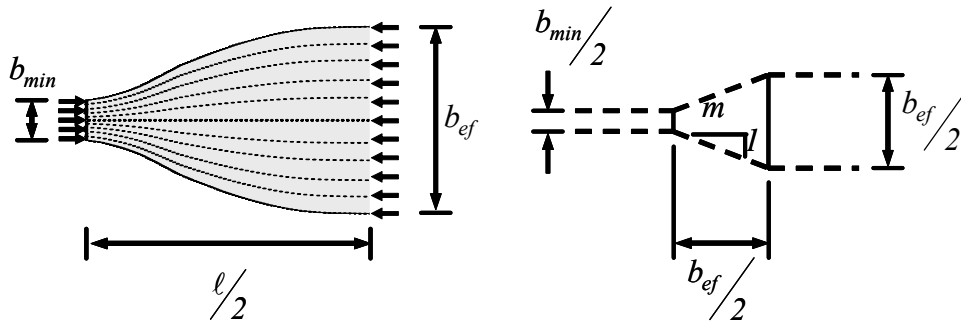
Figure A-15: Dispersion of compression (Left: elastic distribution; Right: equivalent STM) (Schlaich and Weischede 1982)

For this example, the minimum strut area is used to determine the angle of dispersion. At Node B the strut width is 21.3 in. ($a = 21.3in.$). The length of the strut is: $l = \dfrac{d}{\sin\theta} = \dfrac{30in.}{\sin 43.0°} = 44.0in.$ The effective width of the bottle is then $\ell/3$ but not less than a or $b_{ef} = a + \frac{\ell}{6}$. For this example, the second equations governs the width of the strut; which is $b_{ef} = 21.3in. + 44.0in./6 = 28.6in.$ The

slope of the strut in the STM for the bottle-shaped strut is therefore equal to 7.8 ($m = 7.8$). The minimum reinforcement ratio on the cracked plane is:

$$\rho_\perp = \frac{v_R f_c' A_c \sin\theta}{2 f_y bdm} \text{ but not less than } 0.003 \quad \text{(A-14)}$$

$$\rho_\perp = \frac{0.45 \cdot 3.6 ksi \cdot (21.3 in. \times 26 in.) \cdot \sin 43.0°}{2 \cdot 60 ksi \cdot 33 in. \cdot 30 in. \cdot 7.8}$$
$$= 0.0007$$

Where: $\rho_\perp$ = perpendicular reinforcement ratio

$$= \sum \frac{A_{si}}{bs_i} \sin\alpha_i$$

v_R = strut efficiency assuming sufficient reinforcement

A_c = minimum cross-sectional area of the strut

m = slope of the dispersion of compression (Figure A-15)

The calculated minimum reinforcement ratio is lower than the value recommended to control crack widths ($\rho_{\perp,min} = 0.003$). Therefore the value of 0.003 should be used. To satisfy this requirement, No. 5 stirrups spaced at 7 in., and No. 5 longitudinal bars spaced at 12 in. should be used.

A.2.2.4.1.4 Sectional Shear Design

The right-hand portion of the bent cap used in this example lies in the range of reduced shear strength as presented in Chapter 5. Consequently the concrete contribution to shear strength is $1\sqrt{f_c'}b_w d$. The shear strength provided by the concrete is therefore 59.4 kip. The applied shear on the section is 75 kip. The shear reinforcement must be designed for $V_s \geq \frac{V_n}{\phi} - V_c = \frac{75 kip}{0.9} - 59.4 kip = 23.9 kip.$ No. 5 stirrups spaced at 18 in. provide the appropriate strength. However, limitations on maximum spacing and

314

minimum shear reinforcement govern the design. The limits on shear reinforcement from AASHTO LRFD have been adopted in the newly developed model. As such, the reinforcement for the portion of the design using sectional models is No. 5 stirrups and longitudinal bars spaced at 7.5 in. The details of that reinforcement layout were described previously in Section A.2.1.4.

A.2.2.4.1.5 Summary

Using the newly developed models with hydrostatic nodes, the reinforcement required for the bent caps is shown in Figure A-16.
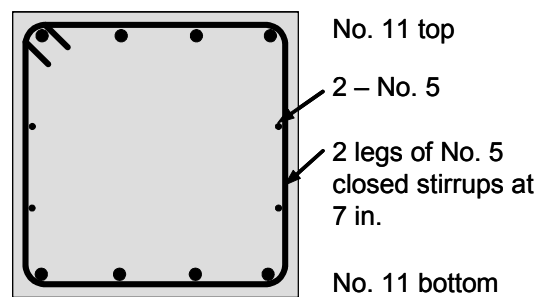
Figure A-16: Cross-section of bent cap using newly developed models with hydrostatic nodes

A.2.2.4.2 *Design Based on the Newly Developed Provisions with Nonhydrostatic Nodes*

Both AASHTO and ACI recommend the use of nonhydrostatic nodes. The newly-developed model can be adapted to nonhydrostatic nodes by using equations presented in Chapter 5. The equations modify the stresses allowed on hydrostatic nodes for used on nonhydrostatic nodes.

In some cases hydrostatic nodes may be impractical. For a beam with a relatively long shear span, and a large bearing area, the use hydrostatic nodes

could prove to be impracticable. The use of nonhydrostatic nodes can lead to better details in such circumstances.

A.2.2.4.2.1 Node A – Nonhydrostatic Conditions

The geometry of Node A using nonhydrostatic conditions is identical to that presented for both AASHTO and ACI as shown in Figure A-6. The allowable efficiencies, and therefore allowable forces, must be altered. For the bottom face of the node, no modification is necessary; the allowable loads are identical for hydrostatic and nonhydrostatic conditions. For the inclined face of the node:

$$k_s = \frac{l_b}{w_s \sin\theta}$$ (A-15)

Where: k_s = the conversion factor for the face of the node associated with a strut

$$k_s = \frac{16in.}{15.3in. \cdot \sin 43.0°}$$
$$= 1.53$$

$$v_{Nonhydrostatic} = k_s v_{Hydrostatic} \leq 0.75 \text{ (For CCT Nodes)} \quad (A-16)$$

Where: $v_{Nonhydrostatic}$ = efficiency factor for use on a nonhydrostatic node

$v_{Hydrostatic}$ = efficiency factor for use on a hydrostatic node

$$v_{Nonhydrostatic} = 1.53 \cdot 0.45$$
$$= 0.69$$

For the left face of the node:

$$k_t = \frac{l_b}{w_t \tan\theta}$$ (A-17)

Where: k_t = the conversion factor for the face of the node associated with a tie

316

$$k_s = \frac{16 in.}{6 in. \cdot \tan 43.0°}$$
$$= 2.86$$

$$v_{Nonhydrostatic} = 2.86 \cdot 0.45$$
$$= 1.29 \le 0.75$$
$$= 0.75$$

Node A is a CCT node, and as such the maximum allowable efficiency factor is 0.75 as per AASHTO LRFD Section 5.6.3.5. The efficiency factor for the left face of the node must be limited to 0.75.

For the left face of the node:

$$\phi P_n = 0.7 \cdot 0.75 \cdot 3.6 ksi \cdot 6 in. \cdot 32 in.$$
$$= 362.9^k > 262.7^k - OK$$

For the inclined face:

$$\phi P_n = 0.7 \cdot 0.69 \cdot 3.6 ksi \cdot 15.3 in. \cdot 32 in.$$
$$= 849.1^k > F_{AB} (= 359.2^k) - OK$$

The modification factor (k_b) for the bottom face is equal to 1.0. Since the bottom face had adequate strength for the hydrostatic conditions, the same is true for the nonhydrostatic conditions.

A.2.2.4.2.2 Node B – Nonhydrostatic Conditions

As with Node A, the geometry of Node B is identical to that used for AASHTO and ACI (Figure A-8). The modification factors for Node B are:

$$k_b = 1.00$$
$$k_s = 1.59$$
$$k_t = 3.53$$

Where: k_b = the conversion factor for the face of the node associated with a bearing

317

Node B is a CCC node and the maximum allowable efficiency is 0.85. The efficiency factor for the inclined faces is $\nu = 1.59 \cdot 0.45 = 0.72$. For the right face the efficiency factor is $\nu = 3.53 \cdot 0.45 = 1.59$; which is greater than the limit. The maximum value (0.85) is used for the right face. The allowable forces on the right and inclined faces are:

For the right face of the node:

$$\phi P_n = 0.7 \cdot 0.85 \cdot 3.6 ksi \cdot 4.4 in. \cdot 26 in.$$
$$= 245.0^k < 262.7^k - NG$$

For the inclined face:

$$\phi P_n = 0.7 \cdot 0.72 \cdot 3.6 ksi \cdot 13.1 in. \cdot 26 in.$$
$$= 618.0^k > F_{AB}(= 359.2^k) - OK$$

The estimated height of Node B (4.4 in.) is extremely conservative. Unless the bent cap is near flexural failure, the node will be much larger than estimated using the depth of the neutral axis. Using the conservative estimate of 4.4 in. for the height of the node showed that the node was only 7% under strength. Therefore the right face of Node B will have adequate strength in the bent cap. The neutral axis depth can be approximated using Eq. 5-22 or 5-23.

A.2.2.4.2.3 Summary

The remainder of the design example using nonhydrostatic nodes is identical to that presented in the previous section regarding hydrostatic nodes. The cross-section is presented in Figure A-16.

A.2.2.5 *Comparison of Designs*

All three design methods (AASHTO, ACI and the newly developed model) indicate that this cap has adequate strength to support the design loads. However, various design procedures recommended differing amounts of shear reinforcement. The reinforcement required by ACI and the newly developed

model are identical. Those two designs require closed stirrups, and horizontal bars near the vertical faces of the member. The stirrup spacing required for both ACI 318-05 and the newly developed procedures is 7 in. The stirrup spacing for the bent cap standard is 10 to 12 in. The longitudinal shear reinforcement is identical for ACI 318, the newly developed procedure, and the standard design.

However, AASHTO requires significantly more reinforcement. The design based on AASHTO STM methods requires stirrups with four legs the stirrups must be spaced at 12 in. Additionally, there must be horizontal bars on the vertical faces of the member as well as along the internal stirrup legs. Currently bent caps use reinforcement layouts that do not include internal stirrup legs. Such an increase in steel to twice the amount currently used seems unwarranted based on the generally good field performance of these structures.

A.2.3 Cap Supporting Type IV Beams

The second example consists of a bent cap that supports two Type IV beams. The beams are spaced 9 ft from center to center, and the columns are spaced at 16 ft 4 in. The beams are not placed symmetrically within the span of the bent cap (Figure A-17).
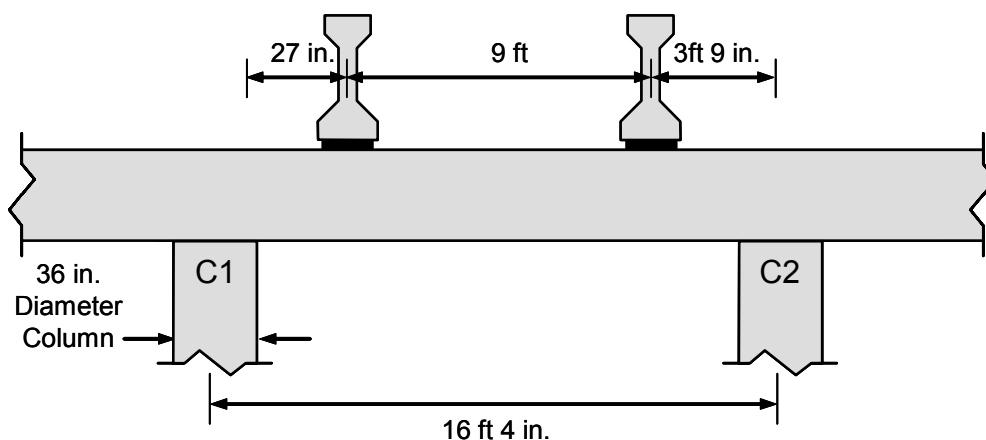
Figure A-17: Bent cap and loading for Example 2

319

When the beam is loaded asymmetrically at multiple points, the truss model is somewhat more complicated. In the case of this example, each of the two loads generates a shear at each end of the beam. The reaction at each end of the cap is the sum of the shears at that location due to the two beam loads. The reaction is not equal to the load applied by the beam nearest the support. If a direct strut were to be used between the load point and the reaction point, that strut would not be in equilibrium in the vertical direction. In order to resolve equilibrium, a more complex truss would need to be developed. The more complex truss would need to distribute the applied loads to both reactions. Rather than develop a complex truss to solve this problem, two simpler trusses can be superimposed. The two trusses are shown in Figure A-18.
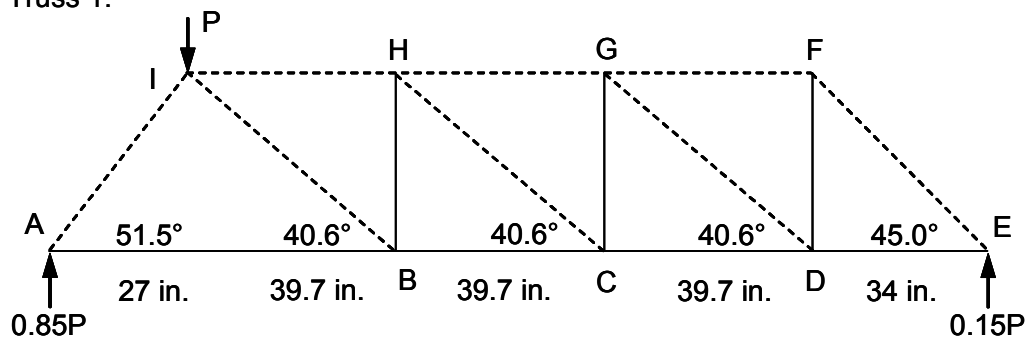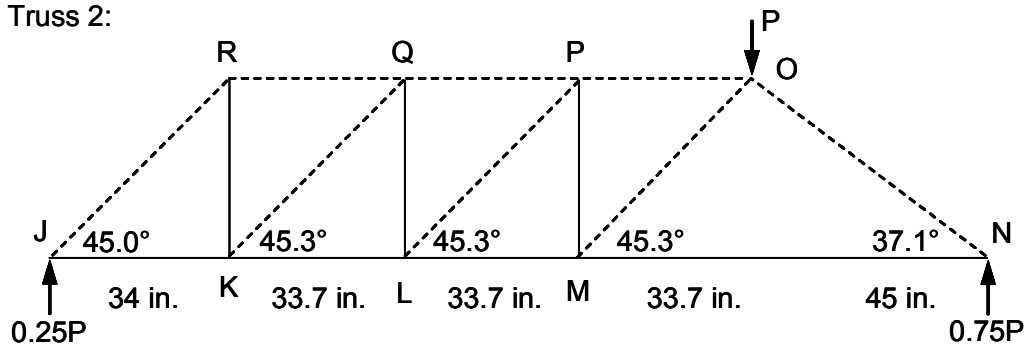
Figure A-18: Truss models for Example 2

The two trusses shown in Figure A-18 were developed as follows: In each case a direct strut connecting the load point and the reaction was used. The remaining portion of the load was handled with a more complex truss. To develop the more complex portion of the truss, a strut acting at 45 degrees was assumed at the reaction that is further from the applied load (at right in Truss 1 and at left in Truss 2). The remaining portion of the beam was then broken into segments of equal length such that the inclined struts were as close to 45 degrees as possible. In both trusses three such segments were used.

Each node uses only half of the available area, and that area is determined as a square that is equivalent to the 36 in. diameter column. Those same assumptions were used for the previous example. The height of the truss was assumed to be equal to jd which was equal to 34 in.

A.2.3.1 Standard Bent Cap Design

The standard bent cap used to support AASHTO Type IV girders is 3 ft 3 in. wide by 3 ft 3 in. deep with an effective depth of 3 ft 0 in. The caps are constructed with concrete that has a specified compressive strength of 3,600 psi.

The longitudinal reinforcement within the cap varies based on the continuity of the cap. However, the longitudinal reinforcement always consists of a single layer of No. 11 bars at the top and bottom of the cross section. The number of bars in the layer varies between four and eight.

The shear reinforcement consists of closed stirrups and longitudinal bars near the vertical faces of the cap. The stirrups are No. 5 bars. For narrow bridges (roadway width equal to 24 ft) the stirrups are spaced at approximately 6 in. For wider bridges, the stirrups are spaced at 10 to 12 in. The tighter stirrup spacing in narrow bridges stems from those caps being supported by only two columns, whereas three columns are used for wider bridges. The skin reinforcement is also

comprised of No. 5 bars. The skin reinforcement is placed such that there are five longitudinal bars along each vertical face of the cap. The spacing between the skin reinforcement and the longitudinal bars is 5 in.

A.2.3.2 Design Based on AASHTO LRFD STM Provisions

Using the load factors associated with AASHTO LRFD, the applied beam loads are 480 kip each. Based on static equilibrium of the trusses the member forces for Truss 1 are:

$$F_{AI} = \frac{408^k}{sin\,51.5°} = 521.3^k$$

$$F_{EF} = \frac{72^k}{sin\,45.0°} = 101.8^k$$

$$F_{DF} = F_{CG} = F_{BH} = 72^k$$

$$F_{DG} = F_{CH} = F_{BI} = \frac{72^k}{sin\,40.6°} = 110.6^k$$

$$F_{GF} = F_{EF}\,cos\,45.0° = 72^k$$

$$F_{GH} = F_{GF} + F_{DG}\,cos\,40.6° = 156.0^k$$

$$F_{HI} = F_{HG} + F_{CH}\,cos\,40.6° = 240.0^k$$

$$F_{DE} = 101.8^k\,cos\,45.0° = 72^k$$

$$F_{CD} = F_{DG}\,cos\,40.6° + F_{DE} = 156.0^k$$

$$F_{BC} = F_{CH}\,cos\,40.6° + F_{CD} = 240.0^k$$

$$F_{AB} = F_{BI}\,cos\,40.6° + F_{BC} = 323.9^k$$

Similarly, the member forces for Truss 2 are:

$$F_{JR} = \frac{120^k}{sin\,45.0°} = 169.7^k$$

$$F_{NO} = \frac{360^k}{sin\,37.1°} = 596.8^k$$

$$F_{KR} = F_{LQ} = F_{MP} = 120^k$$

$$F_{KP} = F_{LP} = F_{MO} = \frac{120^k}{sin\,45.3°} = 168.8^k$$

$$F_{QR} = F_{JR}\,cos\,45.0° = 120^k$$

$$F_{PQ} = F_{QR} + F_{KQ}\,cos\,45.3° = 238.7^k$$

$$F_{NP} = F_{PQ} + F_{LP}\,cos\,45.3° = 357.5^k$$

$$F_{JK} = F_{JR}\,cos\,45.0° = 120^k$$

$$F_{KL} = F_{KQ}\,cos\,45.3° + F_{JK} = 238.7^k$$

$$F_{LM} = F_{LP}\,cos\,45.3° + F_{KL} = 357.4^k$$

$$F_{MN} = F_{NO}\,cos\,45.3° + F_{LM} = 476.1^k$$

A.2.3.2.1 Superposition of Nodes A and J (Node AJ)

Node A from Truss 1 and Node J from Truss 2 are coincident. Therefore those two nodes must be superimposed. The reactions at Nodes A and J can

simply be summed to a single quantity because the forces are collinear. Similarly, the tie forces (F_{AB} and F_{JK}) can be summed. The forces in the struts (F_{AI} and F_{JR}) require a vector sum because they are not collinear. The simplest method to determine the resultant of F_{AI} and F_{JR}, $\overline{F}_L$, is to enforce equilibrium with the reaction force and the tie force as shown in Figure A-19.
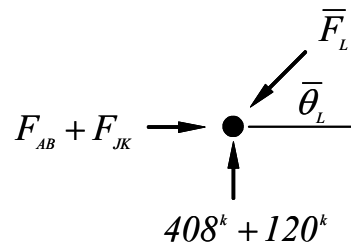
Figure A-19: Superposition of forces at Node AJ

The calculations for the equivalent strut force and angle are shown below:

$$\overline{F}_L = \sqrt{(408^k + 120^k)^2 + (F_{AB} + F_{JK})^2}$$
$$= \sqrt{(408^k + 120^k)^2 + (323.9^k + 120^k)^2}$$
$$= 689.8^k$$

$$\overline{\theta}_L = tan^{-1}\left(\frac{408^k + 120^k}{F_{AB} + F_{JK}}\right)$$
$$= tan^{-1}\left(\frac{408^k + 120^k}{323.9^k + 120^k}\right)$$
$$= 50.0°$$

Using the appropriate angle for the resultant strut abutting Node AJ, the geometry of that node can be determined (Figure A-20). The bottom and left faces of the node are identical to those used for the solution of Example 1. However, the inclined face has changed as shown in the calculations below:

$$w_s = l_b \, \sin\theta + w_t \, \cos\theta$$
$$= 16in. \cdot \sin 50.0° + 6in. \cdot \cos 50.0°$$
$$= 12.3in. + 3.9in. = 16.2in.$$
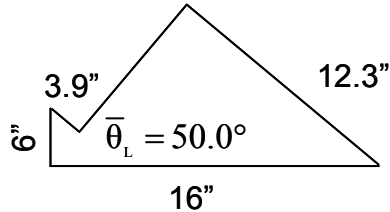
Figure A-20: Elevation of Node AJ

All faces of Node AJ must be checked using AASHTO STM provisions for the allowable stress on a CCT node ($0.75\phi f'_c$). For the bottom face of the node:

$$\phi P_n = 0.7 \cdot 0.75 \cdot 3.6\,ksi \cdot 16in. \cdot 32in.$$
$$= 967.7^k > 528^k - OK$$

For the left face of the node:

$$\phi P_n = 0.7 \cdot 0.75 \cdot 3.6\,ksi \cdot 6in. \cdot 32in.$$
$$= 326.9^k < 443.9^k - NG$$

For the inclined face:

$$\phi P_n = 0.7 \cdot 0.75 \cdot 3.6\,ksi \cdot 16.2in. \cdot 32in.$$
$$= 979.8^k > \overline{F}_L (= 689.8^k) - OK$$

The force acting on the vertical face of the node is greater than the allowable. The node must be increased in size, or the concrete strength must be increased to develop adequate force. The simplest method to increase the allowable force is to use multiple layers of longitudinal reinforcement. The height of the node (6 in.) was based on the location of the longitudinal reinforcement. More layers of longitudinal reinforcement result in a larger node and larger nodes are needed to address the under strength of Node AJ.

A.2.3.2.2 Superposition of Nodes E and N (Node EN)

The superposition of Nodes E and N is performed in the same manner used for Nodes A and J. The equilibrium of the node and the resulting node geometry are shown in Figure A-21.
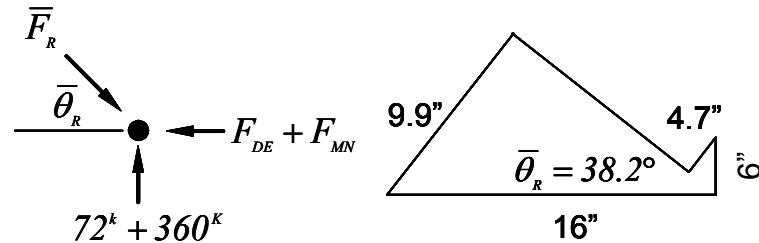
Figure A-21: Details of Node EN

$$\overline{F}_R = \sqrt{\left(72^k + 360^k\right)^2 + \left(F_{DE} + F_{MN}\right)^2}$$
$$= \sqrt{\left(72^k + 360^k\right)^2 + \left(72^k + 476.1^k\right)^2}$$
$$= 697.9^k$$

$$\overline{\theta}_R = tan^{-1}\left(\frac{72^k + 360^k}{F_{DE} + F_{MN}}\right)$$
$$= tan^{-1}\left(\frac{72^k + 360^k}{72^k + 476.1^k}\right)$$
$$= 38.2°$$

The allowable forces on Node EN must be checked just as for Node AJ:

For the bottom face of the node:

$$\phi P_n = 0.7 \cdot 0.75 \cdot 3.6 ksi \cdot 16 in. \cdot 32 in.$$
$$= 967.7^k > 432^k - OK$$

For the right face of the node:

$$\phi P_n = 0.7 \cdot 0.75 \cdot 3.6 ksi \cdot 6 in. \cdot 32 in.$$
$$= 326.9^k < 548.1^k - NG$$

For the inclined face:

$$\phi P_n = 0.7 \cdot 0.75 \cdot 3.6 ksi \cdot 14.6 in. \cdot 32 in.$$
$$= 883.0^k > \overline{F}_R (= 697.9^k) - OK$$

The right face of Node EN has insufficient strength to anchor the resultant tie force. There are two possible solutions. The simplest solution is to use multiple layers of longitudinal reinforcement to increase the height of the node. If the node height was increased to 10 in., there would be adequate strength.

A.2.3.2.3 Nodes I and O

This example consists of a bent cap that supports Type IV beams and the previous example used Type C beams. The Type IV beams are supported on slightly larger bearing pads than the Type C beams (22x26 in. vs. 19x26 in.). The larger bearing area can be used for Nodes I and O. Nodes I and O are not coincident with any other nodes. No superposition is necessary at these locations and the loads applied directly to the nodes can be used for the analysis. Therefore these nodes can be checked using the methods presented in the previous example. Only the portion of the node that abuts the direct strut to the support must be checked just as in Example 1. Such calculations would show that Nodes I and O have adequate strength.

A.2.3.2.4 Resultant Inclined Struts at the Supports

The strength of a resultant struts must be checked at the inclined faces of Nodes AJ and EN. Each strut has a unique efficiency factor based on the AASHTO LRFD STM provisions.

A.2.3.2.4.1 Resultant Strut at the Left Support

Based on Eqns A-1 and A-2, the efficiency factor for the resultant strut at the left support is:

$$\varepsilon_1 = \varepsilon_s + (\varepsilon_s + 0.002)\cot^2 \alpha_s \qquad \text{(A-1)}$$

$$\varepsilon_1 = 0.002 + (0.002 + 0.002)\cot^2 50.0°$$
$$= 0.0048$$

$$v = \frac{1}{0.8 + 170\varepsilon_1} \le 0.85 \qquad \text{(A-2)}$$

$$v = \frac{1}{0.8 + 170 \cdot 0.0048} \le 0.85$$
$$= 0.62 \le 0.85$$

This strut is subject to the same width limitations described in the previous example (two disconnected bearing pads). The strut is limited to 26 in. in width unless interior stirrup legs are provided. The strength of the strut is therefore:

$$\phi P_n = 0.7 \cdot 0.62 \cdot 3.6\,ksi \cdot 16.2in. \cdot 26in.$$
$$= 658.1^k < \overline{F}_L (= 689.8^k) - NG$$

If the strut width were increased to 28 in., the strut would have adequate strength. The bent cap is 39 in. wide, so larger bearing areas would be easy to place on the beam.

The crack control reinforcement as per AASHTO Section 5.6.3.6 necessary for this strut is the same as that calculated for the inclined strut in Example 1. No. 5 stirrups spaced at 12 in. along with No. 5 horizontal bars spaced at 12 in. along the vertical faces of the cap. The stirrups must have four legs, and horizontal bars must also be placed along the internal stirrup legs. This reinforcement comprises four mats of orthogonal reinforcement in the bent cap.

A.2.3.2.4.2 Resultant Strut at the Right Support

The efficiency factor for the strut abutting the right support is 0.45. The strength of the strut is:

$$\phi P_n = 0.7 \cdot 0.45 \cdot 3.6 ksi \cdot 14.6 in. \cdot 26 in.$$
$$= 430.5^k < \overline{F}_L (= 697.9^k) - NG$$

As was the case with the strut abutting the left support, the strut abutting the right support is also insufficient. However, for this strut, even if the full width of the bent cap (39 in.) is used, the strut has insufficient strength as shown in the calculation below:

$$331.1^k \frac{39 in.}{26 in.} = 645.6^k < 697.9^k - NG$$

To gain adequate strength, the area of the inclined face of the node must be increased, or the concrete strength can be increased. If neither of those options is desirable, the depth of the cap can be increased. As the cap depth increases, the angle formed by the strut and the tie increases yielding more efficient, and therefore stronger, struts. The cap design is deficient.

A.2.3.2.5 Sectional Shear Design

The portion of the cap beam between the two applied loads should be designed using sectional models as demonstrated in Example 1. The factored shear force between the beam loads is only 48 kip. The applied shear is less than the concrete contribution to shear strength as calculated in A.2.1.1.4 and the applied shear is greater than one-half of the factored concrete contribution to shear strength. Therefore minimum shear reinforcement requirements and maximum reinforcement spacing limitations control the design for shear reinforcement.

A.2.3.3   Design Based on ACI 318-05 STM Appendix A Provisions

The load factors used by ACI 318 differ from those used by AASHTO LRFD. The factored loads, based on ACI 318-05, are 378.4 kip. The factored forces relevant STM are listed in Table A-2.

328

Table A-2: Loads for use in STM for Example 2

	Loads Based on AASHTO LRFD Load Factors [kip]	Load Based on ACI 318-05 Load Factors [kip]
Beam Load	480.0	378.4
Left Reaction	528.0	416.0
Left Resultant Strut	689.8	543.5
Right Reaction	432.0	340.0
Right Resultant Strut	679.9	535.7

A.2.3.3.1 Node AJ

The geometry of Node AJ for use with ACI 318-05 provisions is the same as that used with AASHTO LRFD (Figure A-20). The node is a CCT node with a maximum efficiency factor of $0.85 \cdot 0.80 = 0.68$. The allowable forces on the node are:

Bottom Face:

$$\phi F_{nn} = 0.75 \cdot 0.85 \cdot 0.80 \cdot 3.6\,ksi \cdot 16in. \cdot 32in.$$
$$= 940.0^k > 416.0^k - OK$$

Left Face:

$$F_{nn} = 0.75 \cdot 0.85 \cdot 0.80 \cdot 3.6\,ksi \cdot 6in. \cdot 32in.$$
$$= 352.5^k > F_{Tie}(= 349.9^k) - OK$$

Inclined Face:

$$F_{nn} = 0.75 \cdot 0.85 \cdot 0.80 \cdot 3.6\,ksi \cdot 16.2in. \cdot 32in.$$
$$= 951.8^k > \overline{F}_L(= 543.5^k) - OK$$

All faces of Node AJ have adequate strength to resist the design forces.

A.2.3.3.2 Node EN

The geometry of Node EN is shown in Figure A-21. Node EN is also a CCT node, and consequently has the same maximum efficiency factor as Node AJ. The allowable forces on the node are:

Bottom Face:

$$\phi F_{nn} = 0.75 \cdot 0.85 \cdot 0.80 \cdot 3.6 ksi \cdot 16 in. \cdot 32 in.$$
$$= 940.0^k > 340.0^k - OK$$

Right Face:

$$F_{nn} = 0.75 \cdot 0.85 \cdot 0.80 \cdot 3.6 ksi \cdot 6 in. \cdot 32 in.$$
$$= 352.5^k > F_{Tie}(= 432.1^k) - NG$$

Inclined Face:

$$F_{nn} = 0.75 \cdot 0.85 \cdot 0.80 \cdot 3.6 ksi \cdot 14.6 in. \cdot 32 in.$$
$$= 857.8^k > \overline{F}_R(= 535.7^k) - OK$$

As with the AASHTO LRFD STM provisions, the ACI 318-05 provisions indicate that Node EN has insufficient strength to anchor the tie. The node strength can be increased by distributing the reinforcement that comprises the tie so that the node is increased in size or the concrete strength can be increased.

A.2.3.3.3 Resultant Inclined Struts at the Supports

The resultant struts that frame into the supports must be checked on the inclined faces of the nodes. For both resultant struts the efficiency factor for use with ACI 318-05 is $0.85 \cdot 0.75 = 0.64$. Sufficient reinforcement will be provided within each strut to warrant this efficiency.

A.2.3.3.3.1 Resultant Strut at the Left Support

The strength of the strut is:

$$F_{ns} = 0.75 \cdot 0.85 \cdot 0.75 \cdot 3.6ksi \cdot 16.2in. \cdot 32in.$$
$$= 892.3^k > \overline{F}_L(= 535.7^k) - OK$$

The reinforcement in the strut must satisfy Eqn. A-8 below:

$$\sum \frac{A_{si}}{bs_i} \sin\alpha_i \geq 0.003 \qquad\qquad (A\text{-}8)$$

For the previous example, the shear reinforcement consisted of No. 5 stirrups spaced and 7 in. and No. 5 horizontal bars spaced at 8 in:

$$\frac{0.62in.^2}{39in. \cdot 7in.} \sin 30.0° + \frac{0.62in.^2}{39in. \cdot 8in.} \sin 50.0° = 0.0027$$

Therefore the same reinforcement (No. 5 stirrups spaced and 7 in. and No. 5 horizontal bars spaced at 6 in) is not sufficient for this example. The spacing between the horizontal shear reinforcing bars must be reduced to 6 in.

$$\frac{0.62in.^2}{39in. \cdot 7in.} \sin 30.0° + \frac{0.62in.^2}{39in. \cdot 6in.} \sin 50.0° = 0.0032$$

A.2.3.3.3.2 Resultant Strut at the Right Support

The strength of the resultant strut at the right support is:

$$F_{ns} = 0.75 \cdot 0.85 \cdot 0.75 \cdot 3.6ksi \cdot 14.6in. \cdot 32in.$$
$$= 670.14^k > \overline{F}_R(= 535.7^k) - OK$$

The reinforcement chosen in for the left strut is also adequate for the right strut:

$$\frac{0.62in.^2}{39in. \cdot 7in.} \sin 51.8° + \frac{0.62in.^2}{39in. \cdot 6in.} \sin 38.2° = 0.0034$$

A.2.3.3.4 Sectional Shear Design

The portion of the bent cap between the two concentrated loads should be designed using sectional methods. The shear between the loads is much less than the one-half of the factored concrete contribution to shear strength. Even though

reinforcement is not required, minimum shear reinforcement is still recommended.

A.2.3.4 Design Based on the Newly Developed Procedures

Just as with Example 1, this example uses the newly developed model along with the load and strength reduction factors from AASHTO LRFD. However, only nonhydrostatic conditions are used for this example. Nonhydrostatic nodes are more practical for design.

A.2.3.4.1 Node AJ

The geometry of Node AJ is identical to that which was used for both AASHTO and ACI based calculations (Figure A-20). The efficiency factor for the node must be calculated. The resultant strut at the left support is at an angle of 50.0 degrees to the longitudinal reinforcement. As such the effective shear span-to-depth ratio is:

$$\left(\frac{a}{d}\right)_{Effective} = \frac{1}{tan\,50.0°} = 0.84$$

The hydrostatic efficiency factor is calculated using Eqn. A-12:

$$v = \frac{27}{a/d\sqrt{f_c'}} \le 0.85 \qquad\qquad (A-12)$$

Where: a = shear span measured from center or reaction to center of load

d = effective depth of the section

$$v = \frac{27}{0.84\sqrt{3600}} \le 0.85$$
$$= 0.53$$

The corresponding conversion factors for the nonhydrostatic nodes are:

$$k_b = 1.0$$

$$k_s = \frac{l_b}{w_s \sin\theta}$$

$$= \frac{16 in.}{16.2 in. \cdot \sin 50.0°}$$

$$= 1.29$$

$$k_t = \frac{l_b}{w_t \tan\theta}$$

$$= \frac{16 in.}{6 in. \cdot \tan 50.0°}$$

$$= 2.24$$

$$vk_b = 0.53 < 0.75$$

$$vk_s = 1.29 \cdot 0.53 = 0.69 < 0.75$$

$$vk_t = 2.24 \cdot 0.53 = 1.19 > 0.75$$

$$= 0.75$$

The conversion factor for the face of the strut anchoring the tie (k_t) is rather large. Using this value of k_t would indicate an excessive efficiency factor. The newly developed model has adopted the limits on nodal efficiency factor from AASHTO LRFD. For a CCT node, that limit is 0.75. Therefore, an efficiency factor of 0.75 is used for the left face of the node. The corresponding allowable forces on the faces of the nodes are:

For the bottom face of the node:

$$\phi P_n = 0.7 \cdot 0.53 \cdot 3.6 ksi \cdot 16 in. \cdot 32 in.$$

$$= 683.8^k > 528^k - OK$$

For the left face of the node:

$$\phi P_n = 0.7 \cdot 0.75 \cdot 3.6 ksi \cdot 6 in. \cdot 32 in.$$

$$= 362.9^k < 443.9^k - NG$$

For the inclined face:

$$\phi P_n = 0.7 \cdot 1.29 \cdot 0.53 \cdot 3.6\,ksi \cdot 16.2in. \cdot 32in.$$
$$= 893.2^k > \overline{F}_L (= 689.8^k) - OK$$

Just as with AASHTO LRFD, the newly developed model indicates that the Node AJ has inadequate strength to anchor the tie force. If the concrete strength were increase to 4,500 psi, Node AJ would have adequate strength:

$$362.9^k \frac{4,500\,psi}{3,600\,psi} = 453.6^k > \overline{F}_L - OK$$

The design value of concrete strength for typical bent caps is 3,600 psi. It is very likely that the actual strength is in excess of this value and is greater than 4,500 psi. The difference between the design value of concrete strength ($f_c' = 3,600\,psi$) and the in situ value is likely enough to increase the strength of Node AJ to acceptable levels.

A.2.3.4.2 Node EN

The hydrostatic efficiency factor for Node EN is 0.35 and the conversion factors are $k_b = 1.0$, $k_s = 1.78$, and $k_t = 3.39$. The corresponding efficiency factors for the bottom, right, and inclined faces or the node are 0.35, 0.75, and 0.62 respectively.

For the bottom face of the node:

$$\phi P_n = 0.7 \cdot 0.35 \cdot 3.6\,ksi \cdot 16in. \cdot 32in.$$
$$= 451.6^k > 432^k - OK$$

For the right face of the node:

$$\phi P_n = 0.7 \cdot 0.75 \cdot 3.6\,ksi \cdot 6in. \cdot 32in.$$
$$= 362.9^k < 548.1^k - NG$$

For the inclined face:

$$\phi P_n = 0.7 \cdot 0.62 \cdot 3.6\,ksi \cdot 14.6\,in. \cdot 32\,in.$$
$$= 730.0^k > \overline{F}_R\,(= 697.9^k\,) - OK$$

The right face of Node EN is inadequate to resist the design forces. In order for the right face of the node to meet strength requirements, the concrete strength would need to be 5,500 psi. Actual field conditions may meet or exceed that strength. If not, multiple layers of longitudinal reinforcement can be used to increase the height of the node. A node height of 9 in. is sufficient to develop adequate strength at Node EN. Additionally, a combination of increased concrete strength and increased node height can be used.

A.2.3.4.3 Resultant Struts

When using the newly developed procedures, the efficiency factor for a node is determined based on the abutting strut. Checking the stresses at the ends of the strut would produce the same results as the calculation of the allowable forces at the nodes. Only the minimum reinforcement on the plane of the expected splitting crack must be checked. The parameters for the minimum reinforcement are shown in

Table A-3. The slope of the dispersion of the compression, m, is determined from Eqn. A-13 and the reinforcement requirement is determined from Eqn. A-14. Note that for both struts, the minimum reinforcement ratio of 0.003, which is intended to address serviceability issues, is much higher than that required for strength based on Eqn A-14.

335

Table A-3: Reinforcement requirements for resultant struts

	Left Resultant Strut	Right Resultant Strut
a [in.]	16.2	14.6
b_{ef} [in]	23.6	18.3
m	6.4	9.9
$\rho_\perp$	0.0009	0.0004

The serviceability reinforcement requirements adopted in the new procedures are identical to those presented in ACI 318-05 Appendix A. Consequently the reinforcement calculated in the previous section for the resultant struts is used for the new procedures. No. 5 stirrups spaced at 7 in. and No. 5 horizontal bars spaced at 12 in. near the vertical faces of the members should be used.

A.2.3.5 Comparison of Designs

The shear reinforcement for the current standard for this bent cap consists of closed stirrups spaced at 10 to 12 in. and longitudinal bars spaced at 5 in. If the cap were designed in accordance with the ACI 318-05 STM provisions, the stirrups would need to be spaced at 7 in. and the longitudinal bars at 6 in. The design based on ACI 318-05 requires a small increase in shear reinforcement over

that which is currently used. It must be noted that the cap designed performed using the ACI 318-05 provisions used a smaller design load than either AASHTO LRFD or the newly developed procedure would require. The design produced using ACI 318-05 calls for more shear reinforcement than is currently used for a load that is less than the design load that is currently used.

The design based on the newly developed procedures requires the same shear reinforcement as the design based on ACI 318 and uses the design loads from AASHTO LRFD. However the newly developed procedure requires that the concrete strength be increased from 3,600 psi to 4,500 psi. These changes are relatively minor, and reflect the performance of these caps in service. In general bent caps designed using the current standard exhibit good performance in the field. However, some caps in the state exhibit signs of damage that is likely due to deficient shear strength.

The cap design based on AASHTO, as was the case for the cap supporting Type C beams, requires significantly more shear reinforcement than the new procedures or the current standard. The design based on AASHTO LRFD requires stirrups with four legs and internal longitudinal shear reinforcement.

A.2.4 Summary of Basic Bent Cap Design Examples

The main difference between the designs produced by the various provisions (ACI 318, AASHTO LRFD, current standard, and the newly developed procedure) was the amount of shear reinforcement required. Both ACI 318-05 and the newly developed procedures requires shear reinforcement very similar to what is currently in use, closed stirrups with horizontal reinforcement along the vertical faces of the members. However, the AASHTO LRFD STM procedure requires the use of additional reinforcement. To satisfy the crack control reinforcement requirement in AASHTO, stirrups with four legs must be

used along with internal layers of longitudinal shear reinforcement. The difference in steel requirements is illustrated by comparing Figure A-10 and Figure A-16.

The commentary in AASHTO LRFD related to the crack control reinforcement requirement states that, "For thicker members multiple grids of reinforcement through the thickness may be required." However, there is no definition given to determine exactly what a "thicker" member is. In a book of example of using AASHTO LRFD STM procedures, Mitchell et al (2004) present a bent cap that is 3 ft wide. In that example multiple grids of reinforcement are used. Since the standard bent caps are not significantly less than 3 ft wide, multiple grids of reinforcement would likely be recommended.

A.3   HAMMERHEAD BENT CAP NO. 1

Plan and elevation drawings of the hammerhead bent cap are shown in Figure A-22. The hatched areas in the plan view represent the bearing seats upon which the beams are set. Each of the three applied load is 1400 kip based on the AASHTO LRFD load factors. The section at the face of the column is shown in Figure A-23. The cap has bundled No. 11 bars for the longitudinal reinforcement, No. 9 bars for the compression reinforcement, and four-legs of No. 7 stirrups. Both AASHTO LRFD STM provisions and the newly developed provisions are used for this example.

The load applied at the center of the cap induces no shear in the cap. Therefore, it is not considered in the truss model. Additionally, the area of the column is greater than the sum of the three bearing areas beneath the beams, so the nodal zone at the top of the column is not critical. With all of these items eliminated from the design process, the only remaining elements are the nodes beneath the exterior concentrated loads (Nodes A) and the abutting struts. The

equilibrium and geometry of Node A are shown in Figure A-24. As with the previous examples, the inclined strut is assumed to act at a quarter-point of the column width.
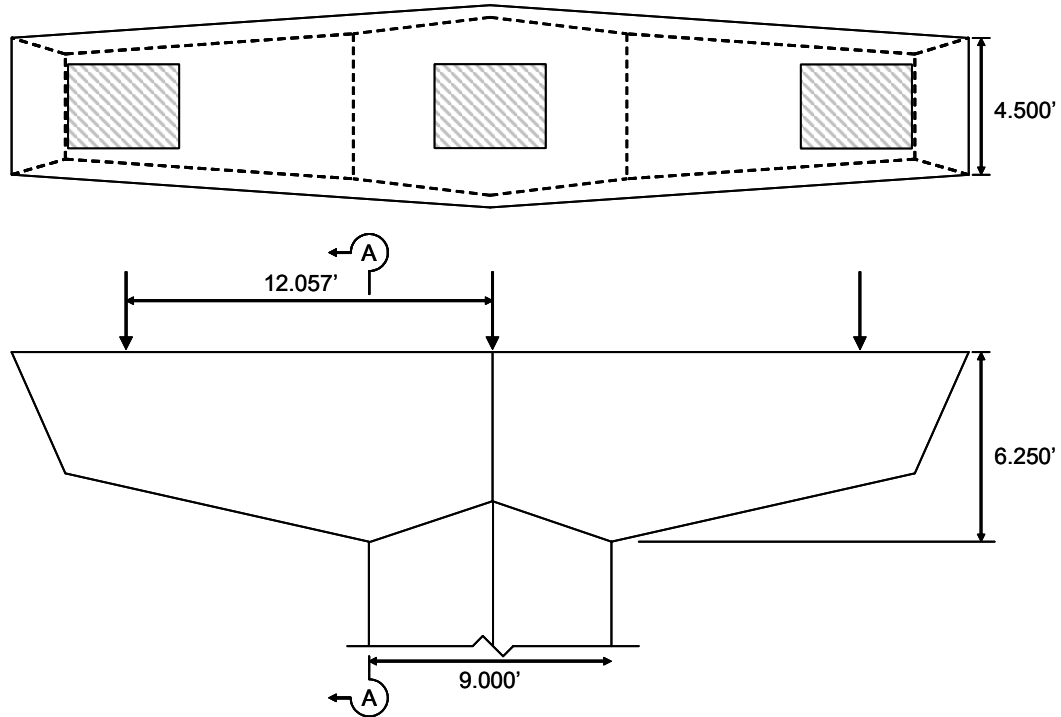
Figure A-22: Hammerhead Bent Cap for Example 3 (Bearing areas are 23 in. x 36 in.)
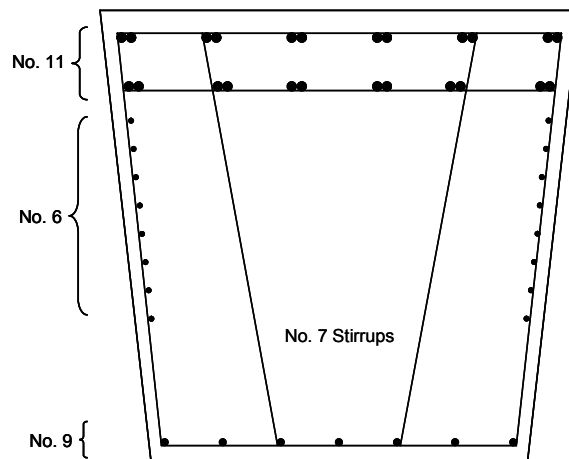
Figure A-23: Section A-A of hammerhead bent cap

$P_u = 1400^k$

$F_T = 2454^k$

$l_b = 36.0in.$
$F_s = 2826^k$
$w_t = 14.0in.$
$w_s = 36.0in. \cdot \sin 29.7° + 14.0in. \cdot \cos 29.7°$
$ = 30.0in.$
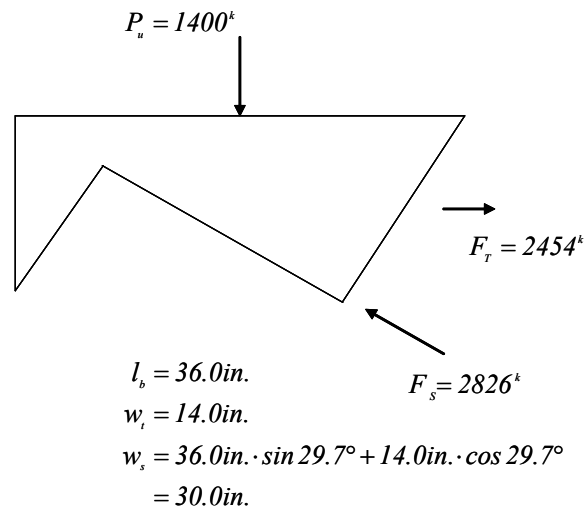
Figure A-24: Details of Node A
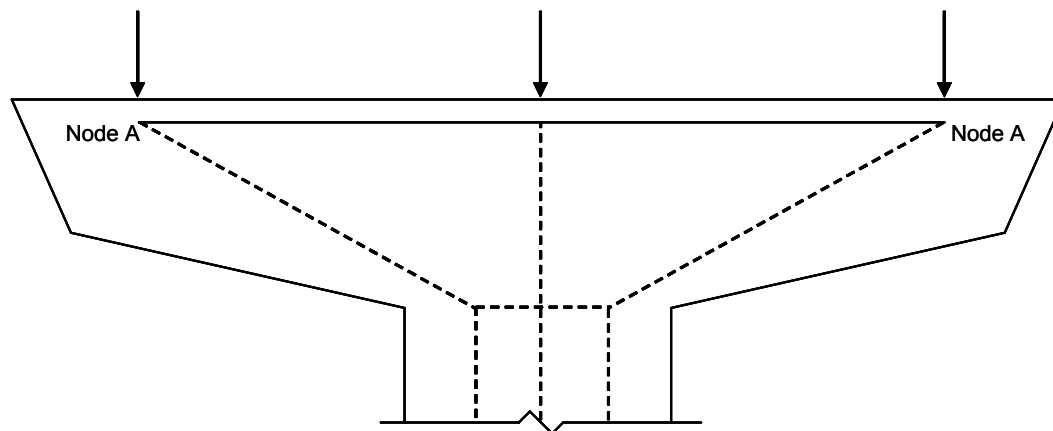
Node A   Node A

Figure A-25: STM used for hammerhead bent cap no. 1

A.3.1   Design Based on AASHTO LRFD STM Provisions

The forces on the faces of the nodes and the end of the strut must be checked. Crack control reinforcement must then be provided.

340

A.3.1.1 Node A

Node A is a CCT node with an efficiency factor of 0.75 as per AASHTO LRFD. The allowable forces on Node A are:

Top Face:

$$\phi P_n = 0.7 \cdot 0.75 \cdot 3.6 ksi \cdot 23 in. \cdot 36 in.$$
$$= 1565^k > P_u (= 1400^k) - OK$$

Left Face:

$$\phi P_n = 0.7 \cdot 0.75 \cdot 3.6 ksi \cdot 23 in. \cdot 14 in.$$
$$= 609^k < F_T (= 2454^k) - NG$$

Inclined Face:

$$\phi P_n = 0.7 \cdot 0.75 \cdot 3.6 ksi \cdot 23 in. \cdot 30 in.$$
$$= 1304^k < F_S (= 2826^k) - NG$$

Two of the node faces have insufficient strength. In order to gain adequate strength on the left face of the node, the node height must be increased to 59 in. The member depth at the left face of the node is only 48 in. Consequently, increased concrete strength, bigger bearing area, or both must be used.

A.3.1.2 Inclined Strut

The available width within the cap is 80 in. Assuming a strain in the direction of the tie, ε_s, is equal to 0.002, the efficiency factor for the strut is:

$$v = \frac{1}{0.8 + 170 \cdot (\varepsilon_s + (\varepsilon_s + 0.002) cot^2 \alpha_s)} \leq 0.85$$
$$= \frac{1}{0.8 + 170 \cdot (0.002 + (0.002 + 0.002) cot^2 29.7°)}$$
$$= 0.31$$

The allowable force in the strut is:

$$\phi P_n = 0.7 \cdot 0.31 \cdot 3.6ksi \cdot 80in. \cdot 30in.$$
$$= 1875^k < F_S(= 2826^k) - NG$$

The strut also has insufficient strength based on the provisions of AASHTO LRFD STM. This strut has only 66% of the required capacity. The cross-section shown in Figure A-23 has reinforcement ratios of 0.0013 and 0.0067 in the horizontal and vertical directions respectively. AASHTO STM requires a reinforcement ratio of at least 0.003 in each direction. Additional horizontal bars are required to satisfy the crack control requirements. However, even if the full width of the cap is used for the strut width, the strut has insufficient strength.

If this bent cap were designed based on AASHTO LRFD STM, major design changes would be required. These changes would be much larger in scope than the increased reinforcement required for the previous examples.

A.3.2 Design Based on Newly Developed Procedures

As with the previous examples, the geometry of the node, in elevation, is the same with the newly developed models as it was with the AASHTO procedures. However, based on the results of the wide beam tests discussed in Chapter 7, the full width of the bent cap is used rather than the area directly beneath the bearing pads. In the wide beam tests the bearing areas were limited to a portion of the width of the beam. The ratio of loaded width to full width is similar for the tests specimens and the bent cap in this example. Based on these assumptions, the area of the top face of the node used for this example is 36x54 in.

A.3.2.1 Node A

The efficiency factors for the node are calculated using Eqns. A-12, A-15, and A-17 as shown below:

342

$$v = \frac{27}{a/d \sqrt{f_c'}} \le 0.85 \qquad\qquad\qquad \text{(A-12)}$$

$$v = \frac{27}{\dfrac{12.057\,ft - \dfrac{9.0\,ft}{4}}{0.9 \cdot 6.25\,ft} \sqrt{3600}} = 0.26$$

$$k_s = \frac{l_b}{w_s \sin\theta} \qquad\qquad\qquad \text{(A-15)}$$

$$k_s = \frac{36\,in.}{30\,in. \cdot \sin 29.7°} = 2.42$$

$$v_s = k_s v \le 0.75$$
$$\qquad = 2.42 \cdot 0.26$$
$$\qquad = .63$$

$$k_t = \frac{l_b}{w_t \tan\theta} \qquad\qquad\qquad \text{(A-17)}$$

$$k_t = \frac{36\,in.}{14\,in. \cdot \tan 29.7°} = 4.51$$

$$v_t = k_t v \le 0.75$$
$$\qquad = 4.51 \cdot 0.26 = 1.17$$
$$\qquad = 0.75$$

The maximum efficiency factor for Node A is 0.75 because it is a CCT node. The allowable forces on the node faces are:

Top Face:

$$\phi P_n = 0.7 \cdot 0.26 \cdot 3.6\,ksi \cdot 54\,in. \cdot 36\,in.$$
$$\qquad = 1274^k < P_u (=1400^k) - NG$$

Left Face:

$$\phi P_n = 0.7 \cdot 0.75 \cdot 3.6\,ksi \cdot 54\,in. \cdot 14\,in.$$
$$\qquad = 1429^k < F_T (=2454^k) - NG$$

Inclined Face:

$$\phi P_n = 0.7 \cdot 0.63 \cdot 3.6\,ksi \cdot 54in. \cdot 30in.$$
$$= 2572^k < F_S (= 2826^k) - NG$$

All three faces of the node do not have the required strength. If the concrete strength is increased to 4,500 psi, the top and inclined faces of the node have adequate strength. The calculations are shown below. In the following calculations the updated values for strength are based on the values calculated above. The values from above are modified by the ratios that indicate the changes brought about by increasing the concrete strength. The first ratio accounts for the decrease in efficiency due to increased concrete strength. In the equation for efficiency factor (Eqn. A-12) the square root of the concrete strength is used. The second ratio accounts directly for the increase in concrete strength.

Top Face:

$$\phi P_n = 1274^k \cdot \frac{\sqrt{3,600\,psi}}{\sqrt{4,500\,psi}} \cdot \frac{4,500\,psi}{3,600\,psi}$$
$$= 1424^k > P_u (= 1400^k) - OK$$

Inclined Face:

$$\phi P_n = 2572^k \cdot \frac{\sqrt{3,600\,psi}}{\sqrt{4,500\,psi}} \cdot \frac{4,500\,psi}{3,600\,psi}$$
$$= 2875^k > F_S (= 2826^k) - OK$$

This increase in concrete strength is not adequate to increase the left face of the node to acceptable levels.

Left Face:

$$\phi P_n = 1429 \cdot \frac{\sqrt{3,600\,psi}}{\sqrt{4,500\,psi}} \cdot \frac{4,500\,psi}{3,600\,psi}$$
$$= 1598^k < F_T (= 2454^k) - NG$$

344

The height of the node must be increased to gain sufficient strength. If the node height is increased to 22 in. the node will have adequate strength on all three sides:

$$\phi P_n = 1598^k \cdot \frac{22in.}{14in.}$$
$$= 2511^k > F_T (= 2454^k) - OK$$

The neutral axis depth approaches one-half of the effective depth as the applied moment approaches zero. Node A is near the tip of a cantilevered beam, and the moment at that point is very nearly zero. Therefore increasing the node height to 22 in. ($d/2 = 24in.$) is a practicable method for eliminating the deficiency.

A.3.2.2 Inclined Strut

The strength of the inclined strut has already been checked at the inclined face of Node A. Only the minimum reinforcement must be determined based on the elastic bottle shape shown in Figure A-15 and Eqn A-14:

$$b_{min} = 30in.$$
$$l = \frac{d}{\sin\theta} = \frac{67.5in.}{\sin 29.7°} = 136.3in.$$
$$b_{ef} = \frac{l}{3} = \frac{136.3in.}{3} = 45.4in. \text{ but not less than } b_{min}$$

$$m = \frac{b_{ef}/2}{b_{ef}/4 - b_{min}/4} = \frac{45.4in./2}{45.4in./4 - 30in./4} = 5.9$$

$$\rho_\perp = \frac{v_R f_c' A_c \sin\theta}{2 f_y bdm} \text{ but not less than } 0.003 \quad \text{(A-14)}$$

345

$$\rho_\perp = \frac{v_R f'_c A_c \sin\theta}{2 f_y bdm}$$

$$= \frac{0.63 \cdot 4500\,psi \cdot (54in. \times 36in.) \cdot \sin 29.7°}{2 \cdot 60000\,psi \cdot 54in. \cdot 67.5in. \cdot 5.9} = 0.0011$$

Equation A-14 yields a perpendicular reinforcement ratio that is less than that required to address serviceability concerns. The minimum perpendicular reinforcement ratio ($\rho_\perp$) is therefore 0.003. The cross-section shown in Figure A-23 indicates the following shear reinforcement: four-legged No. 7 stirrups spaced at 7 in. and horizontal bars (No. 6) spaced at 5 in. along the vertical faces of the member. The perpendicular reinforcement ratio for that reinforcement is:

$$\frac{4 \cdot 0.6in.^2}{54in. \cdot 5in.} \sin 60.3° + \frac{2 \cdot 0.44in.^2}{54in. \cdot 7in.} \sin 29.7° = 0.0089$$

Therefore the cross-section shown in Figure A-23 contains nearly three times the web reinforcement required for the newly developed procedures.

A.3.3   Summary of Hammerhead Bent Cap Example

When using the STM procedures presented in AASHTO LRFD, this bent cap appeared to be grossly undersized and in need of drastic design changes. Based on the newly developed models, only small changes are necessary and some of the web reinforcement could be removed. However the newly developed model used a node area that was rather generous based on test data. If such generous area was used for the node in the AASHTO-based calculations, less drastic changes would be required when applying the AASHTO procedures.

A.4   HAMMERHEAD BENT CAP NO. 2

The second hammerhead cap example is shown in Figure A-26 and the critical cross-section is shown in Figure A-27. For this bent cap, the center load is applied directly over the column and the right load is within the effective depth of

the column face. Neither of these two loads generates the critical design case for shear. The load applied on the left side of the cap creates the greatest shear force on the cap. The shear force on the right side of the column would be less than on the left side. The loads applied to the right side partially rest directly above the column. The design example focuses on the left load. As can be seen in Figure A-26 the shear span-to-depth ratio is 2.2. Therefore sectional models should be used.
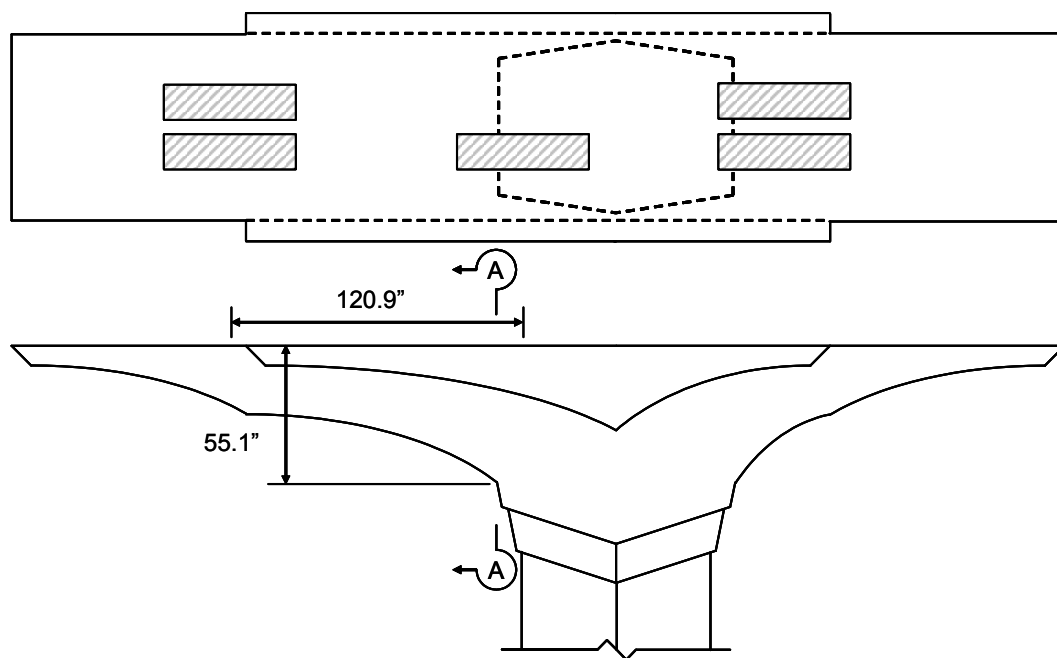
Figure A-26: Plan and elevation views of hammerhead bent cap
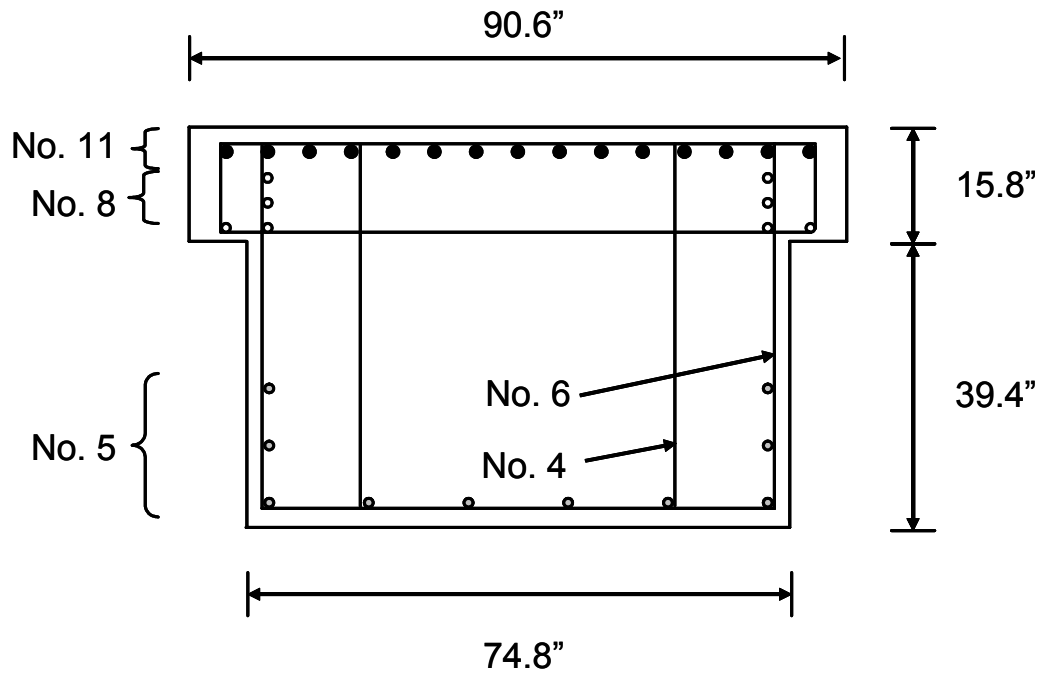
Figure A-27: Cross-section A-A of Hammerhead Cap

A.4.1 Sectional Design Using the Newly Developed Procedures

Based on the AASHTO LRFD load factors, the design load applied on the left portion of the bent cap is 629 kip. This cap has a concentrated load applied between 2d and 6d from the face of the support. The concrete contribution to shear strength is therefore reduced to $V_c = 1\sqrt{f'_c}b_w d$ as per the recommendations presented in Chapter 6. The proper shear reinforcement is determined as follows:

$$V_c = 1\sqrt{f'_c}b_w d \tag{A-18}$$

$$= \sqrt{3,600\,psi} \cdot 74.8in. \cdot 49.5in.$$

$$= 222^{k}$$

$$V_{s} = V_{u} - V_{c}$$

$$= 629^{k} - 222^{k}$$

$$= 407^{k}$$

$$V_{s} = \frac{A_{v}f_{y}d}{s} \rightarrow s \leq \frac{A_{v}f_{y}d}{V_{s}}$$

$$s = \frac{1.28in.^{2} \cdot 60ksi \cdot 74.8in.}{629^{k}}$$

$$= 9.0in.$$

Based only on strength considerations, the stirrup spacing must be less than 9.0 in. However, there are additional limits within AASHTO LRFD for maximum spacing and minimum shear reinforcement. Recall that the detailing requirements presented in AASHTO LRFD have been adopted for use in the newly developed model. The first of these limits is given in Section 5.8.2.5:

$$A_{v} = 0.0316\sqrt{f_{c}'}\frac{b_{w}s}{f_{y}} \qquad \text{(A-5)}$$

$$= 0.0316\sqrt{3.6ksi}\frac{74.8in. \cdot 9.0in.}{60ksi}$$

$$= 0.67in.^{2}$$

The shear reinforcement in the member satisfies the above requirement. The second shear reinforcement requirement is given in Section 5.7.3.4 of AASHTO LRFD:

$$A_{sk} \geq 0.012(d - 30) \leq \frac{A_{s}}{4} \qquad \text{(A-19)}$$

Where: A_{sk} = area of skin reinforcement $\left[\dfrac{in.^{2}}{ft}\right]$

349

$$A_{sk} \geq 0.012(d - 30) \leq \frac{A_s}{4}$$

$$\geq 0.012(49.5in. - 30in.) = 0.234$$

$$\frac{A_s}{4} = \frac{25.06in.^2}{4} = 6.27in.^2$$

$$\therefore A_{sk} = 0.23\frac{in.^2}{ft}$$

In additional the requirements of Eq A-19, the horizontal web reinforcement must be spaced at less than $d/6$. For this example, the maximum spacing is 8.25 in. To satisfy the requirements of Section 5.7.3.4 the horizontal web reinforcement should consist of 7 pairs of No. 4 bars distributed along the vertical faces of the member.

A.4.2 Summary

For this example, the concrete contribution was reduced according to the conclusions of Chapter 6. Even with such reductions, the minimum shear reinforcement governed the design. The results of the design example would therefore be identical if the shear provisions of AASHTO LRFD or the newly developed procedures were used. The current design is adequate to carry the design loads based on the newly developed provisions.

APPENDIX B

Database of Shear Tests

Table B-1: Test specimens included in the shear database

Reference	b [in.]	d [in.]	f'_c [psi]	f_y [ksi]	ρ [%]	ρ_v [%]	Used For STM Database	Conservative Using ACI 318-05 STM Provisions	Conservative Using AASHTO LRFD STM Provisions
	5.0	8.0	8823	60	3.9	0.00	No	-	-
	5.0	8.0	8823	60	3.9	0.00	No	-	-
	5.0	8.0	8823	60	3.9	0.00	No	-	-
	5.0	8.0	8823	60	3.9	0.00	No	-	-
	5.0	8.0	8823	60	3.9	0.00	Yes	Yes	Yes
	5.0	8.0	8823	60	3.9	0.00	Yes	Yes	Yes
	5.0	8.2	8823	60	1.8	0.00	No	-	-
	5.0	8.2	8823	60	1.8	0.00	No	-	-
	5.0	8.2	8823	60	1.8	0.00	No	-	-
	5.0	8.2	8823	60	1.8	0.00	No	-	-
	5.0	8.2	8823	60	1.8	0.00	Yes	No	No
	5.0	8.2	8823	60	1.8	0.00	Yes	No	No
	5.0	8.4	8823	60	0.4	0.00	No	-	-
	5.0	8.4	8823	60	0.4	0.00	No	-	-
	5.0	8.4	8823	60	0.4	0.00	No	-	-
	5.0	8.4	8823	60	0.4	0.00	No	-	-
	5.0	8.4	8823	60	0.4	0.00	Yes	No	No
	5.0	8.4	8823	60	0.4	0.00	Yes	No	No
	5.0	7.9	9715	60	5.0	0.00	No	-	-
	5.0	7.9	9715	60	5.0	0.00	No	-	-
	5.0	7.9	9715	60	5.0	0.00	No	-	-
Ahmad & Lue (1987)	5.0	7.9	9715	60	5.0	0.00	No	-	-
	5.0	7.9	9715	60	5.0	0.00	Yes	No	Yes
	5.0	7.9	9715	60	5.0	0.00	Yes	No	No
	5.0	8.2	9715	60	2.3	0.00	No	-	-
	5.0	8.2	9715	60	2.3	0.00	No	-	-
	5.0	8.2	9715	60	2.3	0.00	No	-	-
	5.0	8.2	9715	60	2.3	0.00	No	-	-
	5.0	8.2	9715	60	2.3	0.00	Yes	No	Yes
	5.0	8.2	9715	60	2.3	0.00	Yes	No	No
	5.0	8.4	9715	60	0.5	0.00	No	-	-
	5.0	8.4	9715	60	0.5	0.00	No	-	-
	5.0	8.4	9715	60	0.5	0.00	No	-	-
	5.0	8.4	9715	60	0.5	0.00	No	-	-
	5.0	8.4	9715	60	0.5	0.00	Yes	No	No
	5.0	8.4	9715	60	0.5	0.00	Yes	No	No
	5.0	7.3	9329	60	6.6	0.00	No	-	-
	5.0	7.3	9329	60	6.6	0.00	No	-	-
	5.0	7.3	9329	60	6.6	0.00	No	-	-
	5.0	7.3	9329	60	6.6	0.00	No	-	-
	5.0	7.3	9329	60	6.6	0.00	Yes	Yes	Yes
	5.0	7.3	9329	60	6.6	0.00	Yes	No	No
	5.0	8.1	9329	60	3.3	0.00	No	-	-
	5.0	8.1	9329	60	3.3	0.00	No	-	-

Reference	b [in.]	d [in.]	f'_c [psi]	f_y [ksi]	ρ [%]	ρ_v [%]	Used For STM Database	Conservative Using ACI 318-05 STM Provisions	Conservative Using AASHTO LRFD STM Provisions
Ahmad & Lue (1987)	5.0	8.1	9329	60	3.3	0.00	No	-	-
	5.0	8.1	9329	60	3.3	0.00	No	-	-
	5.0	8.1	9329	60	3.3	0.00	Yes	No	Yes
	5.0	8.1	9329	60	3.3	0.00	Yes	No	No
	5.0	8.3	9329	60	0.5	0.00	No	-	-
	5.0	8.3	9329	60	0.5	0.00	No	-	-
	5.0	8.3	9329	60	0.5	0.00	No	-	-
	5.0	8.3	9329	60	0.5	0.00	No	-	-
	5.0	8.3	9329	60	0.5	0.00	Yes	No	No
	5.0	8.3	9329	60	0.5	0.00	Yes	No	No
Angelakos et al (2001)	11.8	36.4	3046	73	1.0	0.00	No	-	-
	11.8	36.4	4641	73	1.0	0.00	No	-	-
	11.8	36.4	5511	73	1.0	0.00	No	-	-
	11.8	36.4	9427	73	1.0	0.00	No	-	-
	11.8	36.4	11603	73	1.0	0.00	No	-	-
	11.8	36.4	4641	73	2.1	0.00	No	-	-
	11.8	36.4	4641	73	0.5	0.00	No	-	-
	11.8	36.4	4641	73	0.5	0.08	No	-	-
	11.8	36.4	3046	73	1.0	0.08	No	-	-
	11.8	36.4	5511	73	1.0	0.08	No	-	-
	11.8	36.4	9427	73	1.0	0.08	No	-	-
	11.8	36.4	11603	73	1.0	0.08	No	-	-
	11.8	36.4	5221	73	1.0	0.00	No	-	-
	11.8	36.4	14214	73	1.0	0.00	No	-	-
	11.8	36.4	14214	73	1.0	0.00	No	-	-
	11.8	36.4	5656	73	1.0	0.00	No	-	-
	11.8	36.4	5656	73	1.0	0.00	No	-	-
	11.8	36.4	5366	73	0.8	0.00	No	-	-
	11.8	36.4	14359	73	0.8	0.00	No	-	-
	11.8	36.4	13634	73	0.5	0.00	No	-	-
	11.8	36.4	6817	73	0.8	0.08	No	-	-
Bazant & Kazemi (1991)	1.5	0.8	6790	115	1.7	0.00	No	-	-
	1.5	0.8	6790	115	1.7	0.00	No	-	-
	1.5	0.8	6790	115	1.7	0.00	No	-	-
	1.5	1.6	6790	115	1.7	0.00	No	-	-
	1.5	1.6	6790	115	1.7	0.00	No	-	-
	1.5	1.6	6790	115	1.7	0.00	No	-	-
	1.5	3.2	6790	115	1.7	0.00	No	-	-
	1.5	3.2	6790	115	1.7	0.00	No	-	-
	1.5	3.2	6790	115	1.7	0.00	No	-	-
	1.5	6.4	6790	115	1.7	0.00	No	-	-
	1.5	6.4	6790	115	1.7	0.00	No	-	-
	1.5	6.4	6790	115	1.7	0.00	No	-	-
	1.5	0.8	6700	115	1.6	0.00	No	-	-
	1.5	0.8	6700	115	1.6	0.00	No	-	-
	1.5	0.8	6700	115	1.6	0.00	No	-	-
	1.5	1.6	6700	115	1.6	0.00	No	-	-
	1.5	1.6	6700	115	1.6	0.00	No	-	-
	1.5	1.6	6700	115	1.6	0.00	No	-	-
	1.5	3.3	6700	115	1.6	0.00	No	-	-
	1.5	3.3	6700	115	1.6	0.00	No	-	-
	1.5	3.3	6700	115	1.6	0.00	No	-	-
	1.5	6.5	6700	115	1.6	0.00	No	-	-

Reference	b [in.]	d [in.]	f'_c [psi]	f_y [ksi]	ρ [%]	ρ_v [%]	Used For STM Database	Conservative Using ACI 318-05 STM Provisions	Conservative Using AASHTO LRFD STM Provisions
Bazant & Kazemi (1991)	1.5	6.5	6700	115	1.6	0.00	No	-	-
	1.5	6.5	6700	115	1.6	0.00	No	-	-
	1.5	13.0	6700	115	1.6	0.00	No	-	-
	1.5	13.0	6700	115	1.6	0.00	No	-	-
	1.5	13.0	6700	115	1.6	0.00	No	-	-
Bresler & Scordelis (1963)	12.2	18.2	3270	47	1.8	0.00	No	-	-
	12.0	18.4	3440	47	2.3	0.00	No	-	-
	12.1	18.2	5450	47	2.7	0.00	No	-	-
	12.1	18.4	3490	47	1.8	0.10	No	-	-
	12.0	18.3	3520	47	2.3	0.10	No	-	-
	12.1	18.4	5080	47	2.7	0.10	No	-	-
	9.1	18.2	3590	47	2.4	0.13	No	-	-
	9.0	18.3	3360	47	2.4	0.13	No	-	-
	9.0	18.1	5620	47	3.1	0.13	No	-	-
	6.1	18.3	4290	47	1.8	0.20	No	-	-
	6.0	18.3	3450	47	3.7	0.20	No	-	-
	6.1	18.1	5080	47	3.6	0.20	No	-	-
ao (2001)	11.8	74.3	3980	65	1.5	0.00	No	-	-
	11.8	74.3	3980	65	1.5	0.07	No	-	-
	11.8	74.3	4360	65	0.4	0.00	No	-	-
	11.8	74.3	4460	65	0.4	0.07	No	-	-
Chang & Kesler (1956)	4.0	5.4	4000	48	2.9	0.00	No	-	-
	4.0	5.4	4000	48	1.9	0.00	No	-	-
	4.0	5.4	4000	48	2.4	0.00	No	-	-
	4.0	5.4	4000	48	2.4	0.00	No	-	-
	4.0	5.4	2560	48	1.9	0.00	No	-	-
	4.0	5.4	2560	48	1.9	0.00	No	-	-
	4.0	5.4	2560	48	2.4	0.00	No	-	-
	4.0	5.4	2560	48	2.9	0.00	No	-	-
	4.0	5.4	2160	48	2.4	0.00	No	-	-
	4.0	5.4	2160	48	2.4	0.00	Yes	No	Yes
	4.0	5.4	2160	48	1.9	0.00	No	-	-
	4.0	5.4	2160	48	1.9	0.00	No	-	-
	4.0	5.4	2160	48	2.9	0.00	No	-	-
	4.0	5.4	5600	48	1.9	0.00	No	-	-
	4.0	5.4	5600	48	1.9	0.00	No	-	-
	4.0	5.4	4620	48	1.9	0.00	No	-	-
	4.0	5.4	4600	48	1.9	0.00	No	-	-
	4.0	5.4	4670	48	1.9	0.00	No	-	-
	4.0	5.4	4670	48	1.9	0.00	No	-	-
	4.0	5.4	4670	48	2.9	0.00	No	-	-
	4.0	5.4	4670	48	2.9	0.00	No	-	-
	4.0	5.4	4520	48	2.9	0.00	No	-	-
	4.0	5.4	4520	48	2.9	0.00	No	-	-
	4.0	5.4	4650	48	2.9	0.00	No	-	-
	4.0	5.4	4650	48	2.9	0.00	No	-	-
Clark (1951)	8.0	16.0	3575	47	3.1	0.38	No	-	-
	8.0	16.0	3430	47	3.1	0.38	No	-	-
	8.0	16.0	3395	47	3.1	0.38	No	-	-
	8.0	16.0	3590	47	3.1	0.38	No	-	-
	8.0	16.0	3388	47	3.1	0.37	Yes	Yes	Yes
	8.0	16.0	3680	47	3.1	0.37	Yes	Yes	Yes
	8.0	16.0	3435	47	3.1	0.37	Yes	Yes	Yes
	8.0	16.0	3380	47	3.1	0.37	Yes	Yes	Yes

Reference	b [in.]	d [in.]	f'_c [psi]	f_y [ksi]	ρ [%]	ρ_v [%]	Used For STM Database	Conservative Using ACI 318-05 STM Provisions	Conservative Using AASHTO LRFD STM Provisions
	8.0	16.0	3570	47	3.1	0.37	Yes	Yes	Yes
	8.0	16.0	3370	47	3.1	0.73	Yes	Yes	Yes
	8.0	16.0	3820	47	3.1	0.73	Yes	Yes	Yes
	8.0	16.0	3615	47	3.1	0.73	Yes	Yes	Yes
	8.0	16.0	6110	47	3.1	0.37	Yes	Yes	Yes
	8.0	16.0	3720	47	2.1	0.34	Yes	Yes	Yes
	8.0	16.0	3820	47	2.1	0.34	Yes	Yes	Yes
	8.0	16.0	3475	47	2.1	0.34	Yes	Yes	Yes
	8.0	16.0	4210	47	2.1	0.34	Yes	Yes	Yes
	8.0	16.0	3430	47	2.1	0.69	Yes	Yes	Yes
	8.0	16.0	3625	47	2.1	0.69	Yes	Yes	Yes
	8.0	16.0	3500	47	2.1	0.69	Yes	Yes	Yes
	8.0	16.0	3910	47	2.1	0.69	Yes	Yes	Yes
	8.0	16.0	2040	47	2.1	0.34	Yes	Yes	Yes
	8.0	16.0	2000	47	2.1	0.34	Yes	Yes	Yes
	8.0	16.0	2020	47	2.1	0.34	Yes	Yes	Yes
	8.0	16.0	3550	47	3.1	0.34	Yes	Yes	Yes
	8.0	16.0	6560	47	3.1	0.34	Yes	Yes	Yes
	8.0	16.0	6480	47	3.1	0.34	Yes	Yes	Yes
	8.0	16.0	6900	47	3.1	0.34	Yes	No	Yes
	8.0	16.0	3800	49	1.6	0.46	Yes	Yes	Yes
	8.0	16.0	3790	49	1.6	0.46	Yes	Yes	Yes
	8.0	16.0	3560	49	1.6	0.46	Yes	Yes	Yes
	8.0	16.0	3480	49	1.6	0.61	Yes	Yes	Yes
	8.0	16.0	3755	49	1.6	0.61	Yes	Yes	Yes
	8.0	16.0	3595	49	1.6	0.61	Yes	Yes	Yes
	8.0	16.0	3500	49	1.6	0.61	Yes	Yes	Yes
Clark (1951)	8.0	16.0	4090	49	2.4	0.92	Yes	Yes	Yes
	8.0	16.0	3350	49	1.6	1.22	Yes	Yes	Yes
	6.0	13.0	4010	47	3.4	0.46	Yes	Yes	Yes
	6.0	13.0	4060	47	3.4	0.46	Yes	Yes	Yes
	6.0	13.0	4030	47	3.4	0.46	Yes	Yes	Yes
	6.0	13.0	4375	47	3.4	0.73	Yes	Yes	Yes
	6.0	13.0	4280	47	3.4	0.61	No	-	-
	6.0	13.0	4120	47	3.4	0.61	No	-	-
	6.0	13.0	3790	47	3.4	0.61	No	-	-
	6.0	13.0	3970	47	3.4	0.49	No	-	-
	6.0	13.0	3720	47	3.4	0.49	No	-	-
	6.0	13.0	3200	47	3.4	0.49	No	-	-
	6.0	13.0	4020	47	3.4	0.37	No	-	-
	6.0	13.0	4210	47	3.4	0.37	No	-	-
	6.0	13.0	3930	47	3.4	0.37	No	-	-
	8.0	16.0	3120	54	1.0	0.00	No	-	-
	8.0	16.0	3770	54	1.0	0.00	No	-	-
	8.0	16.0	3435	54	1.0	0.00	No	-	-
	8.0	16.0	3420	54	1.0	0.00	Yes	No	Yes
	8.0	16.0	3468	54	1.0	0.00	Yes	No	Yes
	8.0	16.0	3410	54	1.0	0.00	Yes	No	Yes
	8.0	16.0	3580	54	1.0	0.00	Yes	Yes	Yes
	8.0	16.0	3405	54	1.0	0.00	Yes	Yes	Yes
	8.0	16.0	3420	54	1.0	0.00	Yes	Yes	Yes
	8.0	16.0	3750	54	1.0	0.00	Yes	Yes	Yes
	8.0	16.0	3800	54	1.0	0.00	Yes	Yes	Yes
	8.0	16.0	3765	54	1.0	0.00	Yes	Yes	Yes

Reference	b [in.]	d [in.]	f'_c [psi]	f_y [ksi]	ρ [%]	ρ_v [%]	Used For STM Database	Conservative Using ACI 318-05 STM Provisions	Conservative Using AASHTO LRFD STM Provisions
de Paiva & Siess (1965)	2.0	12.0	3560	46	0.8	0.00	Yes	Yes	Yes
	2.0	12.0	3420	51	0.5	0.00	Yes	Yes	No
	2.0	12.0	5600	46	0.8	0.00	Yes	Yes	No
	2.0	12.0	5240	51	0.5	0.00	Yes	No	No
	3.0	8.0	3380	47	1.7	0.00	Yes	Yes	Yes
	3.0	8.0	2890	47	1.7	1.09	Yes	Yes	Yes
	3.0	8.0	3050	45	0.8	0.00	Yes	No	No
	3.0	8.0	2890	45	2.6	0.00	Yes	Yes	Yes
	3.0	8.0	2910	44	2.6	1.09	Yes	Yes	Yes
	3.0	8.0	5100	47	1.7	0.00	Yes	Yes	Yes
	3.0	8.0	4960	47	0.8	0.00	Yes	No	No
	4.0	6.0	3510	44	1.7	0.00	Yes	Yes	Yes
	4.0	6.0	5360	48	1.7	0.00	Yes	No	Yes
	2.0	12.0	4920	46	0.8	1.42	Yes	Yes	No
	2.0	12.0	4600	45	1.3	1.42	Yes	Yes	Yes
	3.0	8.0	3530	47	0.8	0.94	Yes	No	No
	3.0	8.0	4980	47	1.7	1.31	Yes	Yes	Yes
	4.0	6.0	4970	47	0.8	0.70	Yes	No	No
	4.0	6.0	5030	49	1.7	0.98	Yes	No	Yes
DeCossio & Siess (1960)	6.0	9.9	3050	44	3.4	0.00	No	-	-
	6.0	9.9	3120	45	3.4	0.00	No	-	-
	6.0	9.9	3120	45	3.4	0.00	No	-	-
	6.0	10.0	4570	68	1.0	0.00	No	-	-
	6.0	9.9	3740	52	1.0	0.00	No	-	-
	6.0	9.9	4470	43	1.0	0.00	No	-	-
	6.0	9.9	4440	46	0.3	0.00	No	-	-
Ferguson & Rajagopalan (1968)	6.0	10.4	3440	95	1.7	0.00	No	-	-
	6.1	10.2	5300	95	1.4	0.00	No	-	-
	6.1	10.4	4800	95	1.0	0.00	No	-	-
	6.0	10.5	4200	76	0.8	0.00	No	-	-
	6.0	10.6	4800	73	0.6	0.00	No	-	-
	6.0	10.3	4050	258	0.5	0.00	No	-	-
	6.0	10.3	3640	258	0.5	0.00	No	-	-
	5.9	10.5	4500	258	0.3	0.00	No	-	-
	6.0	10.6	4150	258	0.3	0.00	No	-	-
	6.0	10.6	4300	258	0.3	0.00	No	-	-
Ferguson (1956)	4.0	7.4	4250	40	2.2	0.00	No	-	-
	4.1	7.2	3480	40	2.2	0.00	Yes	No	No
	3.8	7.1	3750	40	2.2	0.00	Yes	No	Yes
	4.0	7.3	3950	40	2.2	0.00	Yes	No	Yes
Foster & Gilbert (1998)	4.9	47.2	13198	62	1.3	0.60	Yes	Yes	Yes
	4.9	47.2	13924	62	1.3	0.60	Yes	Yes	Yes
	4.9	47.2	11603	62	1.3	0.60	Yes	Yes	Yes
	4.9	47.2	11603	62	1.3	0.60	Yes	Yes	Yes
	4.9	27.6	12038	62	2.2	0.60	Yes	Yes	Yes
	4.9	27.6	17404	62	2.2	0.60	Yes	Yes	Yes
	4.9	27.6	11313	62	2.2	0.60	Yes	Yes	Yes
	4.9	27.6	12473	62	2.2	0.60	Yes	No	No
	4.9	27.6	12908	62	2.2	0.00	Yes	Yes	Yes
	4.9	27.6	13489	62	2.2	0.90	Yes	Yes	Yes
	4.9	27.6	15084	62	2.2	0.60	Yes	Yes	Yes
	4.9	27.6	11603	62	2.2	0.60	Yes	Yes	Yes
	4.9	27.6	17404	62	2.2	0.60	Yes	Yes	Yes
	4.9	27.6	11168	62	2.2	0.60	Yes	Yes	Yes

Reference	b [in.]	d [in.]	f'_c [psi]	f_y [ksi]	ρ [%]	ρ_v [%]	Used For STM Database	Conservative Using ACI 318-05 STM Provisions	Conservative Using AASHTO LRFD STM Provisions
Foster & Gilbert (1998)	4.9	27.6	12763	62	2.2	0.60	Yes	Yes	Yes
	4.9	27.6	12908	62	2.2	0.00	Yes	Yes	Yes
Hsuing & Frantz (1985)	6.0	16.5	6235	41	1.8	0.22	No	-	-
	12.0	16.5	6235	44	1.8	0.21	No	-	-
	18.0	16.5	6235	41	1.8	0.22	No	-	-
	18.0	16.5	6235	41	1.8	0.22	No	-	-
Johnson & Ramirez (1989)	12.0	21.2	5280	70	0.2	0.16	No	-	-
	12.0	21.2	5280	70	0.2	0.08	No	-	-
	12.0	21.2	10490	70	0.2	0.08	No	-	-
	12.0	21.2	10490	70	0.2	0.08	No	-	-
	12.0	21.2	8100	70	0.2	0.16	No	-	-
	12.0	21.2	8100	70	0.2	0.00	No	-	-
	12.0	21.2	7440	70	0.2	0.08	No	-	-
	12.0	21.2	7440	70	0.2	0.08	No	-	-
Kani et al (1979)	6.0	10.6	2630	58	0.5	0.00	Yes	No	No
	6.0	10.7	2620	57	0.5	0.00	No	-	-
	6.0	10.6	3000	58	0.5	0.00	No	-	-
	6.0	10.8	2910	57	0.5	0.00	No	-	-
	6.1	10.8	2620	57	0.5	0.00	Yes	No	No
	6.0	10.7	2910	57	0.5	0.00	Yes	No	Yes
	6.0	10.8	4000	58	0.5	0.00	No	-	-
	6.0	11.1	4000	58	0.5	0.00	No	-	-
	6.0	10.9	4060	55	0.5	0.00	Yes	No	No
	6.0	10.8	4060	55	0.5	0.00	Yes	No	No
	6.1	10.9	3800	57	0.5	0.00	Yes	No	No
	6.0	10.7	5280	57	0.5	0.00	Yes	No	No
	6.0	10.9	5020	58	0.5	0.00	No	-	-
	6.0	10.6	5000	58	0.5	0.00	Yes	No	No
	6.0	10.4	4690	58	0.5	0.00	No	-	-
	6.0	10.6	5000	58	0.5	0.00	No	-	-
	5.9	10.6	2800	55	0.8	0.00	No	-	-
	6.2	10.9	2800	55	0.8	0.00	Yes	No	Yes
	6.1	10.8	2560	62	0.7	0.00	No	-	-
	6.1	10.6	2560	62	0.8	0.00	No	-	-
	6.0	10.8	2350	62	0.7	0.00	Yes	No	Yes
	6.1	10.7	2350	59	0.7	0.00	Yes	No	No
	6.0	11.3	2440	61	0.7	0.00	No	-	-
	6.0	10.8	2880	55	0.8	0.00	Yes	No	No
	6.0	10.7	2610	55	0.8	0.00	No	-	-
	6.0	10.8	2610	55	0.8	0.00	No	-	-
	6.1	10.7	2800	55	0.8	0.00	No	-	-
	5.9	10.6	2850	56	0.8	0.00	No	-	-
	6.0	10.7	2850	56	0.8	0.00	No	-	-
	6.0	10.6	3670	61	0.8	0.00	No	-	-
	6.1	10.8	4270	61	0.7	0.00	No	-	-
	6.1	10.6	3670	61	0.8	0.00	No	-	-
	6.0	10.7	3800	56	0.8	0.00	No	-	-
	6.1	10.5	4170	61	0.8	0.00	No	-	-
	6.1	10.5	3850	61	0.8	0.00	No	-	-
	6.1	10.6	3630	61	0.8	0.00	Yes	No	No
	6.0	10.7	3630	66	0.8	0.00	Yes	No	No
	6.3	10.6	3980	59	0.8	0.00	No	-	-
	6.1	10.7	3920	53	0.8	0.00	No	-	-
	6.0	10.8	3920	53	0.8	0.00	No	-	-

Reference	b [in.]	d [in.]	f'_c [psi]	f_y [ksi]	ρ [%]	ρ_v [%]	Used For STM Database	Conservative Using ACI 318-05 STM Provisions	Conservative Using AASHTO LRFD STM Provisions
	6.0	10.8	3700	71	0.8	0.00	Yes	No	No
	6.0	10.6	3700	71	0.8	0.00	No	-	-
	6.0	10.7	3800	56	0.8	0.00	No	-	-
	6.0	10.7	3830	56	0.8	0.00	No	-	-
	6.0	10.8	3830	56	0.8	0.00	No	-	-
	6.0	10.7	4980	55	0.8	0.00	Yes	No	No
	6.1	10.5	4980	55	0.8	0.00	No	-	-
	6.1	10.7	5130	55	0.8	0.00	No	-	-
	6.0	10.7	5130	55	0.8	0.00	No	-	-
	6.2	10.7	4900	60	0.7	0.00	No	-	-
	6.0	10.9	4920	60	0.7	0.00	No	-	-
	6.0	10.7	5130	55	0.8	0.00	No	-	-
	6.1	10.8	5130	55	0.8	0.00	No	-	-
	6.1	10.8	5280	55	0.8	0.00	Yes	No	No
	6.1	11.0	5010	60	0.7	0.00	No	-	-
	6.0	10.8	5280	55	0.8	0.00	Yes	No	No
	6.1	11.2	4920	57	0.7	0.00	No	-	-
	6.0	10.7	2950	48	1.8	0.00	No	-	-
	5.9	10.9	2880	50	1.8	0.00	No	-	-
	6.1	10.7	2230	50	1.8	0.00	No	-	-
	6.1	10.7	2230	50	1.8	0.00	No	-	-
	6.1	10.7	2360	50	1.8	0.00	No	-	-
	6.1	10.7	2280	50	1.8	0.00	Yes	Yes	Yes
	6.1	10.7	2280	50	1.8	0.00	No	-	-
	6.1	10.8	2550	50	1.8	0.00	Yes	Yes	Yes
	6.0	10.9	2610	50	1.8	0.00	No	-	-
Kani et al (1979)	6.0	10.8	2630	58	1.9	0.00	No	-	-
	6.1	10.7	2680	61	1.8	0.00	No	-	-
	6.1	10.8	2880	74	1.8	0.00	No	-	-
	6.1	10.8	2530	61	1.8	0.00	Yes	No	Yes
	5.9	10.8	2530	60	1.9	0.00	Yes	Yes	Yes
	6.0	10.7	3900	57	1.9	0.00	Yes	Yes	Yes
	6.0	10.7	4040	57	1.9	0.00	Yes	Yes	Yes
	6.0	10.7	3560	57	1.9	0.00	Yes	Yes	Yes
	6.0	10.7	3930	57	1.9	0.00	Yes	No	Yes
	6.0	10.7	4320	57	1.9	0.00	No	-	-
	6.0	10.7	4230	57	1.9	0.00	No	-	-
	6.0	10.7	3560	51	1.9	0.00	No	-	-
	6.0	10.7	3650	51	1.9	0.00	No	-	-
	6.0	10.7	3480	51	1.9	0.00	No	-	-
	6.0	10.7	3530	51	1.9	0.00	No	-	-
	6.0	10.7	4000	51	1.9	0.00	No	-	-
	6.0	10.7	4000	51	1.9	0.00	No	-	-
	6.1	10.6	3780	71	1.8	0.00	No	-	-
	6.0	10.8	3780	71	1.8	0.00	No	-	-
	6.1	10.7	4920	57	1.8	0.00	Yes	No	No
	6.1	10.6	4920	56	1.8	0.00	No	-	-
	6.1	10.6	5140	57	1.8	0.00	Yes	No	No
	6.1	10.7	5090	57	1.8	0.00	Yes	No	Yes
	6.1	10.7	5090	57	1.8	0.00	No	-	-
	6.1	10.7	4720	56	1.8	0.00	No	-	-
	6.0	10.9	4800	56	1.8	0.00	Yes	No	Yes
	6.1	10.8	4930	72	1.8	0.00	No	-	-
	6.1	10.7	5190	20	1.8	0.00	No	-	-

Reference	b [in.]	d [in.]	f'_c [psi]	f_y [ksi]	ρ [%]	ρ_v [%]	Used For STM Database	Conservative Using ACI 318-05 STM Provisions	Conservative Using AASHTO LRFD STM Provisions
Kani et al (1979)	6.0	10.9	5020	51	1.8	0.00	No	-	-
	6.1	10.9	5020	51	1.8	0.00	No	-	-
	6.0	10.8	5020	51	1.8	0.00	No	-	-
	6.1	10.6	5250	55	1.8	0.00	No	-	-
	5.9	10.8	5220	55	1.8	0.00	No	-	-
	6.0	10.8	5220	60	1.8	0.00	Yes	No	Yes
	6.0	10.8	3990	50	2.8	0.00	No	-	-
	6.1	10.7	3990	50	2.8	0.00	No	-	-
	6.1	10.7	3980	50	2.7	0.00	No	-	-
	6.0	10.7	3980	50	2.8	0.00	No	-	-
	6.1	10.8	3700	55	2.8	0.00	Yes	Yes	Yes
	6.1	10.6	3950	53	2.7	0.00	Yes	Yes	Yes
	6.0	10.5	4560	58	2.8	0.00	Yes	Yes	Yes
	6.1	10.6	3980	53	2.7	0.00	No	-	-
	6.0	10.6	3980	54	2.7	0.00	No	-	-
	6.1	10.7	4390	54	2.7	0.00	No	-	-
	6.0	10.8	3670	51	2.8	0.00	Yes	Yes	Yes
	6.0	10.8	3670	49	2.8	0.00	No	-	-
	6.0	10.8	3670	49	2.8	0.00	No	-	-
	6.0	10.9	3950	53	2.7	0.00	No	-	-
	6.0	10.8	3800	53	2.7	0.00	No	-	-
	6.0	10.7	3800	53	2.7	0.00	No	-	-
	6.0	10.6	3950	53	2.7	0.00	No	-	-
	6.1	10.8	5100	55	2.7	0.00	Yes	No	No
	6.1	10.7	4920	55	2.7	0.00	No	-	-
	6.0	10.6	5040	54	2.8	0.00	Yes	Yes	Yes
	6.0	10.8	5040	54	2.7	0.00	Yes	Yes	Yes
	6.0	10.8	5100	55	2.7	0.00	Yes	No	Yes
	6.0	10.6	5100	55	2.7	0.00	No	-	-
	6.0	10.8	5010	54	2.7	0.00	No	-	-
	6.2	10.8	5180	55	2.7	0.00	No	-	-
	6.0	10.7	5180	55	2.8	0.00	No	-	-
	6.1	10.7	5100	55	2.7	0.00	No	-	-
	6.0	10.6	5100	55	2.7	0.00	No	-	-
	6.1	10.8	5100	55	2.7	0.00	No	-	-
	6.1	10.9	5320	55	2.7	0.00	No	-	-
	6.0	10.7	5220	60	2.7	0.00	No	-	-
	6.1	10.8	5220	60	2.7	0.00	No	-	-
	6.0	10.8	5280	54	2.7	0.00	No	-	-
	6.0	5.5	3830	56	2.6	0.00	No	-	-
	6.0	5.6	3950	55	2.6	0.00	No	-	-
	6.0	5.4	4060	57	2.7	0.00	No	-	-
	6.0	5.4	4060	57	2.7	0.00	No	-	-
	6.0	5.2	3700	57	2.8	0.00	No	-	-
	6.0	5.4	3700	57	2.8	0.00	Yes	No	Yes
	6.0	5.2	3590	57	2.9	0.00	No	-	-
	6.0	5.3	3590	57	2.8	0.00	No	-	-
	6.0	5.5	3600	57	2.7	0.00	No	-	-
	6.0	5.2	3870	57	2.8	0.00	Yes	No	No
	6.0	5.4	3870	57	2.8	0.00	Yes	No	No
	5.9	5.3	3640	57	2.9	0.00	No	-	-
	6.0	5.4	3950	58	2.7	0.00	No	-	-
	6.0	5.5	3830	54	2.6	0.00	No	-	-
	6.0	5.5	2950	60	2.7	0.00	No	-	-

Reference	b [in.]	d [in.]	f'_c [psi]	f_y [ksi]	ρ [%]	ρ_v [%]	Used For STM Database	Conservative Using ACI 318-05 STM Provisions	Conservative Using AASHTO LRFD STM Provisions
Kani et al (1979)	6.1	5.5	3860	57	2.6	0.00	No	-	-
	6.1	5.5	3880	57	2.6	0.00	No	-	-
	6.0	10.8	3990	50	2.8	0.00	No	-	-
	6.1	10.7	3990	50	2.8	0.00	No	-	-
	6.1	10.7	3980	50	2.7	0.00	No	-	-
	6.0	10.7	3980	50	2.8	0.00	No	-	-
	6.0	10.5	4560	58	2.8	0.00	Yes	Yes	Yes
	6.1	10.6	3980	53	2.7	0.00	No	-	-
	6.0	10.6	3980	54	2.7	0.00	No	-	-
	6.1	10.7	4390	54	2.7	0.00	No	-	-
	6.0	10.8	3670	51	2.8	0.00	Yes	Yes	Yes
	6.0	10.8	3670	49	2.8	0.00	No	-	-
	6.0	10.8	3670	49	2.8	0.00	No	-	-
	6.0	10.9	3950	53	2.7	0.00	No	-	-
	6.0	10.8	3800	53	2.7	0.00	No	-	-
	6.0	10.7	3800	53	2.7	0.00	No	-	-
	6.0	10.6	3950	53	2.7	0.00	No	-	-
	6.2	21.3	3880	51	2.6	0.00	No	-	-
	6.1	21.4	3800	51	2.8	0.00	No	-	-
	6.2	21.3	3730	51	2.8	0.00	No	-	-
	5.9	21.8	3910	54	2.8	0.00	No	-	-
	6.2	21.3	3830	51	2.8	0.00	No	-	-
	6.2	20.8	4400	59	2.8	0.00	Yes	Yes	Yes
	6.2	21.2	3940	59	2.7	0.00	No	-	-
	6.1	21.4	3970	54	2.7	0.00	Yes	Yes	Yes
	6.1	21.4	3970	54	2.7	0.00	No	-	-
	6.0	21.6	3600	56	2.7	0.00	Yes	Yes	Yes
	6.0	20.6	3950	53	2.8	0.00	No	-	-
	6.0	20.6	3960	53	2.8	0.00	No	-	-
	6.0	20.4	4460	54	2.9	0.00	No	-	-
	6.0	21.9	3790	55	2.7	0.00	No	-	-
	6.0	43.2	3900	55	2.7	0.00	Yes	Yes	Yes
	6.1	43.1	3830	54	2.7	0.00	No	-	-
	6.1	43.0	3910	55	2.7	0.00	No	-	-
	6.0	43.2	4280	55	2.7	0.00	No	-	-
	6.1	43.0	4100	55	2.7	0.00	No	-	-
	6.1	43.2	3870	52	2.7	0.00	No	-	-
	6.1	43.1	3870	55	2.7	0.00	No	-	-
	24.1	10.6	3910	55	2.8	0.00	No	-	-
	24.1	10.7	3910	55	2.7	0.00	No	-	-
	24.1	10.7	3940	55	2.7	0.00	No	-	-
	24.1	10.6	3940	55	2.7	0.00	No	-	-
Kong & Rangan (1998)	9.8	11.5	9222	83	2.8	0.16	No	-	-
	9.8	11.5	9222	83	2.8	0.16	No	-	-
	9.8	11.5	9222	83	2.8	0.16	No	-	-
	9.8	11.5	9222	83	2.8	0.16	No	-	-
	9.8	11.5	9222	83	2.8	0.16	No	-	-
	9.8	11.5	9222	83	2.8	0.16	No	-	-
	9.8	11.5	10513	83	2.8	0.11	No	-	-
	9.8	11.5	10513	83	2.8	0.13	No	-	-
	9.8	11.5	10513	83	2.8	0.16	No	-	-
	9.8	11.5	10513	83	2.8	0.16	No	-	-
	9.8	11.5	10513	83	2.8	0.21	No	-	-
	9.8	11.5	10513	83	2.8	0.26	No	-	-

Reference	b [in.]	d [in.]	f'_c [psi]	f_y [ksi]	ρ [%]	ρ_v [%]	Used For STM Database	Conservative Using ACI 318-05 STM Provisions	Conservative Using AASHTO LRFD STM Provisions
Kong & Rangan (1998)	9.8	11.7	9773	92	1.7	0.10	No	-	-
	9.8	11.7	9773	92	1.7	0.10	No	-	-
	9.8	11.5	9773	92	2.8	0.10	No	-	-
	9.8	11.5	9773	92	0.3	0.10	No	-	-
	9.8	11.8	9773	92	3.7	0.10	No	-	-
	9.8	11.8	9773	92	3.7	0.10	No	-	-
	9.8	21.3	12659	83	3.0	0.16	No	-	-
	9.8	17.5	12659	83	3.0	0.16	No	-	-
	9.8	13.6	12659	83	2.8	0.16	No	-	-
	9.8	11.5	12659	83	2.8	0.16	No	-	-
	9.8	9.8	12659	83	3.0	0.16	No	-	-
	9.8	7.8	12659	83	2.8	0.16	No	-	-
	9.8	11.5	12963	83	2.8	0.16	No	-	-
	9.8	11.5	12963	83	2.8	0.16	No	-	-
	9.8	11.5	12963	83	2.8	0.16	No	-	-
	9.8	11.5	12963	83	2.8	0.16	Yes	No	Yes
	9.8	11.5	12963	83	2.8	0.16	Yes	No	No
	9.8	11.5	12963	83	2.8	0.16	Yes	No	No
	9.8	11.7	9991	92	1.7	0.10	No	-	-
	9.8	11.5	9991	92	1.7	0.10	No	-	-
	9.8	11.5	9991	92	2.8	0.10	No	-	-
	9.8	11.8	9991	92	2.7	0.10	No	-	-
	9.8	11.8	9991	92	3.7	0.10	No	-	-
	9.8	11.6	9991	92	3.8	0.10	No	-	-
	9.8	11.6	10846	83	4.5	0.11	No	-	-
	9.8	11.6	10846	83	4.5	0.13	No	-	-
	9.8	11.6	10846	83	4.5	0.16	No	-	-
	9.8	11.6	10846	83	4.5	0.20	No	-	-
	9.8	11.6	10846	83	4.5	0.22	No	-	-
	9.8	11.6	10846	83	4.5	0.26	No	-	-
	9.8	11.5	10817	83	2.8	0.11	No	-	-
	9.8	11.5	10817	83	2.8	0.13	No	-	-
	9.8	11.5	10817	83	2.8	0.16	No	-	-
	9.8	11.5	10817	83	2.8	0.16	No	-	-
	9.8	11.5	10817	83	2.8	0.20	No	-	-
	9.8	11.5	10817	83	2.8	0.22	No	-	-
Kong et al (1970)	3.0	30.0	3120	41	0.5	0.25	Yes	Yes	Yes
	3.0	25.0	3560	41	0.6	0.25	Yes	Yes	Yes
	3.0	20.0	3080	41	0.7	0.25	Yes	Yes	Yes
	3.0	15.0	3080	41	1.0	0.25	Yes	Yes	Yes
	3.0	10.0	3140	41	1.5	0.25	Yes	Yes	Yes
	3.0	30.0	2785	44	0.5	0.86	Yes	Yes	Yes
	3.0	25.0	2700	44	0.6	0.86	Yes	Yes	Yes
	3.0	20.0	2880	44	0.7	0.86	Yes	Yes	Yes
	3.0	15.0	3300	44	1.0	0.86	Yes	Yes	Yes
	3.0	10.0	2920	44	1.5	0.86	Yes	Yes	Yes
	3.0	30.0	3270	41	0.5	0.00	Yes	Yes	Yes
	3.0	25.0	3040	41	0.6	0.00	Yes	Yes	Yes
	3.0	20.0	2790	41	0.7	0.00	Yes	Yes	Yes
	3.0	15.0	3180	41	1.0	0.00	Yes	Yes	Yes
	3.0	10.0	3280	41	1.5	0.00	Yes	Yes	Yes
	3.0	30.0	3190	44	0.5	0.00	Yes	Yes	Yes
	3.0	25.0	3040	44	0.6	0.00	Yes	Yes	Yes
	3.0	20.0	2920	44	0.7	0.00	Yes	Yes	Yes

Reference	b [in.]	d [in.]	f'_c [psi]	f_y [ksi]	ρ [%]	ρ_v [%]	Used For STM Database	Conservative Using ACI 318-05 STM Provisions	Conservative Using AASHTO LRFD STM Provisions
Kong et al (1970)	3.0	15.0	3190	44	1.0	0.00	Yes	Yes	Yes
	3.0	10.0	3280	44	1.5	0.00	Yes	Yes	Yes
	3.0	30.0	2690	41	0.5	0.61	Yes	Yes	Yes
	3.0	25.0	2790	41	0.6	0.61	Yes	Yes	Yes
	3.0	20.0	2920	41	0.7	0.61	Yes	Yes	Yes
	3.0	15.0	3180	41	1.0	0.61	Yes	Yes	Yes
	3.0	10.0	3270	41	1.5	0.61	Yes	Yes	Yes
	3.0	30.0	3782	44	0.5	0.00	Yes	Yes	Yes
	3.0	25.0	3640	44	0.6	0.00	Yes	Yes	Yes
	3.0	20.0	3782	44	0.7	0.00	Yes	Yes	Yes
	3.0	15.0	3782	44	1.0	0.00	Yes	Yes	Yes
	3.0	10.0	3640	44	1.5	0.00	Yes	Yes	Yes
	3.0	30.0	3640	44	0.5	0.00	Yes	Yes	Yes
	3.0	25.0	3782	44	0.6	0.00	Yes	Yes	Yes
	3.0	20.0	3640	44	0.7	0.00	Yes	Yes	Yes
	3.0	15.0	3085	44	1.0	0.00	Yes	Yes	Yes
	3.0	10.0	3085	44	1.5	0.00	Yes	Yes	Yes
Krefeld & Thurston (1966)	8.0	15.4	4440	40	2.1	0.00	No	-	-
	8.0	15.4	4300	40	3.1	0.00	No	-	-
	6.0	12.4	4380	40	3.4	0.00	No	-	-
	6.0	9.4	4360	40	4.5	0.00	No	-	-
	6.0	12.4	2800	40	2.7	0.00	No	-	-
	6.0	12.4	2880	40	2.7	0.00	No	-	-
	6.0	12.4	3280	40	2.7	0.00	No	-	-
	6.0	12.4	3200	40	2.7	0.00	No	-	-
	6.0	12.6	2890	40	0.8	0.00	No	-	-
	6.0	9.6	3000	40	1.1	0.00	No	-	-
	6.0	12.4	2920	40	1.3	0.00	No	-	-
	6.0	12.4	3000	40	1.3	0.00	No	-	-
	6.0	9.4	3220	40	1.8	0.00	No	-	-
	6.0	9.6	3190	40	2.1	0.00	No	-	-
	6.0	12.4	2870	40	2.7	0.00	No	-	-
	6.0	9.4	2980	40	3.5	0.00	No	-	-
	6.0	9.4	3050	40	4.5	0.00	No	-	-
	8.0	9.4	2890	40	5.0	0.00	No	-	-
	6.0	10.1	3180	40	1.0	0.00	No	-	-
	6.0	10.0	3340	40	1.3	0.00	No	-	-
	6.0	10.1	3020	40	2.0	0.00	No	-	-
	6.0	10.0	2390	40	2.6	0.00	No	-	-
	6.0	9.9	2660	40	3.4	0.00	No	-	-
	6.0	9.9	3310	40	4.3	0.00	No	-	-
	6.0	10.1	2750	40	1.0	0.00	No	-	-
	6.0	10.0	3020	40	1.3	0.00	No	-	-
	6.0	10.1	2970	40	2.0	0.00	No	-	-
	6.0	10.0	2980	40	2.6	0.00	No	-	-
	6.0	9.9	2950	40	3.4	0.00	No	-	-
	6.0	9.9	2980	40	4.3	0.00	No	-	-
	6.0	10.1	2730	40	2.0	0.00	No	-	-
	6.0	10.0	3080	40	2.6	0.00	No	-	-
	6.0	9.9	2830	40	3.4	0.00	No	-	-
	6.0	9.9	2770	40	4.3	0.00	No	-	-
	6.0	10.1	3255	40	2.0	0.00	No	-	-
	6.0	10.0	3050	40	2.6	0.00	No	-	-

Reference	b [in.]	d [in.]	f'_c [psi]	f_y [ksi]	ρ [%]	ρ_v [%]	Used For STM Database	Conservative Using ACI 318-05 STM Provisions	Conservative Using AASHTO LRFD STM Provisions
	6.0	9.9	3180	40	3.4	0.00	No	-	-
	6.0	9.9	3100	40	4.3	0.00	No	-	-
	6.0	10.1	3220	40	2.0	0.00	No	-	-
	6.0	10.0	3220	40	2.6	0.00	No	-	-
	6.0	9.9	3310	40	3.4	0.00	No	-	-
	6.0	9.9	3100	40	4.3	0.00	No	-	-
	6.0	9.9	2920	40	3.4	0.00	No	-	-
	6.0	10.1	5010	40	2.0	0.00	No	-	-
	6.0	10.0	4235	40	2.6	0.00	No	-	-
	6.0	9.9	4760	40	3.4	0.00	No	-	-
	6.0	9.9	4990	40	4.3	0.00	No	-	-
	6.0	10.1	4620	40	2.0	0.00	No	-	-
	6.0	10.0	4420	40	2.6	0.00	No	-	-
	6.0	9.9	4760	40	3.4	0.00	No	-	-
	6.0	9.9	4950	40	4.3	0.00	No	-	-
	6.0	10.0	5570	40	2.6	0.00	No	-	-
	6.0	9.9	5430	40	3.4	0.00	No	-	-
	6.0	9.9	5570	40	4.3	0.00	No	-	-
	6.0	10.0	5340	40	2.6	0.00	No	-	-
	6.0	9.9	5430	40	3.4	0.00	No	-	-
	6.0	9.9	4900	40	4.3	0.00	No	-	-
	6.0	10.1	1820	40	2.0	0.00	No	-	-
	6.0	10.0	1870	40	2.6	0.00	No	-	-
	6.0	9.9	2230	40	3.4	0.00	No	-	-
	6.0	9.9	1940	40	4.3	0.00	No	-	-
Krefeld & Thurston (1966)	6.0	10.1	1990	40	2.0	0.00	No	-	-
	6.0	10.0	1870	40	2.6	0.00	No	-	-
	6.0	9.9	2230	40	3.4	0.00	No	-	-
	6.0	9.9	1800	40	4.3	0.00	No	-	-
	6.0	10.1	1770	40	2.0	0.00	No	-	-
	6.0	10.0	2480	40	2.6	0.00	No	-	-
	6.0	9.9	2130	40	3.4	0.00	No	-	-
	6.0	9.9	1980	40	4.3	0.00	No	-	-
	6.0	10.0	2070	40	2.6	0.00	No	-	-
	6.0	9.9	2190	40	3.4	0.00	No	-	-
	8.0	19.0	2430	40	1.6	0.00	No	-	-
	6.0	9.9	5260	40	4.3	0.00	No	-	-
	6.0	9.9	5260	40	4.3	0.00	No	-	-
	6.0	10.0	5180	40	2.6	0.00	No	-	-
	6.0	10.0	5660	40	2.6	0.00	No	-	-
	10.0	17.9	5550	40	2.2	0.00	No	-	-
	10.0	17.9	5550	40	2.2	0.00	No	-	-
	6.0	10.0	5580	50	2.6	0.47	No	-	-
	6.0	10.0	5040	50	2.6	0.27	No	-	-
	6.0	10.0	5040	50	2.6	0.27	No	-	-
	6.0	10.0	5510	50	2.6	0.16	No	-	-
	6.0	10.0	5510	50	2.6	0.16	No	-	-
	6.0	10.0	5660	50	2.6	0.16	No	-	-
	6.0	10.0	5730	50	2.6	0.14	No	-	-
	6.0	10.0	5730	50	2.6	0.14	No	-	-
	10.0	17.9	5410	50	2.2	0.25	No	-	-
	10.0	17.9	5820	50	2.2	0.16	No	-	-
	10.0	17.9	5630	50	2.2	0.11	No	-	-

Reference	b [in.]	d [in.]	f'_c [psi]	f_y [ksi]	ρ [%]	ρ_v [%]	Used For STM Database	Conservative Using ACI 318-05 STM Provisions	Conservative Using AASHTO LRFD STM Provisions
	10.0	17.9	5460	50	2.2	0.11	No	-	-
	10.0	17.9	5640	50	2.2	0.07	No	-	-
	10.0	17.9	5450	54	2.2	0.22	No	-	-
	10.0	17.9	5390	54	2.2	0.11	No	-	-
	10.0	17.9	6000	54	2.2	0.11	No	-	-
	10.0	17.9	3500	54	2.2	0.11	No	-	-
	10.0	17.9	4410	54	2.2	0.11	No	-	-
	10.0	17.9	7030	54	2.2	0.11	No	-	-
	10.0	17.9	6060	54	2.2	0.11	No	-	-
	10.0	17.9	2280	54	2.2	0.11	No	-	-
	10.0	17.9	5360	54	2.2	0.07	No	-	-
	10.0	17.9	5450	54	2.2	0.05	No	-	-
	10.0	17.9	5140	34	2.2	0.22	No	-	-
	10.0	17.9	4970	34	2.2	0.11	No	-	-
	10.0	17.9	5400	75	2.2	0.25	No	-	-
	10.0	17.9	5400	75	2.2	0.16	No	-	-
	10.0	17.9	5880	75	2.2	0.12	No	-	-
	10.0	17.9	5620	75	2.2	0.11	No	-	-
	10.0	17.9	5380	51	2.2	0.25	No	-	-
	10.0	17.9	5750	51	2.2	0.16	No	-	-
	10.0	17.9	5640	51	2.2	0.12	No	-	-
	10.0	17.9	5510	51	2.2	0.11	No	-	-
	10.0	17.9	6190	40	2.2	0.25	No	-	-
	10.0	17.9	6190	40	2.2	0.16	No	-	-
	10.0	17.9	6240	40	2.2	0.12	No	-	-
Krefeld & Thurston (1966)	10.0	17.9	6240	40	2.2	0.11	No	-	-
	8.0	15.4	4240	40	2.1	0.00	No	-	-
	8.0	15.4	3990	40	2.1	0.00	No	-	-
	8.0	15.4	4270	40	3.1	0.00	No	-	-
	8.0	15.4	4290	40	3.1	0.00	No	-	-
	8.0	15.4	4070	40	2.1	0.00	No	-	-
	8.0	15.4	4260	40	3.1	0.00	No	-	-
	6.0	12.4	3910	40	3.4	0.00	No	-	-
	6.0	9.4	4440	40	4.5	0.00	No	-	-
	6.0	12.6	2930	40	0.8	0.00	No	-	-
	6.0	9.6	3300	40	1.1	0.00	No	-	-
	6.0	12.4	2780	40	1.3	0.00	No	-	-
	6.0	9.4	3050	40	1.8	0.00	No	-	-
	6.0	9.6	2660	40	2.1	0.00	No	-	-
	6.0	9.6	3040	40	2.1	0.00	No	-	-
	6.0	12.4	2930	40	2.7	0.00	No	-	-
	6.0	9.4	3080	40	3.5	0.00	No	-	-
	6.0	9.4	3090	40	4.5	0.00	No	-	-
	6.0	9.4	3080	40	4.9	0.00	No	-	-
	6.0	10.1	3180	40	1.0	0.00	No	-	-
	6.0	10.0	3070	40	1.3	0.00	No	-	-
	6.0	10.1	3290	40	2.0	0.00	No	-	-
	6.0	10.0	2590	40	2.6	0.00	No	-	-
	6.0	9.9	2990	40	3.4	0.00	No	-	-
	6.0	9.9	2990	40	4.3	0.00	No	-	-
	6.0	10.1	2750	40	1.0	0.00	No	-	-
	6.0	10.0	3020	40	1.3	0.00	No	-	-
	6.0	10.1	2970	40	2.0	0.00	No	-	-

Reference	b [in.]	d [in.]	f'_c [psi]	f_y [ksi]	ρ [%]	ρ_v [%]	Used For STM Database	Conservative Using ACI 318-05 STM Provisions	Conservative Using AASHTO LRFD STM Provisions
Krefeld & Thurston (1966)	6.0	10.0	2980	40	2.6	0.00	No	-	-
	6.0	9.9	2960	40	3.4	0.00	No	-	-
	6.0	9.9	2980	40	4.3	0.00	No	-	-
	6.0	10.1	2550	40	2.0	0.00	No	-	-
	6.0	10.0	2935	40	2.6	0.00	No	-	-
	6.0	9.9	2800	40	3.4	0.00	No	-	-
	6.0	9.9	2910	40	4.3	0.00	No	-	-
	6.0	10.1	3280	40	2.0	0.00	No	-	-
	6.0	10.0	3205	40	2.6	0.00	No	-	-
	6.0	9.9	3085	40	3.4	0.00	No	-	-
	6.0	9.9	3080	40	4.3	0.00	No	-	-
	6.0	10.1	3220	40	2.0	0.00	No	-	-
	6.0	10.0	3220	40	2.6	0.00	No	-	-
	6.0	9.9	3120	40	3.4	0.00	No	-	-
	6.0	9.9	3045	40	4.3	0.00	No	-	-
	6.0	9.9	2960	40	3.4	0.00	No	-	-
	6.0	10.1	5010	40	2.0	0.00	No	-	-
	6.0	10.0	5280	40	2.6	0.00	No	-	-
	6.0	9.9	4200	40	3.4	0.00	No	-	-
	6.0	9.9	4990	40	4.3	0.00	No	-	-
	6.0	10.0	4590	40	2.6	0.00	No	-	-
	6.0	9.9	4590	40	3.4	0.00	No	-	-
	6.0	9.9	4950	40	4.3	0.00	No	-	-
	6.0	10.0	4680	40	2.6	0.00	No	-	-
	6.0	9.9	4680	40	3.4	0.00	No	-	-
	6.0	9.9	5340	40	4.3	0.00	No	-	-
	6.0	10.1	1820	40	2.0	0.00	No	-	-
	6.0	10.0	1780	40	2.6	0.00	No	-	-
	6.0	9.9	2020	40	3.4	0.00	No	-	-
	6.0	9.9	1940	40	4.3	0.00	No	-	-
	6.0	10.1	1990	40	2.0	0.00	No	-	-
	6.0	10.0	1840	40	2.6	0.00	No	-	-
	6.0	9.9	2170	40	3.4	0.00	No	-	-
	6.0	9.9	1800	40	4.3	0.00	No	-	-
	6.0	10.1	1770	40	2.0	0.00	No	-	-
	6.0	10.0	2480	40	2.6	0.00	No	-	-
	6.0	9.9	2130	40	3.4	0.00	No	-	-
	6.0	9.9	1980	40	4.3	0.00	No	-	-
	6.0	10.1	2200	40	2.0	0.00	No	-	-
	6.0	10.0	2070	40	2.6	0.00	No	-	-
	6.0	9.9	2190	40	3.4	0.00	No	-	-
	6.0	9.9	1850	40	4.3	0.00	No	-	-
	6.0	10.1	1960	40	2.0	0.00	No	-	-
	6.0	10.0	1680	40	2.6	0.00	No	-	-
	6.0	9.9	1620	40	3.4	0.00	No	-	-
	8.0	19.0	3060	40	1.6	0.00	No	-	-
	10.0	17.9	5390	40	2.2	0.00	No	-	-
	6.0	12.4	4250	49	0.3	0.46	No	-	-
	6.0	12.4	4430	49	0.3	0.46	No	-	-
	6.0	12.4	4470	49	0.3	0.49	No	-	-
	6.0	12.4	4330	49	0.3	0.49	No	-	-
	10.0	17.9	4790	54	2.2	0.07	No	-	-
	10.0	17.9	5020	54	2.2	0.05	No	-	-

364

Reference	b [in.]	d [in.]	f'_c [psi]	f_y [ksi]	ρ [%]	ρ_v [%]	Used For STM Database	Conservative Using ACI 318-05 STM Provisions	Conservative Using AASHTO LRFD STM Provisions
	6.0	10.6	3900	41	2.1	0.00	No	-	-
	6.0	10.4	4690	59	2.5	0.00	No	-	-
	6.0	10.4	4470	45	3.2	0.00	No	-	-
	6.0	10.3	4330	46	4.1	0.00	No	-	-
	6.0	10.5	2140	48	1.9	0.00	No	-	-
	6.0	10.3	3800	44	4.1	0.00	No	-	-
Laupa et al (1953)	6.0	10.7	3940	45	1.5	0.00	No	-	-
	6.0	10.7	2140	44	0.9	0.00	No	-	-
	6.0	10.6	2280	42	1.4	0.00	No	-	-
	6.0	10.7	4150	45	0.9	0.00	No	-	-
	6.0	10.7	4070	45	0.6	0.00	No	-	-
	6.0	10.7	2640	45	0.6	0.00	No	-	-
	6.0	10.8	2480	44	0.3	0.00	No	-	-
Lubell et al (2004)	79.1	36.0	9300	67	0.8	0.00	No	-	-
	7.0	21.0	2580	47	2.7	0.00	Yes	Yes	Yes
	7.0	21.0	2990	47	2.7	0.00	Yes	Yes	Yes
	7.0	21.0	3530	47	3.5	0.00	Yes	Yes	Yes
	7.0	21.0	2500	47	3.5	0.00	Yes	Yes	Yes
	7.0	21.0	3140	47	4.3	0.00	Yes	Yes	Yes
	7.0	21.0	2990	47	4.3	0.00	Yes	Yes	Yes
	7.0	21.0	3100	47	2.7	0.00	Yes	Yes	Yes
	7.0	21.0	3320	47	2.7	0.00	Yes	Yes	Yes
	7.0	21.0	3380	47	3.5	0.00	Yes	Yes	Yes
	7.0	21.0	3250	47	3.5	0.00	Yes	Yes	Yes
	7.0	21.0	3150	47	4.3	0.00	Yes	Yes	Yes
	7.0	21.0	3620	47	4.3	0.00	Yes	Yes	Yes
	7.0	21.0	3680	47	4.3	0.52	Yes	Yes	Yes
	7.0	21.0	3250	44	4.3	0.95	Yes	Yes	Yes
	7.0	10.3	4400	44	2.2	0.00	No	-	-
	7.0	10.5	4500	44	2.2	0.00	No	-	-
	7.0	10.6	4500	44	2.2	0.00	No	-	-
	7.0	10.6	4570	44	2.4	0.00	No	-	-
	7.0	10.5	3070	44	1.6	0.00	No	-	-
	7.0	10.6	3130	44	1.6	0.00	No	-	-
Moody et al (1954)	7.0	10.6	2790	44	1.6	0.00	No	-	-
	7.0	10.7	2430	44	1.7	0.00	No	-	-
	7.0	10.6	920	44	0.8	0.00	No	-	-
	7.0	10.7	880	44	0.8	0.00	No	-	-
	7.0	10.8	1000	44	0.8	0.00	No	-	-
	7.0	10.8	980	44	0.8	0.00	No	-	-
	6.0	10.6	5320	44	1.9	0.00	No	-	-
	6.0	10.6	2420	44	1.9	0.00	No	-	-
	6.0	10.6	3740	44	1.9	0.00	No	-	-
	6.0	10.6	2230	44	1.9	0.00	No	-	-
	6.0	10.6	4450	44	1.9	0.00	No	-	-
	6.0	10.6	2290	44	1.9	0.00	No	-	-
	6.0	10.6	4480	44	1.9	0.00	No	-	-
	6.0	10.6	1770	44	1.9	0.00	No	-	-
	6.0	10.6	5970	44	1.9	0.00	No	-	-
	6.0	10.6	3470	44	1.9	0.00	No	-	-
	6.0	10.6	5530	44	1.9	0.00	No	-	-
	6.0	10.6	2930	44	1.9	0.00	No	-	-
	6.0	10.6	5480	44	1.9	0.00	No	-	-
	6.0	10.6	3270	44	1.9	0.00	No	-	-

Reference	b [in.]	d [in.]	f'_c [psi]	f_y [ksi]	ρ [%]	ρ_v [%]	Used For STM Database	Conservative Using ACI 318-05 STM Provisions	Conservative Using AASHTO LRFD STM Provisions
Moody et al (1954)	6.0	10.6	5420	44	1.9	0.00	No	-	-
	6.0	10.6	2370	44	1.9	0.00	No	-	-
Morrow & Viest (1957)	12.0	14.5	2120	68	1.9	0.00	Yes	Yes	Yes
	12.0	14.8	1840	68	0.6	0.00	Yes	Yes	Yes
	12.0	14.3	3270	62	2.5	0.00	Yes	Yes	Yes
	12.0	14.5	3820	59	1.9	0.00	Yes	Yes	Yes
	12.0	14.5	4190	61	1.2	0.00	Yes	Yes	Yes
	12.0	14.0	6590	65	3.8	0.00	Yes	Yes	Yes
	12.0	14.5	6780	66	1.9	0.00	Yes	Yes	Yes
	12.0	14.4	2010	63	1.9	0.00	Yes	Yes	Yes
	12.0	14.8	1640	67	0.6	0.00	Yes	Yes	Yes
	12.0	14.5	4320	59	2.5	0.00	Yes	Yes	Yes
	12.0	14.5	3930	61	1.9	0.00	Yes	Yes	Yes
	12.0	14.4	3510	62	1.2	0.00	Yes	Yes	Yes
	12.0	14.5	4630	60	1.2	0.00	Yes	Yes	Yes
	12.0	14.6	4560	66	1.2	0.00	Yes	Yes	Yes
	12.0	14.7	4580	68	0.6	0.00	Yes	Yes	Yes
	12.0	14.0	6570	65	3.8	0.00	Yes	Yes	Yes
	12.0	14.8	6600	63	1.8	0.00	Yes	Yes	Yes
	12.0	14.3	2130	68	1.9	0.00	Yes	Yes	Yes
	12.1	14.6	1990	67	0.6	0.00	Yes	Yes	Yes
	12.0	14.5	3990	48	2.5	0.00	Yes	Yes	Yes
	12.0	14.5	4690	64	1.9	0.00	Yes	Yes	Yes
	12.0	14.5	4800	62	1.2	0.00	Yes	Yes	Yes
	12.1	13.9	6840	66	3.8	0.00	No	-	-
	12.0	14.5	6360	66	1.9	0.00	Yes	Yes	Yes
	12.0	14.5	5040	55	1.9	0.00	No	-	-
	12.0	14.5	2130	68	1.9	0.00	No	-	-
	12.0	14.5	2130	67	0.6	0.00	No	-	-
	12.0	14.8	3620	48	2.4	0.00	No	-	-
	12.0	14.5	3950	64	1.9	0.00	No	-	-
	12.0	14.5	4120	62	1.2	0.00	No	-	-
	12.1	14.0	5780	64	3.8	0.00	No	-	-
	12.0	14.6	6630	68	1.8	0.00	No	-	-
	12.0	14.4	2370	67	1.9	0.00	No	-	-
	12.0	14.5	3950	63	2.5	0.00	No	-	-
	12.0	14.0	6520	63	3.8	0.00	No	-	-
	12.0	14.3	3950	67	1.9	0.00	No	-	-
	12.0	14.4	4730	68	1.9	0.00	No	-	-
	12.0	14.5	4160	50	1.9	0.00	No	-	-
Oh & Shin (2001)	5.1	19.7	3440	60	1.6	0.00	Yes	Yes	Yes
	5.1	19.7	3440	60	1.6	0.12	Yes	Yes	Yes
	5.1	19.7	3440	60	1.6	0.22	Yes	Yes	Yes
	5.1	19.7	3440	60	1.6	0.34	Yes	Yes	Yes
	5.1	19.7	7121	60	1.6	0.00	Yes	Yes	Yes
	5.1	19.7	7121	60	1.6	0.12	Yes	Yes	Yes
	5.1	19.7	7121	60	1.6	0.22	Yes	Yes	Yes
	5.1	19.7	7121	60	1.6	0.34	Yes	Yes	Yes
	5.1	19.7	7121	60	1.6	0.00	Yes	No	No
	5.1	19.7	7121	60	1.6	0.12	Yes	No	Yes
	5.1	19.7	7121	60	1.6	0.22	Yes	No	No
	5.1	19.7	7121	60	1.6	0.34	Yes	No	No
	5.1	19.7	7121	60	1.6	0.00	Yes	Yes	Yes

Reference	b [in.]	d [in.]	f'_c [psi]	f_y [ksi]	ρ [%]	ρ_v [%]	Used For STM Database	Conservative Using ACI 318-05 STM Provisions	Conservative Using AASHTO LRFD STM Provisions
	5.1	19.7	7121	60	1.6	0.12	Yes	No	Yes
	5.1	19.7	7121	60	1.6	0.22	Yes	No	Yes
	5.1	19.7	7121	60	1.6	0.34	Yes	No	Yes
	5.1	19.7	7121	60	1.6	0.00	Yes	No	Yes
	5.1	19.7	7121	60	1.6	0.12	Yes	No	Yes
	5.1	19.7	7121	60	1.6	0.22	Yes	No	Yes
	5.1	19.7	7121	60	1.6	0.34	Yes	No	Yes
	4.7	19.7	7349	60	1.3	0.13	Yes	No	No
	4.7	19.7	7349	60	1.3	0.13	Yes	No	No
	4.7	19.7	7349	60	1.3	0.13	Yes	No	No
	4.7	19.7	7349	60	1.3	0.13	Yes	No	No
	4.7	19.7	7349	60	1.3	0.13	Yes	No	No
	4.7	19.7	7349	60	1.3	0.24	Yes	No	No
	4.7	19.7	7349	60	1.3	0.37	Yes	No	No
	4.7	19.7	7349	60	1.3	0.13	Yes	No	No
	4.7	19.7	7349	60	1.3	0.13	Yes	No	Yes
	4.7	19.7	7349	60	1.3	0.13	Yes	No	Yes
	4.7	19.7	7349	60	1.3	0.13	Yes	No	Yes
	4.7	19.7	10675	60	1.3	0.13	Yes	No	Yes
Oh & Shin (2001)	4.7	19.7	10675	60	1.3	0.13	Yes	No	No
	4.7	19.7	10675	60	1.3	0.13	Yes	No	No
	4.7	19.7	10675	60	1.3	0.13	Yes	No	No
	4.7	19.7	10675	60	1.3	0.13	Yes	No	No
	4.7	19.7	10675	60	1.3	0.13	Yes	No	No
	4.7	19.7	10675	60	1.3	0.24	Yes	No	No
	4.7	19.7	10675	60	1.3	0.37	Yes	No	No
	4.7	19.7	10675	60	1.3	0.13	Yes	No	No
	4.7	19.7	10675	60	1.3	0.13	Yes	No	No
	4.7	19.7	10675	60	1.3	0.13	Yes	No	Yes
	4.7	19.7	10675	60	1.3	0.13	Yes	No	Yes
	4.7	19.7	10675	60	1.3	0.13	Yes	No	Yes
	5.1	19.7	3440	60	1.6	0.12	Yes	Yes	Yes
	5.1	19.7	3440	60	1.6	0.12	Yes	Yes	Yes
	5.1	19.7	3440	60	1.6	0.12	Yes	Yes	Yes
	5.1	19.7	7121	60	1.6	0.12	Yes	Yes	Yes
	5.1	19.7	7121	60	1.6	0.12	Yes	Yes	Yes
	5.1	19.7	7121	60	1.6	0.12	Yes	No	Yes
	5.1	19.7	7121	60	1.6	0.12	Yes	Yes	Yes
	5.1	19.7	7121	60	1.6	0.12	Yes	Yes	Yes
	5.1	19.7	7121	60	1.6	0.12	Yes	No	Yes
	5.9	12.2	8410	62	3.5	0.14	No	-	-
	5.9	12.2	9135	62	3.5	0.17	No	-	-
	5.9	12.2	8845	62	3.5	0.24	No	-	-
	5.9	12.2	11890	62	4.4	0.14	No	-	-
	5.9	12.2	10875	62	4.4	0.19	No	-	-
	5.9	12.2	11890	62	4.4	0.28	No	-	-
Ozcebe et al (1999)	5.9	12.2	10875	62	2.6	0.14	No	-	-
	5.9	12.2	10875	62	2.6	0.17	No	-	-
	5.9	12.2	10875	62	2.6	0.24	No	-	-
	5.9	12.2	10585	62	3.1	0.14	No	-	-
	5.9	12.2	10585	62	3.7	0.17	No	-	-
	5.9	12.2	10585	62	3.1	0.28	No	-	-
	5.9	12.8	10150	62	1.9	0.14	Yes	Yes	Yes

Reference	b [in.]	d [in.]	f'_c [psi]	f_y [ksi]	ρ [%]	ρ_v [%]	Used For STM Database	Conservative Using ACI 318-05 STM Provisions	Conservative Using AASHTO LRFD STM Provisions
Ramakrishnan & Ananthanarayana (1968)	3.0	15.0	3509	46	0.2	0.00	Yes	No	No
	3.0	20.0	2959	46	0.2	0.00	Yes	Yes	No
	3.1	22.5	3388	46	0.2	0.00	Yes	Yes	Yes
	3.0	30.0	3960	46	0.1	0.00	Yes	Yes	Yes
	3.1	30.0	1778	46	0.1	0.00	Yes	Yes	Yes
	3.0	15.0	2959	46	0.6	0.00	Yes	Yes	No
	3.0	20.0	3091	46	0.5	0.00	Yes	Yes	No
	3.1	22.5	3597	46	0.5	0.00	Yes	Yes	Yes
	3.1	30.0	4114	46	0.3	0.00	Yes	Yes	Yes
	3.0	15.0	3124	46	0.6	0.33	Yes	Yes	No
	3.1	20.0	3542	46	0.5	0.24	Yes	Yes	Yes
	3.0	22.5	2838	46	0.5	0.22	Yes	Yes	Yes
	3.1	30.0	2376	46	0.3	0.16	Yes	Yes	Yes
	3.1	15.0	2205	46	0.2	0.00	Yes	Yes	Yes
	3.1	15.0	1980	46	0.2	0.00	Yes	Yes	Yes
	3.1	20.0	2033	46	0.2	0.00	Yes	Yes	Yes
	3.1	20.0	2073	46	0.2	0.00	Yes	Yes	Yes
	3.1	22.5	2143	46	0.2	0.00	Yes	Yes	Yes
	3.2	30.0	2008	46	0.1	0.00	Yes	Yes	Yes
	3.1	30.0	1533	46	0.1	0.00	Yes	Yes	Yes
	3.2	15.0	1938	46	0.2	0.00	Yes	Yes	Yes
	3.1	15.0	1625	46	0.2	0.00	Yes	Yes	Yes
	3.2	20.0	2020	46	0.2	0.00	Yes	Yes	Yes
	3.1	20.0	1787	46	0.2	0.00	Yes	Yes	Yes
	3.2	22.5	2148	46	0.2	0.00	Yes	Yes	Yes
	3.2	30.0	2140	46	0.1	0.00	Yes	Yes	Yes
Rigotti (2002)	3.7	12.0	4191	64	4.1	0.20	Yes	Yes	Yes
	3.7	12.0	5003	64	4.1	0.20	Yes	Yes	Yes
	3.7	12.0	4191	64	4.1	0.20	Yes	Yes	Yes
	3.7	12.0	4191	64	4.1	0.00	Yes	Yes	Yes
	3.7	12.0	4191	64	4.1	0.00	Yes	Yes	Yes
	3.7	12.0	3698	64	4.1	0.00	Yes	Yes	Yes
	3.7	12.0	4191	64	4.1	0.20	No	-	-
	3.7	12.0	4191	64	4.1	0.20	No	-	-
	3.7	12.0	5003	64	4.1	0.20	No	-	-
	3.7	12.0	2393	64	4.1	0.00	No	-	-
	3.7	12.0	5003	64	4.1	0.00	No	-	-
	3.7	12.0	2393	64	4.1	0.00	No	-	-
Rogowsky et al (1986)	7.9	39.4	3785	59	0.9	0.30	Yes	Yes	Yes
	7.9	39.4	3785	59	0.9	0.00	Yes	Yes	Yes
	7.9	39.4	3887	59	0.9	0.30	Yes	Yes	Yes
	7.9	39.4	3887	59	0.9	0.00	Yes	Yes	Yes
	7.9	39.4	3829	59	0.9	0.00	Yes	Yes	Yes
	7.9	23.6	6150	59	1.0	0.47	Yes	No	Yes
	7.9	23.6	6150	59	1.0	0.00	Yes	No	Yes
	7.9	23.6	6150	59	1.0	0.47	Yes	No	Yes
	7.9	23.6	6150	59	1.0	0.00	Yes	No	No
	7.9	19.7	6266	59	0.8	0.28	Yes	No	Yes
	7.9	19.7	6266	59	0.8	0.00	Yes	No	Yes
	7.9	19.7	6266	59	0.8	0.28	Yes	No	Yes
	7.9	19.7	6266	59	0.8	0.00	Yes	No	Yes
Roller & Russell (1990)	14.0	22.0	17420	59	1.6	0.08	No	-	-
	14.0	22.0	17420	59	3.0	0.44	No	-	-
	14.0	22.0	17420	59	4.6	0.89	No	-	-

Reference	b [in.]	d [in.]	f'_c [psi]	f_y [ksi]	ρ [%]	ρ_v [%]	Used For STM Database	Conservative Using ACI 318-05 STM Provisions	Conservative Using AASHTO LRFD STM Provisions
Roller & Russell (1990)	14.0	22.0	17420	59	6.1	1.27	No	-	-
	14.0	22.0	17420	59	7.0	1.77	No	-	-
	18.0	30.0	10500	65	1.7	0.08	No	-	-
	18.0	30.0	10500	65	1.9	0.16	No	-	-
	18.0	30.0	18170	65	1.9	0.08	No	-	-
	18.0	30.0	18170	65	2.4	0.16	No	-	-
	18.0	30.0	18170	65	2.9	0.23	No	-	-
Sarsam & Al-Musawi (1992)	7.1	9.2	5858	119	0.2	0.09	No	-	-
	7.1	9.2	10919	119	2.2	0.09	No	-	-
	7.1	9.2	5655	119	2.2	0.09	No	-	-
	7.1	9.2	10948	119	2.3	0.09	No	-	-
	7.1	9.2	5829	119	2.2	0.14	No	-	-
	7.1	9.2	10411	119	2.2	0.14	No	-	-
	7.1	9.2	10977	119	2.8	0.09	No	-	-
	7.1	9.2	10716	119	2.8	0.09	No	-	-
	7.1	9.2	10643	119	2.8	0.14	No	-	-
	7.1	9.2	11615	119	2.8	0.19	No	-	-
	7.1	9.2	10165	119	3.5	0.09	No	-	-
	7.1	9.2	10179	119	3.5	0.09	No	-	-
	7.1	9.2	10759	119	3.5	0.14	No	-	-
	7.1	9.2	10977	119	3.5	0.19	No	-	-
Shin et al (1999)	4.9	8.5	7600	60	3.8	0.00	Yes	No	No
	4.9	8.5	7600	60	3.8	0.45	Yes	No	Yes
	4.9	8.5	7600	60	3.8	0.91	Yes	No	Yes
	4.9	8.5	7600	60	3.8	0.14	Yes	Yes	Yes
	4.9	8.5	7600	60	3.8	1.81	Yes	Yes	Yes
	4.9	8.5	7600	60	3.8	0.00	Yes	No	Yes
	4.9	8.5	7600	60	3.8	0.32	Yes	No	Yes
	4.9	8.5	7600	60	3.8	0.65	Yes	Yes	Yes
	4.9	8.5	7600	60	3.8	0.97	Yes	Yes	Yes
	4.9	8.5	7600	60	3.8	1.29	Yes	Yes	Yes
	4.9	8.5	7600	60	3.8	0.00	Yes	No	No
	4.9	8.5	7600	60	3.8	0.25	No	-	-
	4.9	8.5	7600	60	3.8	0.47	No	-	-
	4.9	8.5	7600	60	3.8	0.71	No	-	-
	4.9	8.5	7600	60	3.8	0.94	No	-	-
	4.9	8.5	10600	60	3.8	0.00	Yes	No	No
	4.9	8.5	10600	60	3.8	0.45	Yes	No	Yes
	4.9	8.5	10600	60	3.8	0.91	Yes	No	Yes
	4.9	8.5	10600	60	3.8	1.36	Yes	No	Yes
	4.9	8.5	10600	60	3.8	1.81	Yes	No	Yes
	4.9	8.5	10600	60	3.8	0.00	Yes	No	Yes
	4.9	8.5	10600	60	3.8	0.32	Yes	No	Yes
	4.9	8.5	10600	60	3.8	0.65	Yes	No	Yes
	4.9	8.5	10600	60	3.8	0.97	Yes	Yes	Yes
	4.9	8.5	10600	60	3.8	1.29	Yes	Yes	Yes
	4.9	8.5	10600	60	3.8	0.00	Yes	No	No
	4.9	8.5	10600	60	3.8	0.24	No	-	-
	4.9	8.5	10600	60	3.8	0.47	No	-	-
	4.9	8.5	10600	60	3.8	0.71	No	-	-
	4.9	8.5	10600	60	3.8	0.94	No	-	-
Shioya (1989)	59.1	118.1	3520	52	0.4	0.00	No	-	-
	39.4	78.7	4130	54	0.4	0.00	No	-	-
	19.7	39.4	3170	54	0.4	0.00	No	-	-

Reference	b [in.]	d [in.]	f'_c [psi]	f_y [ksi]	ρ [%]	ρ_v [%]	Used For STM Database	Conservative Using ACI 318-05 STM Provisions	Conservative Using AASHTO LRFD STM Provisions
	11.8	23.6	3070	64	0.4	0.00	No	-	-
	19.7	39.4	3950	54	0.4	0.00	No	-	-
Shioya (1989)	11.8	23.6	3060	64	0.4	0.00	No	-	-
	19.7	39.4	4090	54	0.4	0.00	No	-	-
	11.8	23.6	3960	64	0.4	0.00	No	-	-
	4.0	14.0	2710	63	1.9	0.28	Yes	Yes	Yes
	4.0	14.0	2615	63	1.9	0.28	Yes	Yes	Yes
	4.0	14.0	2330	63	1.9	0.28	Yes	Yes	Yes
	4.0	14.0	2980	63	1.9	0.28	Yes	Yes	Yes
	4.0	14.0	3055	63	1.9	0.28	Yes	Yes	Yes
	4.0	14.0	3145	63	1.9	0.63	Yes	Yes	Yes
	4.0	14.0	2865	63	1.9	0.63	Yes	Yes	Yes
	4.0	14.0	2950	63	1.9	0.63	Yes	Yes	Yes
	4.0	14.0	2775	63	1.9	0.63	Yes	Yes	Yes
	4.0	14.0	2670	63	1.9	1.25	Yes	Yes	Yes
	4.0	14.0	2790	63	1.9	1.25	Yes	Yes	Yes
	4.0	14.0	3020	63	1.9	1.25	Yes	Yes	Yes
	4.0	14.0	2890	63	1.9	1.25	Yes	Yes	Yes
	4.0	14.0	3200	63	1.9	0.24	Yes	Yes	Yes
	4.0	14.0	2915	63	1.9	0.24	Yes	Yes	Yes
	4.0	14.0	3020	63	1.9	0.24	Yes	Yes	Yes
	4.0	14.0	2830	63	1.9	0.24	Yes	Yes	Yes
	4.0	14.0	2780	63	1.9	0.42	Yes	Yes	Yes
	4.0	14.0	2755	63	1.9	0.42	Yes	Yes	Yes
	4.0	14.0	2535	63	1.9	0.42	Yes	Yes	Yes
	4.0	14.0	3160	63	1.9	0.42	Yes	Yes	Yes
	4.0	14.0	2865	63	1.9	0.42	Yes	Yes	Yes
	4.0	14.0	2355	63	1.9	0.63	Yes	Yes	Yes
Smith & Vantsiotis (1982	4.0	14.0	2960	63	1.9	0.77	Yes	Yes	Yes
	4.0	14.0	2755	63	1.9	0.77	Yes	Yes	Yes
	4.0	14.0	2790	63	1.9	0.77	Yes	Yes	Yes
	4.0	14.0	2995	63	1.9	0.70	Yes	Yes	Yes
	4.0	14.0	2480	63	1.9	1.25	Yes	Yes	Yes
	4.0	14.0	2790	63	1.9	0.18	Yes	Yes	Yes
	4.0	14.0	3175	63	1.9	0.18	Yes	Yes	Yes
	4.0	14.0	3290	63	1.9	0.18	Yes	Yes	Yes
	4.0	14.0	3160	63	1.9	0.18	Yes	Yes	Yes
	4.0	14.0	2880	63	1.9	0.31	Yes	Yes	Yes
	4.0	14.0	2790	63	1.9	0.31	Yes	Yes	Yes
	4.0	14.0	2800	63	1.9	0.31	Yes	Yes	Yes
	4.0	14.0	2965	63	1.9	0.31	Yes	Yes	Yes
	4.0	14.0	3010	63	1.9	0.31	Yes	Yes	Yes
	4.0	14.0	3050	63	1.9	0.56	Yes	Yes	Yes
	4.0	14.0	2400	63	1.9	0.56	Yes	Yes	Yes
	4.0	14.0	2650	63	1.9	0.56	Yes	Yes	Yes
	4.0	14.0	2755	63	1.9	0.56	Yes	Yes	Yes
	4.0	14.0	2840	63	1.9	0.77	Yes	Yes	Yes
	4.0	14.0	2690	63	1.9	0.63	Yes	Yes	Yes
	4.0	14.0	2790	63	1.9	0.77	Yes	Yes	Yes
	4.0	14.0	2685	63	1.9	0.77	Yes	Yes	Yes
	4.0	14.0	3080	63	1.9	0.77	Yes	Yes	Yes
	4.0	14.0	2330	63	1.9	0.42	Yes	Yes	Yes
Subedi et al (1986)	3.9	19.7	5366	48	0.8	0.24	Yes	Yes	Yes
	3.9	19.7	5366	47	0.8	0.22	Yes	Yes	Yes

Reference	b [in.]	d [in.]	f'_c [psi]	f_y [ksi]	ρ [%]	ρ_v [%]	Used For STM Database	Conservative Using ACI 318-05 STM Provisions	Conservative Using AASHTO LRFD STM Provisions
Subedi et al (1986)	3.9	35.4	4496	72	0.3	0.21	Yes	Yes	Yes
	3.9	35.4	5149	48	1.1	0.21	Yes	Yes	Yes
	3.9	35.4	6019	55	1.1	0.20	Yes	Yes	Yes
	3.9	19.7	4119	48	0.8	0.24	Yes	Yes	Yes
	3.9	35.4	5062	47	0.3	0.21	Yes	Yes	Yes
	3.9	35.4	5714	31	1.1	0.20	Yes	Yes	Yes
Tan & Lu1996)	5.5	17.5	7120	75	2.6	0.00	Yes	Yes	Yes
	5.5	17.5	6163	75	2.6	0.00	Yes	Yes	Yes
	5.5	17.5	5423	75	2.6	0.00	Yes	Yes	Yes
	5.5	34.8	4524	75	2.6	0.06	Yes	Yes	Yes
	5.5	34.8	4742	75	2.6	0.06	Yes	Yes	Yes
	5.5	34.8	4473	75	2.6	0.06	Yes	Yes	Yes
	5.5	49.3	4756	75	2.6	0.06	Yes	Yes	Yes
	5.5	49.3	5249	75	2.6	0.06	Yes	Yes	Yes
	5.5	49.3	5148	75	2.6	0.06	Yes	Yes	Yes
	5.5	61.4	6177	75	2.6	0.06	Yes	Yes	Yes
	5.5	61.4	5858	75	2.6	0.06	Yes	Yes	Yes
	5.5	61.4	6496	75	2.6	0.06	Yes	Yes	Yes
	4.3	18.2	8532	54	1.2	0.48	Yes	Yes	Yes
	4.3	18.2	7485	54	1.2	0.48	Yes	Yes	Yes
	4.3	18.2	7808	54	1.2	0.48	Yes	Yes	Yes
	4.3	18.2	8310	54	1.2	0.48	Yes	Yes	Yes
	4.3	18.2	8117	54	1.2	0.48	Yes	Yes	No
	4.3	18.2	6624	54	1.2	0.48	Yes	Yes	Yes
	4.3	18.2	7808	54	1.2	0.48	Yes	Yes	Yes
	4.3	18.2	7684	54	1.2	0.48	Yes	Yes	Yes
	4.3	18.2	7417	54	1.2	0.48	Yes	Yes	Yes
	4.3	18.2	6374	54	1.2	0.48	Yes	Yes	Yes
	4.3	18.2	6989	54	1.2	0.48	Yes	No	Yes
	4.3	18.2	6425	54	1.2	0.48	Yes	Yes	Yes
	4.3	18.2	6725	54	1.2	0.48	Yes	Yes	Yes
	4.3	17.4	8164	58	2.6	0.00	Yes	Yes	Yes
	4.3	17.4	8149	58	2.6	2.86	Yes	Yes	Yes
	4.3	17.4	8584	58	2.6	0.00	Yes	Yes	Yes
	4.3	17.4	9251	58	2.6	0.00	Yes	Yes	Yes
	4.3	17.4	8352	58	2.6	0.00	Yes	Yes	Yes
	4.3	17.4	8657	58	2.6	2.86	Yes	Yes	Yes
	4.3	17.4	11252	58	2.6	0.00	Yes	No	No
	4.3	17.4	11252	58	2.6	1.43	Yes	Yes	Yes
	4.3	17.4	11310	58	2.6	0.00	Yes	No	No
	4.3	17.4	12514	58	2.6	0.00	Yes	No	No
	4.3	17.4	12514	58	2.6	0.00	Yes	No	Yes
	4.3	17.4	10919	58	2.6	1.43	Yes	Yes	Yes
	4.3	17.4	11252	58	2.6	0.00	Yes	No	Yes
	4.3	17.4	11252	58	2.6	1.43	Yes	No	Yes
	4.3	17.4	11252	58	2.6	1.43	Yes	Yes	Yes
	4.3	17.4	11310	58	2.6	0.00	Yes	No	Yes
	4.3	17.4	12514	58	2.6	0.00	Yes	No	No
	4.3	17.4	12514	58	2.6	0.00	Yes	No	Yes
	4.3	17.4	11441	58	2.6	1.43	Yes	Yes	Yes
	4.3	17.4	10138	51	2.6	0.48	Yes	Yes	Yes
	4.3	16.5	10138	51	4.1	0.48	Yes	Yes	Yes
	4.3	16.5	9369	51	4.1	0.48	Yes	Yes	Yes

Reference	b [in.]	d [in.]	f'_c [psi]	f_y [ksi]	ρ [%]	ρ_v [%]	Used For STM Database	Conservative Using ACI 318-05 STM Provisions	Conservative Using AASHTO LRFD STM Provisions
Uribe & Alcocer (2001)	13.8	43.3	5134	65	1.6	0.53	Yes	No	Yes
	13.8	43.3	5076	65	1.6	0.53	Yes	No	Yes
Uzel (2003)	4.4	9.1	5191	73	1.2	0.00	No	-	-
	4.4	9.1	5191	73	1.2	0.00	No	-	-
	4.4	9.1	5191	73	1.2	0.00	No	-	-
	4.4	9.1	5191	73	1.2	0.00	No	-	-
	11.8	36.4	6235	80	0.8	0.00	No	-	-
	11.8	24.3	3959	69	0.8	0.00	No	-	-
	11.8	24.3	4539	69	0.8	0.00	No	-	-
	11.8	24.3	4669	82	0.8	0.00	No	-	-
	11.8	36.4	4901	82	0.8	0.00	No	-	-
	11.8	36.4	5249	82	0.8	0.00	No	-	-
	11.8	36.4	5249	82	0.8	0.00	No	-	-
	11.8	34.1	5177	69	2.2	0.00	No	-	-
	11.8	36.4	4901	82	0.8	0.00	No	-	-
	11.8	36.4	5249	82	0.8	0.00	Yes	Yes	Yes
Van Den Berg (1962)	9.0	14.1	8500	40	4.4	0.00	No	-	-
	9.0	14.1	7330	40	4.4	0.00	No	-	-
	9.0	14.1	6160	40	4.4	0.00	No	-	-
	9.0	14.1	6060	40	4.4	0.00	No	-	-
	9.0	14.1	7330	40	4.4	0.00	No	-	-
	9.0	14.1	7050	40	4.4	0.00	No	-	-
	9.0	14.1	5500	40	4.4	0.00	No	-	-
	9.0	14.1	4350	40	4.4	0.00	No	-	-
	9.0	14.1	2570	40	4.4	0.00	No	-	-
	9.0	14.1	4550	40	4.4	0.00	No	-	-
	9.0	14.1	3260	40	4.4	0.00	No	-	-
	9.0	14.1	3970	40	4.4	0.00	No	-	-
	9.0	14.1	3550	40	4.4	0.00	No	-	-
	9.0	14.1	4080	40	4.4	0.00	No	-	-
	9.0	14.1	3810	40	4.4	0.00	No	-	-
	9.0	14.1	4420	40	4.4	0.00	No	-	-
	9.0	14.1	3780	40	4.4	0.00	No	-	-
	9.0	14.1	4160	40	4.4	0.00	No	-	-
	9.0	14.1	4680	40	4.4	0.00	No	-	-
	9.0	14.1	4310	40	4.4	0.00	No	-	-
	9.0	14.1	11220	40	4.4	0.00	No	-	-
	9.0	14.1	8060	40	4.4	0.00	No	-	-
	9.0	14.1	7060	40	4.4	0.00	No	-	-
	9.0	14.1	6190	40	4.4	0.00	No	-	-
	9.0	14.1	3410	40	4.4	0.00	No	-	-
	9.0	14.1	7440	40	4.4	0.00	No	-	-
	9.0	14.1	6640	40	4.4	0.00	No	-	-
	9.0	14.1	7130	40	4.4	0.00	No	-	-
	9.0	14.1	6640	40	4.4	0.00	No	-	-
	9.0	14.1	6750	40	4.4	0.00	No	-	-
	9.0	14.1	7660	40	4.4	0.00	No	-	-
	9.0	14.1	8590	40	4.4	0.00	No	-	-
	9.0	14.1	7300	40	4.4	0.00	No	-	-
	9.0	14.1	8120	40	4.4	0.00	No	-	-
	9.0	14.1	6048	40	4.4	0.00	No	-	-
	9.0	14.1	6830	40	4.4	0.00	No	-	-
	9.0	14.1	7500	40	4.4	0.00	No	-	-

Reference	b [in.]	d [in.]	f'_c [psi]	f_y [ksi]	ρ [%]	ρ_v [%]	Used For STM Database	Conservative Using ACI 318-05 STM Provisions	Conservative Using AASHTO LRFD STM Provisions
	12.0	14.1	7590	40	3.2	0.00	No	-	-
	9.0	14.4	3470	40	3.6	0.00	No	-	-
	9.0	14.5	4010	40	2.6	0.00	No	-	-
Van Den Berg (1962)	9.0	14.5	3900	40	2.4	0.00	No	-	-
	9.0	14.6	4260	40	1.7	0.00	No	-	-
	9.0	14.4	4590	40	2.2	0.00	No	-	-
	9.0	17.6	4510	40	3.5	0.00	No	-	-
	6.0	13.1	3450	40	1.5	0.00	No	-	-
	8.0	15.9	3680	39	3.1	0.00	Yes	Yes	Yes
	8.0	15.9	3330	39	3.1	0.00	Yes	Yes	Yes
Watstein & Mathey (1958)	8.0	15.9	3710	71	1.9	0.00	Yes	Yes	Yes
	8.0	15.9	3830	68	1.9	0.00	Yes	Yes	Yes
	8.0	15.9	3720	105	1.2	0.00	Yes	Yes	Yes
	8.0	15.9	3910	97	1.2	0.00	Yes	Yes	Yes
	8.0	15.9	3250	100	0.8	0.00	Yes	Yes	Yes
	8.0	15.9	3870	100	0.8	0.00	Yes	Yes	Yes
	5.0	8.5	6810	47	0.2	0.00	Yes	Yes	Yes
	5.0	8.5	6000	47	0.2	0.00	Yes	Yes	Yes
	5.0	8.5	5760	47	0.2	0.00	No	-	-
	5.0	8.0	6150	47	3.2	0.05	Yes	Yes	Yes
	5.0	8.0	6300	47	3.2	0.05	Yes	Yes	Yes
	5.0	8.0	6220	47	3.2	0.05	No	-	-
	5.0	8.5	15050	47	2.1	0.00	Yes	Yes	Yes
Xie et al (1994)	5.0	8.5	14990	47	2.1	0.00	Yes	Yes	Yes
	5.0	8.5	15110	47	2.1	0.00	No	-	-
	5.0	7.8	14170	47	4.5	0.39	Yes	Yes	Yes
	5.0	7.8	14460	47	4.5	0.39	Yes	Yes	Yes
	5.0	7.8	15000	47	4.5	0.39	No	-	-
	5.0	7.8	13740	47	4.5	0.39	No	-	-
	5.0	7.8	15760	47	4.5	0.25	No	-	-
	5.0	7.8	15090	47	4.5	0.39	No	-	-
	6.3	14.0	4554	59	1.0	0.00	Yes	Yes	Yes
	6.3	21.9	4554	59	1.0	0.00	Yes	Yes	Yes
	6.3	21.9	4554	59	1.0	0.00	Yes	Yes	Yes
	6.3	27.0	4554	59	1.0	0.00	Yes	Yes	Yes
Yang et al (2003)	6.3	36.8	4554	59	0.9	0.00	Yes	Yes	Yes
	6.3	14.0	11385	59	1.0	0.00	Yes	Yes	No
	6.3	21.9	11385	59	1.0	0.00	Yes	Yes	No
	6.3	27.0	11385	59	1.0	0.00	Yes	Yes	Yes
	14.8	25.8	5221	62	2.5	0.00	No	-	-
	14.8	25.8	5221	62	2.5	0.08	No	-	-
	14.8	25.8	5221	62	2.5	0.08	No	-	-
	14.8	25.8	5221	62	2.5	0.12	No	-	-
	14.8	25.8	9717	62	2.5	0.00	No	-	-
	14.8	25.8	9717	62	2.5	0.08	No	-	-
Yoon et al (1996)	14.8	25.8	9717	62	2.5	0.12	No	-	-
	14.8	25.8	9717	62	2.5	0.16	No	-	-
	14.8	25.8	12618	62	2.5	0.00	No	-	-
	14.8	25.8	12618	62	2.5	0.08	No	-	-
	14.8	25.8	12618	62	2.5	0.12	No	-	-
	14.8	25.8	12618	62	2.5	0.08	No	-	-

Reference	b [in.]	d [in.]	f'_c [psi]	f_y [ksi]	ρ [%]	ρ_v [%]	Used For STM Database	Conservative Using ACI 318-05 STM Provisions	Conservative Using AASHTO LRFD STM Provisions
Yoshida (2000)	11.8	74.3	4873	66	0.7	0.00	No	-	-
	11.8	74.3	4873	66	0.7	0.08	No	-	-
	11.8	74.3	5040	66	0.7	0.07	No	-	-
	11.8	74.3	5040	66	0.7	0.07	No	-	-

References

1. "AASHTO LRFD Bridge Design Specifications, 2nd ed.," 1998, American Association of State Highway and Transportation Officials, Washington, DC.

2. ACI 318-05, 2005, "Building Code Requirements for Structural Concrete and Commentary," American Concrete Institute, Farmington Hills, Michigan.

3. ACI-ASCE Committee 326, 1962, "Shear and Diagonal Tension," American Concrete Institute, Farmington Hills, MI.

4. ASCE-ACI Committee 445, 1998, "Recent Approaches to Shear Design of Structural Concrete," American Concrete Institute, Farmington Hills, MI, 42 pp.

5. ASTM A615/A615M-96a, 1996, "Standard Specification for Deformed and Plain Billet-Steel for Concrete Reinforcement," American Society for Testing and Materials, West Conshohocken, Pennsylvania.

6. ASTM C39/C39M-99, 1999, "Standard Test Method for Compressive Strength of Cylindrical Concrete Specimens," American Society for Testing and Materials, West Conshohocken, Pennsylvania.

7. ASTM C496-96, 1996, "Standard Test Method for Splitting Tensile Strength of Cylindrical Concrete Specimens," American Society for Testing and Materials, West Conshohocken, Pennsylvania.

8. CSA Standard CAN3-A23.3-94, 1994, "Design of Concrete Structures for Buildings with Explanatory Notes," Canadian Standards Association, Rexdale, Ontario.

9. "Structural Concrete: The Textbook on Behavior, Design, and Performance - Volume 2: Basis of Design," 1999, Federation Internationale du Beton (FIB), Lausanna, Switzerland.

10. NZA 3103:1995, 1995, "Concrete Structures Standard," Standards New Zealand.

11. Adebar, P., Kuchma, D., and Collins, M.P., 1990, "Strut-and-Tie Models for the Design of Pile Caps: An Experimental Study," *ACI Structural Journal*, Vol. 87, No. 1, pg. 81-92.

12. Adebar, P. and Zhou, Z., 1993, "Bearing Strength of Compressive Struts Confined by Plain Concrete," *ACI Structural Journal*, Vol. 90, No. 5, pg. 534-541.

13. Adebar, P. and Zhou, Z., 1996, "Design of Deep Pile Caps by Strut-and-Tie Models," *ACI Structural Journal*, Vol. 93, No. 4, pg. 437-448.

14. Aguilar, G., Matamoros, A.B., Parra-Montesinos, G.J., Ramirez, J.A., and Wight, J.K., 2002, "Experimental Evaluation of Design Procedures for Shear Strength of Deep Reinforced Concrete Beams," *ACI Structural Journal*, Vol. 99, No. 4, pp. 539-548.

15. Ahmad, S. A., and Lue, D. M., 1987, "Flexure-Shear Interaction of Reinforced High-Strength Concrete Beams," *ACI Structural Journal*, V. 84, No. 4, pp. 330 – 341.

16. Al-Nahlawi, K., and Wight, J.K., 1992, "Beam Analysis Using Concrete Tensile Strength in Truss Models," *ACI Structural Journal*, Vol. 89, No. 3, pp. 284-289.

17. Alshegeir, A.A. and Ramirez, J.A., 1993, "Analysis and Design of Disturbed Regions with Strut-Tie Models, Parts I and II," Purdue University, Structural Engineering Report No. CE-STR-93-1, Lafayette, Indiana.

18. Anderson, R.B., 1988, *Behavior of CTT-Nodes in Reinforced Concrete Strut-and-Tie Models*, Master's Thesis, University of Texas at Austin.

19. Anderson, N.S., and Ramirez, J.A., 1989, "Detailing of Stirrup Reinforcement," *ACI Structural Journal,* Vol. 86, No. 5, pp. 507-515.

20. Angelakos, D., 1999, "The Influence of Concrete Strength and Longitudinal Reinforcement Ratio on the Shear Strength of Large-Size Reinforced concrete Beams with and without Transverse Reinforcement," Master's Thesis, University of Toronto.

21. Angelakos, D., Bentz, E., and Collins, M. P., 2001, "Effect of Concrete Strength and Minimum Stirrups on Shear Strength of Large Members," *ACI Structural Journal,* V. 98, No. 3, pp. 290 – 300.

22. Ashour, A.F., 2000, "Shear Capacity of Reinforced Concrete Deep beams," *ASCE Journal of Structural Engineering,* Vol. 126, No. 9, pp. 1045-1052.

23. Ashour, A.F., and Rishi, G., 2000, "Tests of Reinforced Concrete Continuous Deep Beams with Web Openings," *ACI Structural Journal,* Vol. 97, No. 3, pp. 418-426.

24. Averbuch, D., and de Buhan, P., 1999, "Shear Design of Reinforced Concrete Deep Beams: A Numerical Approach," *ASCE Journal of Structural Engineering*, Vol. 125, No. 3, pp. 309-318.

25. Baron, M.J., 1966, "*Shear Strength of Reinforced Concrete Beams at Points of Bar Cutoff, ACI Journal,* Vol. 63, No. 1, pp. 127-133.

26. Barton, D.L., 1988, "*Detailing of Structural Concrete Dapped End Beams*," Master's Thesis, University of Texas at Austin.

27. Barton, D.L., Anderson, R.B., Bouadi, A., Jirsa, J.O., and Breen, J.E., "An Investigation of Strut-and-Tie Models for Dapped Beam Details," Center for Transportation Research Report No. CTR 3-5-87/9-1127-1, Austin, Texas, May 1991.

28. Batchelor, B., George, H.K., and Campbell, T.I., 1984, "Effectiveness Factor for Shear in Concrete Beams," *ASCE Journal of Structural Engineering*, Vol. 112, No. 6, pp. 1464-1477.

29. Bažant, Z. P., and Kazemi, M. T., 1991, "Size Effect on Diagonal Shear Failure on Beams without Stirrups," *ACI Structural Journal,* V. 88, No. 3, pp. 268-276.

30. Beaupre, R.J., Powell, L.C., Breen, J.E., and Kreger, M.E., 1988, "Deviation Saddle Behavior and Design for Externally Post-Tensioned Bridges," Center for Transportation Research Report No. CTR 3-5-85/8-365-2, Austin, Texas.

31. Belarbi, A., and Hsu, T.T.C., 1991, "Constitutive laws of reinforced concrete in biaxial tension-compression." *Research Report UHCEE91-2*, Univ. of Houston.

32. Bentz, E.C., 2000, "Sectional Analysis of Reinforced Concrete Members," Doctoral Dissertation, University of Toronto.

33. Bentz, E.C., 2005, "Empirical Modeling of Reinforced Concrete Shear Strength Size Effect for Members without Stirrups," *ACI Structural Journal*, Vol. 102, No. 2.

34. Bergmeister, K., Breen, J.E., Jirsa, J.O., and Kreger, M.E., 1993, "Detailing for Structural Concrete," Center for Transportation Research Report CTR 0-1127-3F, Austin, Texas.

35. Bouadi, A., 1989, "*Behavior of CCT Nodes in Structural Concrete Strut-and-Tied Models*," Master's Thesis, University of Texas at Austin.

36. Breen, J.E., Burdet, O., Roberts, C., Sanders, D., and Wollmann, G., 1994, "Anchorage Zone Reinforcement for Post-Tensioned Concrete Girders," National Cooperative Highway Research Program Report No. 356, Washington, DC.

37. Bresler, B., and Scordelis, A. C., 1963, "Shear Strength of Reinforced Concrete Beams," *ACI Journal,* V. 60, No. 1, pp. 51-72.

38. Burdet, O.L., 1990, "*Analysis and Design of Anchorage Zones in Post-Tensioned Concrete Bridges,*" Doctoral Dissertation, University of Texas at Austin.

39. Cao, S., 2001, *Size Effect and the Influence of Longitudinal Reinforcement on the Shear Response of Large Reinforced Concrete Members,* Master's Thesis, University of Toronto.

40. Chang, T. S., and Kesler, C. E., 1958, "Static and Fatigue Strength in Shear of Beams with Tensile Reinforcement," *ACI Journal,* V. 54, No. 6, pp. 1033-1057.

41. Chen, W.F., 1970, "Double Punch Test for Tensile Strength of Concrete," Journal of the American Concrete Institute, Proceedings Vol. 67, No. 12, pg. 993-995, Detroit, Michigan.

42. Chen, W.F., 1982, *Plasticity in Reinforced Concrete*, McGraw-Hill.

43. Chen, B.S., Hagenberger, M.J., and Breen, J.E., 2002, "Evaluation of Strut-and-Tie Modeling Approach to Dapped Beam with Opening" *ACI Structural Journal*, Vol. 99, No. 4, pp. 445-450.

44. Chung, W., and Ahmad, S.H., 1994, "Model for Shear Critical High-Strength Concrete Deep Beams," *ACI Structural Journal*, Vol. 91, No. 1, pp. 31-41.

45. Clark, A. P., 1951, "Diagonal Tension in Reinforced Concrete Beams," *ACI Journal,* V. 48, No. 10, pp. 145 – 156.

46.   Collins, M.P., and Mitchell, D., 1986, "A Rational Approach to Shear Design – The 1984 Canadian Code Provisions," *ACI Journal*, Vol. 83, No. 6, pg 925-933.

47.   Collins, M.P., Mitchell, D., Adebar, P., and Vecchio, F.J., 1996, "A General Shear Design Method," *ACI Structural Journal*, Vol. 93, No. 1, pp. 36-45.

48.   Collins, M.P., and Mitchell, D., 1997, *Prestressed Concrete Structures*, Response Publications.

49.   Cook, W. and Mitchell, D., 1988, "Studies of Disturbed Regions Near Discontinuities in Reinforced Concrete Members," *ACI Structural Journal*, Vol. 85, No. 2, pg. 206-216.

50.   de Cossio, R. D., and Siess, C. P., 1960, "Behavior and Strength in Shear of Beams and Frames Without Web Reinforcement," *ACI Journal,* V. 56, No. 2, pp. 695-735.

51.   de Paiva, H. A. R., and Siess, C. P., 1965, "Strength and Behavior of Deep Beams," *ASCE Structural Journal,* V. 91, No. 10, pp. 19-41.

52.   Desai, S.B., 1995, "Horizontal web steel a shear reinforcement," *Magazine of Concrete Research,* Vol. 47, No. 171, pp. 143-152.

53.   Fenwick, R.C., and Paulay, T., 1968, "Mechanisms of Shear Resistance of Concrete Beams," *ASCE Journal of Structural Engineering*, Vol. 94, No. 10, pp. 2325-2350.

54.   Ferguson, P. M., 1955, "Some Implication of Recent Diagonal Tension Tests," *ACI Journal,* V. 53, No. 1, pp. 157-172.

55.   Ferguson, P. M., Breen, J. E., and Jirsa, J. O., 1988, *Reinforced Concrete Fundamentals*, 5th ed., John Wiley and Sons.

56. Foster, S.J., 1998, "Design of Non-Flexural Members for Shear," *Cement and Concrete Composites*, Vol. 20, pp. 465-475.

57. Foster, S. J, and Gilbert, R. I., 1996, "The Design of Nonflexural Members with Normal and High-Strength Concrete," *ACI Structural Journal*, Vol. 93, No. 1, pp. 3-10.

58. Foster, S. J, and Gilbert, R. I., 1998, "Experimental Studies on High-Strength Concrete Deep Beams, "*ACI Structural Journal,* V. 95, No. 4, pp. 382-390.

59. Foster, S.J., and Malik, A.R., 2002, "Evaluation of Efficiency Factor Models used in Strut-and-Tie Modeling of Nonflexural Members," *ASCE Journal of Structural Engineering*, Vol. 128, No. 5, pp. 569-577.

60. Guyon, Y., 1953, *Prestressed Concrete*, Contractor's Record LTD, London, England, 543 pp.

61. Hawkins, N.M., 1968, "The bearing strength of concrete loaded through rigid plates," *Magazine of Concrete Research,* Vol. 20, No. 62, pp. 31-40

62. Hawkins, N.M., 1968, "The bearing strength of concrete loaded through flexible plates," *Magazine of Concrete Research,* Vol. 20, No. 63, pp. 95-102.

63. Hawkins, N.M., 1970, "The bearing strength of concrete for strip loading," *Magazine of Concrete Research,* Vol. 22, No. 71, pp. 87-98.

64. Hoang, L.C., and Nielsen, M.P., 1998, "Plasticity Approach to Shear design," *Cement and Concrete Composites*, Vol. 20, pp. 437-453.

65. Hognestad, E., 1951, "A Study of Combined Bending and Axial Load in Reinforced Concrete," Bulletin 399, University of Illinois Engineering Experiment Station, 128 pp.

66. Hong, S, 2000, "Strut-and-Tie Models for Failure Mechanisms for Bar Development in Tension-Tension-Compression Nodal Zone," *ACI Structural Journal*, Vol. 97, No. 1, pp. 111-122.

67. Hong, S., Kim, D., Kim, S, Hong, N.K., 2002, "Shear Strength of Reinforced Concrete Deep Beams with End Anchorage Failure," *ACI Structural Journal*, Vol. 99, No. 1, pp. 12-22.

68. Hong, S., and, Mueller, P., 1996, "Truss Model and Failure Mechanism for Bar Development in CCT Nodes," *ACI Structural Journal*, Vol. 93, No. 5., pp. 564-575.

69. Hwang, S., Lu, W., and Lee, H., 2000, "Shear Strength Prediction for Deep Beams," *ACI Structural Journal*, Vol. 97, No. 3, pp. 367-376.

70. Hsiung, W., and Frantz, G. C., 1985, "Transverse Stirrup Spacing in R/C Beams," *ASCE Structural Journal*, V. 111, No. 2, pp. 353-363.

71. Hsu, T.T.C., 1996, "Toward A Unified Nomenclature for Reinforced-Concrete Theory," *ASCE Journal of Structural Engineering*, Vol. 122, No. 3, pp. 275-283.

72. Hsu, T.T.C., 1998, "Unified Approach to Shear Analysis and Design," *Cement and Concrete Composites*, Vol. 20, pp. 419-435.

73. Johnson, M. K., and Ramirez, J. A., 1989, "Minimum Shear Reinforcement in Beams with Higher Strength Concrete," *ACI Structural Journal,* V. 86, No. 4, pp. 376-382.

74. Kani, G. N. J., 1964, "The Riddle of Shear Failure and Its Solution," *ACI Structural Journal,* V. 61, No. 3, pp. 441-467.

75. Kani, G.N.J., 1966, "Basic Facts Concerning Shear Failure," *ACI Journal*, Vol. 63, No. 6, pp. 675-691.

76. Kani, G.N.J., 1967, "How Safe Are Our Large Reinforced Concrete Beams," *ACI Journal,* Vol. 64, No. 3, pp. 128-141.

77. Kani, G.N.J., 1969, "A Rational Theory for the Function of Web Reinforcement," *ACI Journal*, Vol. 66, No. 3, pp. 185-197.

78. Kani, M. W., Huggins, M. W., and Wittkopp, R. R., 1979, *Kani on Shear in Reinforced Concrete*, University of Toronto Press, 225 pp.

79. Kao, A.M., and Untrauer, R.E., 1975, "Shear Strength of Reinforced Concrete Beams with Bars Terminated in Tension Zones," *ACI Journal*, Vol. 72, No. 12, pp. 720-722.

80. Kim, W.K., and White, R.N., 1991, "Initiation of Shear Cracking in Reinforced Concrete Beams with No Web Reinforcement," *ACI Structural Journal*, Vol. 88, No. 3, pp. 301-308.

81. Kollegger, J, and Mehlhorn, G., 1990, "Experimentelle Untersuchungen zur Bestimmung der Druckfestigkeit des gerissenen Stahlbetons bei einer Querzugbean-spruchung," Report 413, *Deutscher Ausschuss Für Stahlbeton*. (In German)

82. Kong, P. Y. L., and Rangan, B. V., 1998, "Shear Strength of High-Performance Concrete Beams," *ACI Structural Journal,* V. 95, No. 6, pp. 677-68.

83. Kong, F. K., Robins, P. J., and Cole, D. F., 1970, "Web Reinforcement Effects on Deep Beams," *ACI Journal*, V. 67, No. 12, pp. 1010-1016.

84. Kong, F., Robins, P.J., Kirby, D.P., and Short, D.R., 1972, "Deep Beams With Inclined Web Reinforcement," *ACI Journal,* Vol. 69, No. 3, pp. 172-176.

85. Kotsovos, M.D., 1988, "Compressive Force Path Concept: Basis for Reinforced Concrete Ultimate Limit State," *ACI Structural Journal*, Vol. 85, No. 1, pp. 68-75.

86. Kotsovos, M.D., 1988, "Design of reinforced concrete deep beams," *The Structural Engineer*, Vol. 62, No. 2, pp. 28-32.

87. Kotsovos, M.D., 1993, "Mechanisms of 'shear' failure," *Magazine of Concrete Research*, Vol. 35, No. 123, pp. 99-106.

88. Kotsovos, M.D., and Bobrowski, J., 1993, "Design Model for Structural Concrete Based on the Compressive Force Path," *ACI Structural Journal*, Vol. 90, No. 1, pp. 12-20.

89. Kotsovos, M.D., and Lefas, I.D., 1990, "Behavior of Reinforced Concrete Beams Designed in Compliance with the Concept of Compressive Force Path," *ACI Structural Journal*, Vol. 87, No. 2, pp. 127-139.

90. Kotsovos, M.D., and Pavlović, M.N., 2003, "Size effects in beams with small shear span-to-depth ratios," *Computers and Structures*.

91. Krefeld, W. J., and Thurston, C. W., 1966, "Contribution of Longitudinal Steel to Shear Resistance of Reinforced Concrete Beams," *ACI Journal*, V. 63, No. 3, pp. 325-343.

92. Krefeld, W. J., and Thurston, C. W., 1966, "Studies of the Shear Strength and Diagonal Tension Strength of Simply Supported Reinforced Concrete Beams," *ACI Journal*, V. 63, No. 4, pp. 451-474.

93. Kuzmanovic, S., 1998, "An Investigation of the Shear Design of a Reinforced Concrete Box Structure," Master's Thesis, University of Toronto.

94. Lampert, P. and Thürlimann, B., 1971, "Ultimate Strength and Design of Reinforced Concrete Beams in Torsion and Bending," IASBE Publications, No. 31-1, pg. 107-131, Zurich, Switzerland.

95. Laupa, A., Siess, C.P., and Newmark, N.M., 1953, "The Shear Strength of Simple-Span Reinforced Concrete Beams without Web Reinforcement," Structural Research Series No. 52, University of Illinois, Urbana.

96.   Laupa, A., Siess, C. P., and Newmark, N. M., 1953, "The Shear Strength of Reinforced Concrete Beams," *Civil Engineering Studies: Structural Research Series No. 62*, University of Illinois.

97.   Leonhardt, F., and Walther, R., 1962, "Contribution to Treatment of Shear Problems in Reinforced Concrete," *Beton – Stahlbetonbau*, V. 57.

98.   Lubell, A., Sherwood, T., Bentz, E., and Collins, M. P., 2004, "Safe Shear Design of Large, Wide Beams," *Concrete International,* V. 26, No. 1, pp. 67-78.

99.   Lüchinger, P., 1977, "Bruchwiderstand von Kastenträgern aus Stahlbeton unter Torsion, Biegung, und Querkraft (Ultimate Strength of Box-Griders in Reinforced Concrete under Torsion, Bending, and Shear)," Institut für Baustatik und Konstruktion-ETH, Zurich, Switzerland, Bericht Nr. 69.

100.   MacGregor, J.G. and Wight, J.K., 2005, "Reinforced Concrete: Mechanics and Design (4th Edition)," Prentice Hall, Upper Saddle River, New Jersey.

101.   MacGregor, J.G., and Walters, J.R.V., 1967, "Analysis fo Inclined Cracking Shear in Slender Reinforced Concrete Beams," *ACI Journal,* Vol. 64, No. 10, pp. 644-653.

102.   Manuel, R.F., Slight, B.W., and Suter, G.T., 1971, "Deep Beam Behavior Affected by Length and Shear Span Variations," *ACI Journal,* Vol. 68, No. 12, pp. 954-958.

103.   Marti, P., 1985, "Basic Tools in Reinforced Concrete Beam Design," Journal of the American Concrete Institute, Proceeding Vol. 82, No. 1, pg. 46-56, Detroit, Michigan.

104.   Marti, P., 1985, "Truss Models in Detailing," Concrete International, Vol. 7, No. 12, pg. 66-73, Detroit, Michigan.

105.   Marti, P. 1986, "Staggered Shear Design of Simply Supported Concrete beams," *ACI Journal*, Vol. 83, No. 1, pp. 36-41.

106. Marti, P., 1989, "Size Effect in Double-Punch Tests on Concrete Cylinders," ACI Materials Journal, Proceedings Vol. 86, No. 6, pg. 597-601, Detroit, Michigan.

107. Marti, P., 1999, "How to Treat Shear in Structural Concrete," *ACI Structural Journal*, Vol. 96, No. 3, pp. 408-415.

108. Matamoros, A.B., and Wong, K.H., 2003, "Design of Simply Supported Deep Beams Using Strut-and-Tie Models," *ACI Structural Journal*, Vol. 100, No. 6, pp. 704-712.

109. Mau, S.T., and Hsu, T.T.C., 1987, "Shear Strength Prediction for Deep beams with Web Reinforcement," *ACI Structural Journal*, Vol. 84, No. 6, pp. 513-523.

110. Mau, S.T., and Hsu, T.T.C., 1989, "Formula for the Shear Strength of Deep Beams," *ACI Structural Journal*, Vol. 86, No. 5, pp. 516-523.

111. Maxwell, B.S. and Breen, J.E., 2000, "Experimental Evaluation of Strut-and-Tie Model Applied to Deep Beam with Opening," *ACI Structural Journal*, Vol. 97, No. 1, pg. 142-148.

112. Menon, G. and Furlong, R.W., 1977, "Design of Reinforcement for Notched Ends of Prestressed Concrete Girders," Center for Transportation Research Report No. 196-1F, Austin, Texas.

113. Mitchell, D., and Collins, M.P., 1974, "Diagonal Compression Field Theory – A Rational Model for Structural Concrete in Pure Torsion," *ACI Journal,* Vol. 71, No. 8, pp. 396-408.

114. Mitchell, D., Collins, M.P., Bhide, S.B., and Rabbat, B.G., 2004, "AASHTO LRFD Strut-and-Tie Model Design Examples," portland Cement Association, Skokie, IL.

115. Moody, K. G., Viest, I. M., Elstner, R. C., and Hognestad, E., 1954, "Shear Strength of Reinforced Concrete Beams Part 1 – Tests of Simple Beams," *ACI Journal*, V. 51, No. 12, pp. 317-32.

116. Moody, K. G., Viest, I. M., Elstner, R. C., and Hognestad, E., 1954, "Shear Strength of Reinforced Concrete Beams Part 2 – Tests of Restrained beams Without Web Reinforcement

117. Morrow, J., and Viest, I. M., 1957, "Shear Strength of Reinforced Concrete Frame Members Without Web Reinforcement," *ACI Journal*, V. 53, No. 9, pp. 833-869.

118. Mörsch, E., 1902, "Der Eisenbetonbau, seine Theorie und Anwendung (Reinforced Concrete, Theory and Application)," Stuggart, Germany.

119. Mörsch, E., 1924, "Über die Berechnung der Gelenkquader," Beton-und Eisen, No. 12, pg. 156-161, Stuttgart, Germany.

120. Muttoni, A., Schwartz, J., and Thürlimann, B., 1997, *Design of Concrete Structures with Stress Fields*, Birkhäuser.

121. Natrella, M.G., 1963, *Experimental Statistics,* National Bureau of Standards Handbook 91, Washington, D.C.

122. Nielson, M.P., 1998, "*Limit Analysis and Concrete Plasticity, 2ⁿᵈ Edition,*" CRC Press.

123. Niyogi, S.K., 1973, "Bearing Strength of Concrete – Geometric Variations," ASCE Journal of Structural Engineering, Vol. 99, No. 7, pgs. 1471-1490, New York, New York.

124. Niyogi, S.K., 1974, "Concrete Bearing Strength – Support, Mix, Size Effect," ASCE Journal of Structural Engineering, Vol. 100, No. 8, pgs. 1685-1702, New York, New York.

125. Niyogi, S.K., 1975, "Bearing Strength of Reinforced Concrete Blocks," ASCE Journal of Structural Engineering, Vol. 101, No. 5, pgs. 1125-1137, New York, New York.

126. Oh, J. K., and Shin, S. W., 2001, "Shear Strength of Reinforced High-Strength Concrete Deep Beams," *ACI Structural Journal*, V. 98, No. 2, pp. 164-173.

127. Ornelas, I., 2004, "*Behavior of Shear Critical Wide Beams*," Master's Report, University of Texas at Austin.

128. Ottosen, N.S., 1977, "A Failure Criterion for Concrete," *ASCE Journal of Engineering Mechanics*, Vol. 103, No. 4, pp. 527-535.

129. Ozcebe, G., Ersoy, U., and Tankut, T., 1999, "Evaluation of Minimum Shear Reinforcement Requirements for Higher Strength Concrete," *ACI Structural Journal*, V. 96, No. 3, pp. 361-39.

130. Podgorniak-Stanik, B.A., "*The Influence of Concrete Strength, Distribution of Longitudinal Reinforcement, Amount of Transverse Reinforcement and Member Size on Shear Strength of Reinforced Concrete Members*," Master's Thesis, University of Toronto.

131. Poli, S.D., Gambarova P.G., and Karakoç, C., 1987, "Aggregate Interlock Role in R.C. Thin-Webbed Beams in Shear," *ASCE Journal of Structural Engineering*, Vol. 113, No. 1, pp. 1 – 19.

132. Poli, S.D., Prisco, M.D., and Gambarova, P.G., 1991, "Stress Field in Web of RC Thin-Webbed Beams Failing in Shear," *ASCE Journal of Structural Engineering*, Vol. 116, No. 9, pp. 2496-2515.

133. Prisco, M.D., and Gambarova, P.G., 1995, "Comprehensive Model for Study of Shear in Thin-Webbed RC and PC Beams," *ASCE Journal of Structural Engineering*, Vol. 121, No. 12, pp. 1822-1831.

134. Rajagopalan, K. S., and Ferguson, P. M., 1968, "Exploratory Shear Tests Emphasizing Percentage of Longitudinal Steel,' *ACI Journal*, V. 65, No. 8, pp. 634-638.

135. Ramakrishnan, V., and Ananthanarayana, Y., 1968, "Ultimate Strength of Deep Beams in Shear," *ACI Journal*, V. 65, No. 2, pp. 87-98.

136. Ramirez, J. and Breen, J.E., 1983, "Proposed Design Procedures for Shear and Torsion in Reinforced and Prestressed Concrete," Center for Transportation Research Report No. 248-4F, Austin, Texas.

137. Ramirez, J.A., and Breen, J.E., 1991, "Evaluation of Modified Truss-Model Approach for Beams in Shear," *ACI Structural Journal*, Vol. 88, No. 5, pp. 562-571.

138. Reineck, K., 1991, "Ultimate Shear Force of Structural Concrete Members without Transverse Reinforcement Derived from Mechanical Model," *ACI Structural Journal*, Vol. 88, No. 5, pp. 592-602.

139. Reineck, K. (editor), 2002, "Examples for the design of structural concrete with strut-and-tie models (SP208)," American Concrete Institute, Farmington Hills, MI.

140. Reineck, K., Kuchma, D.A., Kim, K.S., and Marx, S., 2003, "Shear Database for Reinforced Concrete Members without Shear Reinforcement," *ACI Structural Journal*, Vol. 100, No. 2, pp. 240-249.

141. Richart, F., 1927, "An Investigation of Web Stresses in Reinforced Concrete Beams," University of Illinois Engineering Experiment Station, Bulletin No. 166, Urbana, Illinois.

142. Ricketts, D.R., 1985, "*Ultimate Behavior of Continuous Deep Reinforced Concrete Beams*," Master's Thesis, University of Alberta.

143.   Rigotti, M., 2002, "*Diagonal Cracking in Reinforced Concrete Deep Beams – An Experimental Investigation,*" Master's Thesis, Concordia University, 220 pp.

144.   Ritter, W., 1899, "Die Bauweise Hennebique (The Hennebique System)," Schweizerische Bauzeitung, Bd. XXXIII, No. 7, Zurich, Switzerland.

145.   Roberts, C., 1990, "*Behavior and Design of the Local Anchorage Zone of Post-Tensioned Concrete Members*," Master's Thesis, The University of Texas at Austin.

146.   Rogowsky, D. M., MacGregor, J. M., and Ong, S. Y., 1986, "Tests of Reinforced Concrete Deep Beams," *ACI Journal*, V. 83, No. 4, pp. 614-623.

147.   Rogowsky, D.M. and MacGregor, J.M., 1986, "Design of Reinforced Concrete Deep Beams," Concrete International, Vol. 6, No. 8, pg. 49-58.

148.   Roller, J. J., and Russell, H. G., 1990, "Shear Strength of High-Strength Concrete Beams with Web Reinforcement," *ACI Structural Journal*, V. 87, No. 2, pp. 191-198.

149.   Russo, G., and Puleri, G., 1997, "Stirrup Effectiveness in Reinforced Concrete Beams in Flexure and Shear," *ACI Structural Journal*, Vol. 94, No. 3, pp. 227-238.

150.   Sanders, D.H., 1990, "*Design and Behavior of Anchorage Zones in Post-Tensioned Concrete Members*," Doctoral Dissertation, University of Texas at Austin.

151.   Sankovich, C.L., 2003, "*An Explanation of the Behavior of Bottle-Shaped Struts Using Stress Fields*," Master's Thesis, University of Texas at Austin.

152. Sarsam, K. F., and Al-Musawi, J. M. S., 1992, "Shear Design of High- and Normal Strength Concrete Beams with Web Reinforcement," *ACI Structural Journal*, V. 89, No. 6, pp. 658-664.

153. Schlaich, M., and Anagnostou, G., 1990, "Stress Fields for Nodes of Strut-and-Tie Models," *ASCE Journal of Structural Engineering*, Vol. 116, No. 1, pp. 13-23.

154. Schlaich, J. and Schäfer, K., 1989, "Konstruieren im Stahlbeton," Betonkalender, pg 563-715, Berlin, Germany.

155. Schlaich, J., and Schäfer, K.,1991 ,"Design and detailing of structural concrete using strut-and-tie models," *The Structural Engineer*, Vol. 69, No. 6, pp. 113-120.

156. Schlaich, J., Schäfer, K., and Jennewein, M., 1987, "Towards a Consistent Design of Structural Concrete," PCI Journal, Vol. 32, No. 3, pg. 74-150, Chicago, Illinois.

157. Schlaich, J. and Weischede, D., 1982, "Detailing of Concrete Structures (in German)," Bulletin d'Information 150, Comité Euro-International du Béton., Paris, 163 pp.

158. Shin, S., Lee, K., Moon, J., and Ghosh, S. K., 1999, "Shear Strength of Reinforced High-Strength Concrete Beams with Shear Span-to-Depth Ratios between 1.5 and 2.5," *ACI Structural Journal*, V. 96, No. 4, pp. 549-556.

159. Shioya, T., 1989, "Shear Properties of Large Reinforced Concrete Members," S*pecial Report,* Institute of Technology, Shimizu Corp., No. 25, 198 pp. (In Japanese)

160. Siao, W.B., 1993, "Strut-and-Tie Model for Shear Behavior in Deep Beams and Pile Caps Failing in Diagonal Splitting," *ACI Structural Journal*, Vol. 90, No. 4, pp. 356-363.

161. Smith, K. N., and Vantsiotis, A. S., 1982, "Shear Strength of Deep Beams," *ACI Journal*, V. 79, No. 3, pp. 201-213.

162. Subedi, N. K., Vardy, A. E., and Kubota, N., 1986, "Reinforced Concrete Deep Beams – Some Test Results," *Magazine of Concrete Research*, V. 38, No. 137, pp. 206-219.

163. Talbot, A., 1909, "Tests of Reinforced Concrete Beams: Resistance to Web Stresses, Series of 1907 and 1908," University of Illinois Engineering Experiment Station, Bulletin No. 29, Urbana, Illinois.

164. Tan, K., Kong, F., Teng, S., and Guan, L., 1995, "High-Strength Concrete Deep Beams with Effective Span and Shear Span Variations," *ACI Structural Journal*, V. 92, No. 4, pp. 1-11.

165. Tan, K., Kong, F., Teng, S., and Weng, L., 1997, "Effect of Web Reinforcement on High-Strength Concrete Deep Beams," *ACI Structural Journal,* V. 94, No. 5, pp. 572-582.

166. Tan, K., Kong, F., and Weng, L., 1998, "High-Strength Reinforced Concrete Deep and Short Beams: Shear Design Equations in North American and UK Practice," *ACI Structural Journal*, Vol. 95, No. 3, pp. 318-329.

167. Tan, K. H., and Lu, H. Y., 1999, "Shear behavior of Large Reinforced Concrete Deep Beams and Code Comparisons," *ACI Structural Journal,* V. 96, No, 5, pp. 836-845.

168. Tan, K., and Mansur, M.A., 1996, "Design Procedure for Reinforced Concrete Beams with Large Web Openings," *ACI Structural Journal*, Vol. 93, No. 4, pp. 404-411.

169. Tan, H. K., Teng, S., Kong, F., and Lu, H., 1997, "Main Tension Steel in High-Strength Concrete Deep and Short Beams," *ACI Structural Journal*, V. 94, No. 6, pp. 752-768.

170. Taylor, H.P.J., 1972, "Shear Strength of Large Beams," *ASCE Journal of Structural Engineering*, Vol. 98, No. 11, pp. 2473-2490.

171. Taylor, R., 1960, "Some shear tests on reinforced concrete beams without shear reinforcement," *Magazine of Concrete Research*, Vol. 12, No. 36, pp. 145-154.

172. Thompson, M.K., 2002, "*The Anchorage Behavior of Headed Reinforcement in CCT Nodes and Lap Splices*," Doctoral Dissertation, University of Texas at Austin.

173. Thompson, M.K., Young, M.J., Jirsa, J.O., Breen, J.E., and Klingner, R.E., 2003, "Anchorage of headed Reinforcement in CCT Nodes," Center for Transportation Research Report 1855-2, University of Texas at Austin.

174. Tompos, E.J., and Frosch, R.J., 2002, "Influence of Beam Size, Longitudinal Reinforcement, and Stirrup Effectiveness on Concrete Shear Strength," *ACI Structural Journal*, Vol. 99, No. 5, pp. 559-567.

175. Uribe, C. M., and Alcocer, S. M., 2001, "Behavior of Deep Beams Designed with Strut-and-Tie Models," Centro Nacional de Prevención de Disastres, 247 pp. (In Spanish)

176. Uzel, A, 2003, *Shear Design of Large Footings*, Doctoral Thesis, University of Toronto, 185 pp.

177. Van Den Berg, F. J., 1962, "Shear Strength of Reinforced Concrete Beams Without Web Reinforcement Part 1 – Distribution of Stresses Over Beam Cross Section," *ACI Journal*, V. 59, No. 10, pp. 1467-1477.

178. Van Den Berg, F. J., 1962, "Shear Strength of Reinforced Concrete Beams Without Web Reinforcement Part 2 – Factors Affecting Load at Diagonal Cracking," *ACI Journal*, V. 59, No. 11, pp. 1587-1599.

179. Van Den Berg, F. J., 1962, "Shear Strength of Reinforced Concrete Beams Without Web Reinforcement Part 3 – Proposed Method for Calculation of Cracking Load," *ACI Journal*, V. 59, No. 12, pp. 1849-1562.

180. Vecchio, F.J., 2000, "Analysis of Shear-Critical Reinforced Concrete Beams," *ACI Structural Journal*, Vol. 97, No. 1, pp. 102-110.

181. Vecchio, F.J., 2000, "Disturbed Stress Field Model for Reinforced Concrete: Formulation," *ASCE Journal of Structural Engineering*, Vol. 126, No. 9, pp. 1070-1077.

182. Vecchio, F.J., 2001, "Disturbed Stress Field Model for Reinforced Concrete: Implementation," *ASCE Journal of Structural Engineering*, Vol. 127, No. 1, pp. 12-20.

183. Vecchio, F.J. and Collins, M.P., 1982, "The Response of Reinforced Concrete to In-Plane Shear and Normal Stresses," The University of Toronto, Department of Civil Engineering Publication No. 82-03, Toronto, Canada.

184. Vecchio, F.J. and Collins, M.P., 1986, "The Modified Compression Field Theory for Reinforced Concrete Elements Subjected to Shear," *ACI Journal,* Vol. 83, No. 2, pg. 219-231.

185. Vecchio, F.J., and Collins, M.P., 1988, "Predicting the Response of Reinforced Concrete Beams Subjected to Shear Using Modified Compression Field Theory," *ACI Structural Journal*, Vol. 85, No. 3, pp. 258-268.

186. Vecchio, F.J, and Collins, M.P., 1993, "Compression Response of Cracked Reinforced Concrete," *ASCE Journal of Structural Engineering*, Vol. 119, No. 12, pp. 3590-3610.

187. Vecchio, F.J., Collins, M.P., and Aspiotis, J., 1994, "High-Strength Concrete Elements Subjected to Shear," *ACI Structural Journal*, Vol. 91, No. 4, pp. 423-433.

188. Vecchio, F.J., Lai, D, and Ng, J., 2001. "Disturbed Stress Field Model for Reinforced Concrete: Validation," *ASCE Journal of Structural Engineering*, Vol. 127, No. 4, pp. 350-358.

189. Walraven, J., and Lenhwalter, N, 1994, "Size Effects in Short Beams Loaded in Shear," *ACI Structural Journal*, Vol. 91, No. 5, pp. 585-593.

190. Warwick, W.B., and Foster, S.J., 1993, "Investigation into the Efficiency Factor Used in non-Flexural Reinforced Concrete Member Design,: UNICIV Report No. R-320, University of New South Wales, Kensington Australia.

191. Watstein, D., and Mathey, R. G., 1958, "Strains in Beams Having Diagonal Cracks," *ACI Journal*, V. 55, No. 12, pp. 717-728.

192. Williams, A., 1979, "The Bearing Capacity of Concrete Loaded Over a Limited Area," Cement and Concrete Association, Technical Report 526, Wexham Springs, Slough, United Kingdom.

193. Wollmann, G.P., 1992, "*Anchorage Zones in Post-Tensioned Concrete Structures,*" Doctoral Dissertation, University of Texas at Austin.

194. Xie, Y., Ahmad, S. H., Yu, T., and Chung, W., 1994, "Shear Ductility of Reinforced Concrete Beams of Normal and High-Strength Concrete," *ACI Structural Journal*, V. 91, No. 2, pp. 140-149.

195. Yang, K., Chung, H., Lee, E, and Eun, H., 2003, "Shear Characteristics of High-Strength Concrete Deep Beams without Shear Reinforcements," *Engineering Structures*, V. 25, pp. 1343-1352.

196. Yoon, Y., Cook, W. D., and Mitchell, D., 1996, "Minimum Shear Reinforcement in Normal, Medium, and High-Strength Concrete Beams," *ACI Structural Journal,* V. 93, No. 5, pp. 1-9.

197. Yoshida, Y., 2000, *Shear Reinforcement for Large Lightly Reinforced Concrete Members,* Master's Thesis, University of Toronto, 150 pp.

198. Young, M.J., 2000, "*Performance of Headed Reinforcing Bars in CCT Nodal Regions*," Master's Thesis, University of Texas at Austin.

199. Yun, Y.M., and Ramirez, J.A, 1996, "Strength of Struts and Nodes in Strut-Tie Model'", *ASCE Journal of Structural Engineering*, Vol. 122, No. 1, pp. 20-29.

200. Zararis, P.D., 2003, "Shear Compression Failure in Reinforced Concrete Deep Beams," *ASCE Journal of Structural Engineering*, Vol. 129, No. 4, pp. 544-553.

201. Zhang, J.-P., 1997, "Diagonal cracking and shear strength of reinforced concrete beams," *Magazine of Concrete Research*, Vol. 49, No. 178, pp. 55-65.

202. Zielinski, Z.A., and Rigotti, M., 1995, "Tests on Shear Capacity of Reinforced Concrete," *ASCE Journal of Structural Engineering*, Vol. 121, No. 11, pp. 1660-1666.

203. Zsutty, T., 1971, "Shear Strength Prediction for Separate Categories of Simple Beam Tests," *ACI Journal,* Vol. 68, No. 2, pp. 138-143.

Vita

Michael Douglas Brown was born on February 19, 1979 in Fort Worth, Texas, son of Verl Douglas Brown and Patricia Word Brown. He attended Crowley High School in Crowley, Texas, and graduated in 1997. After high school he enrolled in The University of Texas at Austin, and in December of 2000, he was awarded the degree of Bachelor of Science in Civil Engineering. In January of 2001, he entered The Graduate School at The University of Texas to pursue a Master of Science degree in Engineering. While pursuing his graduate degree, he worked at the Construction Materials Research Group as a graduate research assistant under K. Folliard. After completing his Master's degree, he began work on his Ph.D. under the supervision of O. Bayrak. Upon completion of his doctoral work, he accepted a faculty position at Ohio University in Athens, Ohio.

Permanent address: 1400 Linwood Lane
                    Fort Worth, Texas 76134

This dissertation was typed by the author.